

UNIVERSIDAD DEL PAÍS VASCO / EUSKAL HERRIKO UNIBERTSITATEA

Escuela Técnica Superior de Ingeniería de Bilbao

Departamento de Ingeniería Química y del Medio Ambiente

# **Development of advanced catalytic systems for the selective hydrogenolysis of biomass-derived polyols**

Dissertation submitted to fulfil the final requirements to obtain the degree of

Ph.D. in Chemical Engineering

by:

**Ms. Sara García Fernández**

Thesis Advisors:

**Dr. Jesús María Requies Martínez**

**Dr. Iñaki Gandarias Goikoetxea**

Bilbao, 2016

*A mis padres y Javi, por su apoyo incondicional*



## Table of contents

Summary.....	2
Resumen.....	7
CHAPTER 1. Introduction.....	13
CHAPTER 2. State of the art: Glycerol hydrogenolysis to propanediols.....	43
CHAPTER 3. Objectives and scope of the thesis.....	77
CHAPTER 4. Experimental.....	81
CHAPTER 5. The role of Pt and WO <sub>x</sub> active phases of the bimetallic Pt/WO <sub>x</sub> /Al <sub>2</sub> O <sub>3</sub> catalysts.....	101
CHAPTER 6. Influence of the support of bimetallic Pt-WO <sub>x</sub> catalysts on glycerol hydrogenolysis.....	127
CHAPTER 7. Mechanistic study of the glycerol hydrogenolysis over Pt/WO <sub>x</sub> /Al <sub>2</sub> O <sub>3</sub> catalysts.....	157
CHAPTER 8. Conclusions and future work.....	187
Appendix: List of acronyms.....	193
Curriculum vitae.....	197

## Summary

A progressive transition from a petroleum-based towards a bio-based economy is completely required in order to achieve a more sustainable society, which implies a reduction of the petroleum dependence and the carbon footprint of modern societies. The development of new transformation processes to convert biomass into fuels and high added value chemicals is the key issue in this transition.

The O/C ratio of the biomass feedstocks, and its derived platform chemicals and building blocks, is commonly higher than that of most commodity chemicals. C–O bond hydrogenolysis appears as one of the best approaches in the deoxygenation of biomass-derived platform chemicals and building blocks. In this sense, the C–O hydrogenolysis of biomass-derived polyols, especially sorbitol, xylitol and glycerol, has attracted a great deal of attention in recent years. These three polyols were identified as ones of the top 13 most important biomass-derived building blocks in the biorefinery industry for the production of high-value chemicals.

The current PhD thesis has focussed on the development of advanced catalytic systems for the selective hydrogenolysis of biomass-derived polyols. For this research, the study of the aqueous glycerol hydrogenolysis to propanediols (PDOs) was selected as a model reaction, but it should not be overlooked that the knowledge gain of this process could be applied in a near future to the valorisation of the more complicated polyols, structurally “analogous” to glycerol, such as sorbitol or xylitol.

In the recent years, the catalytic conversion of glycerol to PDOs has been widely studied by the scientific community. However, only high yields of 1,2-propanediol (1,2-PDO) have been reported, using typically bifunctional systems formed by a hydrogenation metal and an acid or base additive. Nevertheless, the production of the higher added-value 1,3-propanediol (1,3-PDO) is much more challenging. Thus, there is a need for the development of new heterogeneous catalytic systems which are highly selective for the C–O cleavage of the secondary hydroxy group of glycerol.

Up to date, the most effective approach in the production of 1,3-PDO in aqueous phase has shown to be the use of heterogeneous catalysts formed by a highly reducible noble metal with an oxophilic metal (mainly Re or W).

In the present PhD thesis, the bimetallic Pt/WO<sub>x</sub>/Al<sub>2</sub>O<sub>3</sub> catalyst was initially selected for the glycerol hydrogenolysis at 220 °C and 45 bar of H<sub>2</sub>. In order to understand the role of each active phase, two different series of Pt/WO<sub>x</sub>/Al<sub>2</sub>O<sub>3</sub> catalysts,

with different  $\text{WO}_x$  and Pt contents, were prepared through sequential wetness impregnation (WI) method, tested in the reaction and characterised by several techniques.

The  $\text{WO}_x$  incorporation had the most remarkable impact on the increase of the total acidity of the catalyst. In addition, an interesting feature of  $\text{WO}_x/\text{Al}_2\text{O}_3$  catalysts was found: their Brönsted to Lewis acid sites ratio (B/L) can be tuned as a function of the tungsten surface density ( $\rho_w$ ), expressed in W at.  $\text{nm}^{-2}$  of support. Raman spectroscopy of some  $\text{WO}_x/\text{Al}_2\text{O}_3$  catalysts revealed that the  $\rho_w$  parameter controlled the kind of  $\text{WO}_x$  species deposited on the catalyst surface, mainly monotungstates, polytungstates and  $\text{WO}_3$  crystalline nanoparticles ( $\text{WO}_3$  NPs). The combination of this characterisation technique with Fourier transform infrared spectroscopy (FTIR) of adsorbed pyridine showed that the B/L increased with the  $\rho_w$  due to the polytungstate formation, until the emergence of  $\text{WO}_3$  NPs. The polytungstates were found to be the unique species able to delocalize the negative charge required for the formation of Brönsted acid sites.

The results of glycerol hydrogenolysis over  $\text{Pt}/\text{WO}_x/\text{Al}_2\text{O}_3$  catalysts with constant Pt content (1 wt%) and different  $\rho_w$  (1.0-3.9 W at.  $\text{nm}^{-2}$ ) revealed that the maximum yield to 1,3-PDO was achieved with the highest content of dispersed polytungstate species but before the emergence of the  $\text{WO}_3$  NPs (2.4 W at.  $\text{nm}^{-2}$ ), non-well dispersed particles and quite inaccessible to the glycerol reactant.

In addition, the effect of Pt content (1-9 wt%) was studied in the glycerol hydrogenolysis, with constant  $\rho_w$  (nearly the optimum value previously obtained of 2.2 W at.  $\text{nm}^{-2}$ ). As expected, the increase of Pt content enhanced the glycerol conversion since these metal sites were involved in the heterolytic activation of  $\text{H}_2$  molecules into hydrides and protons, which subsequently took part in the activation of the adsorbed glycerol. Moreover, the increase of Pt loading had a remarkable effect on the increase of 1,3-PDO/1,2-PDO ratio. A larger interaction between Pt and  $\text{WO}_x$  sites, or a closer proximity between them, was suggested to be responsible of the greatly enhancement of glycerol conversion and 1,3-PDO/1,2-PDO ratio, at high Pt contents. However, the main drawback was the over-hydrogenolysis of 1,3-PDO to 1-propanol (1-PO). This reaction was partially avoided at 200 °C, enhancing the selectivity towards 1,3-PDO.

To gain more knowledge about some of the main catalytic parameters involved in the reaction, the previous study was deepened by the use of three different aluminium oxide materials as supports of the bimetallic Pt- $\text{WO}_x$  catalysts. For this purpose, pseudo

$\gamma$ -AlO(OH) (pseudo-boehmite) and  $\gamma$ -Al<sub>2</sub>O<sub>3</sub> supports prepared by a sol-gel (SG) method were compared with the previously tested commercial  $\gamma$ -Al<sub>2</sub>O<sub>3</sub> (Al<sup>com</sup>).

The effect of the  $\rho_w$  and Pt-WO<sub>x</sub> interactions was investigated in the aqueous glycerol hydrogenolysis at 200 °C and 45 bar of H<sub>2</sub>.

For this purpose, three different strategies were carried out to modify the  $\rho_w$ : (i) using of catalysts with similar nominal W content of 10 wt%, (ii) catalysts with the highest  $\rho_w$  before the formation of the undesired WO<sub>3</sub> NPs ( $\rho_w^{\text{lim}}$ ), and (iii) catalysts with similar nominal W content of 10 wt% calcined at higher temperature and, therefore, with lower surface area and higher  $\rho_w$ . The Pt loading was kept constant (2 wt%) in all cases.

First of all, the pseudo  $\gamma$ -AlO(OH) support allowed a higher  $\rho_w^{\text{lim}}$  value, since showed a high concentration of hydroxy groups on its surface as compared to that of the  $\gamma$ -Al<sub>2</sub>O<sub>3</sub>. This result indicated that the hydroxy groups are the preferential anchoring sites for the WO<sub>x</sub> species.

The correlation between the results of activity test and catalyst characterisation unequivocally demonstrated that the  $\rho_w$  controlled the selectivity towards 1,3-PDO through the formation of the polytungstate species. However, a balance between the acid and metal sites seemed necessary in order to enhance the Pt-WO<sub>x</sub> interactions or the close proximity between these active sites. Thus, in spite of the pseudo-AlO(OH) support achieved the highest  $\rho_w^{\text{lim}}$ , the Pt/WO<sub>x</sub> on Al<sup>com</sup> catalyst (2Pt9W supported on Al<sup>com</sup>) showed a better yield to 1,3-PDO.

To improve the Pt-WO<sub>x</sub> interactions two strategies were carried out: (i) improving the Pt dispersion of the catalyst which achieved the best results up to that date, with the use of the chemical vapour impregnation (CVI) method for Pt deposition, and, (ii) increasing the Pt loading from 2 to 9 wt%. Despite the CVI method was not able to improve the Pt dispersion of the catalyst prepared by sequential WI, the activity test and characterisation results allowed determine that Pt dispersion was an important parameter in the glycerol hydrogenolysis. A higher Pt dispersion could lead to a higher Pt-WO<sub>x</sub> interaction (or closer proximity), promoting the selective formation of 1,3-PDO from glycerol.

The Pt-WO<sub>x</sub> interactions (or their proximity) were improved by increasing the Pt content from 2 to 9 wt%. The most remarkable effect was found on the glycerol conversion; it increased almost 4 times as the Pt loading increased. Moreover, the increase of Pt loading enhanced the 1,3-PDO/1,2-PDO ratio. Despite the Pt dispersion

decreased with the Pt metal loading, the CO chemisorption results revealed relatively small Pt particles for the catalysts with 9 wt% of Pt (9Pt8W supported on Al<sup>com</sup>). This catalyst showed a considerably high yield to 1,3-PDO of 35.0 % (in 24 h at 200 °C and 45 bar of H<sub>2</sub>).

The great deal of controversy about fundamental parameters involved in the reaction, such as the role of the oxophilic metal in the binding of glycerol or the intermediate species generated, motivated a deeper study of the reaction mechanism.

The glycerol hydrogenolysis was studied by *in-situ* attenuated total reflection infrared (ATR-IR) spectroscopy using the 9Pt8W supported on Al<sup>com</sup> catalyst, at 200 °C and 45 bar of H<sub>2</sub>. This technique proved to be a powerful tool for the catalyst characterisation in real-time since it could register the changes the catalytic surface suffered during the reaction. However, this work highlighted the problems related to the use of solvents with strong IR absorption like water. Although the measurements in water were very hard, it was possible to measure the changes in the interactions of adsorbed molecules and catalyst surface in real-time, as the reactant was consumed and the products were formed.

More interesting mechanistic information was obtained with the *ex-situ* ATR-IR spectroscopy. It was applied to the study of the interactions of the glycerol reactant with different catalyst surfaces ( $\gamma$ -Al<sub>2</sub>O<sub>3</sub> and 9W on  $\gamma$ -Al<sub>2</sub>O<sub>3</sub>), which provided important information about the initial adsorption step. The results suggested that the adsorption took place through the terminal hydroxy group/s of glycerol over both catalysts, but the adsorption strength seemed to be stronger over the catalyst with WO<sub>x</sub>.

Moreover, a preliminary kinetic study was performed in order to determine whether the main products of the glycerol hydrogenolysis (PDOs and 1-PO) compete for the same active sites of glycerol. For these experiments, different aqueous feed solutions formed by glycerol and a product, in a molar ratio of 1:1, were used. An inhibition of the glycerol conversion was found in all cases due to the competitive adsorption for the same active sites between the products and glycerol. PDOs showed a higher competition than 1-PO which could be explained by the higher number of hydroxy groups of PDOs. In addition, the stronger adsorption of 1,3-PDO pointed out that the adsorption of PDOs might also occur preferentially by the terminal hydroxy group.

The traditionally proposed dehydration-hydrogenation mechanism could not explain the very high selectivities towards 1,3-PDO achieved with this kind of catalysts.



To gain more knowledge about the reaction mechanism, the hydrogenolysis of glycerol, 1,2-PDO and 1,3-PDO were carried out under H<sub>2</sub> and N<sub>2</sub> atmospheres, over the 9Pt8W supported on Al<sup>com</sup> catalyst (at 220 °C and 45 bar).

The over-hydrogenolysis of PDOs to 1-PO was the main reaction involved in the PDOs conversion under H<sub>2</sub> atmosphere. It explained why high selectivities towards 1-PO were normally obtained in the glycerol hydrogenolysis. Under N<sub>2</sub> atmosphere, the glycerol conversion decreased almost 4 times and only 1,2-PDO among the PDOs was not obtained. This fact revealed that a high availability of hydrogen is necessary for the glycerol conversion into 1,3-PDO.

The better understanding of some important reaction parameters led to the proposal of a new reaction mechanism for the selective glycerol hydrogenolysis to 1,3-PDO. The WO<sub>x</sub> acid sites might be involved in the first step by anchoring the primary hydroxy group/s of glycerol. Next, a proton coming from a Brønsted acid site (provided by polytungstate species) could protonate the internal hydroxy group of glycerol (with the highest proton affinity). It might be stabilised by the polytungstate species, what was favoured by the stronger glycerol adsorption over the WO<sub>x</sub> sites rather than on those of the  $\gamma$ -Al<sub>2</sub>O<sub>3</sub> support. After dehydration, a secondary carbocation was formed. A hydride specie, coming from the heterolytic activation of molecular H<sub>2</sub> on the Pt active sites, attacked the secondary carbocation. Finally, the hydrolysis of the alkoxide formed yielded the target compound 1,3-PDO.

## Resumen

La progresiva transición desde una economía basada en el petróleo hacia una bio-economía es completamente necesaria para conseguir una sociedad más sostenible, lo cual implica una reducción de la dependencia del petróleo y de la huella de carbono de las sociedades modernas. El desarrollo de nuevos procesos para transformar la biomasa en combustibles y productos químicos de alto valor añadido es la cuestión fundamental en esta transición.

Normalmente, el ratio O/C de las materias primas de la biomasa y, de sus plataformas químicas y bloques químicos constituyentes, es mayor que en mayoría de los productos químicos. La hidrogenólisis del enlace C–O aparece como una de las mejores propuestas para la desoxigenación de las plataformas químicas y bloques químicos derivados de la biomasa. En este contexto, la hidrogenólisis C–O de los polioles derivados de la biomasa, especialmente del sorbitol, xilitol y glicerol, recientemente ha atraído mucha atención. Estos tres polioles han sido identificados como unos de los top-13 bloques químicos constituyentes más importantes en la biorefinería para la obtención de productos químicos de alto valor añadido.

La actual tesis doctoral se ha centrado en el desarrollo de sistemas catalíticos avanzados para la hidrogenólisis selectiva de polioles derivados de la biomasa. Para esta investigación se ha seleccionado el estudio de la hidrogenólisis acuosa de glicerol a propanodiol (PDOs) como modelo de reacción, pero no se debe pasar por alto que el conocimiento adquirido en este proceso podría aplicarse en un futuro cercano a la valorización de polioles más complejos, estructuralmente análogos al glicerol, como el sorbitol o el xilitol.

Recientemente, la conversión catalítica de glicerol a PDOs ha sido ampliamente estudiada por la comunidad científica. Sin embargo, sólo se han obtenido altos rendimientos a 1,2-propanodiol (1,2-PDO) utilizando habitualmente sistemas bifuncionales formados por un metal para la hidrogenación y un ácido o una base como aditivo. Sin embargo, la producción del 1,3-propanodiol (1,3-PDO), de mayor valor añadido, es mucho más compleja. Por ello, es necesario el desarrollo de nuevos sistemas catalíticos heterogéneos altamente selectivos en la ruptura del enlace C-O del grupo hidroxilo secundario del glicerol.

Hasta el momento, la mejora más efectiva en la producción de 1,3-PDO en fase acuosa ha sido el uso de catalizadores heterogéneos formados por un metal noble altamente reducible y un metal oxofílico (principalmente Re o W).

En la presente tesis doctoral, el catalizador bimetalico Pt/WO<sub>x</sub>/Al<sub>2</sub>O<sub>3</sub> ha sido inicialmente seleccionado para la hidrogenólisis de glicerol a 220 °C y 45 bar de H<sub>2</sub>. Para tratar de entender el papel de cada fase activa, 2 diferentes series de catalizadores de Pt/WO<sub>x</sub>/Al<sub>2</sub>O<sub>3</sub>, con diferentes contenidos de WO<sub>x</sub> y Pt, se prepararon mediante el método de impregnación húmeda secuencial (del inglés *wetness impregnation*, WI), se probaron en la reacción y se caracterizaron mediante numerosas técnicas.

La incorporación de WO<sub>x</sub> mostró tener el mayor impacto en el aumento de la acidez total del catalizador. Además, se encontró una interesante característica de los catalizadores de WO<sub>x</sub>/Al<sub>2</sub>O<sub>3</sub>: su ratio de centros ácidos Brønsted a Lewis (B/L) podía modificarse en función de la densidad superficial de tungsteno ( $\rho_w$ ), expresada en at. W nm<sup>-2</sup> de soporte. La espectroscopía Raman de algunos catalizadores de WO<sub>x</sub>/Al<sub>2</sub>O<sub>3</sub> reveló que el parámetro  $\rho_w$  controlaba el tipo de especies de WO<sub>x</sub> depositadas sobre la superficie del catalizador, principalmente monotungstatos, politungstatos y nanopartículas cristalinas de WO<sub>3</sub> (NPs WO<sub>3</sub>). La combinación de esta técnica de caracterización con la espectroscopía infrarroja mediante transformada de Fourier (FTIR) de piridina absorbida mostró que el ratio B/L aumentaba con  $\rho_w$  debido a la formación de politungstatos, hasta la aparición de las WO<sub>3</sub> NPs. Se ha encontrado que los politungstatos son las únicas especies capaces de deslocalizar la carga negativa requerida para la formación de los centros ácidos Brønsted.

Los resultados de la hidrogenólisis de glicerol sobre catalizadores de Pt/WO<sub>x</sub>/Al<sub>2</sub>O<sub>3</sub> con un contenido constante de Pt (1 % peso) y diferentes  $\rho_w$  (1.0-3.9 at. W nm<sup>-2</sup>) revelaron que el mayor rendimiento a 1,3-PDO se obtuvo con el mayor contenido de especies de politungstatos pero antes de la aparición de las NPs WO<sub>3</sub> (2.4 at. W nm<sup>-2</sup>), partículas mal dispersas y bastante inaccesibles al reactivo glicerol.

También se estudió el efecto del contenido de Pt (1-9 % peso) en la hidrogenólisis de glicerol, con un valor constante de  $\rho_w$  (cercano al óptimo encontrado anteriormente de 2.2 at. W nm<sup>-2</sup>). Como era de esperar, el aumento del contenido de Pt mejoró la conversión ya que estos centros metálicos están involucrados en la activación heterolítica de las moléculas de H<sub>2</sub> en hidruros y protones, los cuales posteriormente toman parte en la activación de las moléculas adsorbidas de glicerol. Además, el aumento del contenido de Pt tenía un notable efecto en el aumento del ratio 1,3-

PDO/1,2-PDO. Se ha sugerido que la mayor interacción entre los centros de Pt y los de los  $WO_x$ , o la mayor proximidad entre ellos, a altos contenidos de Pt era la responsable de la gran mejora de la conversión de glicerol y del ratio 1,3-PDO/1,2-PDO. Sin embargo, el principal inconveniente era la sobre-hidrogenólisis de 1,3-PDO a 1-propanol (1-PO). Esta reacción se suprimió parcialmente a 200 °C, mejorando la selectividad a 1,3-PDO.

Para obtener un mayor conocimiento sobre algunos de los principales parámetros involucrados en la reacción, el anterior estudio fue profundizado mediante la utilización de diferentes óxidos de aluminio como soportes de los catalizadores bimetalicos de Pt- $WO_x$ . Con este propósito, se compararon los soportes de pseudo  $\gamma$ -AlO(OH) (pseudo-boehmita) y  $\gamma$ -Al<sub>2</sub>O<sub>3</sub> preparados mediante el método sol-gel (SG) con la previamente utilizada  $\gamma$ -Al<sub>2</sub>O<sub>3</sub> comercial (Al<sup>com</sup>).

Se investigó el efecto de la  $\rho_w$  y de las interacciones Pt- $WO_x$  en la hidrogenólisis acuosa de glicerol a 200 °C y 45 bar de H<sub>2</sub>. Con este propósito, se llevaron a cabo tres estrategias diferentes para modificar la  $\rho_w$ : (i) uso de catalizadores con un contenido nominal de W similar, del 10 % peso, (ii) catalizadores con el mayor valor de posible  $\rho_w$  antes de la aparición de las NPs  $WO_3$  ( $\rho_w^{\text{lim}}$ ), y (iii) catalizadores con un contenido nominal de W similar, del 10 % peso, calcinados a temperaturas más altas y, por tanto, con una menor área superficial y mayor valor de  $\rho_w$ . El contenido de Pt se mantuvo constante en todos los casos (2 % peso).

En primer lugar, el soporte de pseudo-AlO(OH) logró un mayor valor de  $\rho_w^{\text{lim}}$  ya que su superficie mostraba una mayor concentración de grupos hidroxilo comparada con la superficie de la  $\gamma$ -Al<sub>2</sub>O<sub>3</sub>. Este resultado indicaba que los grupos hidroxilos eran los centros preferenciales para el anclaje de las especies de  $WO_x$ .

La correlación entre los resultados de los ensayos de actividad y la caracterización de los catalizadores, demostró de forma inequívoca que la  $\rho_w$  controlaba la selectividad a 1,3-PDO a través de la formación de las especies de politungstos. Sin embargo, parecía necesario un equilibrio entre los centros ácidos y metálicos con el fin de aumentar las interacciones Pt- $WO_x$  o la proximidad entre estos centros activos. Por ello, a pesar de que el soporte de pseudo-AlO(OH) consiguió el valor más alto de  $\rho_w^{\text{lim}}$ , el catalizador de Pt/ $WO_x$  soportado en Al<sup>com</sup> (2Pt9W soportado en Al<sup>com</sup>) mostró un mejor rendimiento a 1,3-PDO.

Para mejorar las interacciones Pt- $WO_x$  se llevaron a cabo dos estrategias: (i) mejorar la dispersión de Pt en el catalizador que había mostrado los mejores resultados

hasta el momento, mediante la utilización del método de impregnación química vapor (del inglés *chemical vapour impregnation*, CVI) para depositar el Pt, y (ii) aumento del contenido de Pt de 2 a 9 % peso. A pesar de que el método CVI no fue capaz de mejorar la dispersión del Pt del catalizador preparado mediante WI, los ensayos de actividad y los resultados de la caracterización permitieron determinar que la dispersión era un parámetro importante en la hidrogenólisis de glicerol. Una mayor dispersión de Pt podría conducir a una mayor interacción Pt-WO<sub>x</sub> (o una mayor proximidad), promoviendo la formación selectiva de 1,3-PDO a partir del glicerol.

Las interacciones Pt-WO<sub>x</sub> (o su proximidad) fueron mejoradas mediante el aumento del contenido de Pt, desde el 2 al 9 % peso. El efecto más remarcable se encontró en la conversión de glicerol; ésta aumentó casi 4 veces con el aumento de la carga de Pt. Además, el incremento del contenido de Pt aumentó el ratio 1,3-PDO/1,2-PDO. A pesar de que la dispersión de Pt disminuía con el aumento del contenido metálico de Pt, los resultados de quimisorción de CO mostraron que las partículas de Pt eran bastantes pequeñas para el catalizador con un 9 % peso (9Pt8W sobre Al<sup>com</sup>). Este catalizador mostró un rendimiento a 1,3-PDO considerablemente elevado del 35 % (en 24 h a 200 °C y 45 bar de H<sub>2</sub>).

La gran controversia sobre ciertos parámetros fundamentales involucrados en la reacción, como el papel del metal oxofílico en el anclaje del glicerol o las especies intermedias generadas, ha motivado la realización de un profundo estudio del mecanismo de reacción.

La hidrogenólisis de glicerol fue estudiada *in-situ* mediante espectroscopía infrarroja de reflexión total atenuada (del inglés *attenuated total reflection infrared*, ATR-IR) utilizando el catalizador 9Pt8W soportado en Al<sup>com</sup>, a 200 °C y 45 bar de H<sub>2</sub>. Esta técnica ha demostrado ser una potente herramienta para la caracterización de catalizadores en tiempo real, ya que puede registrar los cambios que sufre la superficie del catalizador durante la reacción. Sin embargo, este trabajo ha resaltado la problemática relacionada con el uso de disolventes que absorben fuertemente radiación IR como es el caso del agua. Aunque las medidas en agua fueron difíciles, fue posible medir los cambios en las interacciones entre las moléculas adsorbidas y la superficie del catalizador, a medida que los reactivos se iban consumiendo y los productos se iban formando.

Con el uso de la espectroscopía ATR-IR *ex-situ* se obtuvo una información mecanística más interesante. Se aplicó al estudio de las interacciones entre el reactivo

glicerol y la superficie de diferentes catalizadores ( $\gamma\text{-Al}_2\text{O}_3$  and 9W on  $\gamma\text{-Al}_2\text{O}_3$ ), lo que proporcionó importante información acerca de la etapa inicial de adsorción. Los resultados sugirieron que la adsorción tenía lugar a través del grupo/s terminal/es del glicerol sobre los dos catalizadores, pero la fuerza de la adsorción parecía ser mayor sobre el catalizador con  $\text{WO}_x$ .

Además, se llevó a cabo un estudio cinético preliminar para determinar si los principales productos de la hidrogenólisis de glicerol (PDOs y 1-PO) competían por los mismos centros activos que el glicerol. Para estos experimentos, se utilizaron diferentes disoluciones acuosas formadas por el glicerol y un producto, en relación molar 1:1. En todos los casos, se produjo una inhibición de la conversión de glicerol debido a la competencia por los mismos centros activos entre los productos y el glicerol. Los PDOs mostraron una mayor competencia que el 1-PO, lo que podría explicarse por su mayor número de grupos hidroxilo. Además, la más fuerte adsorción del 1,3-PDO indicó que la adsorción de los PDOs también podría ocurrir preferencialmente a través de los hidroxilos terminales.

El mecanismo tradicionalmente propuesto de deshidratación-hidrogenación no puede explicar la alta selectividad a 1,3-PDO conseguida con este tipo de catalizadores. Para obtener un mayor conocimiento sobre el mecanismo de reacción, la hidrogenólisis de glicerol, 1,2-PDO y 1,3-PDO se llevó a cabo en atmósfera de  $\text{H}_2$  y  $\text{N}_2$ , sobre el catalizador de 9Pt8W en  $\text{Al}^{\text{com}}$  (a 220 °C y 45 bar). La sobre-hidrogenólisis de los PDOs a 1-PO fue la principal reacción involucrada en su conversión en atmósfera de  $\text{H}_2$ . Esto explicaba por qué normalmente se obtenían altas selectividades a 1-PO en la hidrogenólisis de glicerol. En atmósfera de  $\text{N}_2$ , la conversión de glicerol se redujo casi 4 veces y sólo se obtuvo 1,2-PDO, entre los PDOs. Este hecho reveló que la alta disponibilidad de  $\text{H}_2$  era necesaria para la conversión de glicerol en 1,3-PDO.

La mejor comprensión de algunos de los parámetros más importantes de la reacción condujo a la proposición de un nuevo mecanismo de reacción para la hidrogenólisis selectiva de 1,3-PDO. Se propuso que los centros ácidos de  $\text{WO}_x$  podrían estar involucrados en la primera etapa, a través del anclaje del glicerol a través de los hidroxilos primarios. Posteriormente, un protón procedente de un ácido Brønsted (proporcionado por las especies de politungstatos) podría protonar el grupo hidroxilo interno del glicerol (de mayor afinidad protónica). Tras la deshidratación, se formaría un carbocatión secundario. Éste podría estabilizarse mediante los politungstatos, lo que estaría favorecido por la más fuerte adsorción del glicerol sobre los centros de  $\text{WO}_x$  que

sobre los del soporte de  $\gamma\text{-Al}_2\text{O}_3$ . Un hidruro, procedente de la activación heterolítica del  $\text{H}_2$  molecular en los centros activos del Pt, atacaría al carbocatión secundario. Finalmente, la hidrólisis del alcóxido formado conduciría a la formación del compuesto de interés, 1,3-PDO.

## **CHAPTER 1. Introduction**





---

**Table of contents**

ABSTRACT.....	17
1.1 BIOMASS AS RENEWABLE FEEDSTOCK .....	17
1.2 THE BIOREFINERY CONCEPT .....	19
1.3 HYDROGENOLYSIS REACTIONS IN BIOMASS UPGRADING.....	22
1.4 UPGRADING OF BIOMASS-DERIVED POLYOLS .....	25
<i>1.4.1 The most interesting biomass-derived polyols as building blocks.....</i>	<i>25</i>
1.4.1.1 Sorbitol .....	25
1.4.1.2 Xylitol.....	26
1.4.1.3 Glycerol .....	27
<i>1.4.2 Hydrogenolysis of biomass-derived polyols.....</i>	<i>29</i>
1.4.2.1 Target products.....	29
1.4.2.2 Catalytic approaches.....	33
REFERENCES.....	37



## Abstract

The aim of the present Chapter is to contextualize the process selected as the object of study of the current thesis, framed in the field of green chemistry and sustainable engineering. This Chapter highlights the interest of this topic from an engineering point of view.

First, the real necessity of a progressive transition from a petroleum-based economy to a bio-based economy is presented. It does not pretend to be a critic overview of the current economy model; it just shows real facts as objectively as possible. Potential industrial processes for the transformation of biomass into interesting and marketable commodity chemicals are briefly discussed, paying particular attention to the process studied in this thesis: *the hydrogenolysis of biomass-derived polyols*.

### 1.1 Biomass as renewable feedstock

Energy availability is essential for the socioeconomic development of any society. Since XIX century fossil fuels, like coal, petroleum and natural gas, are the main energy sources of advanced societies. Undoubtedly, it would have been impossible to hold the rate of the global economic growth and reach the current standard of living of the developed countries without the production and use of these cheap and easily available energy sources.

Nowadays, petroleum is the main world energy source, representing the 33 % of the total, following by coal, 24 %, and natural gas, 30 % [1]. Fossil fuels supplied the 87 % of the world total energy consumption in 2014 [1]. Thus, accessibility and availability of fossil fuels are essential for the economy and well-being of the industrialized societies, being the cause of great magnitude international conflicts. The prospects are not very encouraging. Global energy demand is projected to grow by 37 % by 2040, as the International Energy Agency (IEA) published in the World Energy Outlook 2014 [2]. Other sources of information as the United States Energy Information Agency (EIA) point out even a higher energy demand rise of 56 % for the same period [3]. Where there is a broader consensus is in the dramatic change of the global distribution of energy demand. Most of its rise will come from emerging countries driven by their economic growth. Energy use will essentially flat in much of Europe, Japan, Korea and North America, and consumption rise will be concentrated in the rest

of non-OECD (non-Organization for Economic Cooperation and Development) countries in Asia, 65 % of total, Africa, 8 %, the Middle East 10 %, and Latin America, 8 % (see Fig. 1.1) [2].



Fig. 1.1. World primary energy demand in 2035 (in Mtoe), and share of global growth between 2012-2035 [2].

Formation of fossil fuels took millions of years and they are currently being consumed at a rate that is several orders of magnitude higher than their natural regeneration cycle [4]. Although the controversy about the expected lifetime of fossil fuels is very high, the scientific community agrees that petroleum is the resource with the shortest lifetime, it will last only another 40 years [5]. Petroleum is not only the primary feedstock for liquid fuels, as almost the 4 % of oil is worldwide used for chemicals production [6]. More than 3,000 different compounds are obtained from petroleum, which are afterwards used in fertilizers, plastics, food, pharmaceutical, chemical and textile industries, among others [7].

The large amount of chemical products obtained from these non-renewable resources further aggravates the concern for the depletion of fossil fuels. Moreover, their combustion is considered the main cause of the anthropogenic greenhouse-gases (GHG) emissions, such as carbon dioxide (CO<sub>2</sub>) and methane (CH<sub>4</sub>), and the emission of nitrogen oxides (NO<sub>x</sub>), which contributes to the global warming and climate issues [8,9].

As a consequence of the issues related to the large-scale use of fossil fuels, there is a clear need to find renewable and more sustainable alternatives to produce energy and chemical products. In this regard, biomass is the only sustainable resource of organic carbon currently available on the Earth and, therefore, it has been pointed out as the only alternative to petroleum as the main feedstock for fuels, chemicals, and carbon-based materials production [10]. Biomass constitutes an inexpensive renewable resource

highly available on a global scale, unlike the finite nature of fossil fuels, which could change the current petroleum-based economy toward a more sustainable bio-based one. This transition has multiple economic and environmental advantages: (1) the increase of the energy security by the reduction of many countries dependency on fossil fuel imports, (2) diversification of energy sources, (3) stimulation of regional and rural development, and, (4) increase the sustainability by reducing the emissions GHG, , among others.

Taking into account all of these advantages a new concept was developed: the *biorefinery*. The following section will deepen more into this new concept that will lead to a model more sustainable from an environmental, social and economic point of view.

## 1.2 The biorefinery concept

One of the most exhaustive definitions of the role of biorefinery was recently accomplished by the IEA. They defined it as “*the sustainable processing of biomass into a spectrum of marketable products and energy*” [11]. The biorefinery is an industrial facility or network of facilities that integrates a wide range of technologies for the transformation of biomass feedstocks into their building blocks (carbohydrates, triglycerides, proteins, etc.) and the simultaneous production of biofuels, energy and chemical products of high added value [12]. Biorefinery is “analogous” to the conventional oil refinery, where oil is refined into fuels and chemicals. There, the economic feasibility is partly achieved through the simultaneous production of large volumes of low-value transportation fuels along with lower volumes of more valuable chemicals and carbon-based products. These two concepts are schematically shown in Fig. 1.2.

The technology used in the petroleum refinery is mature because of the broad experience acquired during the last 50 years. Along this time, *heterogeneous catalysis* played a key role in the petroleum refining and chemical processing. Nevertheless, the reactions for conversion of biomass into chemicals typically need to be accomplished in liquid phase, where the solvent is commonly water, rather than the gas phase used for petrochemicals [13]. This fact together with the totally oppose chemical nature of the feedstocks, biomass and petroleum, generated that the catalytic approaches and processing strategies developed for petroleum refinery are not directly applicable in biorefinery. While the catalysts for the conversion of petroleum into chemicals are

focused on selectively functionalize hydrocarbons, the biomass is already highly functionalized and, therefore, the catalysts required should be able to selectively remove some of the functionalities [13,14]. The different processing strategies to obtain chemical products from petroleum and biomass are represented in Fig. 1.3. For these reasons new catalysts and processes are needed for converting biomass into fuels and chemical products.

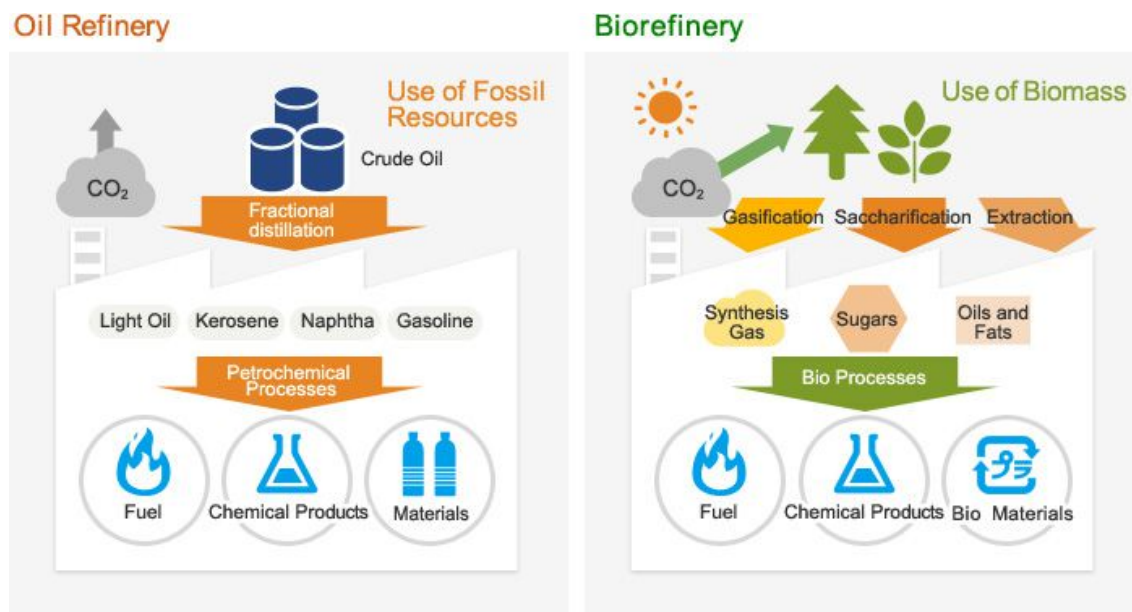


Fig. 1.2. Conventional oil refinery vs. the biorefinery concept [15].

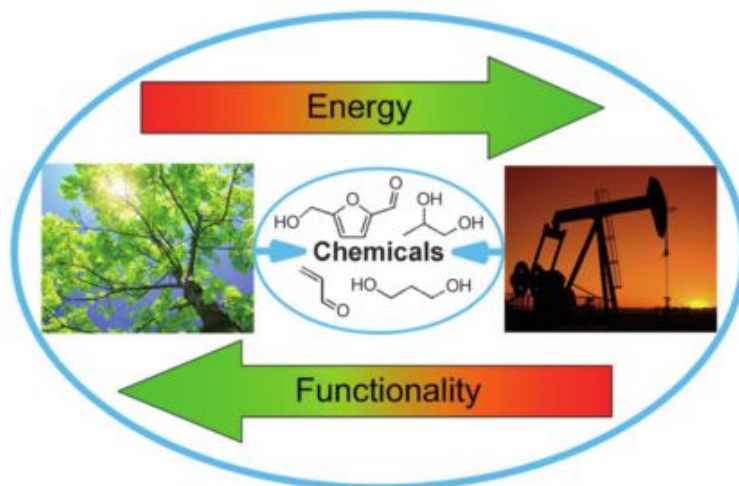


Fig. 1.3. Opposed strategies for chemicals production: de-functionalizing of biomass and functionalizing of petroleum [14].

Biorefinery feedstocks are very diverse. It can be used all kind of biomass including wood and agricultural crops, organic residues (derived from plants and animals, and industrial and municipal wastes) and aquatic biomass, among others.

Nevertheless, the sustainability of the use of biomass is frequently questioned. There is an increasing concern about the use of edible biomass for energy and chemicals production and about the use of extensive lands for energy crops, with the related concerns of loss of biodiversity and land deforestation [16]. However, it is essential to differentiate between the first and second generation technologies. The first ones were developed for the conversion of edible biomass into fuels (so-called *first generation* bio-fuels). Some of the most relevant examples are the use of sugar cane and wheat for the production of ethanol through fermentation of sugars and starches, and the transesterification of vegetable oils, such as palm oil and rapeseed, into biodiesel. By contrast, *second generation* technologies are focused on the conversion of lignocellulosic biomass, such as straw, stover and wood. Lignocellulosic biomass is a non-edible material and, therefore, does not compete with food and feed crops [17]. Thus, the use of lignocellulosic biomass is attracting growing attention as a real sustainable and renewable source.

Lignocellulosic biomass mainly consists of three fractions: cellulose (40-50 %), hemi-cellulose (25-35 %) and lignin (15-20 %) [18,19]. In particular, the conversion of the carbohydrate fraction of lignocellulose (cellulose and hemicellulose) into platform chemicals is of great interest. Fig. 1.4 shows the composition of lignocellulose and the main platform chemicals derived from each fraction.

Commonly, the biomass feedstocks and its derived platform chemicals have a higher O/C ratio than most of the commodity chemicals or fuels. Thus, they required to be deoxygenated [20]. In principle, this deoxygenation can be achieved via C–O bond hydrogenolysis, dehydration, decarbonylation and decarboxylation reactions [21]. Among them, C–O bond hydrogenolysis is of particular significance in the production of high value chemicals [22].

The aim of the next section is to prove the key role of hydrogenolysis reactions in the valorization of some of the most important platform chemicals and building blocks derived from biomass. To that end some relevant examples will be shown.



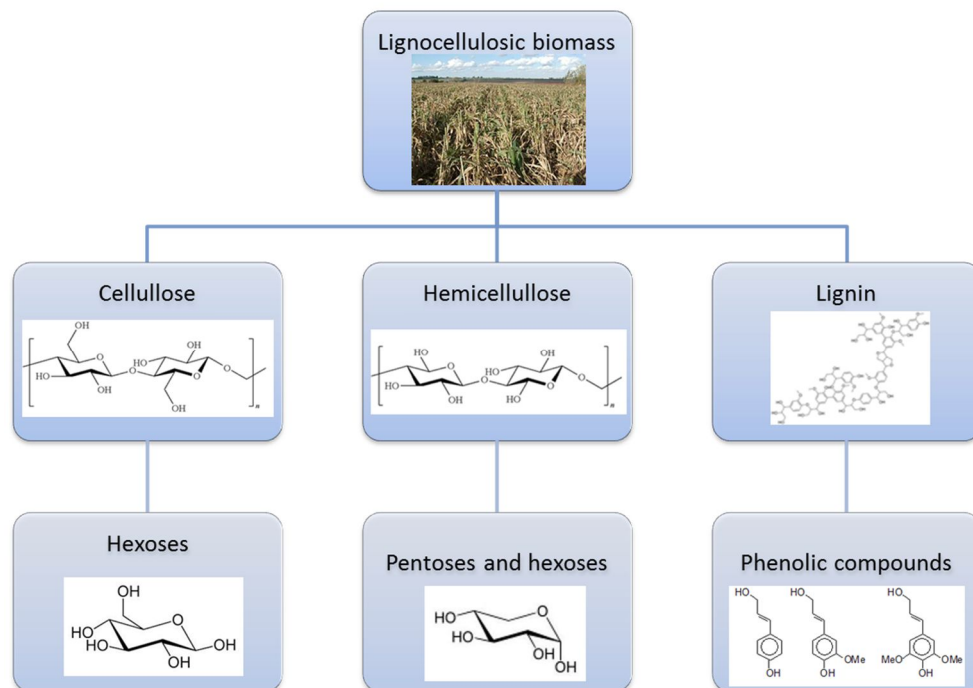


Fig. 1.4. Composition of lignocellulosic biomass and the main platform chemicals obtained.

### 1.3 Hydrogenolysis reactions in biomass upgrading

Hydrogenolysis is defined as a type of reduction that involves a chemical bond dissociation in an organic substrate and the simultaneous addition of hydrogen to the resulting molecular fragments [23]. In general, C–O bond hydrogenolysis is not an easy reaction to achieve. This bond has high activation energy, above most other C–X single bonds (only C–H and C–F bonds are higher) [22]. This makes the C–O bond inert to many reagents and catalysts. The use of heterogeneous catalysts is preferred over the homogeneous ones mainly because it simplifies the separation and reuse of the catalyst after the reaction. Thus, the development of heterogeneous catalysts which show high activity towards C–O bond scission is necessary but also very challenging.

An example of C–O hydrogenolysis is found in the hydrotreating of vegetable oils to liquid alkanes suitable for diesel and jet fuel applications. The vegetable oils, composed of triglycerides (TGs), are deoxygenated using high hydrogen pressures (50–100 bar) and relatively high temperatures (300–400 °C) in the presence of supported metal catalysts [24]. As it is shown in Fig. 1.5, TGs first undergo hydrogenolysis of the C–O bonds forming the free fatty acids along with a molecule of propane [25]. Free fatty acids can undergo oxygen removal by other different pathways: (i) repetitive cycles of hydrogenation-dehydration, hydrodeoxygenation (HDO) to yield n-alkanes

with the same number of carbon atoms as those of the starting free fatty acids and; (ii) decarbonylation/decarboxylation (HDC) that produces a linear alkane with  $n-1$  carbon atoms, releasing  $\text{CO}_x$  molecules [4]. Finally,  $n$ -alkanes are converted into branched hydrocarbons, valuable for green bio-oils, by hydroisomerization reactions, avoiding the undesired chain cracking.

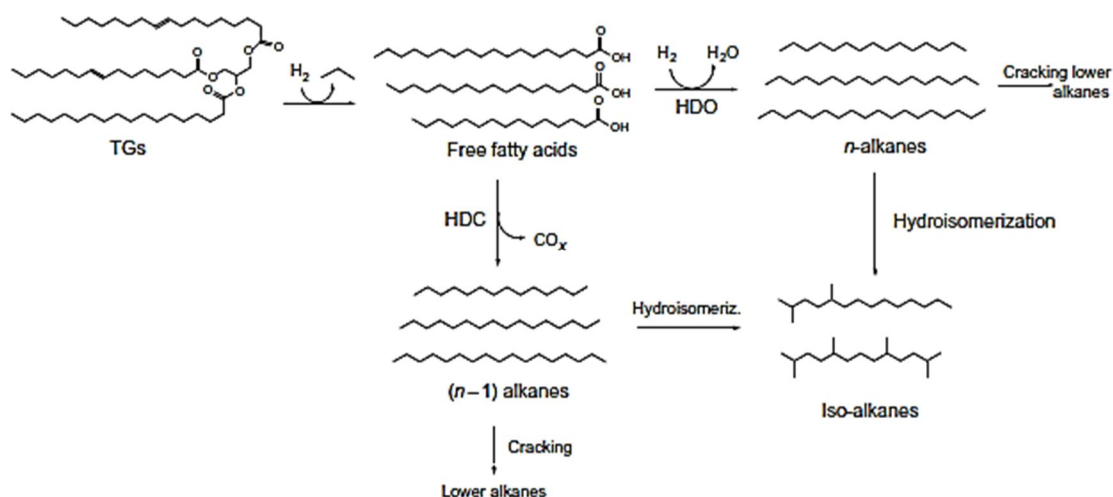


Fig. 1.5. Scheme of the hydrotreating of TGs to green jet fuel and diesel hydrocarbons [4].

The C–O hydrogenolysis is also the main reaction in the transformation of cellulose-derived materials obtained through hydrolysis, such as sorbitol, glucose, and cellobiose, into  $n$ -hexane. For instance, when converting sorbitol into  $n$ -hexane there are six C–O bonds to be cleavage. Huber et al. have intensively investigated this transformation by using different platinum-based catalysts [26–29] obtaining a maximum yield of 70 % into  $n$ -hexane. Recently, Tomishige's group conducted the same reaction over the  $\text{Ir-ReO}_x/\text{SiO}_2$  catalyst combined with the zeolite HZSM-5 as co-catalyst in a biphasic reaction system ( $n$ -dodecane +  $\text{H}_2\text{O}$ ) under mild conditions, obtaining a good yield of 95 % [30]. Furthermore, they attained good results using cellobiose and glucose as starting materials. The direct production of  $n$ -hexane from cellulose has a greater interest. Using the same catalytic system, this group was the first one to achieve the conversion of cellulose into  $n$ -hexane in one-pot obtaining very high yields of 78–83 % [31], from ball-milled cellulose and microcrystalline cellulose, respectively. This transformation consists on the hydrolysis of cellulose to glucose via water-soluble oligosaccharides, hydrogenation of glucose to sorbitol, and successive hydrogenolysis of sorbitol to  $n$ -hexane (Fig. 1.6).

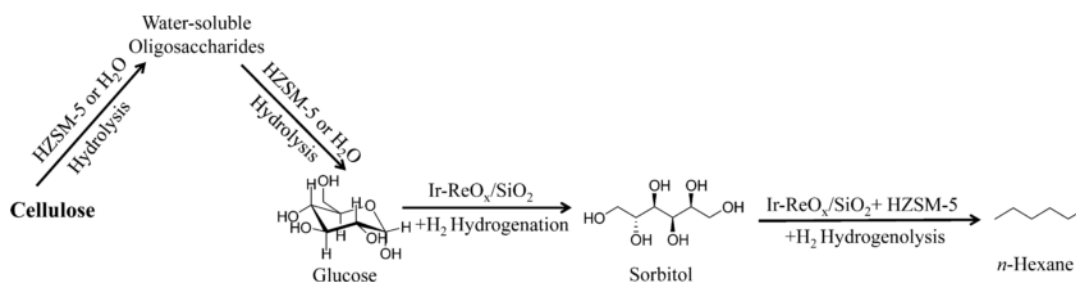


Fig. 1.6. Scheme of the conversion of cellulose into n-hexane [31].

The C–O bond hydrogenolysis plays also a relevant role in the upgrading of some biomass-based building blocks. This is the case of furfural, which is mainly obtained from the dehydration of xylose obtained from the hemicellulose fraction of biomass. Furfural by itself has no value as fuel due to its tendency to polymerize. However, it can be upgraded to 2-methylfuran and polyols, such as 1,5-pentanediol (1,5-PeD) and 1,2-pentanediol (1,2-PeD), which are key building blocks for the production of green fuels and chemicals [23,32,33].

The process is shown in Fig. 1.7 and involves hydrogenation and hydrogenolysis steps. Hydrogenation of furfural can give furfuryl alcohol (FFA) and tetrahydrofurfuryl alcohol (THFA). Hydrogenolysis can also proceed by the reaction of furfural with hydrogen, which can produce 2-methylfuran (2-MF), 2-methyltetrahydrofuran (2-MTHF), cyclopentanone or the polyols 1,5-PeD and 1,2-PeD, which can be used as monomers of polyesters and polyurethanes.

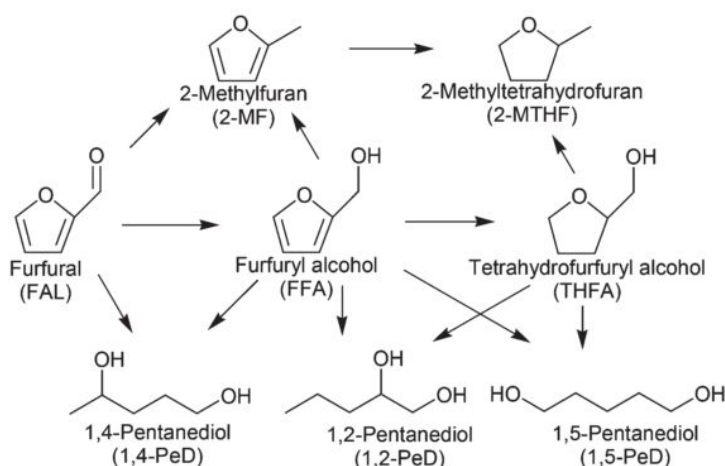


Fig. 1.7. Reaction pathway for furfural conversion to 2-methylfuran and other marketable products [33].

In 2004, the US Department of Energy (DOE) released a publication where 10 target molecules that could be produced from biomass-derived carbohydrates were

described [34]. A new report presents an updated target chemicals based on industrial and scientific advances since 2004 to 2010 [35]. These targets were selected taking into account some different criteria: economics, industrial viability, size of markets, and the ability of the compounds to serve as platform chemicals for the production of derivatives, chemicals and fuels.

Interestingly, among the 13 most important molecules identified as potential building blocks for the production of more interesting chemicals, three were biomass polyols: *sorbitol*, *xylitol* and *glycerol*.

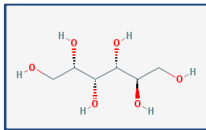
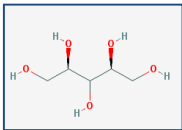
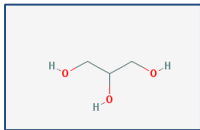
On account of this, the thesis focuses on the valorisation of biomass-derived polyols through hydrogenolysis reactions and it will be discussed in more detail in the following section.

## 1.4 Upgrading of biomass-derived polyols

### 1.4.1 The most interesting biomass-derived polyols as building blocks

The most significant chemical and physical characteristics of sorbitol, xylitol and glycerol are summarized in Table 1.1 in order to facilitate the reading of the next section.

**Table 1.1.** Physicochemical properties of the most interesting biomass-derived polyols as platform chemicals: sorbitol, xylitol and glycerol.

	Sorbitol	Xylitol	Glycerol
<b>Physicochemical properties</b>			
Chemical Formula	C <sub>6</sub> H <sub>14</sub> O <sub>6</sub>	C <sub>5</sub> H <sub>12</sub> O <sub>5</sub>	C <sub>3</sub> H <sub>8</sub> O <sub>3</sub>
Molecular mass (g mol <sup>-1</sup> )	182.17176	152.14578	92.09382
Density (g cm <sup>-3</sup> at 20°C)	1.4890	1.5200	1.2613
Viscosity (cPo at 20°C)	110	300	954
Boiling point (°C)	295	216	290
Melting point (°C)	111	93	18

#### 1.4.1.1 Sorbitol

Sorbitol is a polyol with 6 carbon atoms and an O/C ratio of 1. It is industrially obtained from the catalytic hydrogenation of glucose (from corn, beet or sugar cane)

that possesses a great availability and low cost. On industrial scale, Raney Ni is the catalysts most frequently used in the process.

On the other hand, important attempts are being made for the direct catalytic conversion of cellulose biomass fraction into sorbitol which could imply a significant advance in the biorefinery. This reaction is a two-step process, which includes the hydrolysis of cellulose to glucose and subsequent hydrogenation to the sugar alcohol, sorbitol or mannitol (Fig. 1.8) [36].

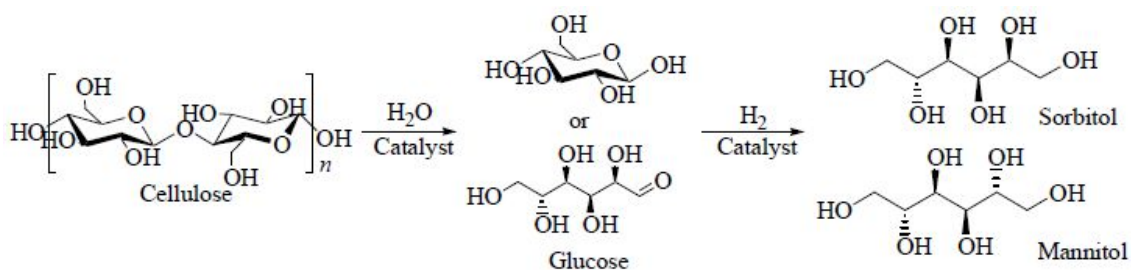


Fig. 1.8. Catalytic conversion of cellulose into sugar alcohols sorbitol and mannitol [36].

For instance, Fukuoka et al. [37] reported 31% yield of sugar alcohols (25 % sorbitol and 6 % to mannitol) in 24 h at 190 °C and 5 MPa H<sub>2</sub> using a Pt/Al<sub>2</sub>O<sub>3</sub> catalysts, and, more recently Sels et al. [38] developed a novel catalyst using carbon nanofibers grown on Ni/γ-Al<sub>2</sub>O<sub>3</sub>, which gave a 50 % sorbitol yield and a 6 % mannitol yield in only 4 h, under 230 °C and 6 MPa H<sub>2</sub>.

The sweetness and low caloric value of sorbitol make it the preferred ingredient in sugar-free products. It is also widely used as pharmaceutical excipient and as humectant and skin conditioning agent in cosmetics and personal care products. Regarding the applications of sorbitol as building block, it should be pointed out the dehydration to isosorbide and anhydrosugars, the hydrogenolysis to glycerol, 1,2-propanediol (1,2-PDO), ethylene-glycol (EG) and lactic acid, and the direct polymerization into branched polysaccharides. These transformations are summarized in Fig. 1.9, in which the circled derivatives are those in commercial use and produced in commodity-scale volume today.

#### 1.4.1.2 Xylitol

Xylitol is a polyol of 5 carbon atoms and an O/C ratio of 1. The catalytic hydrogenation of xylose with hydrogen in a three-phase slurry batch reactor over Raney Ni catalysts [39–41], is the current commercial route of xylitol production. This catalyst, the same used in the sorbitol production from glucose, is usually the preferred

because of its low price and its ease use as a suspended slurry in batch reactions [42]. Nevertheless, its major drawback is the relatively fast deactivation due to accumulation of organic impurities (from the starting material) on the catalyst surface, leading to poisoning of the active sites, and the metal leaching [43–45].

In this particular case the starting material, xylose, is firstly obtained from the hydrolysis and reduction of hemicellulose using e.g. corn cobs or sugar cane [46].

Xylitol is widely used as diabetic sweetener in food and beverage, as freshener in throat drugs and cough syrup to refresh the throat, as humectant in cosmetics, etc. However, recent interest has been devoted in the conversion of xylitol to other chemicals. Some of the main transformations are the oxidation to xylaric and xylonic acid and the hydrogenolysis to glycerol, 1,2-PDO, EG and lactic acid [34]. These and other transformation possibilities are summarized in Fig. 1.9.

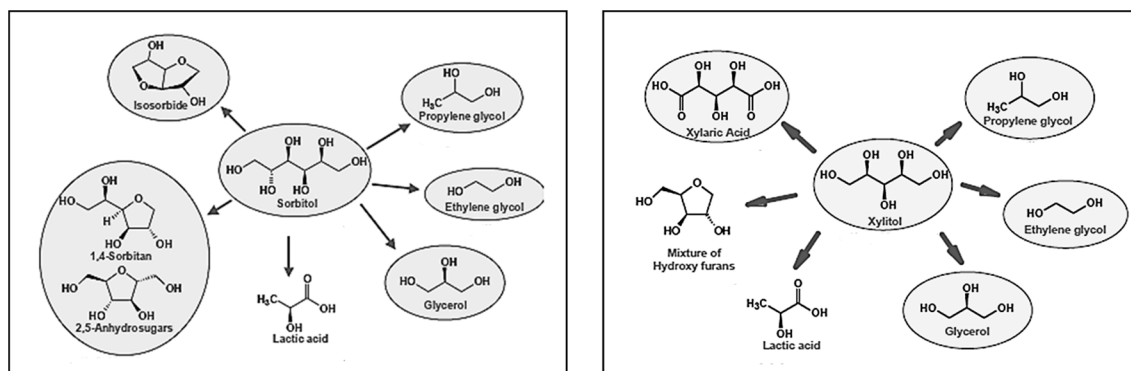


Fig. 1.9. Some of the most important derivatives from sorbitol (left) and xylitol (right).

### 1.4.1.3 Glycerol

Glycerol is the smallest polyol readily available from biomass (3 carbon atoms and an O/C ratio of 1). Until 40's decade the synthesis of glycerol was made from propylene-derived epichlorohydrin, and therefore from fossil fuels. However, nowadays this synthesis route is no longer profitable on a large scale because glycerol is highly and economically available as a by-product of biodiesel production through the transesterification of vegetable oils. The process has even turn around and companies like Dow Chemical and Solvay already possess industrial plants for the production of epichlorohydrin from glycerol [47].

As a consequence of the high demand of green biofuels, the biodiesel sector has been steadily expanding in recent years and a huge quantity of raw glycerol has been placed in the market.

Through the industrial manufacture of biodiesel, by transesterification of animal fats or vegetable oils (both composed of triglycerides) with an alcohol (commonly, methanol or ethanol), for every 10 kg of methyl esters (biodiesel) produced 1 kg of crude glycerol is obtained [48–50]. Fig. 1.10 shows the overall reaction.

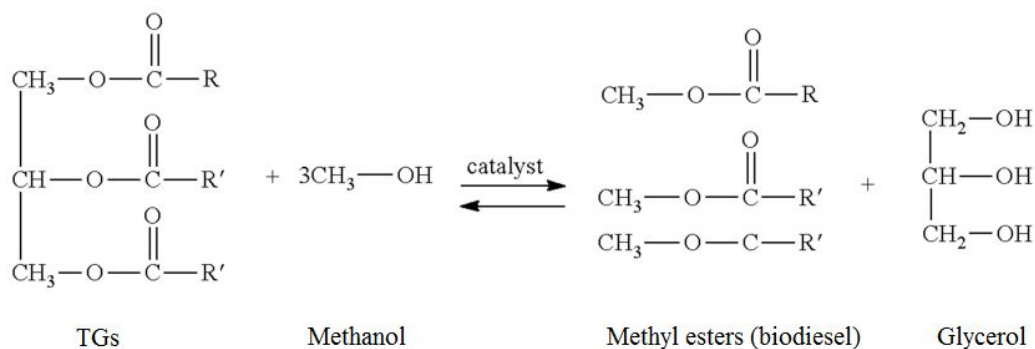


**Fig. 1.10.** Transesterification of triglycerides to methyl esters (biodiesel) and glycerol with methanol [51].

However, the glycerol demand has remained almost unchanged. This combined effect has caused an oversaturation of the traditional glycerol market, which includes the manufacture of cosmetics, soaps, excipient for drugs and food additives, synthesis of alkyl resins, polyurethanes and trinitroglycerine, among others.

Moreover, the raw glycerol obtained in the process must be refined through expensive separation processes to remove impurities (fatty acids, alcohol, and catalyst) like filtration, chemical additions, and fractional vacuum distillation. This refining process is economically unfeasible for small and medium scale plants. Therefore, raw glycerol is nowadays a key problem in biodiesel production and its low sale price has turned this by-product into a residue.

In recent years, several factors, the worldwide economic crisis among others, have slowed down biodiesel production. The best solution to increase the profitability of the biodiesel would be to use glycerol as building block to obtain useful and high added value commodity chemicals.

From a technical point of view and, despite its limited size, the multifunctional structure of glycerol can be used to obtain a wide range of products. In Fig. 1.11 the main applications and transformations of glycerol are summarized.

In spite of the multiple transformations of sorbitol, xylitol and glycerol shown previously, the following section will focus more deeply on the hydrogenolysis reaction of these polyols and the main target products obtained.

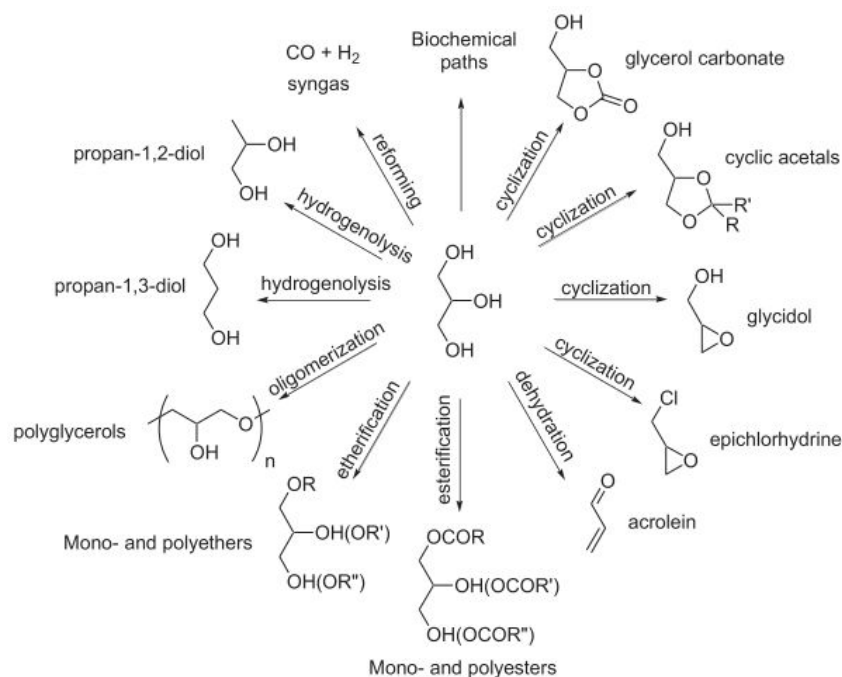


Fig. 1.11. Some of the possible transformations of glycerol [52].

## 1.4.2 Hydrogenolysis of biomass-derived polyols

As it was discussed in the previous section, the hydrogenation of sugars, mainly glucose and xylose, gives rise the respective sugar alcohols, sorbitol and xylitol, at relatively mild conditions and using solid metal catalysts. Through the C–C and C–O hydrogenolysis reactions and under more severe conditions, the sugar alcohols can yield more marketable lower molecular-weight polyols. Among all the possibilities, these are the three most interesting products that can be obtained from this route: **EG**, **1,2-PDO** and **glycerol**. As the traditional market of glycerol is oversaturated, its conversion into EG but more specially into 1,2-PDO and **1,3-PDO** through hydrogenolysis reactions has a higher interest from an industrial point of view.

Below, some relevant information about the main target products of the hydrogenolysis of biomass-derived polyols is shown, as well as the latest catalytic advances in their conversion.

### 1.4.2.1 Target products

*EG*, the simplest diol, is formed by two hydroxyl groups at adjacent positions along the hydrocarbon chain ( $C_2H_6O_2$ ). It is a colourless, odourless and hygroscopic liquid with low viscosity. It is completely miscible with many polar solvents and only slightly soluble in non-polar solvents [53–56]. EG has a low toxicity but produces toxic



metabolites [57] and causes toxicity via several routes, such as ingestion, absorption by skin, and inhalation exposure [57,58].

Traditionally, the industrial route to produce EG has been the hydration of ethylene oxide [59,60]. More recently, synthesis of EG from syngas, mainly obtained from fossil fuels (coal and natural gas) has attracted a great deal of attention. This route is based on the oxidative coupling of CO to form dimethyl oxalate (DMO). The hydrogenation of DMO yields EG.

In spite of its toxicity EG is considered an important commodity chemical and underpins almost every aspect of everyday life. It is used as an antifreeze and coolant in automobiles, as a de-icing fluid for windshields and aircraft, a desiccant for natural gas production, and a precursor for manufacture of polyester fibers and resins [61,62]. In addition, lots of efforts have been devoted to convert EG to hydrogen and chemicals by reforming reactions [63,64]. The global market of EG was estimated in about 20 million metric tonnes in 2010, which was projected to increase 5-10 % per year [56]. It is also noteworthy that the global market demand of EG usually surpasses its production capacity [56].

*1,2-PDO*, more commonly known as propylene glycol, is an alcohol with both a primary and a secondary hydroxy groups with the chemical formula  $C_3H_8O_2$ . It is an oily, colourless, highly hygroscopic organic compound. It is odourless, tasteless and totally soluble in water, chloroform and acetone, among others. It has low toxicity and high stability.

Currently, all commercial production of 1,2-PDO is via the hydrolysis of propylene oxide, obtained from petroleum [65]. Nevertheless, this process presents two principal drawbacks: (i) the two commercial processes to obtain propylene oxide are highly pollutant, using the chlorohydrin or the epoxidation routes [65], and (ii) the resulting reaction mixture, composed of mono-, di- and tri-glycols, requires expensive purification steps through distillation.

The more common commercial names of manufactured 1,2-PDO are Propylene Glycol Industrial (PGI), which designates the grade for general industrial applications, and Propylene Glycol USP/EP (PG USP/EP). This last one meets the requirements of Europe and USA for drugs and can also be used in food, drinks, personal care applications and cosmetics. Among industrial applications, 1,2-PDO is used as an intermediate for the manufacture of other chemicals, especially unsaturated polyester resins and in the manufacture of plastics, paints and coatings (Fig. 1.12). It also plays an

important role as a functional fluid and as a constituent in liquid detergents. Currently, the PGI is replacing EG as antifreeze, especially in food industry applications where it is not possible to use EG due to its high toxicity [50]. According to Dow Chemical, the principal world manufacturer of 1,2-PDO, the global production volume of 1,2-PDO exceeded 2 million tonnes in 2010 [66] and the overall market is expected to grow by nearly 4 % per year in the upcoming years [67].

In spite of the traditional technologies for the production of this polyol are optimized and well established, the growing environmental concerns encourage major industry participants to develop some alternative routes from biomass. Entering this attractive market will not only give them an advantage but will also help them to achieve sustainability in the near future. In this way some of the major companies saw opportunities in the sustainable 1,2-PDO market including Archer Daniels Midland (ADM), Ashland and Cargill. ADM has been successfully producing biomass-derived 1,2-PDO in its Illinois plant since 2011, with a capacity of 100 kilo tonnes per year [68]. They convert bio-glycerol, obtained as by-product in biodiesel manufacture, to industrial PGI through C–O hydrogenolysis reactions using high temperature and pressure conditions. Bio-based 1,2-PDO has proved to reduce between 70-80 % of the GHG emissions as compared with the one obtained from petroleum.

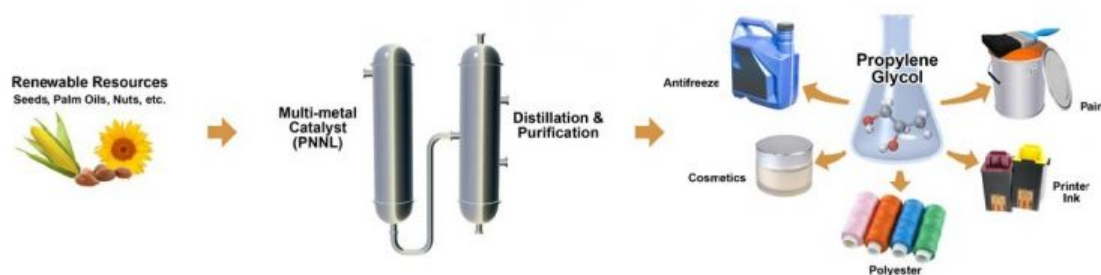


**Fig. 1.12.** Schematic representation of the production of 1,2-PDO from renewable resources and its main industrial applications.

Regarding *1,3-PDO*, it is a linear three-carbon compound with the same chemical formula as 1,2-PDO ( $C_3H_8O_2$ ). They differ each other in that 1,3-PDO has two primary hydroxyl groups. It is also a colourless and odourless compound miscible in water. Moreover, it is a non-toxic and biodegradable organic compound.

The traditional synthesis of 1,3-PDO has been carried out from petroleum, mainly through two routes: hydrolysis of acrolein (Degussa-DuPont process) and the hydroformylation of ethylene oxide (Shell process). However, both routes present a

significant number of drawbacks: (i) expensive facilities are necessary, (ii) the reactions require intermediate steps, (iii) toxic reagents are handled, and, (iv) the yields achieved are not very high (< 43%) [50].

The main use of 1,3-PDO is as a monomer together with terephthalic acid (TPA) in the manufacture of polytrimethylene terephthalate (PTT) polymers, used in turn for the manufacture of fibers and resins. This application represents the 90 % of the use of 1,3-PDO. The remaining 10 % is used as conventional functional fluid in cosmetics, personal care and cleaning products. PTT qualities have been known since 1940, but the high production costs have hindered their entry into market. Nowadays, its market is expected to be 0.1 million tonnes per year [50] and is projected to rise steeply in the coming years.

Due to its commercial interest, some more sustainable production alternatives have been developed. A clear example is the DuPont Tate & Lyle Bioproducts whose bio-based 1,3-PDO is manufactured from renewable raw materials and marketed under the commercial names Susterra® and Zemea®. These products are obtained by a new recently commercialized biological process of fermentation of D-glucose obtained from corn. Once the basic raw material, 1,3-PDO, is obtained the production of PTT polymers is conducted by a copolymerization reaction with pure terephthalic acid. Shell, for its part, has developed the Corterra® polymer and DuPont the Sorona® and Hytrel [69] polymers by this route. Fig. 1.13 shows a scheme of the Sorona® polymer production and its end use in the textile sector.

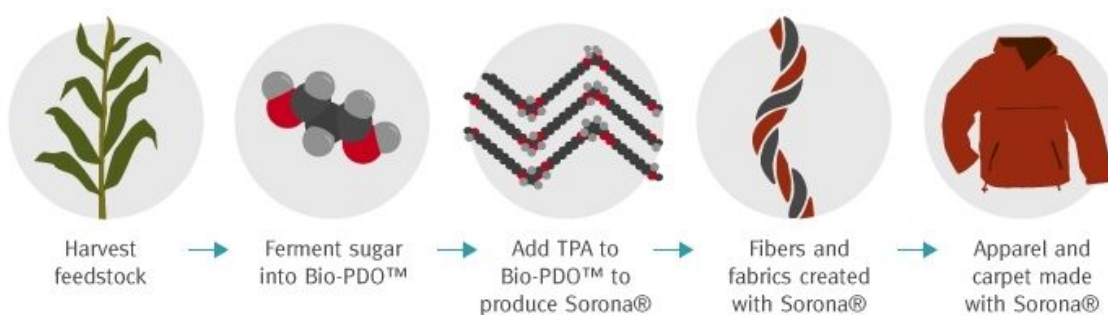


Fig. 1.13. Infographic of the Sorona® polymer production and its use.

It is worth pointing out that biological pathways utilize enzymes to make the desired chemical transformations, typically obtaining very high selectivity. These processes are often kinetically and thermodynamically efficient. Nevertheless, these advantages are usually tempered by the need to “feed” the transforming organism,

which inevitably has a negative impact in the achievable theoretical yield and overall energy and mass balance of the process. Moreover, the reaction product must be isolated from a chemically very complex fermenter broth, which can be very challenging and energy intensive. Another intrinsic challenge to large scale, and especially in batch reactors, is that this kind of process is often self-limiting due to the accumulation of the reaction product which is typically toxic to the transforming organism above a certain concentration [46]. On the contrary, catalytic processes do not suffer from this limitation but may require energy intensive high temperature and pressure reaction conditions.

The importance and increasing demand for these polyols, PDOs and EG, suggest a new possibility for their direct production from the hydrogenolysis of the polyols readily available from lignocellulosic biomass: sorbitol, xylitol and glycerol. In the following section, a brief review of the recent and most important catalytic approaches to these transformations will be summarized.

#### 1.4.2.2 Catalytic approaches

Generally, the major challenge for the hydrogenolysis of biomass-derived polyols into target products is the need to develop active and selective catalysts. In the following Table 1.2 some of the main requirements of the catalysts and the current major technical barriers for the transformation are summarized.

**Table 1.2.** Summary of the main catalytic requirements and technical barriers of the hydrogenolysis of biomass-derived polyols.

Building block	Target product	Catalyst requirements	Technical barriers
Sorbitol	EG, 1,2-PDO	C–C and C–O bonds specificity	Low yields to target products
Xylitol	EG, 1,2-PDO	C–C and C–O bonds specificity	Find low cost xylose stream
Glycerol	1,2-PDO	Selective for primary C–O bond	Tolerance to catalyst poisons
	1,3-PDO	Selective for secondary C–O bond	Low yield, expensive noble metal catalysts and tolerance to catalyst poisons

The hydrogenolysis of sorbitol and xylitol to lower polyols, EG and 1,2-PDO, requires the use of catalysts active and selective towards the specific C–C and C–O bond cleavage. Fig. 1.14 shows the different product distribution of sorbitol

hydrogenolysis according to the C–C bond cleavage and clearly exemplifies the difficulty of obtaining high selectivities towards the target products.

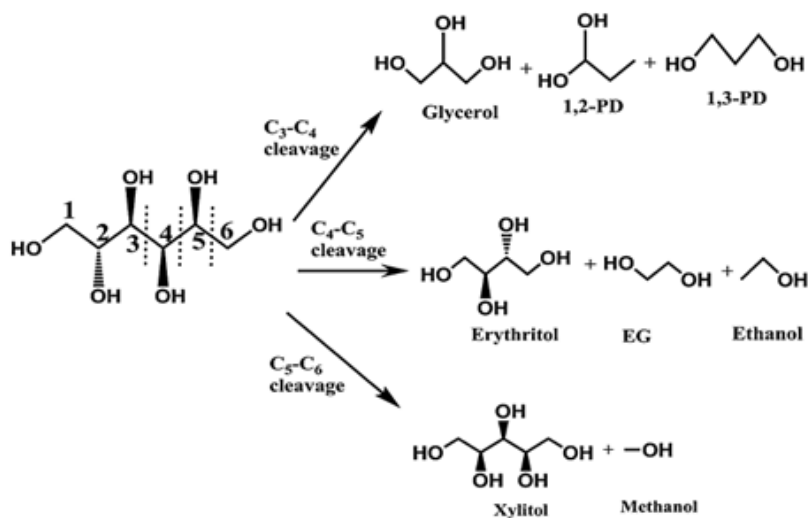


Fig. 1.14. Scheme of sorbitol hydrogenolysis products according to the C–C bond cleavage.

Ni and Ru metals have commonly been employed in the hydrogenolysis of sorbitol and xylitol due to its high C–C breaking ability. They show comparable selectivities towards the two EG and 1,2-PDO [70]. Although Ni-based catalysts usually require harsher reaction conditions (higher reaction temperatures or H<sub>2</sub> pressures), they have recently attracted great attention in polyols hydrogenolysis [71–73] because of their lower price in comparison with the noble metal catalysts.

One of the latest and best approaches in the catalytic hydrogenolysis of sorbitol and xylitol has been the use of a metal catalyst and a basic promoter, which has proved a positive influence on the C–C scission [71].

Banu et al. [74] reported the best results in sorbitol hydrogenolysis to 1,2-PDO (51.8 % yield) and EG (5.2 %) using Ni/NaY catalyst combined with Ca(OH)<sub>2</sub> basic promoter, under the experimental conditions employed (220 °C, 60 bar of H<sub>2</sub>, 6 h of reaction time). However, from the viewpoint of industrial practice the selectivities towards the two glycols are still low.

Recently, Soták et al. [75] reported yields of target glycols (EG and 1,2-PDO) of 71 % for the hydrogenolysis of xylitol at 200 °C and 40 bar of H<sub>2</sub> in only 45 min of reaction time using Ni<sub>2</sub>P/AC catalyst and Ba(OH)<sub>2</sub>·8H<sub>2</sub>O as a basic promoter. However, the main technical barrier for the hydrogenolysis of xylitol is finding a low cost xylose sugar stream [34] as starting material.

One interesting process that could potentially afford a low cost route to glycols may be the hydrogenolysis of mixed sugars that include xylose, arabinose and glucose into 1,2-PDO as the primary product and EG as the secondary product [34].

Concerning the mechanism, it has been proposed that hydrogenolysis of sorbitol and xylitol involves the following key steps: (i) dehydrogenation of polyols to the corresponding aldoses and ketoses on metal sites, (ii) the subsequent C–C bond cleavage via the retro-aldol condensation, which is favored in basic medium, to form glycolaldehyde and glyceraldehyde and, (iii) the hydrogenation of the latter to the selective formation of EG and 1,2-PDO [14,70,76,77]. Xylitol hydrogenolysis is schematized in Fig. 1.15 as example.

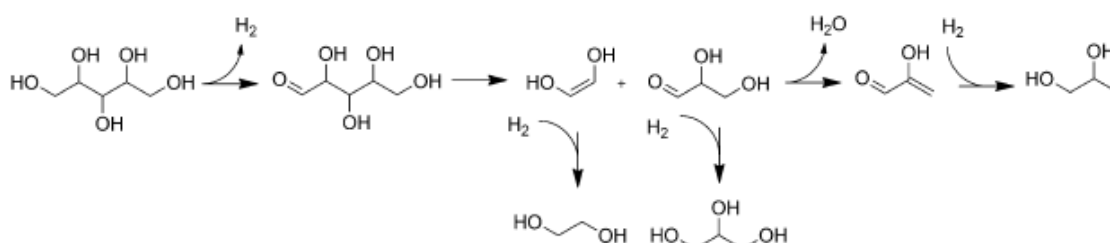


Fig. 1.15. Xylitol hydrogenolysis under alkaline conditions [14].

On the other hand, Zhao et al. [78] suggested another plausible 1,2-PDO formation route through the hydrogenolysis of the glycerol obtained from sorbitol and xylitol.

It is necessary to point out that the production of 1,3-PDO through hydrogenolysis of sorbitol and xylitol has been extremely low or inexistent, up to now. However, its production from glycerol has drawn a great deal of attention in the latest years. The interesting use of 1,3-PDO in the manufacture of PTT polymers makes it even a more valuable chemical target product than other glycols. Thus, the glycerol hydrogenolysis to PDOs, especially 1,3-PDO, is presented as an attractive prospect.

Glycerol conversion into 1,2-PDO and 1,3-PDO requires the development and use of catalysts highly selective towards the primary or secondary C–O bond scission, respectively. Interestingly, since glycerol is structurally analogous to sorbitol and xylitol, all the transformations appropriate to glycerol may be applied to these similar longer chain linear polyols, greatly increasing the diversity of the biorefinery. In the following Chapter 2, a deep analysis of the key parameters involved in the glycerol

hydrogenolysis to PDOs is given, focussing on the latest approaches in the catalyst development and reaction mechanism understanding.

## References

- [1] British Petroleum, BP Statistical Review of World Energy, London (United Kingdom), 2013. [bp.com/statisticalreview](http://bp.com/statisticalreview).
- [2] World Energy Outlook. Executive Summary, Paris (France), 2014. <http://www.iea.org>.
- [3] International Energy Outlook 2013, Washington (U.S.A.), 2013. <http://www.eia.gov/ieo>.
- [4] J.C. Serrano-Ruiz, R. Luque, J.H. Clark, The Role of Heterogeneous Catalysis in the Biorefinery of the Future, in: K. Triantafyllidis, A. Lappas, M. Stöcker (Eds.), *Role Catal. Sustain. Prod. Bio-Fuels Bio-Chemicals*, Elsevier B.V., 2013: pp. 557–576.
- [5] D.A. Simonetti, J. Rass-Hansen, E.L. Kunkes, R.R. Soares, J.A. Dumesic, Coupling of glycerol processing with Fischer-Tropsch synthesis for production of liquid fuels, *Green Chem.* 9 (2007) 1073–1083.
- [6] F. Cherubini, The biorefinery concept: Using biomass instead of oil for producing energy and chemicals, *Energy Convers. Manag.* 51 (2010) 1412–1421.
- [7] M.B. Hocking, *Handbook of Chemical Technology and Pollution Control*, 3rd ed., Elsevier, 2005.
- [8] United States Environmental Protection Agency, (2015). <http://www.epa.gov/climatechange/ghgemissions/global.html>.
- [9] Mitigation of climate change: Contribution of working group III to the fourth assessment report of the Intergovernmental Panel on Climate Change, Cambridge (United Kingdom), 2007.
- [10] A.J. Ragauskas, C.K. Williams, B.H. Davison, G. Britovsek, J. Cairney, C.A. Eckert, et al., The Path Forward for Biofuels and Biomaterials, *Science* (80-. ). 311 (2006) 484–489.
- [11] Biorefineries: adding value to the sustainable utilisation of biomass, Oxford (United Kingdom), 2009. [www.ieabioenergy.com](http://www.ieabioenergy.com).
- [12] A.R. Morais, R. Bogel-Lukasik, Green chemistry and the biorefinery concept, *Sustain. Chem. Process.* 1 (2013) 18.
- [13] B.H. Shanks, Conversion of biorenewable feedstocks: New challenges in heterogeneous catalysis, *Ind. Eng. Chem. Res.* 49 (2010) 10212–10217.
- [14] J. Tendam, U. Hanefeld, Renewable chemicals: Dehydroxylation of glycerol and polyols, *ChemSusChem.* 4 (2011) 1017–1034.
- [15] Nippon Paper Group, <http://www.nipponpapergroup.com/english/research/organize/biomass.html>.
- [16] S. V. Vassilev, C.G. Vassileva, V.S. Vassilev, Advantages and disadvantages of composition and properties of biomass in comparison with coal: An overview, *Fuel.* 158 (2015) 330–350.
- [17] S. Nanda, R. Azargohar, A.K. Dalai, J. a. Kozinski, An assessment on the sustainability of lignocellulosic biomass for biorefining, *Renew. Sustain. Energy Rev.* 50 (2015) 925–941.
- [18] O. Bobleter, Hydrothermal degradation of polymers derived from plants, *Prog. Polym. Sci.* 19 (1994) 797–841.
- [19] G. Dautzenberg, M. Gerhardt, B. Kamm, Bio based fuels and fuel additives from lignocellulose feedstock via the production of levulinic acid and furfural, *Holzforschung.* 65 (2011) 439–451.



- [20] J.P.M. Sanders, J.H. Clark, G.J. Harmsen, H.J. Heeres, J.J. Heijnen, S.R. a Kersten, et al., Process intensification in the future production of base chemicals from biomass, *Chem. Eng. Process. Process Intensif.* 51 (2012) 117–136.
- [21] F. Dong, Y. Zhu, H. Zheng, Y. Zhu, X. Li, Y. Li, Cr-free Cu-catalysts for the selective hydrogenation of biomass-derived furfural to 2-methylfuran: The synergistic effect of metal and acid sites, *J. Mol. Catal. A Chem.* 398 (2015) 140–148.
- [22] H.Y. Zheng, Y.L. Zhu, B.T. Teng, Z.Q. Bai, C.H. Zhang, H.W. Xiang, et al., Towards understanding the reaction pathway in vapour phase hydrogenation of furfural to 2-methylfuran, *J. Mol. Catal. A Chem.* 246 (2006) 18–23.
- [23] S. De, B. Saha, R. Luque, Hydrodeoxygenation processes: Advances on catalytic transformations of biomass-derived platform chemicals into hydrocarbon fuels, *Bioresour. Technol.* 178 (2015) 108–118.
- [24] M.C. Annesini, F. Gironi, W. Guerani, Phase Equilibria of Highly Asymmetric Mixtures Involved in Biodiesel Production, 38 (2014) 67–72.
- [25] I. Kubičková, D. Kubička, Utilization of triglycerides and related feedstocks for production of clean hydrocarbon fuels and petrochemicals: A review, *Waste and Biomass Valorization.* 1 (2010) 293–308.
- [26] G.W. Huber, R.D. Cortright, J. a. Dumesic, Renewable alkanes by aqueous-phase reforming of biomass-derived oxygenates, *Angew. Chemie - Int. Ed.* 43 (2004) 1549–1551.
- [27] N. Li, G.A. Tompsett, G.W. Huber, Renewable High-Octane Gasoline by Aqueous-Phase Hydrodeoxygenation of C5 and C6 Carbohydrates over Pt/Zirconium Phosphate Catalysts, *ChemSusChem.* 3 (2010) 1154–1157.
- [28] L.-Z. Qin, M.-J. Song, C.-L. Chen, Aqueous-phase deoxygenation of glycerol to 1,3-propanediol over Pt/WO<sub>3</sub>/ZrO<sub>2</sub> catalysts in a fixed-bed reactor, *Green Chem.* 12 (2010) 1466.
- [29] Y.T. Kim, J. a. Dumesic, G.W. Huber, Aqueous-phase hydrodeoxygenation of sorbitol: A comparative study of Pt/Zr phosphate and PtReOx/C, *J. Catal.* 304 (2013) 72–85.
- [30] K. Chen, M. Tamura, Z. Yuan, Y. Nakagawa, K. Tomishige, One-Pot Conversion of Sugar and Sugar Polyols to n-Alkanes without C-C Dissociation over the Ir-ReOx/SiO<sub>2</sub> Catalyst Combined with H-ZSM-5, *ChemSusChem.* 6 (2013) 613–621.
- [31] S. Liu, M. Tamura, Y. Nakagawa, K. Tomishige, One-pot conversion of cellulose into n-hexane over the Ir-ReOx/SiO<sub>2</sub> catalyst combined with HZSM-5, *ACS Sustain. Chem. Eng.* 2 (2014) 1819–1827.
- [32] J.P. Lange, E. Van Der Heide, J. Van Buijtenen, R. Price, Furfural-a promising platform for lignocellulosic biofuels, *ChemSusChem.* 5 (2012) 150–166.
- [33] S. Liu, Y. Amada, M. Tamura, Y. Nakagawa, K. Tomishige, One-pot selective conversion of furfural into 1,5-pentanediol over a Pd-added Ir-ReOx/SiO<sub>2</sub> bifunctional catalyst, *Green Chem.* 16 (2014) 617–626.
- [34] T. Werpy, G. Petersen, Top Value Added Chemicals from Biomass, Richland (U.S.A.), 2004.
- [35] J.J. Bozell, G.R. Petersen, Technology development for the production of biobased products from biorefinery carbohydrates-the US Department of Energy’s “Top 10” revisited, *Green Chem.* 12

- (2010) 539.
- [36] J. Ma, W. Yu, M. Wang, X. Jia, F. Lu, J. Xu, Advances in selective catalytic transformation of polyols to value-added chemicals, *Chinese J. Catal.* 34 (2013) 492–507.
- [37] A. Fukuoka, P.L. Dhepe, Catalytic Conversion of Cellulose into Sugar Alcohols, *Angew. Chemie Int. Ed.* 45 (2006) 5161–5163.
- [38] S. de Vyver, J. Geboers, M. Dusselier, H. Schepers, T. Vosch, L. Zhang, et al., Selective Bifunctional Catalytic Conversion of Cellulose over Reshaped Ni Particles at the Tip of Carbon Nanofibers, *ChemSusChem.* 3 (2010) 698–701.
- [39] J. Wisniak, M. Hershkowitz, R. Leibowitz, S. Stein, Hydrogenation of Xylose to Xylitol, *Ind. Eng. Chem. Prod. Res. Dev.* 13 (1974) 75–79.
- [40] M. Hershkowitz, Modelling of a trickle-bed reactor-the hydrogenation of xylose to xylitol, *Chem. Eng. Sci.* 40 (1985) 1309–1311.
- [41] M. Yadav, D.K. Mishra, J.S. Hwang, Catalytic hydrogenation of xylose to xylitol using ruthenium catalyst on NiO modified TiO<sub>2</sub> support, *Appl. Catal. A Gen.* 425-426 (2012) 110–116.
- [42] R.A. Sheldon, H. van Bekkum, Catalytic Hydrogenation and Dehydrogenation, in: *Fine Chem. through Heterog. Catal.*, Wiley-VCH Verlag GmbH, 2000: pp. 351–471.
- [43] K.S.W. Singh, J. Rouquerol, G. Bergeret, P. Gallezot, M. Vaarkamp, D.C. Koningsberger, et al., Characterization of Solid Catalysts, in: G. Ertl, H. Knözinger, F. Schüth, J. Weitkamp (Eds.), *Handb. Heterog. Catal.*, Wiley-VCH Verlag GmbH, 2008: pp. 427–582.
- [44] P. Gallezot, N. Nicolaus, G. Fleche, P. Fuertes, A. Perrard, Glucose Hydrogenation on Ruthenium Catalysts in a Trickle-Bed Reactor, *J. Catal.* 180 (1998) 51–55.
- [45] J.-P. Mikkola, R. Sjöholm, T. Salmi, P. Mäki-Arvela, Xylose hydrogenation: kinetic and NMR studies of the reaction mechanisms, *Catal. Today.* 48 (1999) 73–81.
- [46] M. Schlaf, Selective deoxygenation of sugar polyols to alpha,omega-diols and other oxygen content reduced materials-a new challenge to homogeneous ionic hydrogenation and hydrogenolysis catalysis., *Dalt. Trans.* (2006) 4645–4653.
- [47] Solvay S.A., Solvay to build bio-based epichlorohydrin plant in China to serve largest market in the world, (2012) 1. <http://www.solvay.com>.
- [48] C.-H. (Clayton) Zhou, J.N. Beltramini, Y.-X. Fan, G.Q. (Max) Lu, Chemoselective catalytic conversion of glycerol as a biorenewable source to valuable commodity chemicals, *Chem. Soc. Rev.* 37 (2008) 527–549.
- [49] Z. Chi, D. Pyle, Z. Wen, C. Frear, S. Chen, A laboratory study of producing docosahexaenoic acid from biodiesel-waste glycerol by microalgal fermentation, *Process Biochem.* 42 (2007) 1537–1545.
- [50] M. Pagliaro, M. Rossi, *The Future of Glycerol*, The Royal Society of Chemistry, 2008.
- [51] G. Shah, S. Suri, *Production of biodiesel from feedstock*, US 8545702 B1, 2013.
- [52] C. Len, R. Luque, Continuous flow transformations of glycerol to valuable products: an overview, *Sustain. Chem. Process.* 2 (2014) 1–10.
- [53] C. Staples, Fate, effects and potential environmental risks of ethylene glycol: a review,

- Chemosphere. 43 (2001) 377–383.
- [54] R. Mosser-Ruck, K. Devineau, D. Charpentier, M. Cathelineau, Effects of ethylene glycol saturation protocols on XRD patterns: A critical review and discussion, *Clays Clay Miner.* 53 (2005) 631–638.
- [55] R. Gomes, R.G. Liteplo, M.E. Meek, M. Lewis, Concise International Chemical Assessment Document 54: Ethylene oxide, Ottawa (Canada), 2002.
- [56] H. Yue, Y. Zhao, X. Ma, J. Gong, Ethylene glycol: properties, synthesis, and applications, *Chem. Soc. Rev.* 41 (2012) 4218.
- [57] M. Lovrić, P. Granić, M. Čubrilo-Turek, Z. Lalić, J. Sertić, Ethylene glycol poisoning, *Forensic Sci. Int.* 170 (2007) 179–184.
- [58] C. Guo, K.E. McMartin, The cytotoxicity of oxalate, metabolite of ethylene glycol, is due to calcium oxalate monohydrate formation, *Toxicology.* 208 (2005) 347–355.
- [59] Y. Li, B. Yue, S. Yan, W. Yang, Z. Xie, Q. Chen, et al., Preparation of ethylene glycol via catalytic hydration with highly efficient supported niobia catalyst, *Catal. Letters.* 95 (2004) 163–166.
- [60] J.W. van Hal, J.S. Ledford, X. Zhang, Investigation of three types of catalysts for the hydration of ethylene oxide (EO) to monoethylene glycol (MEG), *Catal. Today.* 123 (2007) 310–315.
- [61] G. Xu, Y. Li, Z. Li, H.-J. Wang, Kinetics of the Hydrogenation of Diethyl Oxalate to Ethylene Glycol, *Ind. Eng. Chem. Res.* 34 (1995) 2371–2378.
- [62] L. Chen, P. Guo, M. Qiao, S. Yan, H. Li, W. Shen, et al., Cu/SiO<sub>2</sub> catalysts prepared by the ammonia-evaporation method: Texture, structure, and catalytic performance in hydrogenation of dimethyl oxalate to ethylene glycol, 257 (2008) 172–180.
- [63] G.W. Huber, J.W. Shabaker, S.T. Evans, J.A. Dumesic, Aqueous-phase reforming of ethylene glycol over supported Pt and Pd bimetallic catalysts, 62 (2006) 226–235.
- [64] G.W. Huber, J.W. Shabaker, J.A. Dumesic, Raney Ni-Sn Catalyst for H<sub>2</sub> Production from Biomass-Derived Hydrocarbons, 300 (2003) 2075–2077.
- [65] A.E. Martin, F.H. Murphy, Propylene Glycols, 2008.
- [66] The Dow Chemical, DOW™ Propylene Glycol, 2013. [www.dow.com](http://www.dow.com).
- [67] M. Pagliaro, Glycerol: The Platform Biochemical of the Chemical Industry, Digital ed, 2013.
- [68] ADM Announces Successful Start-Up of Renewable, Biobased Propylene Glycol Facility in Decatur, 2015. <http://www.adm.com>.
- [69] DuPont™ Sorona EP thermoplastic polymer®, 2007. [www.dupont.com](http://www.dupont.com).
- [70] J. Sun, H. Liu, Selective hydrogenolysis of biomass-derived xylitol to ethylene glycol and propylene glycol on Ni/C and basic oxide-promoted Ni/C catalysts, *Catal. Today.* 234 (2014) 75–82.
- [71] X. Chen, X. Wang, S. Yao, X. Mu, Hydrogenolysis of biomass-derived sorbitol to glycols and glycerol over Ni-MgO catalysts, *Catal. Commun.* 39 (2013) 86–89.
- [72] L. Zhou, A. Wang, C. Li, M. Zheng, T. Zhang, Selective Production of 1,2-Propylene Glycol from Jerusalem Artichoke Tuber using Ni-W<sub>2</sub>C/AC Catalysts, *ChemSusChem.* 5 (2012) 932–938.

- 
- [73] L. Ye, X. Duan, H. Lin, Y. Yuan, Improved performance of magnetically recoverable Ce-promoted Ni/Al<sub>2</sub>O<sub>3</sub> catalysts for aqueous-phase hydrogenolysis of sorbitol to glycols, *Catal. Today*. 183 (2012) 65–71.
- [74] M. Banu, P. Venuvanalingam, R. Shanmugam, B. Viswanathan, S. Sivasanker, Sorbitol hydrogenolysis over Ni, Pt and Ru supported on NaY, *Top. Catal.* 55 (2012) 897–907.
- [75] T. Soták, T. Schmidt, M. Hronec, Hydrogenolysis of polyalcohols in the presence of metal phosphide catalysts, *Appl. Catal. A Gen.* 459 (2013) 26–33.
- [76] K. Wang, M.C. Hawley, T.D. Furney, Mechanism Study of Sugar and Sugar Alcohol Hydrogenolysis Using 1,3-Diol Model Compounds, *Ind. Eng. Chem. Res.* 34 (1995) 3766–3770.
- [77] I.M. Leo, M.L. Granados, J.L.G. Fierro, R. Mariscal, Sorbitol hydrogenolysis to glycols by supported ruthenium catalysts, *Chinese J. Catal.* 35 (2014) 614–621.
- [78] L. Zhao, J.H. Zhou, Z.J. Sui, X.G. Zhou, Hydrogenolysis of sorbitol to glycols over carbon nanofiber supported ruthenium catalyst, *Chem. Eng. Sci.* 65 (2010) 30–35.



**CHAPTER 2. State of the art:  
Glycerol hydrogenolysis to propanediols**



---

**Table of contents**

ABSTRACT.....	47
2.1 GLYCEROL HYDROGENOLYSIS OVER CONVENTIONAL CATALYSTS .....	47
2.1.1 <i>Monometallic noble metals</i> .....	47
2.1.2 <i>Noble metal combined with an acid</i> .....	50
2.1.3 <i>Noble metal combined with a base</i> .....	54
2.1.4 <i>Non-noble metals</i> .....	56
2.2 CATALYSTS FOR THE SELECTIVE PRODUCTION OF 1,3-PDO.....	58
2.2.1 <i>The required features of a heterogeneous catalyst</i> .....	58
2.2.2 <i>Bi-functional catalysts based on Rhenium</i> .....	59
2.2.3 <i>Bi-functional catalyst based on Tungsten</i> .....	63
2.3 CONCLUSION AND OUTLOOK.....	70
REFERENCES.....	72





## Abstract

The utilization of 1,3-propanediol (1,3-PDO) in the production of the widely used polytrimethylene terephthalate polymers (PTT) has turned it into one of the most interesting compounds that can be obtained from glycerol. However, the selective production of 1,3-PDO is very challenging and most conventional catalytic systems yield 1,2-propanediol (1,2-PDO) as the main product. As a consequence of this, the reaction mechanisms and catalysts for the selective production of 1,2-PDO are well developed. By contrast, some important reaction aspects related to 1,3-PDO production remain unclear.

It is not by far the aim of the current state of the art to address all the vast literature related to glycerol hydrogenolysis to propanediols (PDOs). Instead, the most relevant works have been selected in order to discuss the main catalytic systems utilized, the effect of the operating reaction conditions and the proposed reaction mechanisms.

It is worth pointing out that glycerol hydrogenolysis to PDOs can serve as a model reaction and that the conclusions and advances obtained in this process can be applied to the valorisation of more complicated molecules, such as other biomass-derived polyols.

## 2.1 Glycerol hydrogenolysis over conventional catalysts

The first feature that a catalyst for hydrogenolysis reactions must show is the ability to activate hydrogen molecules. Hydrogen is known to be activated over a metal surface. Typical metals used are noble metals, such as Ru, Pt or Pd, and non-noble transition metals, specially Cu and Ni [1,2]. This section has been divided according to the type of metal that activates the hydrogen, even though sometimes it is difficult to draw a clear line.

### 2.1.1 Monometallic noble metals

Noble metals are widely used in hydrogenation reactions because of their ability to activate hydrogen molecules. Among them, Ru-based catalysts have been frequently used as an active component in the hydrogenolysis of glycerol (Table 2.1).

**Table 2.1.** Examples of glycerol hydrogenolysis over noble metal catalysts on neutral supports.

Catalyst	H <sub>2</sub> (bar)	Temp. (°C)	Glycerol/water/ catalyst (g)	Time (h)	Conv. (%)	Product selectivity (%)	Ref.
10% Ru/C	60	210	6.5/154/n.r.	<sup>a</sup>	<sup>a</sup>	1,2-PDO (12), EG (47), ethane (26)	[3]
5% Pt/C	14	200	50/10/2.5	24	35	1,2-PDO (83)	[1]
5% Pd/C	14	200	50/10/2.5	24	5	1,2-PDO (72)	[1]
5% Ru/C	14	200	50/10/2.5	24	44	1,2-PDO (40)	[1]
5% Ru/TiO <sub>2</sub>	50	180	1/4/0.1	12	90	1,2-PDO (21), EG (41)	[4]
5% Ru/SiO <sub>2</sub>	50	180	1/4/0.1	12	3	1,2-PDO (55), EG (12)	[4]
5% Rh/SiO <sub>2</sub>	80	120	0.4/21/0.15	10	7	1,2-PDO (38), 1,3-PDO (8), 1-PO (35), 2-PO (13)	[5]

Metal content in wt %, n.r.= not reported, <sup>a</sup> very low conversion.

Montassier's group [3,6] was one of the first to study this process. They used Ru/C as catalyst at 210 °C and 60 bar of H<sub>2</sub>, obtaining 47 % selectivity towards ethylene glycol (EG) as major product, but low selectivity towards 1,2-PDO (12 %), at low glycerol conversions [3].

Montassier et al. proposed a reaction mechanism for the formation of 1,2-PDO over Ru/C composed by the following three steps: (i) reversible glycerol dehydrogenation to glyceraldehyde in metal sites, (ii) dehydration of glyceraldehyde to 2-hydroxyacrolein and through subsequent keto-enol tautomerism to pyruvaldehyde and, (iii) hydrogenation of this intermediate to 1,2-PDO (*dehydrogenation-dehydration-hydrogenation mechanism*). They proposed that the dehydration of glyceraldehyde takes place by a nucleophilic reaction with water or with adsorbed hydroxy groups of the catalyst. Moreover, they suggested that the formation of EG is produced via retro-aldol reaction of glyceraldehyde to glycolaldehyde and subsequent hydrogenation. The reaction mechanism is shown in Fig. 2.1.

In later studies carried out by Dasari et al. [1] over Ru/C under milder reaction conditions, 1,2-PDO was obtained as the main product (40 % selectivity). In the same work, they also compared the activities of various commercial hydrogenation catalysts in the glycerol hydrogenolysis, at 200 °C and 14 bar of H<sub>2</sub>. Pd/C showed very low activity, but high selectivity towards 1,2-PDO (73 %). However, Pt/C showed higher selectivity towards 1,2-PDO (83 %) and higher yield (29 %) than Ru/C (40 % selectivity and 18 % yield). Nevertheless, other non-noble-metal catalysts such as copper chromite (Cu<sub>2</sub>Cr<sub>2</sub>O<sub>5</sub>) showed even higher yield (Table 2.4).

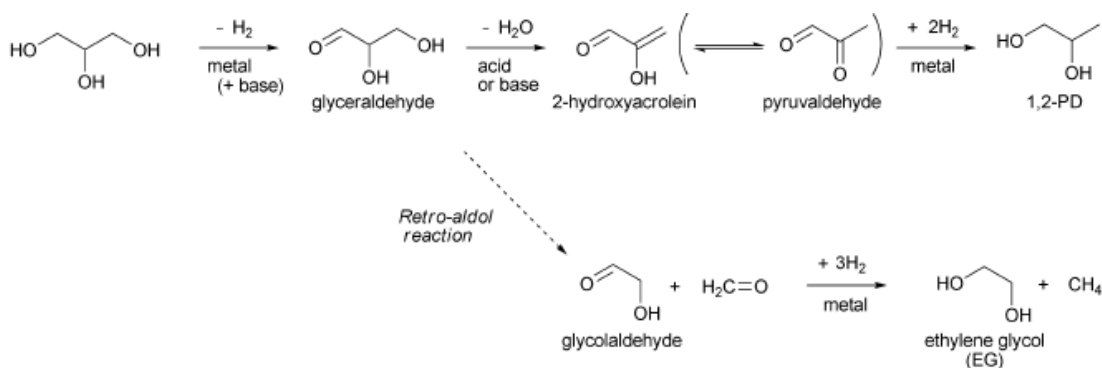


**Fig. 2.1.** Scheme of the glycerol hydrogenolysis to 1,2-PDO and EG proposed by Montassier et al. [3,6]: *dehydrogenation-dehydration-hydrogenation* mechanism.

Dasari's group also suggested an alternative reaction mechanism based on their experiments in which the formation of acetol (hydroxyl acetone) together with 1,2-PDO was observed. Moreover, they found that the reaction takes place even in the absence of water (1,2-PDO yield of 50 % with Cu<sub>2</sub>Cr<sub>2</sub>O<sub>5</sub>), and since the catalyst was reduced in H<sub>2</sub> stream prior to the reaction, there were no surface hydroxy groups taking part in the reaction. These facts contradict the mechanism proposed by Montassier et al. Their novel mechanism does not include water present in the form of surface hydroxy groups or as a part of reactants. The reaction mechanism proposed is formed by two steps: (i) dehydration of glycerol to acetol, and (ii) hydrogenation of acetol to 1,2-PDO (*dehydration-hydrogenation mechanism*).

Later Feng et al. [4] studied the effect of the support and of the catalyst pre-reduction temperature on the catalytic performance of Ru supported catalysts in the hydrogenolysis of glycerol. Among the tested supports (NaY, SiO<sub>2</sub>, Al<sub>2</sub>O<sub>3</sub> and TiO<sub>2</sub>), Ru supported on TiO<sub>2</sub> exhibited the highest glycerol conversion (90 %). However, the selectivity towards 1,2-PDO was only 21 % and the production of EG was favoured under the reaction conditions (see Table 2.1). On the other hand, Ru/SiO<sub>2</sub> showed the lowest activity, but with a much higher selectivity towards 1,2-PDO than that of EG (55 % and 12 % selectivity, respectively). Moderate glycerol conversion (34 %) and 1,2-PDO selectivity (47 %) were obtained for Ru/Al<sub>2</sub>O<sub>3</sub> catalyst. They reached to the conclusion that the support material could influence the metal particle size and the reaction routes. Moreover, they found that pre-reduction temperature had also a high influence in the activity of the catalyst, fundamentally by modifying the metal particle size, which usually increased with the reduction temperature, and as a consequence of this, glycerol conversion decreased.

Under a much lower temperature of 120 °C, Furikado et al. [5] compared the behaviour of various supported noble-metal catalysts (Rh, Ru, Pt and Pd over C, SiO<sub>2</sub> and Al<sub>2</sub>O<sub>3</sub>) in the aqueous phase glycerol hydrogenolysis. Pd and Pt supported catalyst showed less than 1 % glycerol conversion and so did all the noble-metals supported on Al<sub>2</sub>O<sub>3</sub>. Among all the catalysts tested, Rh/SiO<sub>2</sub> showed the highest glycerol conversion (7 %) and moderate selectivity towards 1,2-PDO (38 %). It is worth mentioning that with this catalyst 1,3-PDO was observed as a reaction product with an 8 % selectivity. This group also investigated the effect of reaction temperature concluding that in order to maximize the yield of 1,2-PDO, the reaction should be carried out at low temperatures. In this way, the C–O over-hydrogenolysis of PDOs to lower alcohols (mainly 1-PO and 2-PO) and the C–C hydrogenolysis to degradation products (EG, ethanol, methanol and methane) are minimized.

As a general remark, monometallic noble-metal catalysts show high activity in the C–C bond hydrogenolysis and, therefore, are not very selective towards the PDOs, giving in most cases EG in quite high yields. In order to improve the selectivity towards PDOs several approaches have been carried out. The most remarkable approaches have been the addition of either an acid or a base as a co-catalyst, or the use of bi-functional metal/acid or metal/base catalysts, which will be described in the next section.

## 2.1.2 Noble metal combined with an acid

**Table 2.2.** Examples of glycerol hydrogenolysis over noble metal catalysts combined with an acid.

Catalyst	H <sub>2</sub> (bar)	Temp. (°C)	Glycerol/water/ catalyst + additive (g)	Time (h)	Conv. (%)	Product selectivity (%)	Ref.
5% Ru/C + Al <sub>2</sub> O <sub>3</sub>	80	120	4/16/0.15 + 0.3	10	79	1,2-PDO (75), 1-PO (8), 2-PO (2), EG (7)	[2]
3% Ru/C + Nb <sub>2</sub> O <sub>5</sub>	60	180	10/40/0.3 + 0.3	8	45	1,2-PDO (61), EG (29)	[7]
5% Rh/C + H <sub>2</sub> WO <sub>4</sub>	80	180	15/65/5 + 1.25	168	21	1,2-PDO (70), 1,3-PDO (6)	[8]
	80	180	15/65 <sup>b</sup> /5 + 1.25	168	32	1,2-PDO (6), 1,3-PDO (12)	[8]
	80	180	15/65 <sup>c</sup> /5 + 1.25	48	15	1,2-PDO (13), 1,3-PDO (13)	[8]
1% Pt/ASA	45 <sup>a</sup>	220	8/32/1.3	24	23	1,2-PDO (35), 1,3-PDO (1), 1-PO + 2-PO (13)	[9]

Metal content in wt %, n.r.= not reported, <sup>a</sup> inert atmosphere, <sup>b</sup> sulfolane media, <sup>c</sup> dioxane media.

One of the first works in which a noble metal was combined with an acid was the work carried out by Tomishige's group [2,10]. They combined Ru/C with various Brønsted acid co-catalysts, such as Amberlyst 15 (A15) ion-exchange resin, sulfonated zirconia, zeolites, and homogeneous H<sub>2</sub>SO<sub>4</sub>. They found that A15 was the most effective co-catalyst among them, obtaining very high glycerol conversion and selectivity towards 1,2-PDO (79 % and 75 %, respectively) [2] (more details in Table 2.2). The hydrogenolysis of 1,2-PDO over Ru/C + A15 proceeded with similar selectivities towards 1-PO (36 %) and 2-PO (31 %), while that of glycerol gave higher selectivities towards 1-PO, suggesting that 1-PO was mainly formed through the over-hydrogenolysis of 1,3-PDO.

They also found that the yield of 1,2-PDO increased drastically by the presence of A15, whereas the yield of 1,3-PDO + 1-PO was not influenced by the acid co-catalyst. Based on these results, the authors concluded that the formation of 1,3-PDO was catalysed only by Ru/C. In contrast, the formation of 1,2-PDO was catalysed by both, A15 and Ru/C.

The good performance of acetol hydrogenation under Ru/C + A15 confirmed that glycerol hydrogenolysis to 1,2-PDO in acid conditions occurs following the *dehydration-hydrogenation* route, previously proposed by Dasari et al. [1]: the dehydration of glycerol to acetol is catalysed by A15 and the subsequent hydrogenation of acetol to 1,2-PDO is catalysed on the Ru metallic sites. In addition, the C–O hydrogenolysis rate increases with increasing H<sub>2</sub> pressure, which contradicts the *dehydrogenation-dehydration-hydrogenation* mechanism proposed by Montassier et al., because high hydrogen pressures should disfavour the initial dehydrogenation step.

Tomishige's group also proposed that 1,3-PDO can be formed in a similar way via 3-hydroxypropanal (3-HPA), as dehydration intermediate from glycerol and its subsequent hydrogenation gives the desired product [10] (Fig. 2.2). This transformation was mainly catalysed by Ru/C as it was explained above.

The lower selectivity towards 1,3-PDO might be explained by two factors: (i) its high reactivity under operating conditions, comparable to that of glycerol, and higher than the reactivity of 1,2-PDO, and (ii) acetol is thermodynamically more stable than 3-HPA [11]. This might be the main reason for the greatly higher selectivities towards 1,2-PDO than 1,3-PDO frequently obtained under conventional catalytic systems.

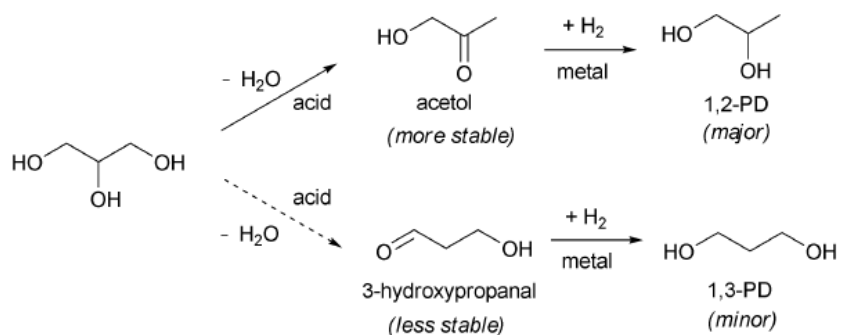


**Fig. 2.2.** Scheme of the glycerol hydrogenolysis to PDOs: *dehydration-hydrogenation* mechanism [12].

The main drawback of the A15 is its low thermal stability. To avoid this problem, other works using thermally more stable inorganic solid acids were carried out. Balaraju et al. [7] studied the influence of the acidity of the catalysts on glycerol conversion and selectivity using commercial Ru/C with different inorganic solid acids as co-catalysts, such as niobia (Nb<sub>2</sub>O<sub>5</sub>), 12-tungstophosphoric acid supported on zirconia (TPA/ZrO<sub>2</sub>), cesium salt of TPA (CsTPA) and cesium salt of TPA supported on zirconia (CsTPA/ZrO<sub>2</sub>). They found a linear correlation between glycerol conversion and the total acidity of the catalysts. Glycerol conversion increased with increasing acidity, which indicates that the acid sites play a role in the dehydration of glycerol to acetol. The presence of acetol as a reaction product confirmed this hypothesis. Among the different acid co-catalysts tested, Nb<sub>2</sub>O<sub>5</sub> and TPA/ZrO<sub>2</sub>, with moderate acid sites, showed the maximum conversion and almost identical selectivities (45 % glycerol conversion and 61 % selectivity towards 1,2-PDO for Nb<sub>2</sub>O<sub>5</sub> co-catalyst).

The positive effect of the addition of a homogeneous acid was highlighted in the work of Chaminand et al. [8]. The addition of H<sub>2</sub>WO<sub>4</sub> to the reaction medium increased both, glycerol conversion and the selectivity towards PDOs. Interestingly, they obtained high 1,2-PDO selectivity (70 %) but also small amounts of 1,3-PDO (6 % selectivity) combining Rh/C and H<sub>2</sub>WO<sub>4</sub> in aqueous medium. Their work showed that the nature of the solvent has a dramatic effect on the reaction rate and product distribution. In sulfolane media, the main product was 1-PO and a high 1,3-PDO/1,2-PDO ratio of 2 was obtained. However, the selectivity values of both PDOs were relatively low. Using dioxane as solvent the C–C bond cleavage was favoured and significant amounts of EG, ethanol and methanol were detected. In spite of the promising results using organic polar solvents, water is the preferred solvent from a green chemistry point of view since biodiesel-derived glycerol is obtained in aqueous phase after the transesterification

reaction of vegetable oils, and since water is also obtained as a product in hydrogenolysis reactions.

More recently, Gandarias et al. [9] investigated the selective glycerol hydrogenolysis to 1,2-PDO over Pt supported on amorphous silico-alumina (Pt/ASA) under mild conditions (220 °C and 45 bar). They compared the results obtained under H<sub>2</sub> and N<sub>2</sub> atmospheres. Under N<sub>2</sub>, the hydrogen required in the hydrogenolysis reaction is *in-situ* obtained from the aqueous phase reforming (APR) of glycerol. The scheme of this novel process is shown in Fig. 2.3.

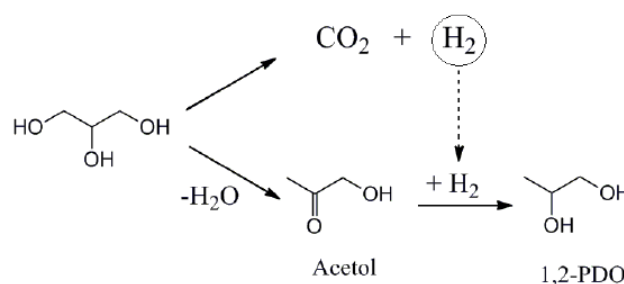


Fig. 2.3. Glycerol APR combined with hydrogenolysis to 1,2-PDO [13].

The hydrogen obtained in this way seemed to be as effective as the hydrogen provided directly from the gas phase (20 and 23 % glycerol conversion in 24 h under H<sub>2</sub> and N<sub>2</sub> atmospheres, respectively). In spite of this, low selectivity values towards PDOs were achieved as compared to other results published in the literature, mainly because of the high C–O bond cleavage ability of the Pt/ASA catalyst which leads to the over-hydrogenolysis of PDOs to 1-PO and 2-PO. Moreover, they compared the activity and product distribution obtained with the support ASA and with Pt/ASA, in order to establish the role of the metallic (Pt) and acid sites (of the support) in the reaction. In the experiments with ASA support, dehydrated products were dominant, while in the experiments with Pt/ASA major product came from the hydrogenation reactions.

This novel process to obtain hydrogen presents some advantages over the traditional use of molecular hydrogen: (i) avoid the necessity to use molecular hydrogen which is still derived from fossil fuels and is dangerous to handle, (ii) could lead to work under milder conditions of temperature and pressures, since the *in-situ* hydrogen is produced on the active sites of the catalyst, and does not require high pressures unlike molecular hydrogen externally added.



### 2.1.3 Noble metal combined with a base

Other remarkable approach in the glycerol hydrogenolysis was the combination of noble metals with a base. Some of the most relevant results are summarized in Table 2.3.

**Table 2.3** Examples of glycerol hydrogenolysis over noble metal catalysts combined with a base.

Catalyst	H <sub>2</sub> (bar)	Temp. (°C)	Glycerol/water/ + additive (g) catalyst	Time (h)	Conv. (%)	Product selectivity (%)	Ref.
5% Ru/TiO <sub>2</sub> + LiOH	30	170	1/4/0.10 + 0.024	12	90	1,2-PDO (87), EG (7)	[14]
5% Ru/C + CaO	40	200	1.5/150/0.1 + 0.084	5	50	1,2-PDO (46), lactate (32), EG (16)	[15]
3% Pt/C + CaO	40	200	1.5/150/0.1 + 0.084	5	40	1,2-PDO (71), lactate (19), EG (9)	[15]
2% Pt/HLT	30	220	4/16/0.5	20	92	1,2-PDO (93)	[16]
2.7% Pt/NaY	n.r. <sup>a</sup>	230	8.4/33.6/1.6	15	85	1,2-PDO (65), 1-PO + 2-PO (7), ethanol (10)	[17]

Metal content in wt %, n.r.= not reported, <sup>a</sup> inert atmosphere.

Feng et al. [14] studied the effect of different base additives in the performance of a Ru/TiO<sub>2</sub> catalyst in aqueous glycerol hydrogenolysis under mild conditions (170 °C and 30 bar of H<sub>2</sub>). The addition of LiOH base dramatically increased the glycerol conversion and the selectivity towards 1,2-PDO, obtaining very good results after 12 h reaction time (90 % conversion and 87 % selectivity). Moreover, they studied the effect of the amount of LiOH base on the reaction. Interestingly, increasing the amount of LiOH glycerol conversion and selectivity towards 1,2-PDO initially exhibited an increase and finally reached a maximum, after which they began to decrease. By contrast, the selectivity towards EG decreased with the increase of LiOH amount. This interesting behavior is explained by the three steps *dehydrogenation-dehydration-hydrogenation* route (see scheme in Fig. 2.1) mentioned above, since the base can mainly promote the dehydration of glyceraldehyde to pyruvaldehyde.

In other works, Maris and Davis evaluated the behaviour of commercial carbon-supported Ru and Pt catalysts in the aqueous phase glycerol hydrogenolysis, at 200 °C and 40 bar H<sub>2</sub>, with and without the addition of a base [15,18]. At neutral conditions, Ru/C showed higher glycerol conversion than Pt/C (40 % vs 13 %), whereas the activity

was greater promoted over Pt than over Ru using NaOH or CaO as base additives. Their results could also be explained by the three step mechanism. The first step, the dehydrogenation of glycerol to glyceraldehyde, is suggested to occur on the metallic sites but it can be also enhanced by the presence of a base. However, the second step, the dehydration of glyceraldehyde to pyruvaldehyde, is mainly catalyzed by the base. They also proposed that the high formation of lactic acid (in its conjugated base form, lactate) occurred through internal Cannizzaro reaction of pyruvaldehyde catalyzed by the base [19]. Thus, the selectivity towards 1,2-PDO was not very high in any cases. The formation of EG was suggested to occur by two routes. On Ru/C it was mainly formed by the C–C bond cleavage of glyceraldehyde. In contrast, since Pt is not effective for the cleavage of C–C bond, formation of EG most likely proceeds through a base-catalysed retro-aldol route. The best results were obtained for Pt/C with CaO as additive, obtaining a 40 % glycerol conversion, with 71 % selectivity towards 1,2-PDO and moderate selectivity towards lactate (19 %).

It is worth mentioning the more recent work carried out by Yuan et al. [16] in which they found an excellent catalyst for the selective hydrogenolysis of glycerol to 1,2-PDO. Among the catalyst tested, Pt/HBeta, Pt/HZSM-5, Pt/C, Pt/Al<sub>2</sub>O<sub>3</sub>, Pt/MgO and Pt/hydrotalcite (Pt/HLT), the latter catalyst exhibited the best results: 92 % glycerol conversion and 93 % selectivity towards 1,2-PDO, under mild reaction condition (220 °C and 30 bar of H<sub>2</sub>, in 20 h reaction time). They correlated the results of the different catalysts with their alkalinity and Pt particles size. Although the detected Pt particles sizes in Pt/HZSM-5 and Pt/HBeta were smaller than that in Pt/MgO, their activities were very low because of their poor alkalinity (less than 10 % glycerol conversion). On basic supports, the predominant activity of Pt/HLT than that of Pt/MgO (92 % vs 50 % glycerol conversion) could be partially caused by its highly dispersed Pt particles.

High yield of 1,2-PDO (57 %) was also reported by D'Hondt et al. [17] combining the APR and the hydrogenolysis of glycerol. The reaction was carried out under inert atmosphere using Pt/NaY catalyst at 230 °C and 15 h reaction time. Simultaneously to the production of hydrogen through APR of glycerol, other molecules of glycerol are dehydrated on the acid sites of the support to yield acetol as intermediate. The last hydrogenation step of acetol on metal sites gives 1,2-PDO.

It is worth to point out that in alkaline conditions only marginal 1,3-PDO selectivities have been reported.

### 2.1.4 Non-noble metals

Generally, noble metals are more active than non-noble metals in the C–C and C–O bond hydrogenolysis reactions which usually lead to poor selectivities towards PDOs. Thus, some non-noble metal were tested in the glycerol hydrogenolysis. The most relevant results are displayed in Table 2.4.

**Table 2.4** Examples of glycerol hydrogenolysis over non-noble metal catalysts.

Catalyst	H <sub>2</sub> (bar)	Temp. (°C)	Glycerol/water/ catalyst (g)	Time (h)	Conv. (%)	Product selectivity (%)	Ref.
Cu <sub>2</sub> Cr <sub>2</sub> O <sub>5</sub>	21	200	20/10/2.5	24	65	1,2-PDO (90)	[1]
Raney® Cu	15	205	<sup>a</sup> / <sup>a</sup> /n.r.	<sup>b</sup>	100	1,2-PDO (94)	[20]
Raney® Ni	10	190	8/0/2	44	97	1,2-PDO (71), ethanol (19), CO <sub>2</sub> (10)	[21]
32% Cu/	50	200	36/24/1.8	10	20	1,2-PDO (80), EG (3)	[22]
ZnO/Al <sub>2</sub> O <sub>3</sub>	6	190	<sup>c</sup>	n.r.	96	1,2-PDO (92)	[22]
15% Cu/MgO + NaOH	30	180	6/2/1 + 0.125	20	82	1,2-PDO (96)	[23]
Cu <sub>0.4</sub> /Mg <sub>5.6</sub> Al <sub>2</sub> O <sub>8.6</sub>	30	220	7.1/2.4/1	20	99	1,2-PDO (97), 1-PO (1), EG (2)	[24]
20% Ni-15%Cu/ Al <sub>2</sub> O <sub>3</sub> + formic acid	45 <sup>d</sup>	220	5.5/131/2.7 + 0.45 g h <sup>-1</sup>	24	90	1,2-PDO (82)	[25]

Metal content in wt %, n.r. = not reported, <sup>a</sup> 80 wt% glycerol/water, feed rate = 3 mL h<sup>-1</sup>, H<sub>2</sub>/glycerol molar ratio = 68, <sup>b</sup> 5 days on stream, <sup>c</sup> WHSV = 0.08 h<sup>-1</sup>, H<sub>2</sub>/glycerol molar ratio = 144, <sup>d</sup> N<sub>2</sub> atmosphere.

Among the non-noble metals, Cu has been extensively studied because of its poor hydrogenolytic activity towards C–C bond and its high selectivity towards C–O bond cleavage [1,6].

This feature of Cu-based catalysts was observed in the work of Dasari et al. [1] in which they studied a large list of heterogeneous commercial catalysts, including noble (Ru, Pt, Pd on C) and non-noble metals (Cu<sub>2</sub>Cr<sub>2</sub>O<sub>5</sub>, Raney Ni and Raney Cu). Catalysts based on Ru or Pd showed low selectivity towards 1,2-PDO (less than 50%) due to the competitive hydrogenolysis of C–C and C–O bonds leading to the formation of lower alcohols (C<3) and gases. On the other hand, Cu-based catalysts exhibited higher selectivity towards 1,2-PDO with little selectivity towards EG and other degradation by-products. Among all, Cu<sub>2</sub>Cr<sub>2</sub>O<sub>5</sub> was identified as the most effective

catalyst for the reaction under quite mild conditions (see Table 2.4). In this work, they proposed the *dehydration-hydrogenation* mechanism of glycerol to 1,2-PDO, based on the evidences found.

More recently, Schmidt et al. [20] reported a very high yield of 1,2-PDO (94 %) using Raney<sup>®</sup> Cu as catalyst in a continuous fixed bed reactor. According to the authors, continuous operation is preferred for its higher catalyst/feed ratio (offsetting the low specific activity of Cu based catalysts) and its ability to remove by-products such as water and CO<sub>2</sub>, thereby minimizing the equilibrium constraints which had led to low net batch yields.

Good yield of 1,2-PDO (69 %) was obtained using a Raney<sup>®</sup> Ni catalyst for the hydrogenolysis of glycerol, at 190 °C and 10 bar of H<sub>2</sub>, in the absence of solvent [21]. The only by-products detected were ethanol and CO<sub>2</sub>.

Interestingly, Huang et al. [22] reported the glycerol hydrogenolysis in liquid and vapour phases over a Cu/ZnO/Al<sub>2</sub>O<sub>3</sub> catalyst. A 1,2-PDO selectivity of 92 % at 96 % glycerol conversion was achieved in vapour phase, at 190 °C and 6 bar of H<sub>2</sub>. Nevertheless, the liquid-phase hydrogenolysis required more severe conditions (200 °C and 50 bar of H<sub>2</sub>) and showed much lower yields of 1,2-PDO. In spite of lower yields, working in liquid phase instead of gas can greatly increase the economic viability of the process: (i) The required reaction volume is lower, which allows the reduction of the reactor dimensions, and (ii) the energy supply is also lower, since it is not necessary to evaporate the reaction solution.

In the glycerol hydrogenolysis to 1,2-PDO over co-precipitated CuO/MgO catalysts at 180 °C and 30 bar of H<sub>2</sub>, the glycerol conversion and the selectivity reached 72 % and 98 %, respectively [26]. The addition of a small amount of NaOH as base additive further increased the conversion to 82 % without a significant change in 1,2-PDO selectivity. The preparation method of co-precipitation led to smaller Cu and MgO particles sizes than those obtained using the impregnation method, which were more active for glycerol hydrogenolysis.

An extremely effective catalyst for glycerol hydrogenolysis to 1,2-PDO proved to be the highly dispersed Cu on a layered solid base, Cu<sub>0.4</sub>/Mg<sub>5.6</sub>Al<sub>2</sub>O<sub>8.6</sub> (99 % glycerol conversion and 97 % selectivity towards 1,2-PDO). They compared the activity of the catalyst synthesized by different methods and found a correlation between the Cu particle size and the activity: It was higher for smaller particle sizes. Moreover, their research showed a particular behaviour of the catalyst: A little amount of NaOH further

increased the activity without promoting the cleavage of C–C bonds and, therefore, without a loss of the selectivity towards 1,2-PDO. This suggests that, under these operating conditions, the hydrogenolysis of glycerol to 1,2-PDO proceeded through the three steps *dehydrogenation-dehydration-hydrogenation* mechanism.

Recently, our research group has integrated the glycerol hydrogenolysis and a new *in-situ* process to generate the required hydrogen: Catalytic transfer hydrogenation (CTH) using hydrogen donors [25,27,28]. The reaction was investigated over bimetallic Ni-Cu/Al<sub>2</sub>O<sub>3</sub> catalysts under inert atmosphere and using different hydrogen donor molecules. Formic acid proved to be the most effective one. The formation of a Ni–Cu alloy during the reduction of the catalyst decreased the active Ni ensemble size, and consequently promoted the selective hydrogenolysis of the C–O bond instead of the C–C bond hydrogenolysis. It was also observed that an optimum balance between the acid sites of the Al<sub>2</sub>O<sub>3</sub> support and the metal sites is necessary in order to maximize the yield of 1,2-PDO. Moreover, it was found that the use of hydrogen donors could lead to the use of milder reaction conditions [28], especially when catalysts active at temperatures lower than 180 °C are utilized.

This opened a new interesting field in glycerol hydrogenolysis. Under optimized operating conditions, a glycerol conversion of 90 % and a selectivity towards 1,2-PDO of 82 % were obtained [25].

## **2.2 Catalysts for the selective production of 1,3-PDO**

### **2.2.1 The required features of a heterogeneous catalyst**

As stated above, conventional monometallic noble metals show moderate selectivities towards 1,2-PDO, and negligible formation of 1,3-PDO. EG and other degradation products resulting from the C–C hydrogenolysis are also produced. The combination of noble metal catalysts with an appropriate amount of an acid or, more efficiently, of a base promotes the formation of 1,2-PDO from glycerol. As it has been described above, two main mechanisms have been proposed depending on whether the reaction is carried out under alkali (*dehydrogenation-dehydration-hydrogenation* mechanism in Fig. 2.1) or acid conditions (*dehydration-hydrogenation* mechanism in Fig. 2.2).

In order to promote the 1,3-PDO/1,2-PDO ratio, a catalyst showing high selectivity towards the C–O cleavage of the secondary hydroxy group of glycerol is

required. A better understanding of the reaction mechanism is, therefore, a key aspect to develop new active and selective catalytic systems.

An early patent of Celanese Corporation discussed the effect of  $\text{H}_2\text{WO}_4$  acid addition to the reaction medium in the production of 1,3-PDO from glycerol, using a homogeneous  $\text{Rh}(\text{CO})_2$  catalysts and 1,3-dimethyl-2-imidazolidinone (DMI) as solvent [29]. They suggested that  $\text{H}_2\text{WO}_4$  is not a mere protic acid and that it plays a relevant role in the reaction, because when it was replaced by  $\text{H}_2\text{SO}_4$  the formation of PDOs and 1-PO was limited. The effect of  $\text{H}_2\text{WO}_4$  was also studied by Chaminand et al. with a  $\text{Rh}/\text{C}$  catalyst [8], showing a 4 % yield of 1,3-PDO in sulfolane solution at 180 °C and 80 bar after 168 h reaction time (Table 2.2). In other works, a similar promotion of 1,3-PDO selectivity was observed when W- and Re-based homogeneous acids were added into the reaction medium [30,31].

However, the use of heterogeneous catalysts is preferred because it simplifies the separation and reuse of the catalyst after the reaction and allows direct interactions between the hydrogenation active metals and the acid promoters. Thus, the use of bi-functional catalysts, using Re or W oxides together with a hydrogenation active metal, has been investigated in the recent years. The main results reported using these catalytic systems are described in the following sections and are summarized in Tables 2.5 and 2.6, respectively.

### 2.2.2 Bi-functional catalysts based on Rhenium

Tomishige's group carried out a broad study regarding the addition of different oxophilic metals to  $\text{Rh}/\text{SiO}_2$  catalysts [32]. They found that Re, Mo and W enhanced the activity of the  $\text{Rh}/\text{SiO}_2$  catalyst in the aqueous phase glycerol hydrogenolysis. The best results were obtained with the addition of Re, which enhanced both the conversion of glycerol and the selectivity towards 1,3-PDO:  $\text{Rh}-\text{ReO}_x/\text{SiO}_2$  showed 37 times higher 1,3-PDO yield (11 %) than the monometallic  $\text{Rh}/\text{SiO}_2$  catalyst. The Extended X-Ray Absorption Fine Structure (EXAFS) results showed the presence of Re-O, Re-Re and, interestingly, direct Re-Rh bonds without oxygen atoms between species. Based on experimental results they suggested that the glycerol hydrogenolysis proceeds on the interface between Rh metal and partially reduced  $\text{ReO}_x$  clusters attached to Rh. In Fig. 2.4 the suggested structure of  $\text{Rh}-\text{ReO}_x/\text{SiO}_2$  is shown.

**Table 2.5** Glycerol hydrogenolysis over noble metal combined with Re oxide.

Catalyst	H <sub>2</sub> (bar)	Temp. (°C)	Glycerol/water/ catalyst (g)	Time (h)	Conv. (%)	Product selectivity (%)	Ref.
4% Rh-ReO <sub>x</sub> /SiO <sub>2</sub> (Re/Rh=0.9)	80	120	4/16/0.15	5	78	1,3-PDO (14), 1,2-PDO (38), 1-PO (35), 2-PO (12)	[32]
4% Ir-ReO <sub>x</sub> /SiO <sub>2</sub> (Re/Rh=1.8)+ H <sub>2</sub> SO <sub>4</sub>	80	120	4/1/0.15 + <sup>c</sup>	36	81	1,3-PDO (46), 1,2-PDO (4), 1-PO (41), 2-PO (6)	[33]
3% Ru-ReO <sub>x</sub> / SiO <sub>2</sub> (Re/Ru=0.9)	80	160	4.4/6.6/0.15	8	51	1,3-PDO (8), 1,2-PDO (49), 1-PO (26), 2-PO (6)	[34]
4% Rh-ReO <sub>x</sub> /C (Re/Rh=0.5)	34	120	<sup>b</sup>	4	14	1,3-PDO (10), 1,2-PDO (26), 1-PO (27), 2-PO (11)	[35]
6% Pt-5% ReO <sub>x</sub> /C sinterized	40	170	n.r.	8	45	1,3-PDO (29), 1,2-PDO (27), 1-PO (30), 2-PO (14)	[36]

Metal content and metal ratio in wt %, <sup>a</sup> Molar ratio, <sup>b</sup> 5 wt% glycerol/water, catalyst/reactant mass ratio=1/9, <sup>c</sup> H<sup>+</sup>/Ir=1.

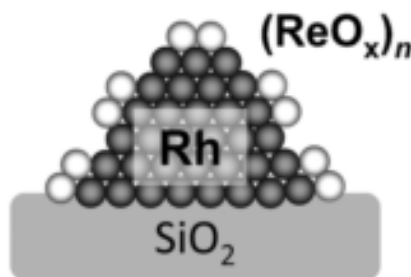


**Fig. 2.4.** Proposed structure of Rh-ReO<sub>x</sub>/SiO<sub>2</sub> catalyst [12].

Thereafter, the same group tested the effect of Re addition on Ir/SiO<sub>2</sub> catalysts [32,37] in aqueous phase glycerol hydrogenolysis. They found that the additive effect over Ir on the selectivity towards 1,3-PDO was much more pronounced than that observed over Rh. Using small amounts of H<sub>2</sub>SO<sub>4</sub> as homogeneous co-catalyst, a very significant 1,3-PDO yield of 38 % was reported [32]. Interestingly, the positive effect of H<sub>2</sub>SO<sub>4</sub> on the production of 1,3-PDO over the Ir-ReO<sub>x</sub>/SiO<sub>2</sub> catalyst was saturated at H<sup>+</sup>/Re = 1 (Fig. 2.5). Both activity and selectivity were almost unchanged between H<sup>+</sup>/Ir

= 1 and 12.4, indicating that the acidity did not promote the hydrogenolysis reaction and that *dehydration-hydrogenation* route via 3-HPA is minor over Ir–ReO<sub>x</sub>/SiO<sub>2</sub> catalyst.

Moreover, the relatively low reaction temperature used (120 °C) with this system suggested that a different mechanism is more plausible due to the endothermic character of the initial dehydration step. In base of the results, they proposed an energetically more favoured *direct hydrogenolysis mechanism*, which consisted on: (i) glycerol adsorption on the surface of ReO<sub>x</sub> cluster at the terminal position to form 2,3-dihydroxypropoxide (the more stable coordination mode of glycerol on Re species), (ii) hydrogen activation on the Ir-metal and hydride attack to the 2-position of the 2,3-dihydroxypropoxide to produce 3-hydroxypropoxide, or hydride attack to the 3-position forming 2-hydroxypropoxide, and, (iii) hydrolysis of 3-hydroxypropoxide and 2-hydroxypropoxide to give 1,3-PDO and 1,2-PDO, respectively.

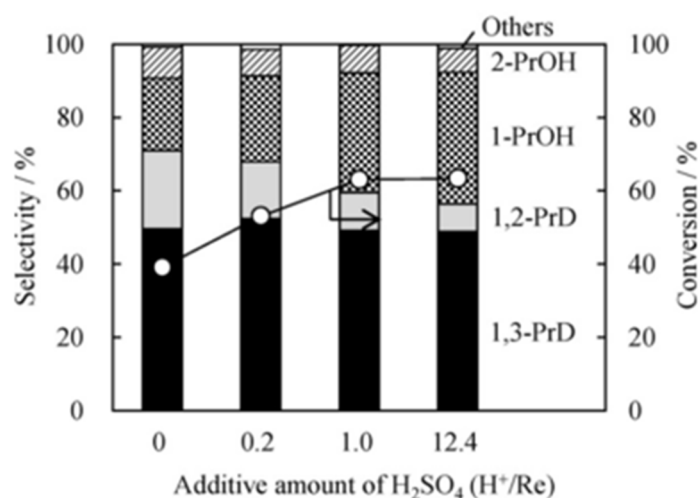


**Fig. 2.5.** Dependence of the glycerol hydrogenolysis over Ir–ReO<sub>x</sub>/SiO<sub>2</sub> (Re/Ir=1) on additive amount of H<sub>2</sub>SO<sub>4</sub> (conditions in Table 2.5) [37].

According to the authors, the key factors to obtain high 1,3-PDO selectivity could rely on: (i) the preferential terminal alkoxide formation during glycerol adsorption due to a steric effect induced by large Re clusters formation, and (ii) the higher formation of the 3-hydroxypropoxide via the more stable 6-membered-ring transition state in contrast to the unstable 7-membered-ring transition state for the formation of the 2-hydroxypropoxide. The proposed transition states can be observed in the Fig. 2.6.



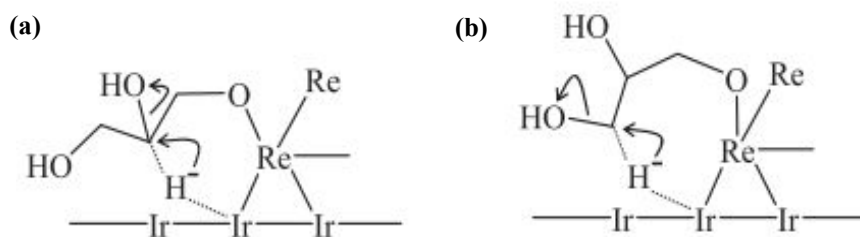


**Fig. 2.6.** Structures of the transition states: (a) 2,3-dihydroxypropoxide and (b) 1,3-dihydroxypropoxide formation and hydride attack proposed by Tomishige's group [37].

In another work, the catalytic performance of the bimetallic Ru-ReO<sub>x</sub>/SiO<sub>2</sub> was compared with that of monometallic Ru/SiO<sub>2</sub> catalyst in the hydrogenolysis of glycerol under 160 °C, and 80 bar of H<sub>2</sub> [34]. The incorporation of ReO<sub>x</sub> greatly promoted the glycerol conversion. However, ReO<sub>x</sub>/SiO<sub>2</sub> alone had almost no activity (< 2 % glycerol conversion). They found that the pre-treatment conditions had a great influence on the catalytic performance. High reduction temperatures promoted the particles sintering, decreasing the metals dispersion on the support, which in turn led to lower glycerol conversions. Under optimal reduction conditions they obtained a 4 % yield of 1,3-PDO, with 1,2-PDO still as the major reaction product.

An interesting work regarding C-O hydrogenolysis of polyols (glycerol among others) and cyclic-ethers derived from biomass over Rh-ReO<sub>x</sub>/C was carried out by Dumesic's group in 2011 [35]. The catalyst proved to be selective in the hydrogenolysis of secondary C-O bonds. In view of their results, it is clear that the position of the hydroxy group in the reactant molecule enormously affects its reactivity. Noteworthy, the results from density functional theory (DFT) suggested that hydroxy groups on Re atoms associated with Rh are acidic, which was confirmed by temperature-programmed desorption of NH<sub>3</sub> (TPD-NH<sub>3</sub>). These results are in good agreement with the previously suggested acid nature of hydroxy groups on Re [38]. Due to the oxophilic nature of Re, they form a strong binding with oxygen atoms and are the responsible for proton donation leading to the formation of carbenium ion transition states. Based on the experimental trends for polyols, they proposed a new *direct hydrogenolysis mechanism*, different from the one proposed by Tomishige's group, which consists on: (i) initial protonation-dehydration with the formation of a carbenium ion, catalysed by Brønsted acid sites, (ii) stabilisation of the carbenium ion through hydride transfer from primary-

CH<sub>2</sub>OH group leading to the formation of more stable oxocarbenium intermediates, and (iii) final hydride attack to the oxocarbenium ion. Fig. 2.7 displays the new proposed mechanism.

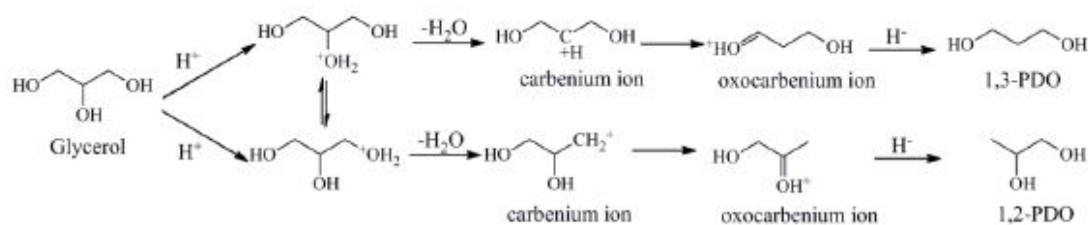


Fig. 2.7. Reaction mechanism for glycerol hydrogenolysis proposed by Dumesic's group, adapted from [39].

According to the results obtained in the hydrogenolysis of the diols studied (1,2- and  $\alpha,\omega$ -diols of C4-C6 compounds), 1,2-diols were more reactive than  $\alpha,\omega$ -diols and the hydrogenolysis of the secondary hydroxy group was significantly higher, leading mainly to the formation of the corresponding primary alcohol. They correlated this higher reactivity with the intermediate formation of the more stable secondary carbocation over the primary one.

Daniel et al. [36] combined Pt and ReO<sub>x</sub> supported on C (Pt-ReO<sub>x</sub>/C) and also found a promoting effect of Re in the selective production of 1,3-PDO from glycerol. The best result (13 % yield of 1,3-PDO) was obtained with a catalyst synthesized at elevated temperatures (700 °C), which resulted in a better atomic mixing of the Pt and Re components without severely decreasing the metals dispersion. Regarding the role of the oxophilic ReO<sub>x</sub> clusters, Daniel et al. proposed that they might facilitate the glycerol hydrogenolysis by the direct activation of a C-OH bond. This suggestion differs from the role as glycerol anchoring sites proposed by Tomishige's group [32].

In spite of the quite high selectivities towards 1,3-PDO reported, the use of ReO<sub>x</sub> shows some drawbacks: (i) They are frequently reduced from +7 to an average valence  $\leq +4$  in presence of noble metal at certain temperatures (during the reduction and/or the reaction), greatly changing its morphology, and (ii) some Re oxide species, such as Re<sub>2</sub>O<sub>7</sub>, are very soluble on water, which compromises its stability and reusability [40].

### 2.2.3 Bi-functional catalyst based on Tungsten

Supported heteropoly acids have been used in several industrial processes mainly related to catalytic oxidation reactions [41,42]. Recently, heteropoly acids have been tested in other catalytic reactions, such as glycerol hydrogenolysis. They possess

unique physicochemical properties, such as a very strong Brønsted acidity and redox properties, which can be tuned by varying their loadings [43]. Keggin type structure heteropoly acids are used in the majority of the applications. In general, the Keggin structure consists of heteropoly anions of the formula  $[\text{XM}_{12}\text{O}_{40}]^{n-}$ , where X is the heteroatom ( $\text{P}^{5+}$ ,  $\text{Si}^{4+}$ , etc.) and M is the added atom ( $\text{Mo}^{6+}$ ,  $\text{W}^{6+}$ , etc.). The crystal structure is based on a central tetrahedron  $\text{XO}_4$  surrounded by 12 edge- and corner-sharing metal-oxygen octahedral  $\text{MO}_6$  as it is shown in Fig. 2.8.

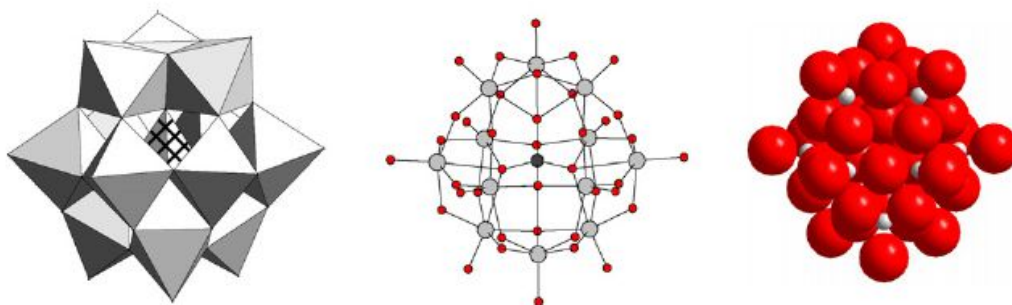


**Fig. 2.8.** The structure of the Keggin heteropoly anion  $[\alpha\text{-XM}_{12}\text{O}_{40}]^{n-}$  in polyhedral (left), ball-and-stick (middle) and space-filling (right) representations [43].

Zhu et al. [44] combined the use of the Cu metal with an heteropoly acid containing  $\text{W}^{6+}$ , 12-tungstosilicic acid,  $\text{H}_4\text{SiW}_{12}\text{O}_{40}$  (HSiW), supported on  $\text{SiO}_2$  for the glycerol hydrogenolysis in vapour phase. Under the optimized operating conditions (see Table 2.6) a very high glycerol conversion of 83 % and moderate selectivities to PDOs (32 % and 22 % to 1,3-PDO and 1,2-PDO, respectively) were obtained. In spite of the good results, evaporation of glycerol is energy-consuming and the liquid-phase catalytic process is preferred.

The same group investigated the glycerol hydrogenolysis in aqueous phase using Pt-HSiW/ $\text{SiO}_2$  type catalysts [45]. The catalysts were prepared by impregnation of Pt/ $\text{SiO}_2$  catalysts with aqueous solutions containing the desired amount of HSiW. CO-chemisorption measurements showed that low loadings of HSiW (until 15 wt %) promoted the Pt dispersion, whereas at higher HSiW contents a partial covering of the Pt metal surface with HSiW occurred, decreasing Pt dispersion and, therefore, the glycerol conversion. The HSiW content of 15 wt % proved to be the most efficient, probably due to the combination of a good Pt dispersion and an optimum acidity. Higher HSiW loadings could provide an excess of total acidity but in exchange for a decrease on Pt dispersion. Interestingly, the incorporation of HSiW to the Pt/ $\text{SiO}_2$  catalyst increased the number of acid sites, mainly strong Brønsted acid sites which it

was reported that play a key role in the dehydration of glycerol to 3-HPA [46,47], which could be subsequently hydrogenated to form 1,3-PDO (according to *dehydration-hydrogenation* mechanism) or further dehydrated to produce acrolein, the precursor of 1-PO.

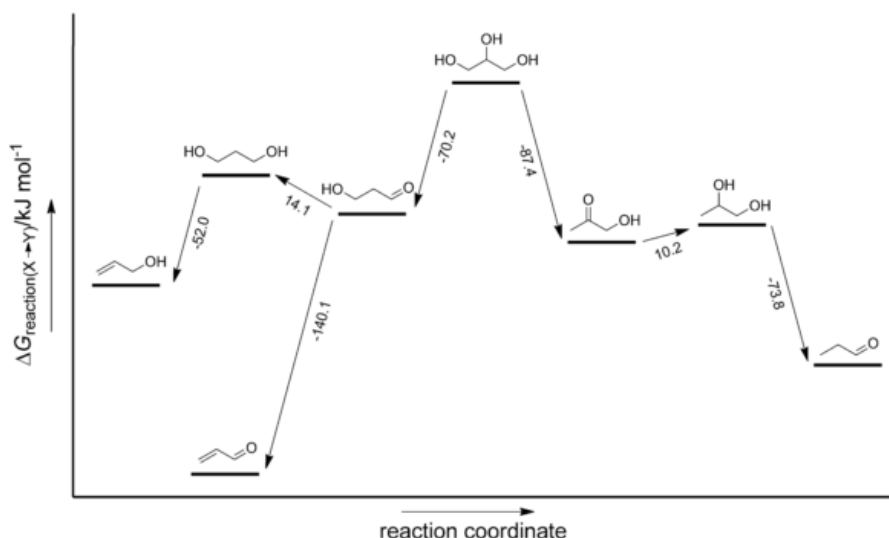
**Table 2.6** Glycerol hydrogenolysis over noble metal combined with W.

Catalyst	H <sub>2</sub> (bar)	Temp. (°C)	Glycerol/water/ catalyst (g)	Time (h)	Conv. (%)	Product selectivity (%)	Ref.
10%Cu-15%HSiW/ SiO <sub>2</sub>	5.4	210	<sup>a</sup>	24	83	1,3-PDO (32), 1,2- PDO (22)	[44]
2%Pt-15%HSiW/ SiO <sub>2</sub>	50	200	<sup>b</sup>	24	81	1,3-PDO (39)	[45]
2% Pt/WO <sub>3</sub> /ZrO <sub>2</sub> (wt% W/Pt= 8)	80	170	0.28/0.21 <sup>c</sup> /0.1	18	n.r.	1,3-PDO (24) <sup>d</sup> , 1,2- PDO (13) <sup>d</sup> , 1-PO (28) <sup>d</sup>	[48]
3%Pt/WO <sub>3</sub> /ZrO <sub>2</sub> (wt% W/Pt= 3.3)	40	130	<sup>e</sup> / <sup>f</sup>	24	70	1,3-PDO (46), 1,2- PDO (3)	[39]
2%Pt/WO <sub>3</sub> /TiO <sub>2</sub> /SiO <sub>2</sub> (wt% W/Pt=1.3; wt %Ti/Pt=2)	55	180	4/37 <sup>f</sup>	12	15	1,3-PDO (51), 1,2- PDO (9), 1-PO (25), 2-PO (8)	[49]
5%Pt-WO <sub>3</sub> /Al <sub>2</sub> O <sub>3</sub> (wt% W/Pt= 1)	30	160	12/121/4	3	20	1,3-PDO (67), 1,2- PDO (4)	[31]
2%Pt/WO <sub>3</sub> / "AlO(OH)" (wt% W/Pt= 2)	50	180	0.09/3/0.1	12	100	1,3-PDO (66), 1,2- PDO (2), 1-PO (11), 2-PO (6)	[50]

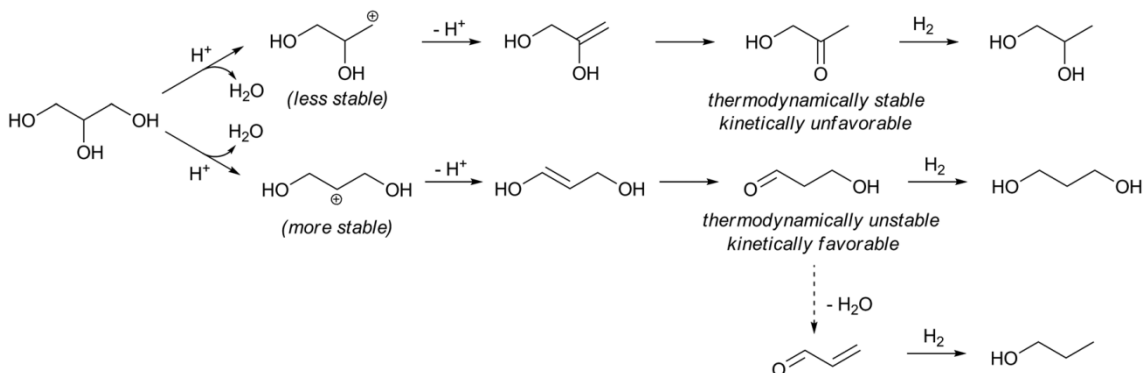
Metal content and metal ratio in wt %, <sup>a</sup> WHSV= 0.08 h<sup>-1</sup>, H<sub>2</sub>/glycerol molar ratio = 144, <sup>b</sup> WHSV= 0.045 h<sup>-1</sup>, H<sub>2</sub>/glycerol molar ratio = 137, <sup>c</sup> DMI solvent, <sup>d</sup> Product yield, <sup>e</sup> 60 wt% glycerol/water, feed rate = 0.5 mL h<sup>-1</sup>, H<sub>2</sub>/glycerol molar ratio = 0.12, <sup>f</sup> 2mL catalyst.

Fig. 2.9 exemplifies the difficulties in achieving high 1,3-PDO selectivities: (i) From a thermodynamic point of view, the formation of acetol through glycerol dehydration is thermodynamically more favoured than the formation of 3-HPA, and (ii) whenever 3-HPA is formed, its dehydration to acrolein is also preferred over hydrogenation to 1,3-PDO. Thus, the formation of 1,3-PDO should be kinetically controlled [51,52]. According to this, the glycerol *dehydration-hydrogenation* mechanism was suggested to occur via cationic intermediates as shown in Fig. 2.10.

The secondary carbocation that leads to the formation of the 3-HPA intermediate is more stable than the primary carbocation that leads to the formation of acetol.



**Fig. 2.9.** Reaction energies for glycerol to 1,2-PDO, 1,3-PDO, acrolein and their possible intermediates (3-HPA and acetol) and degradation products, modified from [53].



**Fig. 2.10.** Glycerol dehydration-hydrogenation mechanism to PDOs formation via carbocation intermediates.

In view of the results obtained by Zhu et al. with Pt-HSiW/SiO<sub>2</sub>, the authors affirmed that Brønsted acid sites are indispensable to selectively transform glycerol into 1,3-PDO. At optimum reaction conditions, the optimized Pt-HSiW/SiO<sub>2</sub> catalyst showed a 31 % yield of 1,3-PDO (glycerol conversion of 81 % and selectivity towards 1,3-PDO of 39 %). They also tested Cu-HSiW/SiO<sub>2</sub> catalyst under the same conditions obtaining only 9 % of glycerol conversion and 1,3-PDO selectivity.

The use of heteropoly acids has become an interesting approach in the glycerol hydrogenolysis into 1,3-PDO. However, there are not enough evidences about its real

role in the selective production of 1,3-PDO. In addition, heteropoly acids usually possess low thermal stability which sometimes limits their catalytic applications.

The incorporation of W oxides on a support together with an active hydrogenation metal is also a very effective approach. It is necessary to point out that some of the works cited in this section were published after the start of current Thesis, at the end of 2012.

The use of W oxides is preferred over that of Re oxides, because it avoids most of the main problems of stability associated to the use of Re oxides (described in the previous section 2.2.2). Unlike the Re oxides, W oxides are almost insoluble. In addition to this, significantly higher temperatures are required to reduce W oxide species. Thus, more robust and stable W-based catalytic systems appear as a better option.

In the work published by Kurosaka et al. [48] in 2008, catalysts containing Pt noble metal and  $\text{WO}_3$  were prepared on different supports (HY,  $\text{TiO}_2$ ,  $\text{Al}_2\text{O}_3$ ,  $\text{SiO}_2$ - $\text{Al}_2\text{O}_3$ ,  $\text{ZrO}_2$  and AlMCM-41) and tested in the glycerol hydrogenolysis using DMI as solvent. All the supports tested gave 1,2-PDO and 1,3-PDO in yields higher than 6 %, but the best result was obtained when  $\text{ZrO}_2$  was used as support: 1,3-PDO yield of 24 % with a 1,3-PDO/1,2-PDO molar ratio of about 2, under 170 °C, 80 bar of  $\text{H}_2$  and 18 h reaction time. However, 1-PO and 2-PO formation was also very high (27 % yield), probably because of the over-hydrogenolysis of PDOs. According to the X-ray diffraction (XRD) results of different catalysts, those which showed peaks related to Pt and  $\text{WO}_3$  gave PDOs in lower yields (<11%). These results highlight the importance of the high dispersion of both Pt and  $\text{WO}_3$  for the effective glycerol hydrogenolysis to PDOs. They also investigated other noble metals like Pt, Pd, Rh, Ru and Ir supported on  $\text{WO}_3/\text{ZrO}_2$  and concluded that metal dispersion (no peaks of metals detected in XRD) was not the responsible of the different catalytic behaviour but the metal type itself. The most active one was Pt.

In order to elucidate the role of Pt,  $\text{WO}_3$  and the  $\text{ZrO}_2$  support in the reaction, different catalysts were prepared and tested. For this purpose, Pt/ $\text{ZrO}_2$ , Pt/ $\text{WO}_3$  or  $\text{WO}_3/\text{ZrO}_2$  catalyst, prepared through conventional wetness impregnation, and co-impregnated Pt- $\text{WO}_3$  over  $\text{ZrO}_2$ , were tested in the reaction and compared with the results obtained with Pt/ $\text{WO}_3/\text{ZrO}_2$  catalyst. None of the new catalytic systems catalysed the reaction efficiently (yields of PDOs < 13 %). In view of these results, they

concluded that Pt/WO<sub>3</sub>/ZrO<sub>2</sub> is not a mere bi-functional catalyst and the active sites for the hydrogenolysis of glycerol to 1,3-PDO may be only on this catalyst conformation.

The weakness of the previous study was the use of a polar organic solvent, DMI, since it reduces the environmental and economic viability of the process. As it was mentioned above, water appears as the best green solvent.

In this context, Qin et al. [39] reported the use of the same kind of catalyst, Pt/WO<sub>3</sub>/ZrO<sub>2</sub>, in the aqueous phase glycerol hydrogenolysis using a fixed-bed continuous flow reactor. A high 1,3-PDO yield of 32 % and very high 1,3-PDO/1,2-PDO molar ratio of 18 were reported. Product distribution and glycerol conversion varied with the catalyst composition, catalysts pre-treatment, and the reaction conditions. As the Pt content increased (from 1 to 4 wt %) glycerol conversion greatly increased (from 14 % to 84 %). Regarding product distribution, 1,2-PDO selectivity remained very low in any case but 1,3-PDO increased with increasing Pt and reached a maximum at a Pt content of 3 wt %. For higher contents, the selectivity towards 1-PO increased remarkably at expense of the 1,3-PDO formation. These results indicate that an excess of Pt content promotes the over hydrogenolysis of PDOs to 1-PO. The effect of the amount of W (from 5 to 15 wt %) was also studied.

The maximum glycerol conversion and 1,3-PDO yield was found at a W content of 10 wt %, which is slightly higher than the theoretical monolayer of WO<sub>x</sub> on ZrO<sub>2</sub>. This term is defined as the maximum theoretical amount of the two-dimensional tungsten (in this case) in contact with the oxide support [54]. The TPD-NH<sub>3</sub> results were in agreement with previous reports in which the acidity of WO<sub>x</sub>/ZrO<sub>2</sub> catalysts increased with the WO<sub>x</sub> loading up to the monolayer coverage [55]. The increase of H<sub>2</sub> pressure provided a positive effect on the glycerol hydrogenolysis to 1,3-PDO and 1-PO, which might be due to the increase in the concentration of protons and hydride ions formed through the activation and spillover of H<sub>2</sub> on the Pt active sites.

Gong et al. [49] investigated the glycerol hydrogenolysis over Pt/WO<sub>3</sub>/TiO<sub>2</sub>/SiO<sub>2</sub> catalysts obtaining 1,3-PDO in a yield of 8 % and a 1,3-PDO/1,2-PDO molar ratio of 5. The main contribution of this work was the elucidation of the role of TiO<sub>2</sub> promoting the Pt dispersion, as shown by XRD patterns and transmission electron microscopy (TEM) images. The TPD-NH<sub>3</sub> and Fourier transform infrared spectroscopy (FTIR) of adsorbed pyridine results showed that WO<sub>3</sub> species improved the acidity of the catalyst, providing mainly weak Brönsted acid sites, which played a key role in the selective formation of 1,3-PDO.

In the patent of Suzuki et al. [31] of KAO Corporation an impressive selectivity towards 1,3-PDO of 67 % at 20 % glycerol conversion was reported. The catalyst used was Pt-WO<sub>3</sub>/Al<sub>2</sub>O<sub>3</sub> prepared by impregnation of a commercial Pt/Al<sub>2</sub>O<sub>3</sub> with a salt containing W. The good selectivity result, the best until that date, inspired us to design and study new catalytic systems based on Pt, WO<sub>x</sub> and Al<sub>2</sub>O<sub>3</sub>.

However, by far the highest yield of 1,3-PDO reported to date was recently obtained by Kaneda et al. [50] using Pt and WO<sub>3</sub> supported on “boehmite” catalyst (denoted as Pt/WO<sub>3</sub>/AlO(OH)). This value was 66 % at complete glycerol conversion, at 180 °C, 50 bar of H<sub>2</sub> and after 12 h reaction time. In a previous work carried out by the same group they developed a Pt-AlO<sub>x</sub>/WO<sub>3</sub> catalyst (AlO<sub>x</sub> added to Pt/WO<sub>3</sub>) for the selective hydrogenolysis of glycerol to 1,3-PDO in water, achieving also high 1,3-PDO yields (41 %) [56]. They proposed a plausible reaction mechanism, which is shown in Fig. 2.11.

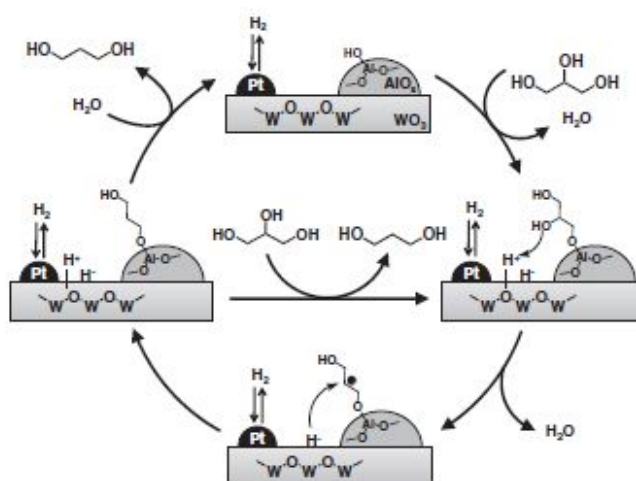


Fig. 2.11. Reaction mechanism proposed by Arundhati et al. [56] over Pt-AlO<sub>x</sub>/WO<sub>3</sub> catalyst.

According to this reaction mechanism, glycerol is adsorbed on the AlO<sub>x</sub> surface forming a primary alkoxide. Protonation of a secondary hydroxy group of the alkoxide and successive dehydration give a secondary carbocation, which is quickly attacked by a hydride specie generated through the activation of H<sub>2</sub> on Pt metal sites and hydrogen spillover onto the WO<sub>3</sub> surface. Further hydrolysis yields 1,3-PDO. In spite of the extraordinary results obtained, the hypothesis postulated by the authors is not totally reliable. They attributed the high yield to the plentiful Al–OH groups in the boehmite support which would promote the formation of Al-alkoxide species. However, the high temperatures used in the catalyst pre-treatment (800 °C) and the XRD results indicate a



different alumina structure than boehmite (possibly  $\gamma$ -Al<sub>2</sub>O<sub>3</sub>) and therefore the absence of many hydroxy groups. The authors did not explain why Pt and Al work much better than other elements. Other noble metals can similarly activate H<sub>2</sub>, and many metal cations can form an alkoxide structure. Furthermore, the formation of Al-alkoxide is not proved in this work and the W-alkoxide formation should not be excluded.

### **2.3 Conclusion and outlook**

There is a considerable research dealing with the catalytic conversion of glycerol to 1,2-PDO in which high yields (> 95 %) have been reported, using typically bi-functional systems formed by a hydrogenation metal and an acid or a base as additive. Nevertheless, the selective production of 1,3-PDO is more challenging. The control of the 1,3-PDO/1,2-PDO ratio, which requires highly selective C–O cleavage of the primary or secondary hydroxy groups of glycerol, is strongly dependent on the catalyst used. Thus, there is a need for the development and understanding of new selective catalytic systems in order to obtain the more valuable 1,3-PDO. From an economic and environmental point of view, glycerol hydrogenolysis in liquid phase using water as solvent is the best choice since biodiesel-derived glycerol is obtained in aqueous phase through the transesterification of vegetable oils, and since water is also formed as a product during the hydrogenolysis reactions.

The combination of a highly reducible noble metal with an oxophilic metal (mainly Re or W) has opened the window to a new class of bi-functional heterogeneous catalysts for the selective C–O hydrogenolysis of glycerol to the high added-value 1,3-PDO. These kinds of catalysts can also be applied for other deoxygenation process of biomass derived building blocks. A precise control of the catalyst structure, such as the selection of the noble metal, the modifier and support, the control of particle size and metal dispersion, the structure of the modifier, and the acidity, among other factors, are totally necessary.

In spite of the intense work carried out, the overall reaction mechanism of PDOs formation over those catalysts still remains unclear. The most frequently proposed mechanism is the two-step *dehydration-hydrogenation* route, via acetol or 3-HPA intermediates for the 1,2-PDO and 1,3-PDO production, respectively. However, other *direct mechanisms* have been proposed in which different alkoxide and carbocationic species are formed. The great deal of controversy about fundamental reaction

parameters, such as the role of the oxophilic metal in the binding of glycerol, the intermediate species generated and the effect of noble metal and oxophilic metal interactions, has encouraged us to carry out a deeper study of the catalytic system formed by Pt, WO<sub>x</sub> and Al<sub>2</sub>O<sub>3</sub>, which was reported to be effective in the selective production of 1,3-PDO from glycerol.

## References

- [1] M.A. Dasari, P.P. Kiatsimkul, W.R. Sutterlin, G.J. Suppes, Low-pressure hydrogenolysis of glycerol to propylene glycol, *Appl. Catal. A Gen.* 281 (2005) 225–231.
- [2] T. Miyazawa, S. Koso, K. Kunimori, K. Tomishige, Development of a Ru/C catalyst for glycerol hydrogenolysis in combination with an ion-exchange resin, *Appl. Catal. A Gen.* 318 (2007) 244–251.
- [3] C. Montassier, J.C. Ménézo, J. Moukolo, J. Naja, L.C. Hoang, J. Barbier, et al., Polyol conversions into furanic derivatives on bimetallic catalysts: Cu-Ru, Cu-Pt and Ru-Cu, *J. Mol. Catal.* 70 (1991) 65–84.
- [4] J. Feng, H. Fu, J. Wang, R. Li, H. Chen, X. Li, Hydrogenolysis of glycerol to glycols over ruthenium catalysts: Effect of support and catalyst reduction temperature, *Catal. Commun.* 9 (2008) 1458–1464.
- [5] I. Furikado, T. Miyazawa, S. Koso, A. Shima, K. Kunimori, K. Tomishige, Catalytic performance of Rh/SiO<sub>2</sub> in glycerol reaction under hydrogen, *Green Chem.* 9 (2007) 582.
- [6] C. Montassier, D. Giraud, J. Barbier, Polyol Conversion by Liquid Phase Heterogeneous Catalysis Over Metals, *Heterog. Catal. Fine Chem. an Int. Symp.* 41 (1988) 165–170.
- [7] M. Balaraju, V. Rekha, P.S.S. Prasad, B.L. a P. Devi, R.B.N. Prasad, N. Lingaiah, Influence of solid acids as co-catalysts on glycerol hydrogenolysis to propylene glycol over Ru/C catalysts, *Appl. Catal. A Gen.* 354 (2009) 82–87.
- [8] J. Chaminand, L. auren. Djakovitch, P. Gallezot, P. Marion, C. Pinel, C. Rosier, Glycerol hydrogenolysis on heterogeneous catalysts, *Green Chem.* 6 (2004) 359.
- [9] I. Gandarias, P.L. Arias, J. Requies, M.B. Güemez, J.L.G. Fierro, Hydrogenolysis of glycerol to propanediols over a Pt/ASA catalyst: The role of acid and metal sites on product selectivity and the reaction mechanism, *Appl. Catal. B Environ.* 97 (2010) 248–256.
- [10] Y. Kusunoki, T. Miyazawa, K. Kunimori, K. Tomishige, Highly active metal-acid bifunctional catalyst system for hydrogenolysis of glycerol under mild reaction conditions, *Catal. Commun.* 6 (2005) 645–649.
- [11] M. Y. Nakagawa, T. and K. Tomishige, Catalytic materials for the hydrogenolysis of glycerol to 1,3-propanediol, *J. Mater. Chem. A.* 2 (2014) 6688–6702.
- [12] Y. Nakagawa, K. Tomishige, Heterogeneous catalysis of the glycerol hydrogenolysis, *Catal. Sci. Technol.* 1 (2011) 179.
- [13] I. Gandarias, P.L. Arias, Hydrotreating Catalytic Processes for Oxygen Removal in the Upgrading of Bio-Oils and Bio-Chemicals, in: Z. Fang (Ed.), *Liq. Gaseous Solid Biofuels - Convers. Tech.*, 1st ed., InTech, 2013.
- [14] J. Feng, J. Wang, Y. Zhou, H. Fu, H. Chen, X. Li, Effect of Base Additives on the Selective Hydrogenolysis of Glycerol over Ru/TiO<sub>2</sub> Catalyst, *Chem. Lett.* 36 (2007) 1274–1275.
- [15] E.P. Maris, W.C. Ketchie, M. Murayama, R.J. Davis, Glycerol hydrogenolysis on carbon-supported PtRu and AuRu bimetallic catalysts, *J. Catal.* 251 (2007) 281–294.
- [16] Z. Yuan, P. Wu, J. Gao, X. Lu, Z. Hou, X. Zheng, Pt/Solid-Base: A Predominant Catalyst for Glycerol Hydrogenolysis in a Base-Free Aqueous Solution, *Catal. Letters.* 130 (2009) 261–265.

- [17] E. D'Hondt, S. Van de Vyver, B.F. Sels, P. a Jacobs, Catalytic glycerol conversion into 1,2-propanediol in absence of added hydrogen., *Chem. Commun.* (2008) 6011–6012.
- [18] E.P. Maris, R.J. Davis, Hydrogenolysis of glycerol over carbon-supported Ru and Pt catalysts, *J. Catal.* 249 (2007) 328–337.
- [19] C.A. Ramírez-López, J.R. Ochoa-Gómez, M. Fernández-Santos, O. Gómez-Jiménez-Aberasturi, A. Alonso-Vicario, J. Torrecilla-Soria, Synthesis of lactic acid by alkaline hydrothermal conversion of glycerol at high glycerol concentration, *Ind. Eng. Chem. Res.* 49 (2010) 6270–6278.
- [20] S. Schmidt, S. Tanielyan, N. Marin, G. Alvez, R. Augustine, Selective Conversion of Glycerol to Propylene Glycol Over Fixed Bed Raney® Cu Catalysts, *Top. Catal.* 53 (2010) 1214–1216.
- [21] A. Perosa, P. Tundo, Selective hydrogenolysis of glycerol with raney nickel, *Ind. Eng. Chem. Res.* 44 (2005) 8535–8537.
- [22] L. Huang, Y.-L. Zhu, H.-Y. Zheng, Y.-W. Li, Z.-Y. Zeng, Continuous production of 1,2-propanediol by the selective hydrogenolysis of solvent-free glycerol under mild conditions, *J. Chem. Technol. Biotechnol.* 83 (2008) 1670–1675.
- [23] Z. Yuan, J. Wang, L. Wang, W. Xie, P. Chen, Z. Hou, et al., Biodiesel derived glycerol hydrogenolysis to 1,2-propanediol on Cu/MgO catalysts, *Bioresour. Technol.* 101 (2010) 7088–7092.
- [24] Z. Yuan, L. Wang, J. Wang, S. Xia, P. Chen, Z. Hou, et al., Hydrogenolysis of glycerol over homogenously dispersed copper on solid base catalysts, *Appl. Catal. B Environ.* 101 (2011) 431–440.
- [25] I. Gandarias, J. Requies, P.L. Arias, U. Armbruster, A. Martin, Liquid-phase glycerol hydrogenolysis by formic acid over Ni-Cu/Al<sub>2</sub>O<sub>3</sub> catalysts, *J. Catal.* 290 (2012) 79–89.
- [26] Z. Yuan, J. Wang, L. Wang, W. Xie, P. Chen, Z. Hou, et al., Biodiesel derived glycerol hydrogenolysis to 1,2-propanediol on Cu/MgO catalysts., *Bioresour. Technol.* 101 (2010) 7099–103.
- [27] I. Gandarias, P.L. Arias, S.G. Fernández, J. Requies, M. El Doukkali, M.B. Güemez, Hydrogenolysis through catalytic transfer hydrogenation: Glycerol conversion to 1,2-propanediol, *Catal. Today.* 195 (2012) 22–31.
- [28] I. Gandarias, S.G. Fernández, M. El Doukkali, J. Requies, P.L. Arias, Physicochemical Study of Glycerol Hydrogenolysis Over a Ni-Cu/Al<sub>2</sub>O<sub>3</sub> Catalyst Using Formic Acid as the Hydrogen Source, *Top. Catal.* 56 (2013) 995–1007.
- [29] T.M. Che, Production of propanediols, US 4,642,394, 1987.
- [30] L. Ma, D. He, Z. Li, Promoting effect of rhenium on catalytic performance of Ru catalysts in hydrogenolysis of glycerol to propanediol, *Catal. Commun.* 9 (2008) 2489–2495.
- [31] N. Suzuki, Y. Yoshikawa, M. Takahashi, M. Tamura, Process fro producing product of hydrogenolysis of polyhydric alcohol, US 7,799,957 B2, 2010.
- [32] Y. Shinmi, S. Koso, T. Kubota, Y. Nakagawa, K. Tomishige, Modification of Rh/SiO<sub>2</sub> catalyst for the hydrogenolysis of glycerol in water, *Appl. Catal. B Environ.* 94 (2010) 318–326.
- [33] Y. Nakagawa, Y. Shinmi, S. Koso, K. Tomishige, Direct hydrogenolysis of glycerol into 1,3-

- propanediol over rhenium-modified iridium catalyst, *J. Catal.* 272 (2010) 191–194.
- [34] L. Ma, D. He, Influence of catalyst pretreatment on catalytic properties and performances of Ru-Re/SiO<sub>2</sub> in glycerol hydrogenolysis to propanediols, *Catal. Today.* 149 (2010) 148–156.
- [35] M. Chia, Y.J. Pagán-Torres, D. Hibbitts, Q. Tan, H.N. Pham, A.K. Datye, et al., Selective Hydrogenolysis of Polyols and Cyclic Ethers over Bifunctional Surface Sites on Rhodium–Rhenium Catalysts, *J. Am. Chem. Soc.* 133 (2011) 12675–12689.
- [36] O.M. Daniel, A. Delariva, E.L. Kunkes, A.K. Datye, J. a. Dumesic, R.J. Davis, X-ray Absorption Spectroscopy of Bimetallic Pt-Re Catalysts for Hydrogenolysis of Glycerol to Propanediols, *ChemCatChem.* 2 (2010) 1107–1114.
- [37] Y. Amada, Y. Shinmi, S. Koso, T. Kubota, Y. Nakagawa, K. Tomishige, Reaction mechanism of the glycerol hydrogenolysis to 1,3-propanediol over Ir-ReO<sub>x</sub>/SiO<sub>2</sub> catalyst, *Appl. Catal. B Environ.* 105 (2011) 117–127.
- [38] D.L. King, L. Zhang, G. Xia, A.M. Karim, D.J. Heldebrant, X. Wang, et al., Aqueous phase reforming of glycerol for hydrogen production over Pt-Re supported on carbon, *Appl. Catal. B Environ.* 99 (2010) 206–213.
- [39] L.-Z. Qin, M.-J. Song, C.-L. Chen, Aqueous-phase deoxygenation of glycerol to 1,3-propanediol over Pt/WO<sub>3</sub>/ZrO<sub>2</sub> catalysts in a fixed-bed reactor, *Green Chem.* 12 (2010) 1466.
- [40] L. Zhang, A.M. Karim, M.H. Engelhard, Z. Wei, D.L. King, Y. Wang, Correlation of Pt-Re surface properties with reaction pathways for the aqueous-phase reforming of glycerol, *J. Catal.* 287 (2012) 37–43.
- [41] N. Mizuno, M. Misono, Heterogeneous catalysis., *Chem. Rev.* 98 (1998) 199–217.
- [42] I. V. Kozhevnikov, Catalysis by heteropoly acids and multicomponent polyoxometalates in liquid-phase reactions, *Chem. Rev.* 98 (1998) 171–198.
- [43] I. V Kozhevnikov, Sustainable heterogeneous acid catalysis by heteropoly acids, *J. Mol. Catal. A Chem.* 262 (2007) 86–92.
- [44] L. Huang, Y. Zhu, H. Zheng, G. Ding, Y. Li, Direct conversion of glycerol into 1,3-propanediol over Cu-H<sub>4</sub>SiW<sub>12</sub>O<sub>40</sub>/SiO<sub>2</sub> in vapor phase, *Catal. Letters.* 131 (2009) 312–320.
- [45] S. Zhu, Y. Qiu, Y. Zhu, S. Hao, H. Zheng, Y. Li, Hydrogenolysis of glycerol to 1,3-propanediol over bifunctional catalysts containing Pt and heteropolyacids, *Catal. Today.* 212 (2013) 120–126.
- [46] A. Alhanash, E.F. Kozhevnikova, I. V. Kozhevnikov, Gas-phase dehydration of glycerol to acrolein catalysed by caesium heteropoly salt, *Appl. Catal. A Gen.* 378 (2010) 11–18.
- [47] F. Cavani, S. Guidetti, L. Marinelli, M. Piccinini, E. Ghedini, M. Signoretto, The control of selectivity in gas-phase glycerol dehydration to acrolein catalysed by sulfated zirconia, *Appl. Catal. B Environ.* 100 (2010) 197–204.
- [48] T. Kurosaka, H. Maruyama, I. Naribayashi, Y. Sasaki, Production of 1,3-propanediol by hydrogenolysis of glycerol catalyzed by Pt/WO<sub>3</sub>/ZrO<sub>2</sub>, *Catal. Commun.* 9 (2008) 1360–1363.
- [49] L. Gong, Y. Lu, Y. Ding, R. Lin, J. Li, W. Dong, et al., Selective hydrogenolysis of glycerol to 1,3-propanediol over a Pt/WO<sub>3</sub>/TiO<sub>2</sub>/SiO<sub>2</sub> catalyst in aqueous media, *Appl. Catal. A Gen.* 390 (2010) 119–126.
- [50] R. Arundhathi, T. Mizugaki, T. Mitsudome, K. Jitsukawa, K. Kaneda, Highly selective

- hydrogenolysis of glycerol to 1,3-propanediol over a boehmite-supported platinum/tungsten catalyst, *ChemSusChem*. 6 (2013) 1345–1347.
- [51] J. Tendam, U. Hanefeld, Renewable chemicals: Dehydroxylation of glycerol and polyols, *ChemSusChem*. 4 (2011) 1017–1034.
- [52] J. TenDam, K. Djanashvili, F. Kapteijn, U. Hanefeld, Pt/Al<sub>2</sub>O<sub>3</sub> Catalyzed 1,3-Propanediol Formation from Glycerol using Tungsten Additives, *ChemCatChem*. 5 (2013) 497–505.
- [53] M.R. Nimlos, S.J. Blanksby, X. Qian, M.E. Himmel, D.K. Johnson, Mechanisms of Glycerol Dehydration, *J. Phys. Chem. A*. 110 (2006) 6145–6156.
- [54] I.E. Wachs, B.M. Weckhuysen, Structure and reactivity of surface vanadium oxide species on oxide supports, *Appl. Catal. A Gen.* 157. 157 (1997) 67–90.
- [55] C.D. Baertsch, K.T. Komala, Y. Chua, E. Iglesia, Genesis of Brønsted Acid Sites during Dehydration of 2-Butanol on Tungsten Oxide Catalysts, *J. Catal.* 57 (2002) 44–57.
- [56] T. Mizugaki, T. Yamakawa, R. Arundhati, T. Mitsudome, K. Jitsukawa, K. Kaneda, Selective hydrogenolysis of glycerol to 1,3-propanediol catalyzed by Pt nanoparticles-AlO<sub>x</sub>/WO<sub>3</sub>, *Chem. Lett.* 41 (2012) 1720–1722.



## **CHAPTER 3.**

### **Objectives and scope of the thesis**





In the Chapter 1 of the present Ph.D Thesis, some evidences were provided in order to show that a progressive transition from a petroleum-based towards a bio-based economy is completely required in order to achieve a more sustainable society. As it was stated in the Chapter 2, special attention has recently been devoted to a particular transformation process of biomass into marketable commodity chemicals: the hydrogenolysis of biomass-derived polyols.

The main objective of the current PhD Thesis is the **development of advanced catalytic systems for the selective hydrogenolysis of biomass-derived polyols**. This work aims to have an academic interest, being useful for the scientific community, and serve as a contribution in the field of green chemistry and sustainable engineering, and especially in the field of hydrogenolysis reactions.

For this research, the **aqueous glycerol hydrogenolysis to propanediols** was selected as a model reaction. From an economic and environmental standpoint, the use of water as solvent is the best choice since the bio-glycerol obtained through the transesterification of vegetable oils is obtained in aqueous phase, and since water is always a by-product in the hydrogenolysis reactions. It should not be overlooked that the conclusions and advances achieved in this process could be applied to the valorisation of the more complicated biomass-derived polyols, structurally “analogous” to glycerol, such as sorbitol or xylitol.

In order to achieve the main objective of this Thesis satisfactorily, some partial goals have to be fulfilled:

- Selection and development of highly active and selective catalytic systems in the C–O glycerol hydrogenolysis. The precise selection of the metal, the modifier as well as the support is totally necessary in order to develop an efficient catalyst. The promising results reported with catalytic systems formed by Pt, WO<sub>x</sub> and Al<sub>2</sub>O<sub>3</sub>, encouraged us to choice this system as the object of study.
- Study the catalytic behaviour and its correlation with the activity test results. For this purpose, some fresh and used catalysts should be analysed with conventional and advanced characterisation techniques. This exhaustive study should lead to the understanding of the factors affecting the selective C–O

cleavage of the primary or secondary hydroxy groups of glycerol, which is strongly dependent on the catalyst structure.

- Optimization of the reaction conditions and catalytic structure in order to develop a catalyst which maximizes the formation of the most interesting target product “1,3-propanediol”.
- Elucidation of the reaction mechanism involved in the production of propanediols, emphasising in the mechanism of 1,3-propanediol.

Noteworthy, the catalytic selective conversion of bio-glycerol into propanediols, and especially into 1,3-propanediol, could significantly improve the cost-competitiveness of biodiesel industry, which currently faces some difficulties. However, this process is still far from being scaled-up to the industry.

## **CHAPTER 4. Experimental**



## Table of contents

ABSTRACT.....	85
4.1 CATALYST PREPARATION.....	85
4.1.1 <i>Pt/WO<sub>x</sub> on conventional <math>\gamma</math>-Al<sub>2</sub>O<sub>3</sub> support</i> .....	85
4.1.2 <i>Pt/WO<sub>x</sub> on non-conventional supports</i> .....	86
4.1.3 <i>Pt loaded on WO<sub>x</sub>/Al<sub>2</sub>O<sub>3</sub> through chemical vapour impregnation</i> .....	87
4.2 CATALYST LAYER PREPARATION ON THE INTERNAL REFLECTION ELEMENT.....	88
4.3 ACTIVITY TEST.....	89
4.3.1 <i>Batch autoclave</i> .....	89
4.3.2 <i>Kinetic study</i> .....	90
4.4 CATALYST CHARACTERISATION.....	91
4.4.1 <i>Chemical analysis</i> .....	91
4.4.2 <i>N<sub>2</sub> physisorption</i> .....	91
4.4.3 <i>CO chemisorption</i> .....	92
4.4.4 <i>TEM</i> .....	92
4.4.5 <i>SEM</i> .....	92
4.4.6 <i>XRD</i> .....	92
4.4.7 <i>Raman spectroscopy</i> .....	93
4.4.8 <i>XPS</i> .....	93
4.4.9 <i>H<sub>2</sub>-TPR</i> .....	93
4.4.10 <i>NH<sub>3</sub> adsorption microcalorimetry</i> .....	93
4.4.11 <i>FTIR spectroscopy of adsorbed pyridine</i> .....	94
4.4.12 <i>In-situ ATR-IR spectroscopy</i> .....	95
4.4.13 <i>Ex-situ ATR-IR spectroscopy</i> .....	97
REFERENCES.....	99



## Abstract

Herein, all the experimental techniques and conditions used along the present Doctoral Thesis are described in detail. It has been developed with the aim to make the reading of the Thesis more pleasant without any repetition in the next sections. Moreover, it will be easier for the reader to find any required technical information. In the following chapters references are made to the corresponding section of this Chapter 4.

## 4.1 Catalyst preparation

### 4.1.1 Pt/WO<sub>x</sub> on conventional $\gamma$ -Al<sub>2</sub>O<sub>3</sub> support

These catalysts were prepared by sequential wetness impregnation (WI) method. The typical procedure followed for catalysts preparation is detailed below. Commercial  $\gamma$ -Al<sub>2</sub>O<sub>3</sub> (Merck,  $\geq 99.9\%$ ) was used as support, and it was impregnated using the appropriate amounts of ammonium metatungstate ((NH<sub>4</sub>)<sub>6</sub>(H<sub>2</sub>W<sub>12</sub>O<sub>40</sub>).nH<sub>2</sub>O, Sigma-Aldrich,  $\geq 99.99\%$ ) dissolved in deionized water. Impregnated samples were dried at 110 °C overnight and subsequently calcined in air from room temperature up to 450 °C at a heating rate of 2 °C min<sup>-1</sup>. This temperature was hold for 4 h. Pt was then loaded on supported tungsten oxide catalysts by wetness impregnation using tetraammineplatinum (II) nitrate ((Pt(NH<sub>3</sub>)<sub>4</sub>(NO<sub>3</sub>)<sub>2</sub>, Sigma-Aldrich,  $\geq 99.995\%$ ) as precursor. The resulting catalysts were dried and calcined following the same procedure as above at 300 or 450 °C. The calcination temperature applied will be specified in each case.

Henceforth, the prepared Pt/WO<sub>3</sub>/Al<sub>2</sub>O<sub>3</sub> samples by WI are denoted as  $xPt_yW$ , where  $x$  refers to the Pt content in weight percent (wt %) in the final catalyst and  $y$  to the W content related to the alumina support (in terms of wt % of W/ $\gamma$ -Al<sub>2</sub>O<sub>3</sub>), both of them measured by ICP-OES. The tungsten surface density (expressed in W atoms nm<sup>-2</sup> of support) was calculated based on the following equation (Eq. 4.1),

$$\rho_W [W \text{ atoms nm}^{-2} \text{ of support}] = \frac{\left(\frac{x_W}{M_W}\right)_{NA}}{S_{Al_2O_3}[1-(x_{WO_3}+x_{PtO})]} \quad \text{Eq. 4.1}$$

where  $x_w$  is the mass fraction of the W species in the final catalyst, NA is the Avogadro number,  $M_w$  is the W atomic weight, and  $S_{Al_2O_3}$  is the initial BET surface area



of the calcined support of  $\gamma$ -Al<sub>2</sub>O<sub>3</sub>. In this case, it was assumed that all the tungsten oxide species presented in the catalyst were WO<sub>3</sub> and the platinum oxides were PtO.

#### 4.1.2 Pt/WO<sub>x</sub> on non-conventional supports

In order to study the effect of the physicochemical characteristics of the support on the glycerol hydrogenolysis reaction, three different Al-based supports were tested. The same commercial  $\gamma$ -Al<sub>2</sub>O<sub>3</sub> (Al<sup>com</sup>) used in the previous section (4.1.1) was one of the supports used. The other two supports were prepared by the acid sol-gel (SG) method.

The SG method was carried out in a similar way described in other works published by our group [1]. First, aluminum isopropoxide, AIP (Al[OCH(CH<sub>3</sub>)<sub>2</sub>]<sub>3</sub>, Sigma-Aldrich 99.995%), was hydrolyzed at 40 °C using a molar ratio H<sub>2</sub>O/AIP of 100. The pH was adjusted to 4.0-4.2 (acid conditions) by adding HNO<sub>3</sub> aqueous solution (1.5 M). The solution was allowed to peptize for 45 min under vigorous stirring. The sol formed was then placed in a sonicator equipment for 30 min at 40 °C. Afterwards, the solvent was removed by drying at 65 °C for 48 h. The solid material obtained was dried overnight in a heater at 110 °C. The SG material obtained by this procedure has a pseudo-boehmite (pseudo  $\gamma$ -AlO(OH)) structure according to the XRD analysis (see section 6.2.1.1 of the Chapter 6). A fraction of this material was used as support without any treatment and was denoted as Al<sup>SG</sup>. Other fraction was calcined at 450 °C (in air at 2 °C min<sup>-1</sup> for 4 h) and it was converted into  $\gamma$ -Al<sub>2</sub>O<sub>3</sub>, also used as support in this study (Al<sup>SG</sup>).

Then, (NH<sub>4</sub>)<sub>6</sub>(H<sub>2</sub>W<sub>12</sub>O<sub>40</sub>).nH<sub>2</sub>O was incorporated into the support following the same procedure described in the section 4.1.1. The resulted catalysts were calcined at 450 °C (or 800 °C) in air at 2 °C min<sup>-1</sup> heating rate and holding the final temperature for 4 h. Thereafter, Pt(NH<sub>3</sub>)<sub>4</sub>(NO<sub>3</sub>)<sub>2</sub> was also incorporated in tungstated alumina materials according to the section 4.1.1. The final catalyst was calcined, as above, at 300 °C.

Prepared Pt/WO<sub>3</sub>/Al<sub>2</sub>O<sub>3</sub> samples are denoted as *xPtyW support*, where *x* refers to the Pt content in the final catalyst (wt % Pt), *y* to the W content related to the alumina support (wt % of W/ $\gamma$ -Al<sub>2</sub>O<sub>3</sub>), both measured by ICP-OES, and the *support* specifies the material used in each case (Al<sup>com</sup>, Al<sup>SG</sup> or Al<sup>SG'</sup>).

### 4.1.3 Pt loaded on $\text{WO}_x/\text{Al}_2\text{O}_3$ through chemical vapour impregnation

The chemical vapour impregnation method (CVI) developed by Forde et al. [2,3] was used for depositing the Pt onto calcined  $\text{WO}_x/\text{Al}_2\text{O}_3$  (prepared according to the section 4.1.1) and improve its dispersion over the support. For this purpose, platinum acetylacetonate, (from Sigma-Aldrich, 99.9%) was used as precursor and was physically mixed with  $\text{WO}_x/\text{Al}_2\text{O}_3$  sample (10W, concretely). The mixed was transferred to a Schlenk flask with a magnetic stirrer and a tube sealed. The sublimation and deposition of the organometallic Pt-precursor onto the support was achieved by heating the mixed at 140 °C for 1 h under a constant vacuum ( $10^{-3}$  mbar) and stirring. The temperature selected enabled the sublimation of the organometallic precursor without decomposition.

The resulted catalyst was reduced for 1 h at 400 °C, with a heating ramp of 5 °C  $\text{min}^{-1}$ , under a pure  $\text{H}_2$  stream (100  $\text{NmL min}^{-1}$ ) in order to fully pyrolyse the Pt-precursor. Table 4.1 summarizes the nomenclature for the catalysts used in this Thesis

**Table 4.1.** Catalyst nomenclature description.

Section	Name	Description
4.1.1	$x\text{Pt}y\text{W}(z)$	Impregnation of W on commercial $\gamma\text{-Al}_2\text{O}_3$ followed by Pt impregnation x=wt % Pt on final catalyst, y= wt % W on commercial $\gamma\text{-Al}_2\text{O}_3$ , z= W surface density (W atoms $\text{nm}^{-2}$ of support)
4.1.2	$x\text{Pt}y\text{W support}$	Impregnation of W on <i>support</i> followed by Pt impregnation x=wt % Pt on final catalyst, y= wt % W on <i>support</i> ( $\text{Al}^{\text{com}}$ , $\text{Al}^{\text{SG}}$ or $\text{Al}^{\text{SG}}$ )
4.1.2	$\text{Al}^{\text{com}}$	Commercial $\gamma\text{-Al}_2\text{O}_3$
4.1.2	$\text{Al}^{\text{SG}}$	Pseudo $\gamma\text{-AlO(OH)}$ prepared by acid SG method (without thermal treatment)
4.1.2	$\text{Al}^{\text{SG}}$	$\gamma\text{-Al}_2\text{O}_3$ obtained through calcination at 450 °C of $\gamma\text{-AlO(OH)}$ prepared by acid SG method
4.1.3	$x\text{Pt}^{\text{CVI}}y\text{W Al}^{\text{com}}$	Impregnation of W on commercial $\gamma\text{-Al}_2\text{O}_3$ followed by Pt loading by chemical vapor impregnation (CVI) method; x=wt % Pt on final catalyst, y= wt % W on commercial $\gamma\text{-Al}_2\text{O}_3$ .

## 4.2 Catalyst layer preparation on the internal reflection element

For the investigation of reactants adsorption and *in-situ* reaction on catalytic active sites by Attenuated Total Reflection Infrared (ATR-IR) spectroscopy the catalysts were first prepared according to the previous method described in 4.1.1 section. After the impregnation of Pt precursor on tungstated  $\text{Al}_2\text{O}_3$ , these catalysts were calcined at 300 °C. Subsequently, they were reduced at 300 °C for 1 h at a 5 °C  $\text{min}^{-1}$  heating rate in a flow of pure  $\text{H}_2$  (100  $\text{Nml min}^{-1}$ ).

Thereafter, aqueous solutions of the catalysts were prepared. First, Milli-Q water was degassed for 2 h using a glass bubbler and a flow of pure Ar at room temperature, in order to remove the dissolved  $\text{O}_2$ . Typically, 50 mg of reduced catalyst were finely crushed and added to 10 mL of degassed-water. To prepare a homogeneous aqueous suspension of the catalyst the mixture was stirred in a sonicator for 24 h at room temperature.

The investigation of the catalysts surface requires the catalyst to be immobilised on the internal reflection element (IRE) of the ATR-IR equipment. In this research two different IREs were used: ZnSe for *ex-situ* ATR-IR spectroscopy and Si crystal for *in-situ* ATR-IR spectroscopy. In order to do it, two drops of the catalyst suspension were deposited on the IRE and the water was evaporated in a vacuum desiccator for 1 h. The process was repeated until a homogeneous layer was obtained and the IRE was completely covered. This method conducts to the preparation of steady layers as it was reported in previous works [4,5]. Some examples of catalysts layers prepared are shown in Fig. 4.1 and 4.2.

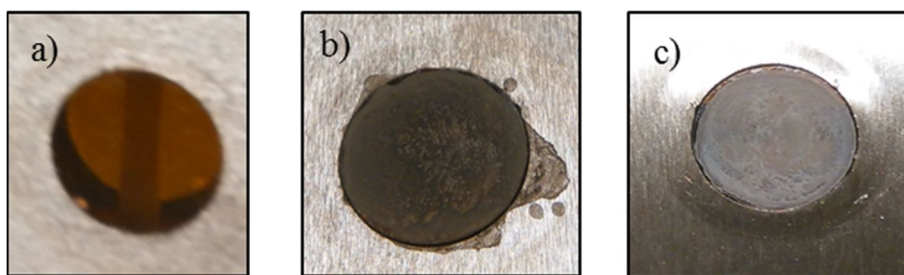


**Fig. 4.1.** ZnSe IRE (a),  $\text{Pt}/\text{WO}_x/\text{Al}_2\text{O}_3$  (b) and  $\text{WO}_x/\text{Al}_2\text{O}_3$  (c) catalysts layer on ZnSe IRE.

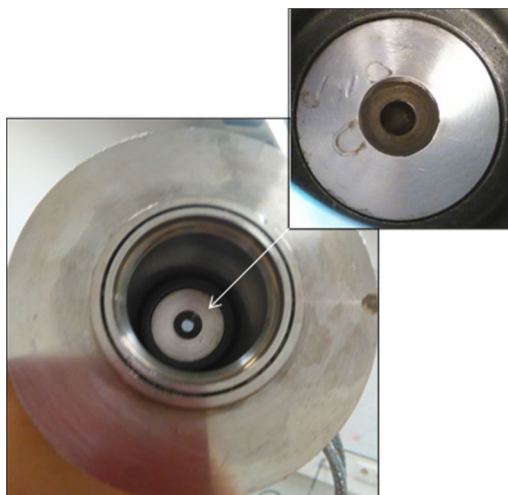


Fig. 4.2. Si IRE for *in-situ* ATR-IR spectroscopy (bottom) and Pt/WO<sub>x</sub>/Al<sub>2</sub>O<sub>3</sub> catalyst layer on Si IRE (top).

## 4.3 Activity test

### 4.3.1 Batch autoclave

Some activity tests were carried out in a 50-mL stainless steel autoclave (PID Eng&Tech., Spain) with a stirring rate of 550 rpm (Fig. 4.3). Typically, 0.35 g of catalyst powder (300-500  $\mu\text{m}$ ) was introduced into a catalytic basket inside the autoclave (maintaining the  $0.166 \text{ g}_{\text{catalyst}} \text{ g}^{-1}_{\text{reactant}}$  ratio constant).

Prior to the activity test, the catalyst was *in situ* reduced under a stream of pure H<sub>2</sub> (100 NmL/min) at 300 or 450 °C for 1 h (the reduction temperature will be specified in each catalyst). After reduction, the reactor was cooled down to the reaction temperature (180-220 °C) and the H<sub>2</sub> (in some test N<sub>2</sub>) pressure was increased up to 20 bar. The reactant solution (usually, 42 mL of 5 wt % glycerol aqueous solution), placed into a feed cylinder at 50 bar of H<sub>2</sub> pressure, was fed into the reactor taking advantage of the pressure difference and by circulating a continuous flow of H<sub>2</sub> (or N<sub>2</sub>) from the cylinder to the reactor for about 5 min. Thereafter, the pressure was increased up to the 45 bar.

During the 24 h reaction time of experiments, 4 liquid samples were taken along the first 7 h and a last sample was taken at 24 h, after reactants were cooled down (< 40 °C). In the 16 h-experiments, only the last liquid sample was taken. These samples were analysed using 1,4-butanediol (Sigma–Aldrich, 99.99%) as the internal standard with a gas chromatograph (GC, Agilent Technologies, 7890 A) equipped with a Meta-Wax capillary column (diameter 0.53 mm, length 30 m), a flame ionization detector (FID), and a thermal conductivity detector (TCD). After 16 or 24 h of reaction, the gas phase

was collected in a gas bag and analysed with another GC-TCD-FID equipped with a molecular sieve column (HP-MOLESIEVE, diameter 0.535 mm, length 30 m) and a capillary column (HP PLOT/Q, diameter 0.320 mm, length 30 m). The glycerol conversion and the selectivity towards liquid products were calculated based on the following equations (Eq. 4.2 and 4.3):

$$\text{Glycerol conversion (\%)} = \frac{\sum C\text{-based mol of all liquid product}_{t=t}}{C\text{-based mol of glycerol}_{t=0}} \times 100 \quad \text{Eq.4.2}$$

$$\text{Liquid product selectivity (\%)} = \frac{C\text{-based mol of the product}_{t=t}}{\sum C\text{-based mol of all liquid products}_{t=t}} \times 100 \quad \text{Eq.4.3}$$

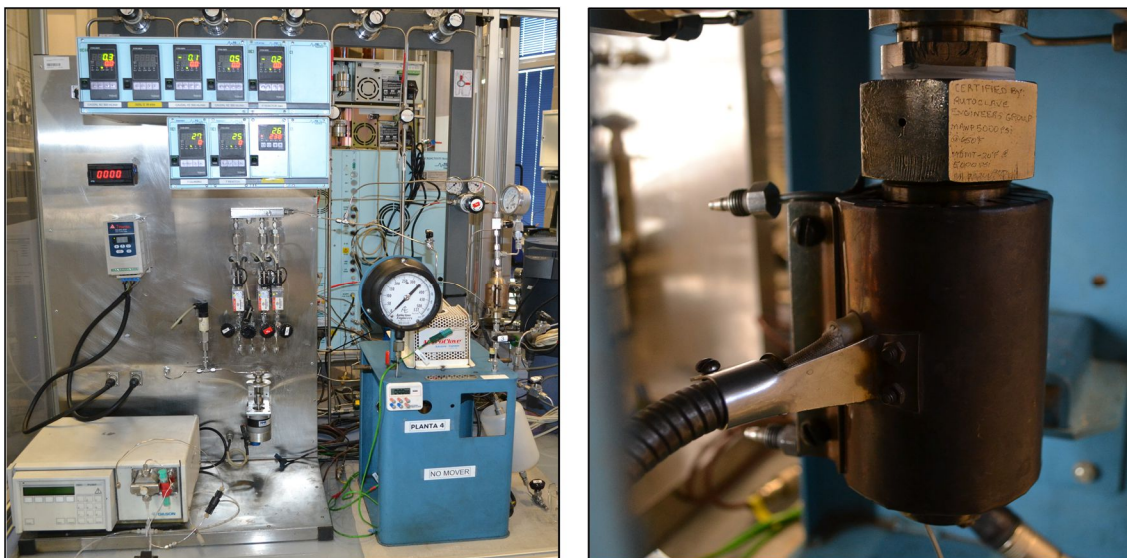


Fig. 4.3. Overall batch autoclave system (left) with 50-mL reactor (right).

### 4.3.2 Kinetic study

Kinetic studies were carried out in 4 similar stainless steel autoclaves of 50 mL capacity (RWTH Aachen University, Germany). Typically, 0.08 g of 9Pt8W catalyst (prepared according to the section 4.1.1) and 10 mL of reactant solution were placed in each autoclave.

The calcination temperature of the final Pt/WO<sub>x</sub>/Al<sub>2</sub>O<sub>3</sub> catalyst was 300 °C and was *ex-situ* reduced at the same temperature for 1 h using a H<sub>2</sub> flow of 100 NmL min<sup>-1</sup> prior to the activity tests. The feed was modified in each experiment and it will be specified during the discussion of the results. However, the catalyst to glycerol ratio was kept constant and equal to 0.166 g<sub>catalyst</sub> g<sup>-1</sup><sub>glycerol</sub>. The systems were then purged and pressurized up to 25 bar of H<sub>2</sub>. Afterwards, they were placed in hotplates with a

magnetic stirring of 550 rpm and heated up to 200 °C (see Fig. 4.4). After 2 h reaction time the autoclaves were immediately cooled down in an ice-bath.

A known amount of 1,4-butanediol (Sigma–Aldrich, 99.99%) aqueous solution was added to the reaction mixture external standard, and a sample was then taken and analysed in a GC-TCD-FID (6890 N, Agilent Technologies) equipped with a Supra-Wax capillary column (diameter 0.53 mm, length 30 m).



Fig. 4.4. Autoclaves used for kinetic study.

## 4.4 Catalyst characterisation

### 4.4.1 Chemical analysis

The chemical analysis of the calcined catalyst was carried out by inductively coupled plasma optical emission spectrometry (ICP-OES) using a Perkin-Elmer Optima 2000 instrument. Previously to the analysis, the solid samples were digested in a microwave oven in an acid mixture (3 mL of HNO<sub>3</sub>, 2 mL of HCl and 3 mL of HF), heating from room temperature up to 180 °C, with a heating ramp of 7 °C min<sup>-1</sup>, for 30 min. The samples totally decomposed were then diluted in 100 mL-flask with water. The sample amount (80-100 mg) was previously calculated with the premise that its concentration in the solution should be within the instrument detection range.

### 4.4.2 N<sub>2</sub> physisorption

Textural properties (surface area, pore volume, and pore size distributions) were obtained by N<sub>2</sub> physisorption at -196 °C using a Quantachrome AUTOSORB-1C-TCD instrument. All samples were dried at 300 °C overnight under high vacuum prior to the

physisorption measurements. The surface area was calculated using the Brunauer, Emmett, and Teller (BET) method, and the pore size distributions were obtained using the Barrett–Joyner–Halenda (BJH) method applied to the desorption branch of the isotherms.

#### **4.4.3 CO chemisorption**

The measurements were performed in an AUTOSORB-iQ equipment. Prior to adsorption, all samples were outgassed in He flow at 120 °C for 3 h and subsequently reduced at 450 °C under a stream of pure H<sub>2</sub> for 1 h (similar to reaction conditions). The samples were cooled down to room temperature and evacuated under He flow for 2 h. After that, CO chemisorption uptakes were measured by pulses of pure CO at 40 °C (or 35 °C).

The CO/Pt adsorption stoichiometry employed for the estimation of the Pt size and metal dispersion was 1.

#### **4.4.4 TEM**

Transmission electron microscopy (TEM) images were obtained in a Philips SuperTwin CM200 apparatus operated at 200 kV and equipped with LaB6 filament and EDAX EDS microanalysis system. The samples were pre-reduced at 450 °C (similar to reaction conditions) and then dispersed into ethanol solvent and placed on a carbon-coated copper grid (300 Mesh) followed by drying under vacuum.

#### **4.4.5 SEM**

Scanning electron microscopy (SEM) was employed to examine the morphology of some reduced Pt/WO<sub>x</sub>/Al catalysts. For this purpose a JEOL JSM-6400 apparatus equipped with a W filament was used. The fresh catalyst samples were previously reduced at 300 °C for 1 h (similar to reaction conditions).

#### **4.4.6 XRD**

X-ray diffraction (XRD) studies of the reduced catalyst were recorded on an Xpert-Pro instrument with a PW3050/60 goniometer and a Cu anode at current of 40 mA and voltage of 40 kV, in a 2θ range from 10° to 90° with a 0.026° step size. The patterns were compared with the power diffraction files (PDF) by Xpert-Pro High Score tool.

*In-situ* XRD was carried out on the same system, in a high-temperature chamber. The sample was mounted in a high-temperature cell and heated at 2 °C min<sup>-1</sup> under stationary air.

#### 4.4.7 Raman spectroscopy

In order to determine the species present in the samples and the interaction between the platinum and tungsten species, the Raman spectra of the calcined catalysts were determined. The equipment employed was a Renishaw InVia microscope with Ar ion laser (Modu-Laser) using 514 nm laser excitation. The spectra of the catalysts, in powder form, were recorded at ambient temperature within the 150–1500 cm<sup>-1</sup> region.

#### 4.4.8 XPS

XPS spectra of the reduced samples (fresh and some used samples) were obtained on a VG Escalab 200R spectrometer equipped with a hemispherical electron analyser and Mg K $\alpha$  (h $\nu$  = 1253.6 eV) X-ray source. Binding energy ( $E_b$ ) values were referred to the C1s peak at 284.6 eV. The recorded XPS signals were analysed using a nonlinear Shirley-type background and decomposed into subcomponents by Gaussian–Lorentzian functions.

#### 4.4.9 H<sub>2</sub>-TPR

The reducibility study of the surface species was carried out on a Quantachrome AUTOSORB-1C-TCD apparatus. Temperature programme reduction (TPR) profiles were obtained using 0.3 g of a catalyst powder. The samples were reduced in a flowing gas of 5 vol% H<sub>2</sub> in Ar (50 mL min<sup>-1</sup> of total flow rate) increasing the temperature from 40 °C up to 1100 °C at 10 °C min<sup>-1</sup>. A TCD detector downstream of the sample monitored changes in the concentration of H<sub>2</sub>.

The samples were thermally pre-treated, prior to the analysis, in order to eliminate the water and impurities from the surface. For this purpose, they were heated at 250 °C under a He stream for 2 h.

#### 4.4.10 NH<sub>3</sub> adsorption microcalorimetry

Adsorption microcalorimetry measurements were performed at 80 °C in a volumetric line linked to a heat-flow microcalorimeter (Tian-Calvet type, C80 from



Setaram) in order to measure the whole acidity as well as the strength of the catalytic sites present in the samples.

Ammonia ( $\text{NH}_3$ ) was used as a basic probe molecule to titrate the surface acid sites. 0.1 g of the powder calcined sample was pre-treated under vacuum at 250 °C overnight (about 12 h) and subsequently evacuated at the same temperature for 1 h prior to the measurements.

Small successive  $\text{NH}_3$  injections were sent onto the sample until a final  $\text{NH}_3$  equilibrium pressure of about 67 Pa. For each dose, the adsorption heat and the pressure of the adsorbate, this last measured by means of a differential Barocel capacitance manometer (Datametries), were recorded by a computer. Following the first adsorption isotherm, the sample was outgassed under vacuum for 30 min at the same temperature and a second adsorption isotherm was performed until the equilibrium pressure of 27 Pa was attained. The irreversible volume of  $\text{NH}_3$  ( $V_{\text{irr}}$ ), associated with the strongly chemisorbed  $\text{NH}_3$ , was calculated from the difference between the first and second volumetric isotherms at 27 Pa. A picture of the equipment and the operation scheme are shown in Fig. 4.5.

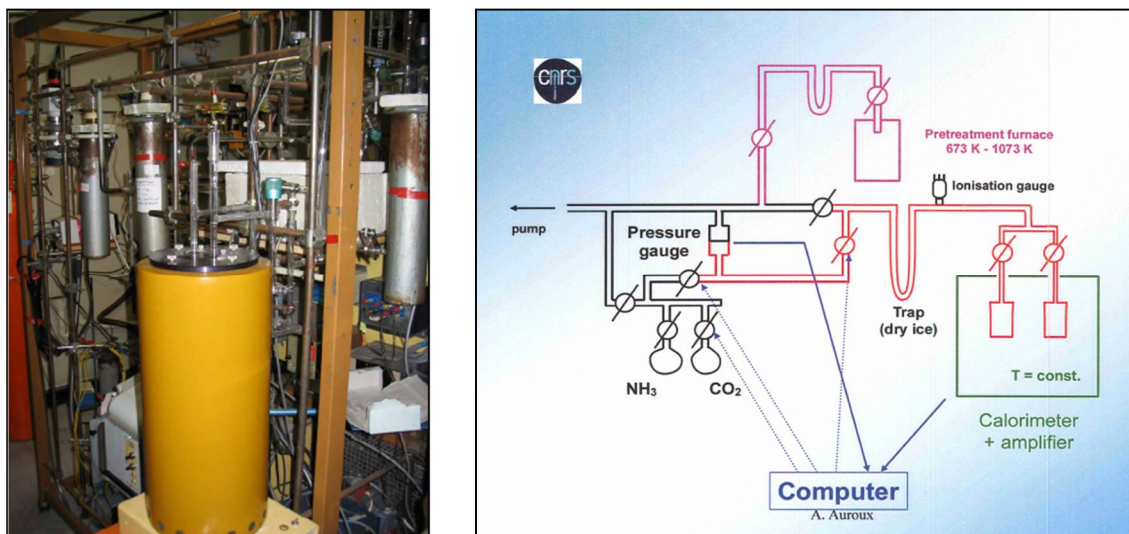


Fig. 4.5. C80 microcalorimeter equipment used at the Institut de Recherches sur la Catalyse et l'Environnement de Lyon (IRCELYON), France, (left), and operation scheme (right).

#### 4.4.11 FTIR spectroscopy of adsorbed pyridine

The Fourier transform infrared (FTIR) spectroscopy of adsorbed pyridine analyses were carried out in order to study the nature (type and strength) of acid sites on the surface of different  $\text{WO}_x/\text{Al}_2\text{O}_3$  and  $\text{Pt}/\text{WO}_x/\text{Al}_2\text{O}_3$  samples. Infrared transmission

spectra were recorded on Nicolet 8700 FTIR spectrometer equipped with an extended KBr beam splitter and a mercury cadmium telluride (MCT) detector.

The samples were pressed into a 30-35 mg of self-supporting wafers, having a surface area of about 2 cm<sup>2</sup>, which were placed into an infrared quartz cell, with CaF<sub>2</sub> windows, connected to a vacuum line.

Pellets were pre-treated under vacuum (about 10<sup>-5</sup> Pa) with an oxygen flow and by a slow heating of 2 °C min<sup>-1</sup> up to 350 °C. Then, they were outgassed at the same temperature for 1 h. A known amount of pyridine was introduced into the cell at room temperature.

Spectra were recorded after pyridine desorption by evacuation for 15 min under vacuum at different temperatures (200 °C and 300 °C) with a spectral resolution of 2 cm<sup>-1</sup> and 32 scans per spectra. All reported spectra were obtained by subtracting the spectrum of the activated catalyst (after pre-treatment but before pyridine adsorption) from those after pyridine adsorption. A schematic representation of the procedure is represented in Fig. 4.6.

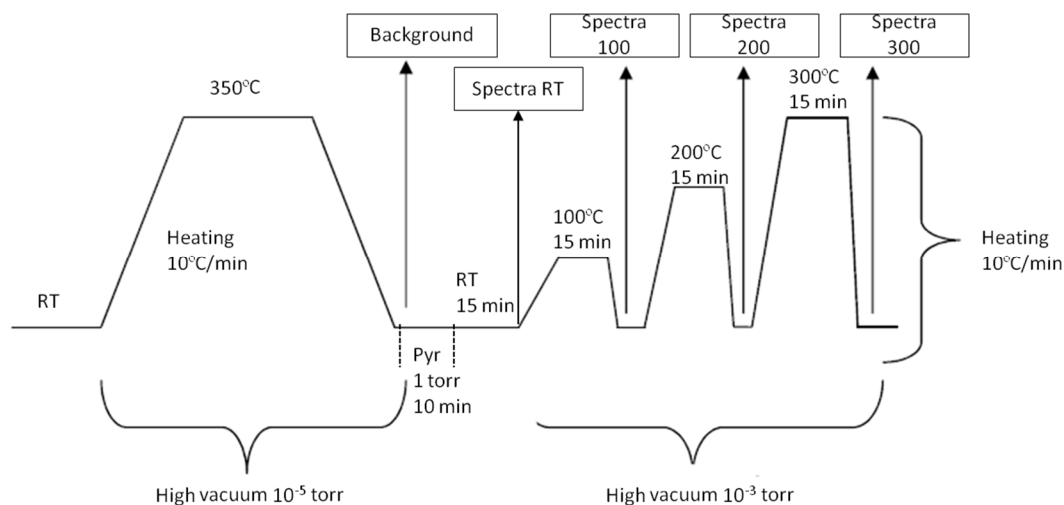


Fig. 4.6. Scheme of the FTIR of adsorbed pyridine measurements carried out.

#### 4.4.12 *In-situ* ATR-IR spectroscopy

In order to study the surface species involved in glycerol hydrogenolysis reaction, such as reactants, intermediates and products, and also the catalytic surface, some *in-situ* ATR-IR spectroscopy measurements were carried out. The experiments were conducted in a ReactIR 45m FTIR spectrometer (Mettler Toledo) with liquid N<sub>2</sub>-cooled MCT detector. This equipment is an *in-situ* mid-infrared based system that

allows monitoring the reaction in real-time and, thus, obtaining a deeper and real reaction information. It is connected to an autoclave, in which the reaction is performed through a K4 conduit to sentinel. The Silicon (Si) crystal used as IRE, placed on the bottom part of the autoclave, was coated with the catalyst layer prepared as explained above in section 4.2.

The schematic representation of the autoclave setup with the IRE of the ATR-IR is shown in Fig. 4.7. In Fig. 4.8 real pictures of the equipment (used at The Debye Institute for Nanomaterials Science of the Utrecht University, The Netherlands) are illustrated.

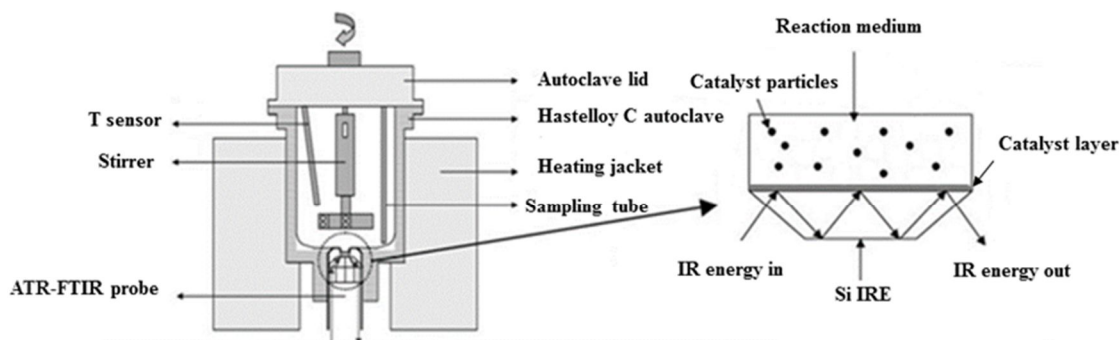
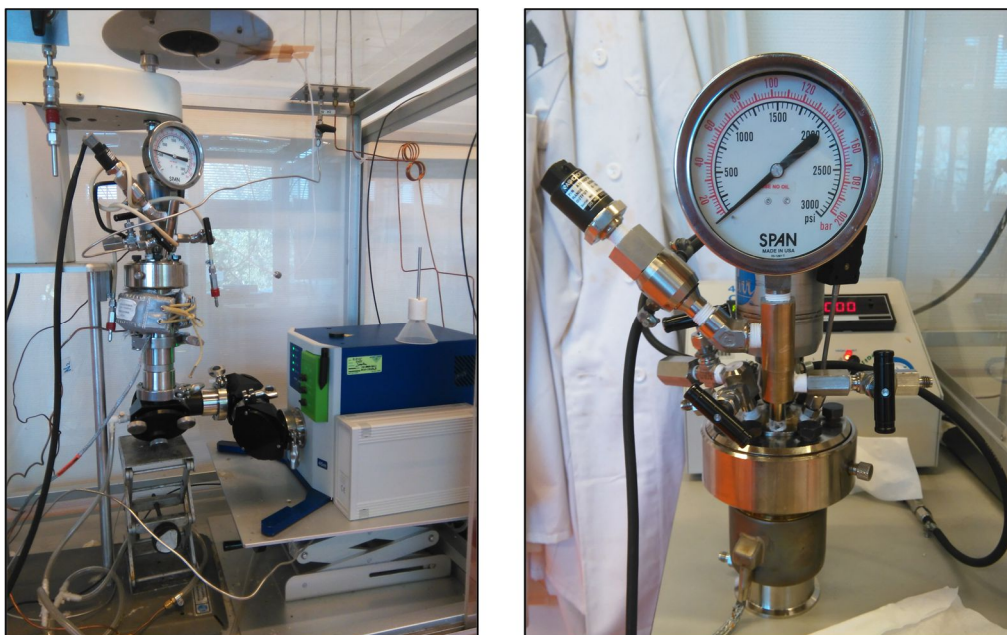


Fig. 4.7. Schematic representation of the autoclave setup and ATR-IR principle, modified from [6].

The reactant solution, typically 20 mL glycerol (Sigma-Aldrich, 99.0 %) in Milli-Q water, was placed in the autoclave. Thereafter, the 9Pt8W catalyst in powder form (420-500  $\mu\text{m}$ ) was introduced into the autoclave. The glycerol concentration varied from 5 to 30 wt%, but the catalyst to glycerol ratio was kept constant (0.166  $\text{g}_{\text{catalyst}} \text{g}_{\text{reactant}}^{-1}$ ). The catalyst was prepared according to the section 4.1.1, calcining the resulting Pt/ $\text{WO}_x/\text{Al}_2\text{O}_3$  catalyst at 300 °C. Prior to the activity test, the catalyst was *ex-situ* reduced under a stream of pure  $\text{H}_2$ , or  $\text{N}_2$  in some experiments, (100  $\text{NmL min}^{-1}$ ) at 300 °C for 1 h. The reactor was then purged 5 times with  $\text{H}_2$  (or  $\text{N}_2$ ). Afterwards, the pressure was increased up to the 35 bar and the heating and stirring (550 rpm) started. The reaction started when the temperature and pressure reached the operation values of 200 °C and 45 bar.



**Fig. 4.8.** *In-situ* ATR-IR set up (right) and the autoclave (left) used at The Debye Institute for Nanomaterials Science of the Utrecht University, The Netherlands.

The liquid and gaseous samples were taken when reaction finished at 16 h reaction time and after the system was cooled down ( $T < 40\text{ }^{\circ}\text{C}$ ). The composition of the gas phase was analysed in a micro GC (Varian, 490 GC) equipped with a COX 1m and a CP-Sil-5CB 6m columns (Agilent Technologies). The liquid sample was analysed using 1,4-butanediol (Sigma-Aldrich, 99.9%) as internal standard with a GC-TCD-FID (Agilent Technologies, 7890 A) equipped with a Meta-Wax capillary column (diameter 0.53 mm, length 30 m).

During the experiments, spectra were collected every 2 min for 6 h, at 15 min for the next 2 h and every 30 min for the rest 8 h. The measurements were also registered during the heating. Each spectrum was collected using a resolution of  $4\text{ cm}^{-1}$  and 64 scans in the  $4000\text{-}650\text{ cm}^{-1}$  scan region.

Blank-experiments were carried out following the same procedure but using pure solvents as reactants, Milli-Q water.

#### 4.4.13 *Ex-situ* ATR-IR spectroscopy

The surface chemistry of some catalysts (commercial  $\gamma\text{-Al}_2\text{O}_3$  and  $\text{WO}_x/\text{Al}_2\text{O}_3$ ) was studied through *ex-situ* ATR-IR spectroscopy. The measurements were carried out in a TENSOR 37 instrument (from Bruker) equipped with a horizontal ATR accessory (FastIR from Harrick) and a zinc selenide ( $\text{ZnSe}$ ) crystal as IRE. Fig. 4.9 shows the equipment employed for the research.

Typically, the catalyst was immobilised on the IRE surface according to the section 4.2 and was recorded and used as the background. Then, a drop of a glycerol aqueous solution (or water) was deposited over the catalyst layer and the spectra were collected. In some cases, the water loaded sample spectrum was subtracted from the spectrum of the glycerol loaded sample over the same catalyst. After glycerol loading, the moisture of the layer was removed under high vacuum (HV) for 1 h and spectra were registered at room temperature and pressure (RTP).

All spectra were recorded at  $4\text{ cm}^{-1}$  of resolution and 64 scans per spectrum in the  $4000\text{-}650\text{ cm}^{-1}$  region.

In order to note vibrational shifts, the IRE was also fully covered by pure glycerol (Sigma-Aldrich, 99.0 %) and a glycerol aqueous solution.

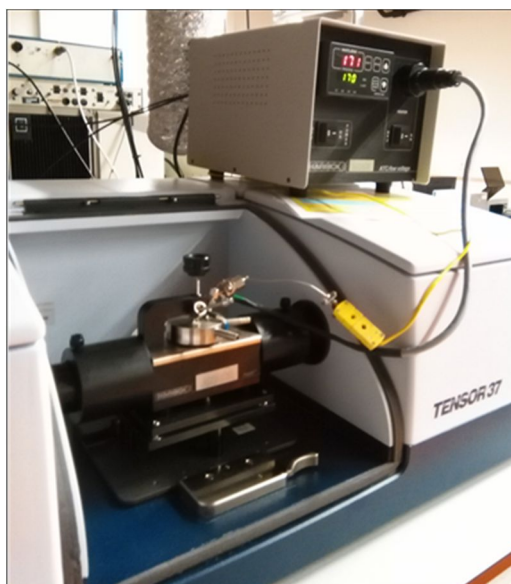


**Fig. 4.9.** *Ex-situ* ATR-IR set up used at the Debye Institute for Nanomaterials Science of the Utrecht University, The Netherlands.

## References

- [1] M. El Doukkali, A. Iriondo, J.F. Cambra, L. Jalowiecki-Duhamel, a. S. Mamede, F. Dumeignil, et al., Pt monometallic and bimetallic catalysts prepared by acid sol-gel method for liquid phase reforming of bioglycerol, *J. Mol. Catal. A Chem.* 368-369 (2013) 125–136.
- [2] M.M. Forde, L. Kesavan, M.I. Bin Saiman, Q. He, N. Dimitratos, J.A. Lopez-Sanchez, et al., High activity redox catalysts synthesized by chemical vapor impregnation, *ACS Nano.* 8 (2014) 957–969.
- [3] M.M. Forde, R.D. Armstrong, R. McVicker, P.P. Wells, N. Dimitratos, Q. He, et al., Light alkane oxidation using catalysts prepared by chemical vapour impregnation: tuning alcohol selectivity through catalyst pre-treatment, *Chem. Sci.* (2014) 3603–3616.
- [4] R. He, R.R. Davda, J. a Dumesic, In Situ ATR-IR Spectroscopic and Reaction Kinetics Studies of Water-Gas Shift and Methanol Reforming on Pt / Al<sub>2</sub>O<sub>3</sub> Catalysts in Vapor and Liquid Phases, *J. Phys. Chem. B.* (2005) 2810–2820.
- [5] I. Ortiz-Hernández, C.T. Williams, In Situ Investigation of Solid - Liquid Catalytic Interfaces by Attenuated Total Reflection Infrared Spectroscopy, *Langmuir.* 19 (2003) 2956–2962.
- [6] G.M. Hamminga, G. Mul, J.A. Moulijn, Real-time in situ ATR-FTIR analysis of the liquid phase hydrogenation of  $\gamma$ -butyrolactone over Cu-ZnO catalysts: A mechanistic study by varying lactone ring size, *Chem. Eng. Sci.* 59 (2004) 5479–5485.



**CHAPTER 5.**  
**The role of Pt and WO<sub>x</sub> active phases of the  
bimetallic Pt/WO<sub>x</sub>/Al<sub>2</sub>O<sub>3</sub> catalysts**

**Extracted from the article:** *New approaches to the Pt/WO<sub>x</sub>/Al<sub>2</sub>O<sub>3</sub> catalytic system behavior for the selective glycerol hydrogenolysis to 1,3-propanediol*

**Authors:** S. García-Fernández, I. Gandarias, J. Requies, M.B. Güemez, S. Bennici, A. Auroux, P.L. Arias.

**Journal, volume and pages:** Journal of Catalysis 323, 65-75

**Date of publication:** March 2015

**Selected as one of the four Featured Articles from the March 2015 issue by the Editor-in-chief Prof. Johannes Lercher**





## Table of contents

ABSTRACT.....	105
5.1 EXPERIMENTAL .....	106
5.1.1 Catalyst preparation .....	106
5.1.2 Catalyst characterisation .....	106
5.1.3 Activity test.....	106
5.2 RESULTS AND DISCUSSION .....	106
5.2.1 Catalyst characterisation .....	106
5.2.1.1 N <sub>2</sub> -physisorption.....	106
5.2.1.2 CO chemisorption.....	107
5.2.1.3 TEM.....	108
5.2.1.4 XRD.....	108
5.2.1.5 Raman spectroscopy .....	110
5.2.1.6 XPS.....	111
5.2.1.7 H <sub>2</sub> TPR.....	113
5.2.1.8 NH <sub>3</sub> adsorption microcalorimetry .....	115
5.2.1.9 FTIR spectroscopy of adsorbed pyridine.....	116
5.2.2 <i>Effect of tungsten surface density on glycerol conversion and selectivity to PDOs</i> .....	118
5.2.3 <i>Effect of platinum metal content on glycerol conversion and selectivity to PDOs</i> .....	120
5.3 PROPOSED REACTION MECHANISM .....	122
5.4 CONCLUSIONS .....	124
ACKNOWLEDGMENTS.....	124
REFERENCES.....	125



## Abstract

Although the hydrogenolysis of glycerol to 1,2-propanediol (1,2-PDO) is already well developed, the production of the more valuable 1,3-propanediol (1,3-PDO) is still a challenge. To achieve this aim, it is essential to design catalysts showing high selectivity toward the C–O cleavage of the secondary hydroxy group of glycerol.

In this work, two different series of Pt/WO<sub>x</sub>/Al<sub>2</sub>O<sub>3</sub> catalytic systems were studied for the selective hydrogenolysis of glycerol to 1,3-PDO. The results reveal the necessity to control the tungsten surface density in order to obtain highly dispersed polytungstate species, which are able to produce Brønsted acidity and are involved in the selective formation of 1,3-PDO.

After optimization of the tungsten surface density, the effect of platinum content was also studied. It was found that by improving the interactions between platinum and tungsten oxides, it is possible to increase the selectivity toward 1,3-PDO. Under optimized reaction conditions, a selectivity toward 1,3-PDO of 51.9 % at 53.1 % glycerol conversion was obtained. Based on the characterization and activity test results, a reaction mechanism for the Pt-WO<sub>x</sub> catalytic system in glycerol hydrogenolysis to 1,3-PDO was also proposed.

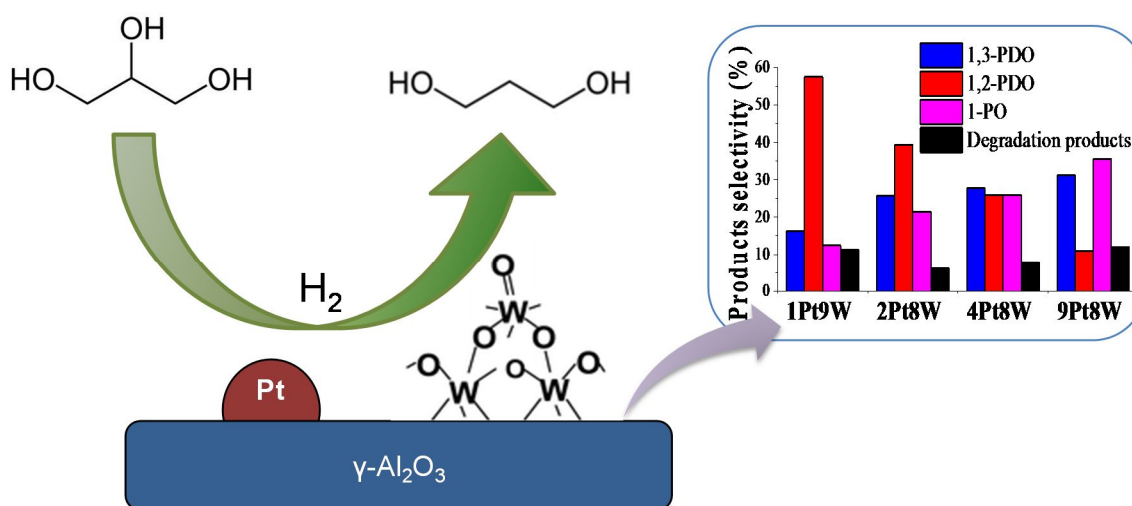


Fig. 5.1. Graphical abstract

## **5.1 Experimental**

### **5.1.1 Catalyst preparation**

Pt/WO<sub>x</sub>/Al<sub>2</sub>O<sub>3</sub> catalysts were prepared by sequential wetness impregnation method. The typical procedure followed for the preparation is detailed in section 4.1.1 of Chapter 4. The resulting Pt/WO<sub>x</sub>/Al<sub>2</sub>O<sub>3</sub> catalysts were finally calcined at 450 °C. They are denoted as xPt<sub>y</sub>W(z) as it was explained in the same section.

### **5.1.2 Catalyst characterisation**

The physicochemical properties of the catalysts measured by N<sub>2</sub> physisorption, H<sub>2</sub> temperature programmed reduction (H<sub>2</sub>-TPR), Fourier transform infrared (FTIR) spectroscopy of adsorbed pyridine, Raman spectroscopy, X-ray diffraction (XRD), X-ray photoelectronic spectroscopy (XPS), NH<sub>3</sub> adsorption calorimetry, transmission electron microscopy (TEM), and CO chemisorption techniques.

Detailed information about the equipments and conditions used in each of the characterisation techniques employed are described in the section 4.4 of Chapter 4.

### **5.1.3 Activity test**

The activity tests were carried out in an autoclave following the procedure described in section 4.3.1 of Chapter 4. The catalysts were reduced at 450 °C prior to the activity tests and, typically, the reaction was conducted at 220 °C.

## **5.2 Results and discussion**

### **5.2.1 Catalyst characterisation**

#### **5.2.1.1 N<sub>2</sub>-physisorption**

The textural properties of the calcined catalysts are shown in Table 5.1. The catalysts surface area was reduced in all the catalysts as compared to the  $\gamma$ -alumina support ( $S_{\text{BET}}$  of 140 m<sup>2</sup> g<sup>-1</sup>) as the tungsten surface density increased. This could be due to the blocking or filling of  $\gamma$ -alumina pores when the tungsten oxide species were added. The reduction in pore volume of the catalysts in comparison with the bulk support (pore volume of 0.23 cm<sup>3</sup> g<sup>-1</sup>) can be explained through the same assumption. The incorporation of the platinum oxide on the tungstated support had the same effect.

**Table 5.1.** Textural properties of the catalyst and its activity results obtained after 24 h reaction time, 220 °C and 45 bar pressure

Catalyst <sup>a</sup>	$S_{\text{BET}}$ (m <sup>2</sup> g <sup>-1</sup> )	Pore volume (cm <sup>3</sup> g <sup>-1</sup> )	Glycerol conversion (%)	Product selectivity (%)			
				1,3-PDO	1,2-PDO	1-PO	Degradation products <sup>b</sup>
1Pt1W (0.2)	128	0.24	25.6	0.0	78.2	1.9	19.9
1Pt5W (1.0)	111	0.22	22.2	3.1	76.3	3.5	17.2
1Pt9W (2.4)	104	0.19	16.7	16.4	57.5	12.4	11.3
1Pt14W (3.9)	96	0.18	11.6	10.9	60.9	20.7	7.5
1Pt19W (5.9)	79	0.15	5.5	11.2	59.5	29.3	0.0
2Pt8W (2.2)	105	0.19	25.6	25.7	39.3	21.5	6.1
4Pt8W (2.2)	-	-	42.1	27.8	25.9	25.9	7.8
9Pt8W (2.2)	81	0.15	60.3	31.2	11.0	35.6	12.0
9Pt8W (2.2) <sup>c</sup>	81	0.15	53.1 <sup>c</sup>	51.9 <sup>c</sup>	9.5 <sup>c</sup>	24.8 <sup>c</sup>	1.2 <sup>c</sup>

<sup>a</sup> Tungsten surface density in brackets (W at. nm<sup>-2</sup>)

<sup>b</sup> Main degradation products: ethylene glycol, ethanol, methane

<sup>c</sup> Results obtained for 9Pt8W (2.2) catalyst at 200 °C reaction temperature

### 5.2.1.2 CO chemisorption

The tungsten oxides present in the Pt/WO<sub>x</sub>/Al<sub>2</sub>O<sub>3</sub> catalysts do not adsorb CO [1]; therefore, CO chemisorption was used to measure the platinum particle size and metal dispersion on platinum loaded samples. Depending on the type of adsorption sites, the average of CO/Pt adsorption stoichiometry usually varies from 1 to 2 because CO chemisorbs in various forms [2]. The most widely CO/Pt adsorption stoichiometry used for the calculation of platinum size and metal dispersion is a ratio of 1 [2,3]. In order to facilitate the comparison with other works, the same value was assumed in this article. The results are shown in Table 5.2. It can be noted that increasing the platinum loading, the metal size notably increased, from 4.1 to 26.4 nm for 2Pt8W and 9Pt8W catalyst, respectively, and with the resultant decline in platinum dispersion (from 27.3 % to 4.3 %, respectively).

**Table 5.2.** Pt particle size and dispersion obtained by CO-chemisorption at 40°C

Catalyst <sup>a</sup>	Pt size (nm)	Pt dispersion (%)
2Pt8W (2.2)	4.1	27.3
4Pt8W (2.2)	11.2	10.1
9Pt8W (2.2)	26.4	4.3

### 5.2.1.3 TEM

Fig. 5.2 (a) and (b) shows the TEM images of 1Pt9W and 9Pt8W catalysts. Although the TEM images do not allow a clear visual discrimination among platinum and tungsten oxide clusters (neither by shape nor contrast), it is interesting to note that only particles with diameters  $\leq 5$  nm were found. EDS microanalysis on different specific particles allowed to differentiate certain platinum particles from the tungsten oxides at low platinum content. In Fig. 5.2 (a), a platinum particle (circle) of a diameter lower than 1 nm surrounded by tungsten oxides well dispersed in the catalyst surface can be seen. For 9Pt8W sample, the differentiation was absolutely impossible even by EDS microanalysis, which reveals the closer proximity between these species at higher platinum contents. Both, platinum and tungsten, characteristic X-ray peaks were obtained around throughout the sample investigated (Fig. 5.2 (b)).

The particle sizes obtained by TEM are commonly smaller than those from chemisorption uptakes as Iglesia et al. reported [3]. In this case, the platinum particle size estimated from TEM (5 nm) and CO chemisorption (26 nm) measurements is significantly different for the 9Pt8W catalyst.

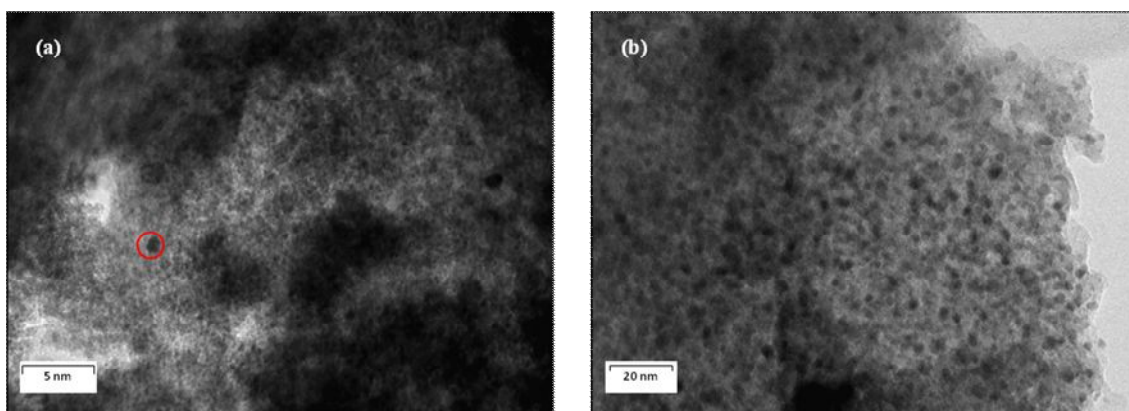


**Fig. 5.2.** TEM images of fresh reduced (a) 1Pt9W and (b) 9Pt8W catalysts

### 5.2.1.4 XRD

The structure of the reduced (at reaction conditions) fresh Pt/WO<sub>x</sub>/Al<sub>2</sub>O<sub>3</sub> catalysts was analysed by XRD (Fig. 5.3). The XRD patterns of the catalysts with a constant Pt content (1 wt %) and different WO<sub>x</sub> loading reveal that only diffraction peaks related to crystalline  $\gamma$ -alumina ( $2\theta = 37.5^\circ, 45.4^\circ, 66.9^\circ$ ) [4] were observed for catalyst with a tungsten surface density lower than 2.4 Wat. nm<sup>-2</sup>. However, diffraction peaks characteristic of monoclinic-WO<sub>3</sub> phase (m-WO<sub>3</sub>) ( $2\theta = 23.5^\circ, 33.3^\circ$ ) were observed for a tungsten surface density of 3.9 Wat. nm<sup>-2</sup> [5]. This indicates the

formation of  $\text{WO}_3$  crystalline nanoparticles ( $\text{WO}_3$  NPs) of around 5 nm at high tungsten surface density values. These results are in good agreement with the Raman spectroscopy and XPS results. The absence of platinum diffraction peaks revealed the homogeneous dispersion of this metal on the catalyst.

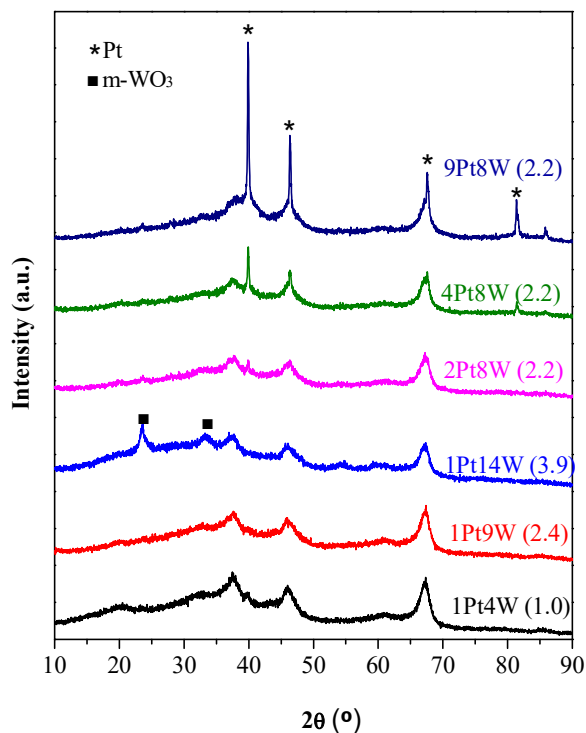


**Fig. 5.3.** XRD patterns of fresh reduced  $\text{WO}_x/\text{Al}_2\text{O}_3$  and  $\text{Pt}/\text{WO}_x/\text{Al}_2\text{O}_3$  catalysts. Tungsten surface density (W at.  $\text{nm}^{-2}$ ) in brackets.

As it can be observed in the XRD patterns of the catalysts with a constant tungsten surface density of about 2.2-2.4  $\text{W at. nm}^{-2}$ , for platinum loadings higher than 2 wt %, large and narrow peaks characteristic of metallic platinum ( $2\theta = 39.9^\circ$ ,  $46.4^\circ$ ,  $67.6^\circ$ ) [6] started to be observed. There was no evidence of the presence of platinum oxides, which means that the complete reduction of the catalyst was attained at the reduction conditions used. As the platinum content raised from 2 wt % to 4 wt %, the platinum crystallite size also increased considerably but remained almost constant for higher platinum contents (9 wt %). This trend was supported by CO chemisorption and TEM technique results. However, the platinum particle size values obtained by XRD are considerably higher, probably due to the most dominant contribution of some big platinum particles formed on this bulk type analysis and to the very small clusters being undetectable because of the detection limit of this technique was 3 nm.



### 5.2.1.5 Raman spectroscopy

Tungsten surface density determines the different types of tungsten oxides species that are deposited on the surface of the catalyst, namely surface monotungstate species (coordinated structure: WO<sub>4</sub>), polytungstates (coordinated structure: WO<sub>5</sub>/WO<sub>6</sub>), and WO<sub>3</sub> crystalline nanoparticles (NPs) [7].

Raman spectroscopy was used to differentiate the species present on the catalysts surface, and the spectra of calcined catalysts are shown in Fig. 5.4. The  $\gamma$ -alumina support has no Raman active modes [7]. The Raman bands of Pt/WO<sub>x</sub>/Al<sub>2</sub>O<sub>3</sub> catalysts appearing in the 970-1008 cm<sup>-1</sup> region can be attributed to W=O vibration bands of mono- and polytungstate species [7]. The progressive shift of the position of this band to higher wavenumbers, from 971 cm<sup>-1</sup> to 1008 cm<sup>-1</sup>, as the tungsten density increases from 0.2 Wat. nm<sup>-2</sup> up to 3.9 Wat. nm<sup>-2</sup>, can be ascribed to an increase of the polytungstates to monotungstates ratio [8].

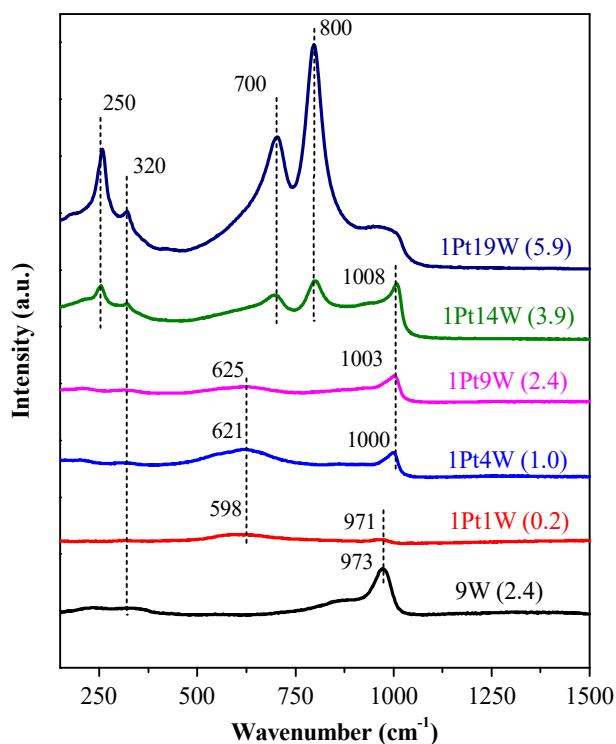


Fig. 5.4. Raman spectra of the calcined catalysts. Tungsten surface density (W at. nm<sup>-2</sup>) in brackets.

Typical WO<sub>3</sub> NP bands at 800, 700, and 250 cm<sup>-1</sup> could be observed at densities  $\geq 3.9$  Wat. nm<sup>-2</sup>, which are assigned to W–O stretching, W–O bending, and W–O–W deformation modes of octahedrally coordinated WO<sub>3</sub> crystals [9]. These NPs correspond to m-WO<sub>3</sub> phase as the XRD results revealed. The formation of WO<sub>3</sub> NPs on the catalyst surface is due to the aggregation and sintering of tungsten oxides before

reaching the theoretical  $\gamma$ -alumina monolayer coverage ( $7 \text{ Wat. nm}^{-2}$ ). This value was calculated by Barton et al. at [10] assuming corner sharing  $\text{WO}_x$  octahedra with bond distances derived from  $m\text{-WO}_3$ . These data suggest that there are a fixed number of binding sites for tungsten oxides on  $\gamma$ -alumina surface. It is widely suggested this species anchor to the  $\gamma$ -alumina support by titrating the surface hydroxyls [11]. One possible assumption is that  $\text{WO}_3$  NPs start forming once all the surface hydroxyls are titrated. However, we cannot exclude the possibility that the formation of NPs starts before all the anchoring sites are occupied. At the highest tungsten surface density of  $5.9 \text{ Wat. nm}^{-2}$ , the  $m\text{-WO}_3$  is the predominant phase detected by Raman spectroscopy.

For the 9W catalyst, the band corresponding to polytungstates appears at  $973 \text{ cm}^{-1}$ . When 1 wt % of platinum was incorporated into  $\text{WO}_x/\text{Al}_2\text{O}_3$  (1Pt9W), a shift to a higher wavenumber occurred (from  $973 \text{ cm}^{-1}$  to  $1003 \text{ cm}^{-1}$ ). This shift might be due to the interaction between platinum and surface tungsten oxides that affects the distortion of the oxotungsten species. This approach was also found over  $\text{Pd-WO}_x/\text{TiO}_2$  system by Taylor et al. [12]. In  $\text{Pt/WO}_x/\text{Al}_2\text{O}_3$  catalytic systems, it appears that the transfer of electrons from the metallic platinum to the  $\text{WO}_x$  increases the  $\text{W=O}$  bond strength.

#### 5.2.1.6 XPS

XPS measurements were carried out to identify the surface chemical species, its oxidation state and to estimate the metal dispersion on the catalyst surface for  $\text{WO}_x/\text{Al}_2\text{O}_3$  and  $\text{Pt/WO}_x/\text{Al}_2\text{O}_3$  reduced samples.

For tungstated samples (without platinum), Al2p and W4f were used to study the Al and W elements, respectively. Fig. 5.5 shows the intensity ratio of the W4f and Al2p photoelectrons,  $(I_{\text{W}}/I_{\text{Al}})_{\text{XPS}}$ , compared to the bulk W/Al atomic ratio,  $(\text{W}/\text{Al})_{\text{bulk}}$ . The Kerkhof- Moulijn model (K-M model) has been used mainly to estimate the maximum concentration of tungsten at which a deviation from monolayer deposition occurs [13]. It can be observed that experimental and predicted by K-M model (black straight line) values almost match for tungsten surface density values below  $2.4 \text{ Wat. nm}^{-2}$ . The fact that the sample with 14 wt % W ( $3.9 \text{ Wat. nm}^{-2}$ ) slightly deviates from the linearity reveals that the  $\text{WO}_3$  is not only forming a two-dimensional phase in the catalyst surface, but also a small fraction of  $\text{WO}_3$  begins to form three-dimensional clusters ( $\text{WO}_3$  NPs). These results agree with previously shown XRD results and show that  $\text{WO}_3$  NPs are formed at tungsten surface density values below the theoretical monolayer content of  $7 \text{ Wat. nm}^{-2}$  [10]).

For Pt/WO<sub>x</sub>/Al<sub>2</sub>O<sub>3</sub> samples, due to the overlapping of Al2p and Pt4f lines, the Pt4d lines were used to study the platinum species on the catalyst surface, although this line is weaker. The E<sub>b</sub> obtained in the Pt4d<sub>5/2</sub> (314.8-315.9 eV) spectral region for the investigated samples (see Table 5.3) shows that the platinum species are completely reduced under the reduction conditions used [14]. Moreover, the E<sub>b</sub> of W4f<sub>7/2</sub> peaks can be associated with the existence of both WO<sub>3</sub> [15] and aluminum tungstates (Al<sub>2</sub>(WO<sub>4</sub>)<sub>3</sub>) [16]. However, due to the relative low calcination temperature used in catalyst preparation (450 °C), it can be assumed that aluminium tungstates were not formed or in negligible proportion.

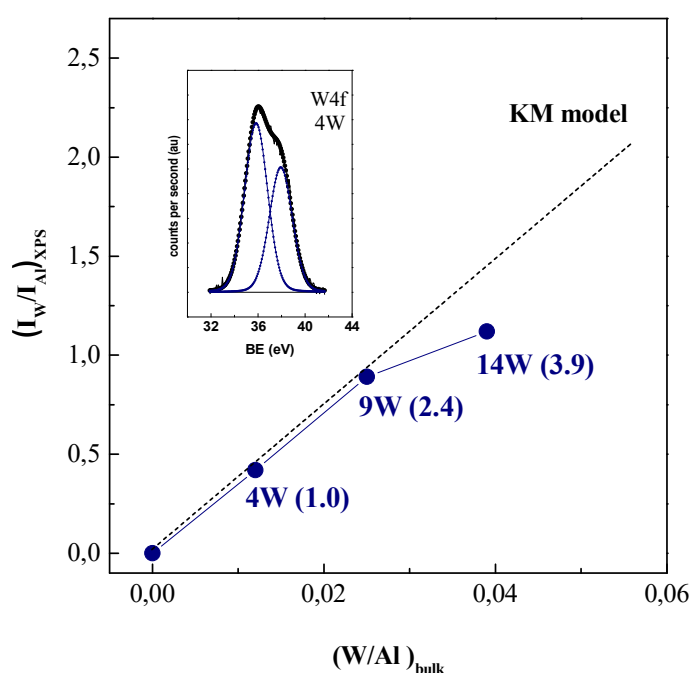


**Fig. 5.5.** Intensity ratio,  $(I_{W4f}/I_{Al2p})_{XPS}$ , of the W4f and Al2p photoelectrons against the bulk atomic ratio,  $(W/Al)_{bulk}$ . The black line corresponds to Kerkhof–Moulijn model. Tungsten surface density (W at. nm<sup>-2</sup>) in brackets.

The XPS peak intensities were used to calculate the atomic relative contents of the Pt/WO<sub>x</sub>/Al<sub>2</sub>O<sub>3</sub> reduced samples, which are given in Table 5.3. These surface atomic ratios of Pt and W related to Al were there compared with the bulk ratios obtained from ICP-OES. For fresh reduced catalysts with low platinum contents of 1 wt %, it can be observed that Pt/Al surface ratios are rather similar to the bulk ratios, which suggests a good platinum dispersion, even at high tungsten oxide contents (1Pt14W sample). For higher platinum loadings, considerably smaller atomic surface ratios than bulk ratios were obtained, which might be a consequence of a worse platinum dispersion.

**Table 5.3.** Bulk atomic ratio obtained from ICP-OES, surface atomic ratio obtained from XPS and BE of the Pt and W elements

Catalyst <sup>a</sup>	Pt/Al		W/Al		E <sub>b</sub>	
	Bulk	Surface	Bulk	Surface	Pt 4d <sub>5/2</sub>	W 4f <sub>7/2</sub>
1Pt4W (1.0)	0.003	0.003	0.011	0.029	315.0	35.5
1Pt9W (2.4)	0.004	0.003	0.027	0.056	314.9	35.6
1Pt14W (3.9)	0.004	0.003	0.045	0.080	315.0	35.8
4Pt8W (2.2)	0.012	0.007	0.026	0.032	314.9	35.9
4Pt8W (2.2) <sup>b</sup>	0.012	0.004	0.026	0.052	314.9	35.8
9Pt8W (2.2)	0.028	0.010	0.023	0.028	314.8	35.9
9Pt8W (2.2) <sup>b</sup>	0.028	0.007	0.023	0.041	315.9	35.9

<sup>a</sup> Tungsten surface density in brackets (W at. nm<sup>-2</sup>)

<sup>b</sup> Catalyst after use in glycerol hydrogenolysis reaction at 220 °C

XPS can provide further information about the metal anchoring sites. Kwak et al. [17] observed that when platinum was supported on bare  $\gamma$ -alumina, it was anchored at specific Al<sup>3+</sup> sites. In the case of WO<sub>x</sub> species, it is widely suggested that they anchor to the  $\gamma$ -alumina support by titrating the surface hydroxyls [11]. However, we are not aware of studies concerning the sites where platinum is incorporated on the WO<sub>x</sub>/Al<sub>2</sub>O<sub>3</sub> surface. The W/Al surface ratio results of the investigated samples can reveal further information about these sites. A remarkable decrease in W/Al surface ratio was found as the platinum loading increased on 1 wt % to 9 wt % (0.056 to 0.028) for the fresh reduced samples. This may be an indication that the platinum could partially be anchored at the WO<sub>x</sub> sites at high platinum loadings, in addition being anchored to the Al<sup>3+</sup> sites. Nevertheless, further research is required to corroborate this hypothesis. Interestingly, XPS results of used catalysts (reaction at 220 °C) revealed an important decline in Pt/Al and an increase in W/Al surface ratios comparing to the ones of the fresh catalysts, which suggests a potential dispersion loss of the platinum on the tungsten oxide sites under the hydrothermal reaction conditions employed. These reaction conditions might also affect the oxidation state of Pt species, as the shift of the E<sub>b</sub> of Pt 4d<sub>5/2</sub> for the used catalyst with the highest Pt content (9Pt8W) suggests.

### 5.2.1.7 H<sub>2</sub> TPR

The H<sub>2</sub>-TPR profiles of the catalysts are shown in Fig. 5.6. In the temperature range studied (40-1100 °C), the  $\gamma$ -alumina support cannot be reduced (not shown). Although the complete reduction of WO<sub>x</sub>/Al<sub>2</sub>O<sub>3</sub> catalysts requires temperatures higher

than 1100 °C, it is possible to verify that the initial reduction temperature decreases as the tungsten surface density increases. This could indicate that the interaction between WO<sub>x</sub> species and the support is stronger at low tungsten surface densities. The appearance of a peak at 780 °C for the 14W (3.9 W at. nm<sup>-2</sup>) catalyst may be related to the presence of WO<sub>3</sub> NPs as Raman spectroscopy and XPS, among other techniques, revealed. The 4Pt catalyst TPR profile shows two main peaks at 133 and 260 °C, which are attributed to the reduction of platinum oxides [18]. The appearance of small reduction peaks between 400 and 600 °C is probably due to platinum species highly interacting with the support. The tungsten oxides incorporation (4Pt8W catalyst) notably reduced the platinum reduction peaks, which were detected with the maxima at 120, 230, and 470 °C. This decrease in the reduction temperature of platinum oxides indicates an interaction between platinum and tungsten oxides, which generates more reducible platinum species.

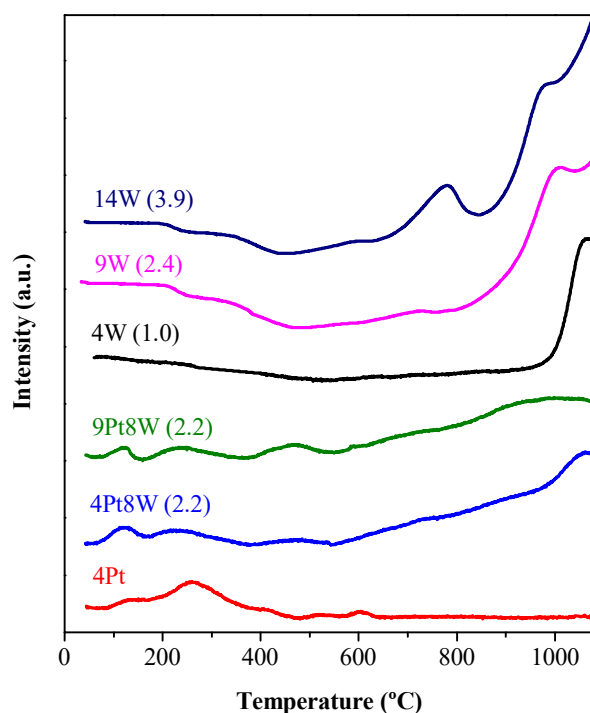


**Fig. 5.6.** H<sub>2</sub>-TPR of the calcined fresh catalysts. Tungsten surface density (W at. nm<sup>-2</sup>) in brackets

Concerning the reduction of WO<sub>x</sub> species in the catalysts containing platinum, it started at a temperature around 550 °C, in contrast to the catalyst without Pt (9W), for which higher temperatures were required. The spillover of the H<sub>2</sub> molecules on the platinum sites seems to facilitate WO<sub>x</sub> reduction. It has to be noticed that this effect is

more noticeable as the platinum content increases, which reveals that Pt and W phases are in closer proximity, which was also observed by XPS and TEM analysis.

### 5.2.1.8 NH<sub>3</sub> adsorption microcalorimetry

The amounts of NH<sub>3</sub> adsorbed at 80 °C and the corresponding interaction energies with the catalysts were determined by means of a volumetry-calorimetry coupled technique. Table 5.4 gives the total number of acid sites (estimated by  $V_{\text{tot}}$ ), the number of strong acid sites ( $V_{\text{irr}}$ ) as well as the initial differential heat of NH<sub>3</sub> adsorption ( $Q_{\text{init}}$ ).

**Table 5.4.** Initial heats of adsorption, total, and irreversible amounts of NH<sub>3</sub> adsorbed at an equilibrium pressure of 27 Pa, measured by NH<sub>3</sub> adsorption microcalorimetry.

Catalyst <sup>a</sup>	Acidity		
	$Q_{\text{init}}^{\text{b}}$ (kJ mol <sup>-1</sup> )	$V_{\text{tot}}^{\text{c}}$ (μmol NH <sub>3</sub> g <sup>-1</sup> )	$V_{\text{irr}}^{\text{d}}$ (μmol NH <sub>3</sub> g <sup>-1</sup> )
γ-Al <sub>2</sub> O <sub>3</sub>	179	219	120
9W (2.4)	235	287	153
2Pt8W (2.2)	222	260	147
4Pt8W(2.2)	224	278	161
4Pt	178	235	129

<sup>a</sup> Tungsten surface density in brackets (W at. nm<sup>-2</sup>)

<sup>b</sup> Initial heat evolved in the first dose of NH<sub>3</sub>

<sup>c</sup> Total amount of NH<sub>3</sub> retained as determined at 27 Pa of equilibrium pressure

<sup>d</sup> Irreversibly adsorbed amount of NH<sub>3</sub> as determined from the difference between the amounts adsorbed in the first and second adsorptions isotherms at 27 Pa

The volumetric adsorption isotherms (NH<sub>3</sub> uptake vs. equilibrium pressure) and differential heats of NH<sub>3</sub> adsorption (differential heats vs. NH<sub>3</sub> uptake) are reported in Fig. 5.7 (a) and (b), respectively. The volumetric isotherms of the studied samples displayed in all cases an initial vertical section proportional to the amount of strongly chemisorbed NH<sub>3</sub> [18]. The incorporation of tungsten oxide to the γ-alumina support increases the total acidity, as it is indicated by the total amount of NH<sub>3</sub> retained at 27 Pa of equilibrium pressure ( $V_{\text{tot}}$ ), as it can be observed in Fig. 5.7 (a) and Table 5.4. It has to be noticed that the catalysts with tungsten (with and without platinum) presented similar capacity to adsorb the NH<sub>3</sub> probe. The small variations might be due to differences in the real tungsten content. The non-tungstated catalyst (4Pt) presented a whole acidity similar to the one showed by the γ-alumina support, which indicates that the tungsten had the most remarkable impact on the total acidity of the catalyst.

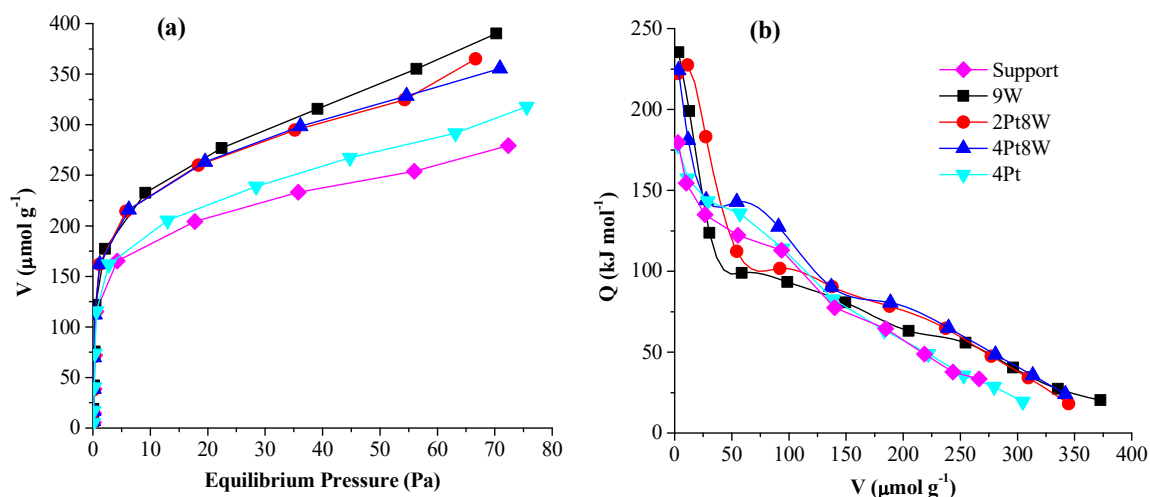


**Fig. 5.7.** (a) Volumetric adsorption isotherms, NH<sub>3</sub> uptake in μmol g<sup>-1</sup> vs. equilibrium pressure and (b) differential heats of NH<sub>3</sub> adsorption, differential heats in kJ mol<sup>-1</sup> vs. NH<sub>3</sub> uptake in μmol g<sup>-1</sup>. Tungsten surface density (W at. nm<sup>-2</sup>) in brackets.

Slight changes can be observed in the differential heats profiles as it is shown in Fig. 5.7 (b). In all cases, the heats of adsorption showed a decreasing trend upon increasing coverage, as usually observed for heterogeneous surfaces. The heterogeneity of the studied samples is due to the presence of acidic sites of different nature and strengths [19–22]. All the tungstated alumina investigated samples exhibited high initial  $Q_{\text{init}}$  (>200 kJ mol<sup>-1</sup>) and  $V_{\text{irr}}$ , very similar to each other, which are characteristic of the strongest acid sites, whereas lower values were presented by the  $\gamma$ -alumina support and the catalysts without tungsten.

It can also be seen in Fig. 5.7 (b) that the presence of relatively high amounts of platinum (4 wt %) enhanced the content of medium strength acid sites, which seems to be independent of the presence of tungsten.

#### 5.2.1.9 FTIR spectroscopy of adsorbed pyridine

The effect of the tungsten oxide content (and tungsten surface density) and the effect of the incorporation of platinum on WO<sub>x</sub>/Al<sub>2</sub>O<sub>3</sub> were studied by FTIR of adsorbed pyridine on the samples after successive heating at 200 and 300 °C (Fig. 5.8). Brönsted and Lewis acid sites are easily identified and distinguished by examination of the 1700-1400 cm<sup>-1</sup> range [23].

The type and strength of acidity on  $\gamma$ -Al<sub>2</sub>O<sub>3</sub> has been a matter of controversy for some time. In this work, the pyridine adsorbed on the  $\gamma$ -Al<sub>2</sub>O<sub>3</sub> support led to the following main bands at 200 °C in this frequency range: 1614 (ν<sub>8a</sub>) cm<sup>-1</sup>, 1578 (ν<sub>8b</sub>)

$\text{cm}^{-1}$ , and  $1450$  ( $\nu_{19b}$ )  $\text{cm}^{-1}$ , which can be assigned to coordinately bonded pyridine on Lewis acid sites [24]. Another band at  $1493$  ( $\nu_{19a}$ )  $\text{cm}^{-1}$  was found, which is common of both vibrations due to pyridinium ion ( $\text{PyH}^+$ ), produced by the reaction of pyridine with Brönsted sites, and coordinately bonded pyridine on Lewis sites. However, the non-appearance of another  $\text{PyH}^+$  bands seems to indicate the exclusive Lewis character of the  $\gamma\text{-Al}_2\text{O}_3$  support acid sites.

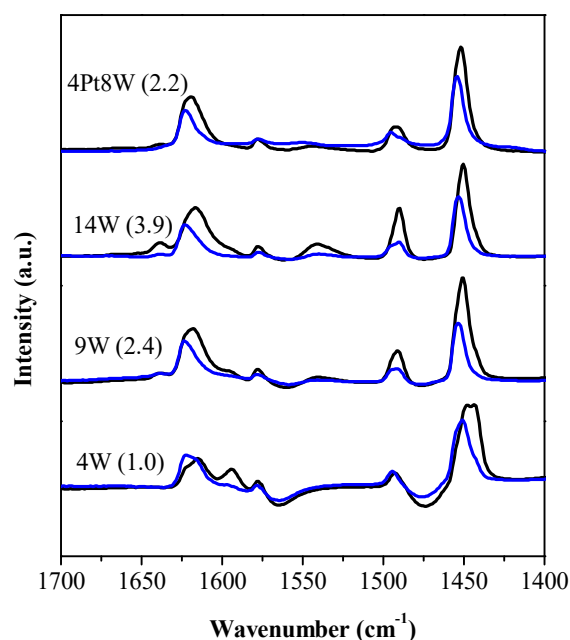


**Fig. 5.8.** FTIR of adsorbed pyridine on fresh calcined  $\text{WO}_x/\text{Al}_2\text{O}_3$  and  $\text{Pt}/\text{WO}_x/\text{Al}_2\text{O}_3$  catalysts. Desorption temperature of  $200\text{ }^\circ\text{C}$  (black line) and  $300\text{ }^\circ\text{C}$  (blue line). Tungsten surface density (W at.  $\text{nm}^{-2}$ ) in brackets.

The three characteristic bands of Lewis sites present on  $\gamma$ -alumina and the band at about  $1490\text{ cm}^{-1}$  have also been observed for all the samples studied. Tungsten surface density plays a key role in the formation of the Brönsted acid sites on the catalyst surface. No evidence of Brönsted characteristic bands was found at low densities of  $1.0\text{ Wat. nm}^{-2}$ , so the acidity appears to be almost solely due to Lewis acid sites. On  $\gamma\text{-Al}_2\text{O}_3$  tungstated samples, common bands related to  $\text{PyH}^+$  began to appear at densities  $\geq 2.4\text{ Wat. nm}^{-2}$ . On  $9\text{W}$  ( $2.4\text{ Wat. nm}^{-2}$ ) catalyst at  $200\text{ }^\circ\text{C}$ , these bands were found at  $1540\text{ cm}^{-1}$  and  $1638\text{ cm}^{-1}$ , supporting the presence of Brönsted sites [24]. The isolated tungsten oxide species, observed by Raman spectroscopy at low tungsten surface densities ( $< 2.4\text{ Wat. nm}^{-2}$ ), cannot delocalize the negative charge required for the formation of Brönsted acid sites. However, at higher densities, polytungstates started to be formed resulting in the formation of an extended network of tungsten oxide species, over which an excess negative charge may be delocalized [10,25].



Qualitatively, the intensities of the IR bands of Lewis sites progressively decreased as the desorption temperature increased and shifted toward higher wavenumbers, which confirms the high strength of the Lewis sites. The same trend was observed for Brönsted sites.

In order to make a semi-quantitatively study of the samples acidity, the area of 1450 cm<sup>-1</sup> peak for Lewis sites and the area of 1540 cm<sup>-1</sup> peak for Brönsted sites were used. In Table 5.5, the results of the Brönsted to Lewis ratio (B/L) at the different pyridine desorption temperatures are shown. It can be noticed that WO<sub>3</sub> NPs formed at high tungsten surface densities (> 3.9 Wat. nm<sup>-2</sup>) had not a contribution to the catalyst acidity, displaying slightly lower B/L ratio than the sample with 2.4 Wat. nm<sup>-2</sup>.

**Table 5.5.** Brönsted to Lewis acid sites ratio (B/L) obtained from the FTIR of adsorbed pyridine

Catalyst <sup>a</sup>	B/L ratio at 200 °C	B/L ratio at 300 °C
γ-Al <sub>2</sub> O <sub>3</sub>	0.00	0.00
4W (1.0)	0.00	0.00
9W (2.4)	0.25	0.19
14W (3.9)	0.23	0.15
4Pt8W (2.2)	0.28	<sup>b</sup>

<sup>a</sup> Tungsten surface density in brackets (W at. nm<sup>-2</sup>)

<sup>b</sup> The area was too low to be integrated but not equal to zero

On the other hand, for 9W and 4Pt8W, samples with a close tungsten surface density (2.4 and 2.2 Wat. nm<sup>-2</sup>, respectively), the decrease of the Lewis acidity was more noticeable than the Brönsted acidity decrease after desorption at 200 °C; therefore, the B/L ratio increased. However, Brönsted sites were hardly observed at 300 °C for the catalyst containing platinum (4Pt8W). This could mean that the presence of platinum reduced the strength of Brönsted acid sites.

It is worth adding that the hydrogen atoms forming by H<sub>2</sub> dissociation, during the catalyst pretreatment and along the reaction, could be involved in the generation and maintenance of Brönsted sites [9].

### **5.2.2 Effect of tungsten surface density on glycerol conversion and selectivity to PDOs**

The effect of tungsten surface density was investigated in the aqueous phase glycerol hydrogenolysis. It is widely suggested that the production of 1,3-PDO from

glycerol requires the presence of Brønsted acid sites [26] but also a hydrogenation metal able to activate the molecular  $H_2$  present in the reacting atmosphere. As we have shown above, an interesting feature of the supported  $WO_x/Al_2O_3$  catalysts is that their B/L acidity can be tuned as a function of the tungsten surface density. The activity test results are presented in Fig. 5.9 (a) and (b) obtained at 24 h reaction time, 220 °C and 45 bar with the catalyst containing 1 wt % of Pt and different tungsten surface density values.

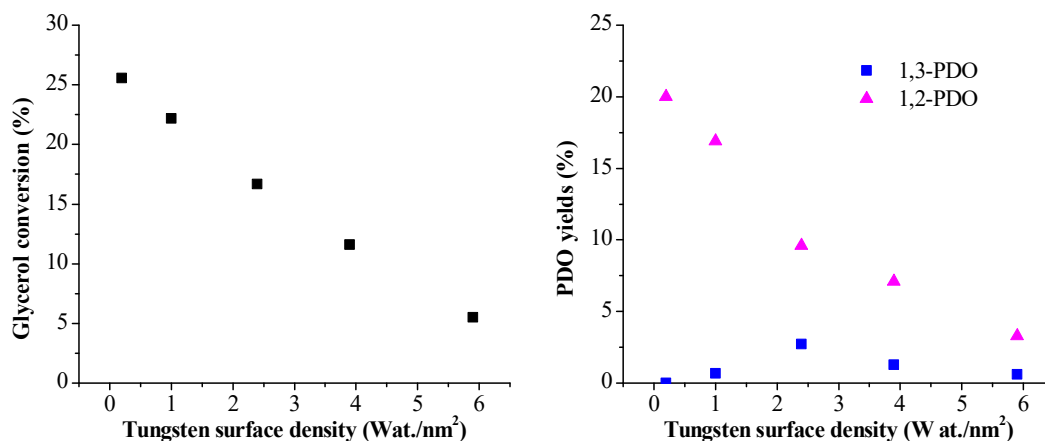


**Fig. 5.9.** (a) Glycerol conversion values and (b) PDOs yields obtained for  $Pt/WO_x/Al_2O_3$  catalysts with 1 wt % Pt as a function of the tungsten surface density, in the hydrogenolysis of glycerol at 220 °C, 45 bar  $H_2$  pressure, and 24 h reaction time.

Glycerol conversion diminished with increasing tungsten surface density as it is shown in Fig. 5.9 (a). On the other hand, it can be observed a different trend in the PDOs yields. Whereas 1,2-PDO yield decreased as the tungsten density increased, the 1,3-PDO production was increased to a maximum value and then decreased as it can be seen in Fig. 5.9 (b). The progressive coverage of the hydroxyl groups of the  $\gamma$ -alumina by the tungsten oxides, as the tungsten surface density increases [8], may explain the observed decrease in the glycerol conversion. It seems that tungsten oxide sites are less active than those of the  $\gamma$ -alumina support for the hydrogenolysis reaction of glycerol. This feature was not observed when other supports such as silica or zirconia were used [26,27]. The strong interaction between the  $\gamma$ -alumina support and tungsten oxide and therefore the low interaction between platinum and tungsten oxides, at low platinum loadings, could be the reason for this poor glycerol conversion.

The incorporation of the tungsten oxide enhances the total acidity of the catalyst, as observed from the  $NH_3$  adsorption calorimetry results. B/L ratio also increased with increasing the tungsten surface density due to the generation of polytungstate species, as

the FTIR of adsorbed pyridine (Table 5.5) and the Raman spectroscopy (Fig. 5.4) analysis showed. This fact causes a decrease in the 1,2-PDO yield and an increase in the 1,3-PDO yield until a density of 2.4 Wat. nm<sup>-2</sup> was reached. For higher tungsten surface densities, the formation of crystalline WO<sub>3</sub> NPs has a negative effect on the 1,3-PDO yield due to the over-hydrogenolysis reactions obtaining 1-PO as the main by-product. This effect cannot be just related to the catalyst acidity, because small acidity differences were found between WO<sub>x</sub>/Al<sub>2</sub>O<sub>3</sub> containing WO<sub>3</sub> NPs and the sample with the maximum polytungstate content and without these WO<sub>3</sub> NPs (see Table 5.5 entries 3 and 4). This aspect is later discussed with the proposed reaction mechanism.

Therefore, it seems that the presence of highly dispersed polytungstate species in the catalyst surface, which provide Brönsted acid sites, is necessary in order to produce 1,3-PDO by hydrogenolysis of glycerol. It was found that the optimum surface density of tungsten that maximizes the production of 1,3-PDO at these conditions is 2.4 Wat. nm<sup>-2</sup>, obtaining a maximum 1,3-PDO selectivity of 16.4% (2.7% yield).

### **5.2.3 Effect of platinum metal content on glycerol conversion and selectivity to PDOs**

The effect of platinum content of Pt/WO<sub>x</sub>/Al<sub>2</sub>O<sub>3</sub> catalysts was also studied in the glycerol hydrogenolysis reaction. A series of catalysts with different platinum content and similar tungsten surface density, nearly the optimum value previously obtained (2.2 Wat. nm<sup>-2</sup>), were prepared and tested.

The activity results are represented in Fig. 5.10 (a) and (b), and the values are given in Table 5.1. As expected, when the platinum content increased, the glycerol conversion also increased, from 25.6 % for 1 wt % Pt to 60.3 % for 9 wt % Pt. The hydrogen molecules present in the reacting atmosphere might be dissociatively adsorbed on platinum metal giving rise to hydrogen atoms that are subsequently involved in the activation of the adsorbed glycerol molecule and in the later transformation to the products. The electronic interactions, observed by TPR and Raman spectroscopy, between platinum and the highly dispersed polytungstates could also contribute to increasing the activation of H<sub>2</sub> molecules on the platinum active sites. These interactions were more pronounced as the platinum content increased. On the other hand, glycerol conversion does not seem to be clearly correlated to the platinum dispersion, because the highest values were obtained at the lowest platinum dispersions.

More interestingly, the platinum content had not only an effect on glycerol conversion but it also affected PDOs selectivity. It must be added that the most remarkable effect of platinum loading was found in the 1,2-PDO selectivity: it decreased from 57.2 % for 1 wt % platinum catalyst to 11.0 % for 9 wt % platinum content catalyst, as it can be observed in Fig. 5.10 (b). The 1,3-PDO selectivity increased slightly and progressively with the platinum content increase. For the catalyst with 1 wt % of platinum, the 1,3-PDO selectivity was only of 16.4 %, whereas the platinum content increases up to 9 wt % enhanced this value until 31.2 %.

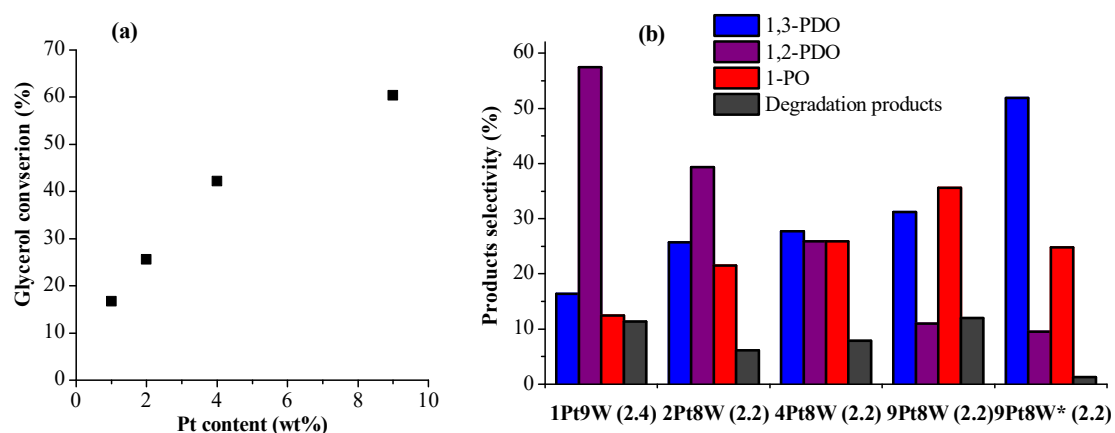


**Fig. 5.10.** (a) Glycerol conversion values and (b) product selectivities obtained for Pt/WO<sub>x</sub>/Al<sub>2</sub>O<sub>3</sub> catalysts with a constant tungsten surface density as a function of the platinum content, in the hydrogenolysis of glycerol at 220 °C (200 °C for 9Pt8W\* catalyst), 45 bar H<sub>2</sub> pressure, and 24 h reaction time.

The amount of platinum does not significantly contribute neither to the total acidity nor to the relative B/L ratio, as it was observed by NH<sub>3</sub> adsorption calorimetry and FTIR of the adsorbed pyridine techniques. Therefore, the effect of the platinum loading on the PDOs relative formation must be related to other factors. The XPS results suggested that for high platinum contents (>5 wt %), it anchors to the tungsten oxides sites (in addition to the Al<sup>3+</sup> preferential anchoring sites). Although this hypothesis must be confirmed by other techniques, it is clear that the closer proximity between the Pt and WO<sub>x</sub> active sites seems to enhance the selectivity toward 1,3-PDO while decreasing the selectivity of 1,2-PDO. The main drawback is that the formation of 1,3-PDO seems to be accompanied by the over-hydrogenolysis to 1-PO. In order to avoid the undesirable reactions, the reaction temperature was decreased to 200 °C for the 9Pt8W catalyst. The results, shown in Table 5.1, indicate that the over-

hydrogenolysis of 1,3-PDO to 1-PO was partially avoided at 200 °C, enhancing the 1,3-PDO selectivity up to 51.9% (27.6% yield).

### 5.3 Proposed reaction mechanism

The most accepted mechanism for the formation of PDOs from glycerol hydrogenolysis is the *dehydration-hydrogenation* route. In the first step, glycerol is dehydrated to acetol or 3-hydroxypropanal (3-HPA), while in the second step, these intermediates are hydrogenated to 1,2 and 1,3-PDO, respectively. The formation of acetol is thermodynamically favoured due to its higher stability as compared to 3-HPA, which explains why normally 1,2-PDO is the major product on glycerol hydrogenolysis. Our activity tests and characterization results match with previously reported studies that indicate that Brönsted acidity is required for the production of 1,3-PDO: The maximum selectivity toward 1,3-PDO was obtained at the tungstate surface density showing the highest B/L ratio (at 2.4 Wat. nm<sup>-2</sup>). However, there are some important evidences suggesting that the formation of 1,3-PDO cannot be only related to the amount of Brönsted acid sites.

Recently, Tomishige's group [28] studied the influence that adding different concentrations of H<sub>2</sub>SO<sub>4</sub> as acid co-catalyst had on the glycerol hydrogenolysis reaction, over another noble metal-oxophilic metal catalytic system (Ir-ReO<sub>x</sub>/SiO<sub>2</sub>). Interestingly, the positive effect of H<sub>2</sub>SO<sub>4</sub> on the production of 1,3-PDO over the Ir-ReO<sub>x</sub>/SiO<sub>2</sub> catalyst was saturated at H<sup>+</sup>/Re = 1. Both activity and selectivity were almost unchanged between H<sup>+</sup>/Ir = 1 and 12.4. Similarly, in our results, the yield of 1,3-PDO was more than two times higher with the 1Pt9W catalyst compared with the 1Pt14W catalyst even though both catalysts presented similar B/L ratios. In addition to this, it was observed that the amount of Pt and the interaction between Pt and WO<sub>x</sub> active sites also affect the selectivity toward 1,3-PDO.

For Pt-W-Al catalysts, Kaneda et al. proposed a mechanism [29,30] which involved an initial glycerol adsorption on Al-OH site forming an alkoxide specie. As it has been mentioned above, the tungsten oxide species anchor to the  $\gamma$ -Al<sub>2</sub>O<sub>3</sub> support at its surface hydroxyls [11], and therefore, an increase in tungsten surface density should imply a decrease in Al-OH sites.

We suggest that glycerol is adsorbed on tungsten active sites forming an alkoxide (see reaction scheme in Fig. 5.11). Next, a proton, coming from a Brönsted

acid site provided by polytungstate species, protonates the secondary hydroxyl group of the alkoxide. After dehydration, a secondary carbocation is formed. The adsorbed carbocation is attacked by a hydride specie generated on the Pt active sites. Further hydrolysis yields 1,3-PDO. The key step in this reaction seems to be the fast hydrogenation of the secondary carbocation in order to avoid its conversion into acrolein (precursor of 1-PO). The stabilization of the carbocation might be crucial at this point. It was suggested that only the polytungstate species are able to delocalize the negative charge required for the carbocation intermediate stabilization, instead of the monotungstate and  $\text{WO}_3$  NPs species [10]. This explains well the reason why the best results (at similar platinum content of 1 wt %) were obtained for the catalyst in which more polytungstate species are generated before the  $\text{WO}_3$  NPs formation.

These  $\text{WO}_3$  NPs are not only inactive for the carbocation stabilization, but they also are tridimensional structures that limit the accessibility of the glycerol to the polytungstate acid sites. Another important factor is the close proximity between the Pt and the  $\text{WO}_x$  active sites, which might facilitate the attack of the hydride species for the fast hydrogenation of the secondary carbocation. This explains the higher selectivities toward 1,3-PDO that are obtained at higher Pt contents.

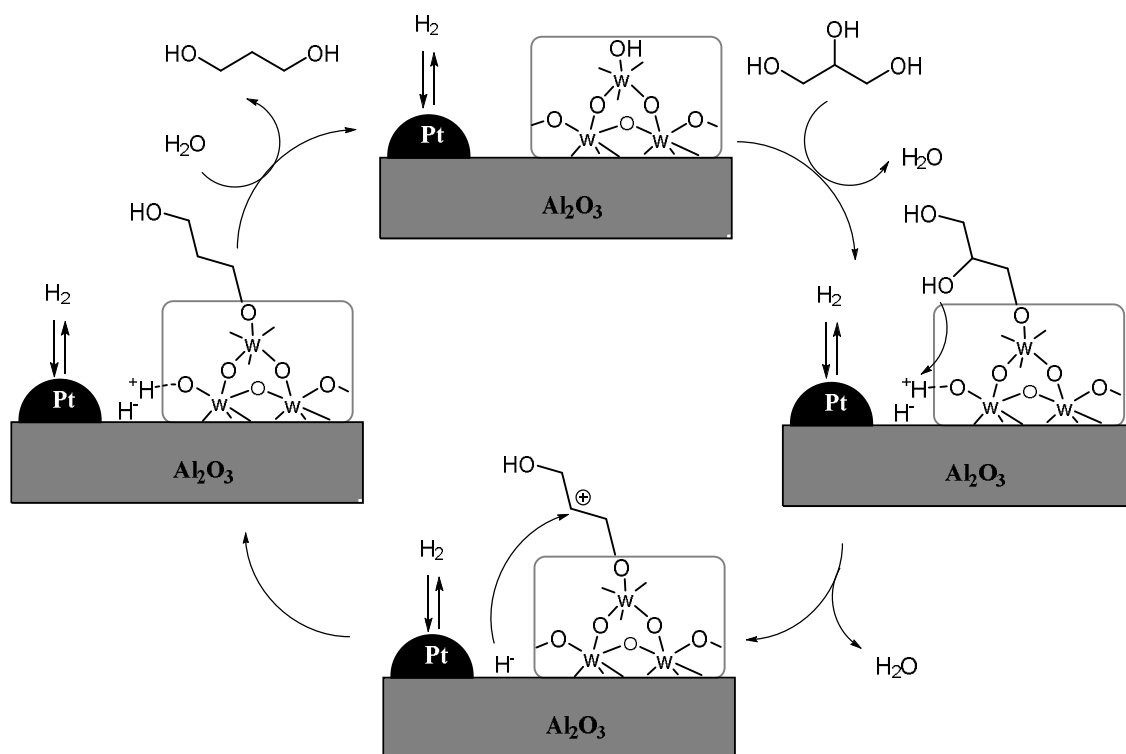


Fig. 5.11. Reaction mechanism proposed for glycerol hydrogenolysis to 1,3-PDO.

## **5.4 Conclusions**

In this work, it has been demonstrated that the bimetallic Pt/WO<sub>x</sub>/Al<sub>2</sub>O<sub>3</sub> catalytic system is effective for the selective hydrogenolysis of glycerol to 1,3-PDO. This study proved that 1,3-PDO selectivity depends on the tungsten surface density that controls the kind of tungsten oxide species deposited on the catalyst surface. The maximum selectivity was achieved when the highest content of polytungstate species are formed but before the appearance of WO<sub>3</sub> NPs, concluding that in order to selectively obtain 1,3-PDO, the presence of highly dispersed polytungstate species is required. These species are able to delocalize the negative charge required for the formation of Brønsted acid sites. However, the results from this work also indicate that not only acidity plays a role in the selective hydrogenolysis of glycerol to 1,3-PDO, but also the platinum and tungsten oxides sites interactions may be involved. The closer proximity between platinum and tungsten oxides at high platinum content and the electronic interactions between acid and metallic sites could be the responsible for the enhancement of the 1,3-PDO yields. Further research should allow improving Pt-WO<sub>x</sub> synergies and as a result the yield to 1,3-PDO.

## **Acknowledgments**

This work was supported by University of the Basque Country (UPV/EHU), European Union through the European Regional Development Fund (FEDER) (Spanish MICIN Project: CTQ2012-38204-C03-03), and the Basque Government (Researcher Training Programme of the Department of Education, Universities and Research). The authors also gratefully acknowledge Prof. José Luis García Fierro from Institute of Catalysis and Petrochemistry of Madrid for the technical support in the XPS measurements.

## References

- [1] C. Pfaff, M.J. Pérez Zurita, C. Scott, P. Patiño, M.R. Goldwasser, J. Goldwasser, et al., Absolute surface coverage of tungsten-alumina catalysts, *Catal. Letters*. 49 (1997) 13–16.
- [2] K.S.W. Singh, J. Rouquerol, G. Bergeret, P. Gallezot, M. Vaarkamp, D.C. Koningsberger, et al., Characterization of Solid Catalysts, in: G. Ertl, H. Knözinger, F. Schüth, J. Weitkamp (Eds.), *Handb. Heterog. Catal.*, Wiley-VCH Verlag GmbH, 2008: pp. 427–582.
- [3] A.D. Allian, K. Takanebe, K.L. Furdala, X. Hao, T.J. Truex, J. Cai, et al., Chemisorption of CO and Mechanism of CO Oxidation on Supported Platinum Nanoclusters, *J. Am. Chem. Soc.* 134 (2012) 743.
- [4] A. Karakonstantis, L., Bourikas, K., Lycourghiotis, Tungsten–Oxo-Species Deposited on Alumina, *J. Catal.* 162 (1996) 295–305.
- [5] M.I. Zaki, N.E. Fouad, S. a a Mansour, a. I.M. Rabee, Structure-reduction correlation of supported tungsten(VI)-oxo-species, *Appl. Surf. Sci.* 282 (2013) 898–907.
- [6] M.-Y. Kim, J.-H. Park, C.-H. Shin, S.-W. Han, G. Seo, Dispersion Improvement of Platinum Catalysts Supported on Silica, Silica-Alumina and Alumina by Titania Incorporation and pH Adjustment, *Catal. Letters*. 133 (2009) 288–297.
- [7] X. Wu, L. Zhang, D. Weng, S. Liu, Z. Si, J. Fan, Total oxidation of propane on Pt/WOx/Al<sub>2</sub>O<sub>3</sub> catalysts by formation of metastable Pt delta+ species interacted with WOx clusters, *J. Hazard. Mater.* 225-226 (2012) 146–154.
- [8] I.E. Wachs, T. Kim, E.I. Ross, Catalysis science of the solid acidity of model supported tungsten oxide catalysts, *Catal. Today*. 116 (2006) 162–168.
- [9] D.G. Barton, M. Shtein, R.D. Wilson, S.L. Soled, E. Iglesia, Structure and Electronic Properties of Solid Acids Based on Tungsten Oxide Nanostructures, (1999) 630–640.
- [10] D.G. Barton, S.L. Soled, G.D. Meitzner, F. G.A., E. Iglesia, Structural and Catalytic Characterization of Solid Acids Based on Zirconia Modified by Tungsten Oxide, *J. Catal.* 181 (1999) 57–72.
- [11] M.M. Ostromecki, L.J. Burcham, I.E. Wachs, The influence of metal oxide additives on the molecular structures of surface tungsten oxide species on alumina. II. In situ conditions, *J. Mol. Catal. A Chem.* 132 (1998) 59–71.
- [12] M.N. Taylor, W. Zhou, T. Garcia, B. Solsona, A.F. Carley, C.J. Kiely, et al., Synergy between tungsten and palladium supported on titania for the catalytic total oxidation of propane, *J. Catal.* 285 (2012) 103–114.
- [13] V. León, A simplified Kerkhof-Moulijn model for dispersion quantification from XPS atomic concentrations, *Surf. Sci.* 339 (1995) L931–L934.
- [14] J.Z. Shyu, K. Otto, Identification of platinum phases on  $\gamma$ -alumina by XPS, *Appl. Surf. Sci.* 32 (1988) 246–252.
- [15] S.F. Ho, S. Contarini, J.W. Rabalais, Ion-beam-induced chemical changes in the oxyanions (Moyn-) and oxides (Mox) where M = chromium, molybdenum, tungsten, vanadium, niobium and tantalum, *J. Phys. Chem.* 91 (1987) 4779–4788.



- [16] W. Grünert, E.S. Shpiro, R. Feldhaus, K. Anders, G.V. Antoshin, K.M. Minachev, Reduction behavior and metathesis activity of WO<sub>3</sub>/Al<sub>2</sub>O<sub>3</sub> catalysts I. An XPS investigation of WO<sub>3</sub>/Al<sub>2</sub>O<sub>3</sub> catalysts, *J. Catal.* 107 (1987) 522–534.
- [17] J.H. Kwak, J. Hu, D. Mei, C.-W. Yi, D.H. Kim, C.H.F. Peden, et al., Coordinatively unsaturated Al<sup>3+</sup> centers as binding sites for active catalyst phases of platinum on gamma-Al<sub>2</sub>O<sub>3</sub>, *Science*. 325 (2009) 1670–1673.
- [18] D. Sprinceana, M. Caldararu, N. Ionescu, A. Auroux, Calorimetric Study of the Acidity and Interface Effects of Tin Dioxide Layers Deposited on Another Metal Oxide, *J. Therm. Anal. Calorim.* 56 (1999) 109–115.
- [19] S. Bennici, A. Auroux, Thermal Analysis and Calorimetric Methods, in: S.D. Jackson, J.S.J. Hargreaves (Eds.), *Met. Oxide Catal.*, Wiley-VCH Verlag GmbH & Co. KGaA, 2009: pp. 391–441.
- [20] A. Auroux, D. Sprinceana, A. Gervasini, Support Effects on de-NO<sub>x</sub> Catalytic Properties of Supported Tin Oxides, *J. Catal.* 195 (2000) 140–150.
- [21] a. Auroux, Acidity characterization by microcalorimetry and relationship with reactivity, *Top. Catal.* 4 (1997) 71–89.
- [22] C. Busco, A. Barbaglia, M. Broyer, V. Bolis, G.M. Foddanu, P. Ugliengo, Characterisation of Lewis and Brønsted acidic sites in H-MFI and H-BEA zeolites: A thermodynamic and ab initio study, *Thermochim. Acta.* 418 (2004) 3–9.
- [23] E. Parry, An infrared study of pyridine adsorbed on acidic solids. Characterization of surface acidity, *J. Catal.* 2 (1963) 371–379.
- [24] G. Busca, The surface acidity of solid oxides and its characterization by IR spectroscopic methods. An attempt at systematization, *Phys. Chem. Chem. Phys.* 1 (1999) 723–736.
- [25] J. Macht, E. Iglesia, Structure and function of oxide nanostructures: catalytic consequences of size and composition., *Phys. Chem. Chem. Phys.* 10 (2008) 5331–5343.
- [26] L.-Z. Qin, M.-J. Song, C.-L. Chen, Aqueous-phase deoxygenation of glycerol to 1,3-propanediol over Pt/WO<sub>3</sub>/ZrO<sub>2</sub> catalysts in a fixed-bed reactor, *Green Chem.* 12 (2010) 1466.
- [27] L. Gong, Y. Lu, Y. Ding, R. Lin, J. Li, W. Dong, et al., Selective hydrogenolysis of glycerol to 1,3-propanediol over a Pt/WO<sub>3</sub>/TiO<sub>2</sub>/SiO<sub>2</sub> catalyst in aqueous media, *Appl. Catal. A Gen.* 390 (2010) 119–126.
- [28] Y. Amada, Y. Shinmi, S. Koso, T. Kubota, Y. Nakagawa, K. Tomishige, Reaction mechanism of the glycerol hydrogenolysis to 1,3-propanediol over Ir-ReO<sub>x</sub>/SiO<sub>2</sub> catalyst, *Appl. Catal. B Environ.* 105 (2011) 117–127.
- [29] T. Mizugaki, T. Yamakawa, R. Arundhathi, T. Mitsudome, K. Jitsukawa, K. Kaneda, Selective hydrogenolysis of glycerol to 1,3-propanediol catalyzed by Pt nanoparticles-AlO<sub>x</sub>/WO<sub>3</sub>, *Chem. Lett.* 41 (2012) 1720–1722.
- [30] R. Arundhathi, T. Mizugaki, T. Mitsudome, K. Jitsukawa, K. Kaneda, Highly selective hydrogenolysis of glycerol to 1,3-propanediol over a boehmite-supported platinum/tungsten catalyst, *ChemSusChem.* 6 (2013) 1345–1347.

## **CHAPTER 6.**

### **Influence of the support of bimetallic Pt-WO<sub>x</sub> catalysts on glycerol hydrogenolysis**



---

**Table of contents**

ABSTRACT.....	131
6.1 EXPERIMENTAL .....	131
6.1.1 Catalyst preparation .....	131
6.1.2 Catalyst characterisation .....	132
6.1.3 Activity tests .....	132
6.2 RESULTS AND DISCUSSION .....	132
6.2.1 Effect of the tungsten surface density and Pt-WO <sub>x</sub> interactions .....	132
6.2.1.1 XRD.....	133
6.2.1.2 Chemical composition and textural properties.....	136
6.2.1.3 Raman spectroscopy.....	139
6.2.1.4 SEM.....	142
6.2.1.5 H <sub>2</sub> -TPR .....	145
6.2.1.6 Activity tests .....	147
6.2.2 Effect of the Pt dispersion and the Pt-WO <sub>x</sub> interactions .....	149
6.2.2.1 Effect of Pt dispersion .....	149
6.2.2.2 Effect of Pt loading.....	151
6.3 CONCLUSIONS.....	153
REFERENCES.....	154



## Abstract

In the metal supported catalysis, the starting material of the support has a direct influence on the active sites formation, the metal dispersion and interactions, and the catalyst stability [1,2], among other properties. In this Chapter 6, three aluminium oxide materials, with a different nature, were used as supports of the bimetallic Pt-WO<sub>x</sub> catalysts. Those catalysts were tested in the glycerol hydrogenolysis in order to gain more knowledge about some of the main catalytic parameters involved in the reaction. For this purpose, pseudo boehmite ( $\gamma$ -AlO(OH)) and alumina ( $\gamma$ -Al<sub>2</sub>O<sub>3</sub>) prepared by a sol-gel (SG) method were compared with the previously tested commercial  $\gamma$ -Al<sub>2</sub>O<sub>3</sub> (Al<sup>com</sup>). According to the literature, the pseudo  $\gamma$ -AlO(OH) is a useful material for the synthesis of  $\gamma$ -Al<sub>2</sub>O<sub>3</sub> since is the precursor that requires less energy [3,4].

In Chapter 5 it was reported that the kind of WO<sub>x</sub> species present on the catalyst surface, which is controlled by the tungsten surface density ( $\rho_w$ ), is a crucial factor in the glycerol hydrogenolysis to 1,3-propanediol (1,3-PDO). The different WO<sub>x</sub> species that may be present on the catalyst surface are: monotungstates (WO<sub>4</sub>), polytungstates (WO<sub>5</sub>/WO<sub>6</sub>) and WO<sub>3</sub> nanoparticles (NPs) [5,6]. More precisely, our previous findings showed that polymeric WO<sub>x</sub>, polytungstates, were the only species able to delocalize the negative charge required for the formation and stabilisation of Brønsted acid sites, which are directly involved in the 1,3-PDO formation. An important decrease of the 1,3-PDO yield was reported as soon as the WO<sub>3</sub> NPs started to appear.

Taking into account all these facts, in the current Chapter the importance of the  $\rho_w$  parameter was demonstrated unequivocally. Other parameters such as the Pt-WO<sub>x</sub> interactions seemed to have an enormous influence in the reaction as well. Interestingly, the dispersion of Pt was also found to play a key role, mainly in the conversion of glycerol.

## 6.1 Experimental

### 6.1.1 Catalyst preparation

The procedure for the preparation of the Pt/WO<sub>x</sub> catalysts on non-conventional Al-based supports (denoted as *xPtyW support*) through the wetness impregnation (WI) method was described in the section 4.1.2 of the Chapter 4. These catalysts were tested

in the glycerol hydrogenolysis in order to study the effect of the support on different parameters of the catalysts as well as on their activity and selectivity.

The chemical vapour impregnation (CVI) technique was used for preparing highly dispersed Pt nanoparticles over WO<sub>x</sub>/Al<sub>2</sub>O<sub>3</sub> samples (described in section 4.1.3) and was used for studying the effect of the Pt dispersion on the glycerol hydrogenolysis. This catalyst was denoted as xPt<sup>CVI</sup><sub>y</sub>W Al<sup>com</sup>. More details about the nomenclature for the catalysts employed can be found in the Table 4.1 of Chapter 4.

### **6.1.2 Catalyst characterisation**

The elemental, textural and structural properties of the catalysts were measured by N<sub>2</sub> physisorption, inductively coupled plasma optical emission spectrometry (ICP-OES), temperature programme reduction with a constant flow of H<sub>2</sub> (H<sub>2</sub>-TPR), CO chemisorption, Raman spectroscopy, X-ray diffraction (XRD) and scanning electron microscopy (SEM) techniques.

The equipments, as well as the conditions, used in each of the characterisation methods employed in this Chapter 6 were described in detail in the section 4.4 of Chapter 4.

### **6.1.3 Activity tests**

The activity tests were carried out in the autoclave described in the section 4.3.1 of Chapter 4. Prior to the activity test, the catalysts were *in-situ* reduced for 1 h under a stream of pure H<sub>2</sub> (100 NmL/min) at 300 °C, with the exception of the sample prepared by CVI which required higher reduction temperatures (400 °C).

## **6.2 Results and discussion**

### **6.2.1 Effect of the tungsten surface density and Pt-WO<sub>x</sub> interactions**

The effect of the tungsten surface density ( $\rho_w$ ) and Pt-WO<sub>x</sub> interactions was investigated in the aqueous glycerol hydrogenolysis. For this purpose, three different Al-based supports were used: commercial  $\gamma$ -Al<sub>2</sub>O<sub>3</sub> (Al<sup>com</sup>), and  $\gamma$ -Al<sub>2</sub>O<sub>3</sub> and pseudo  $\gamma$ -AlO(OH) prepared by the SG method, denoted as Al<sup>SG</sup> and Al<sup>SG'</sup>, respectively (structural details in the section 6.2.1.1).

In order to modify the  $\rho_w$  values of the Pt/WO<sub>x</sub>/Al-based catalysts and to study the effect of this parameter on the activity test, three different strategies were carried out. In all these cases the Pt loading remained constant (2 wt%):

1. Using of catalysts with a nominal W content of 10 wt% supported on the different Al-based materials. In spite of their similar W content, they have a different  $\rho_w$  due to the different  $S_{BET}$  of their supports (see section 6.2.1.2).
2. Using of Pt/WO<sub>x</sub> samples with the highest possible  $\rho_w$  before the formation of the undesired WO<sub>3</sub> NPs. In the case of Al<sup>com</sup> support, a nominal 10 wt% W loading provides this behaviour, whereas W loadings of 15 wt% and 23 wt% were necessary in the case of Al<sup>SG</sup> and Al<sup>SG'</sup>, respectively (more details in the section 6.2.1.3).
3. Increasing the  $\rho_w$  by raising the calcination temperature (800 °C instead of 450 °C) and, therefore, decreasing the surface area of the catalysts. For this purpose, two Pt/WO<sub>x</sub> catalysts with a nominal W content of 10 wt% supported on Al<sup>SG</sup> and Al<sup>SG'</sup> were used.

In the following sections the results of characterisation techniques and their correlation with the results of the activity tests are discussed.

### 6.2.1.1 XRD

The XRD diffraction patterns of the Al-based support prepared by SG method, without any thermal treatment (Al<sup>SG'</sup>), revealed broad and strong diffraction peaks at  $2\theta = 13.8^\circ$ ,  $28.4^\circ$ ,  $38.8^\circ$ ,  $65.0^\circ$  and  $72.1^\circ$  (see Fig. 6.1 (a)). According to the criteria established by the International Centre for Diffraction Data, the sample showed some differences with respect to a well-crystallized  $\gamma$ -AlO(OH), like the notably broadening and intensity loss in the diffraction peaks, which was more pronounced in the (020) reflexion at  $13.8^\circ$  [7,8]. This indicates that the sample was poorly crystallized as compared to the  $\gamma$ -AlO(OH) and showed a pseudo  $\gamma$ -AlO(OH) structure instead [3,9].

The structural evolution of the Al<sup>SG'</sup> support with the temperature, under air atmosphere, was *in-situ* studied by XRD and can be observed in Fig. 6.2. The characteristic peaks of pseudo  $\gamma$ -AlO(OH) became weaker and some others became more visible as the calcination temperature increased. At 450 °C no diffractions peaks of pseudo  $\gamma$ -AlO(OH) were observed, and the appearance of some new peaks at  $2\theta = 36.6^\circ$ ,  $46.0^\circ$  and  $66.9^\circ$ , revealed a phase change from pseudo  $\gamma$ -AlO(OH) to  $\gamma$ -Al<sub>2</sub>O<sub>3</sub> (see the Eq. 6.1) [10,11]. Based on this phase transformation the Al<sup>SG'</sup> support calcined at 450



°C was denoted as Al<sup>SG</sup>. The detailed diffraction peaks of both structures are shown in Fig. 6.1. The peak positions and intensities remained unchanged within the 450-550 °C range. These results are in good agreement with previous works on the thermal transformation of the  $\gamma$ -AlO(OH) [12,13].

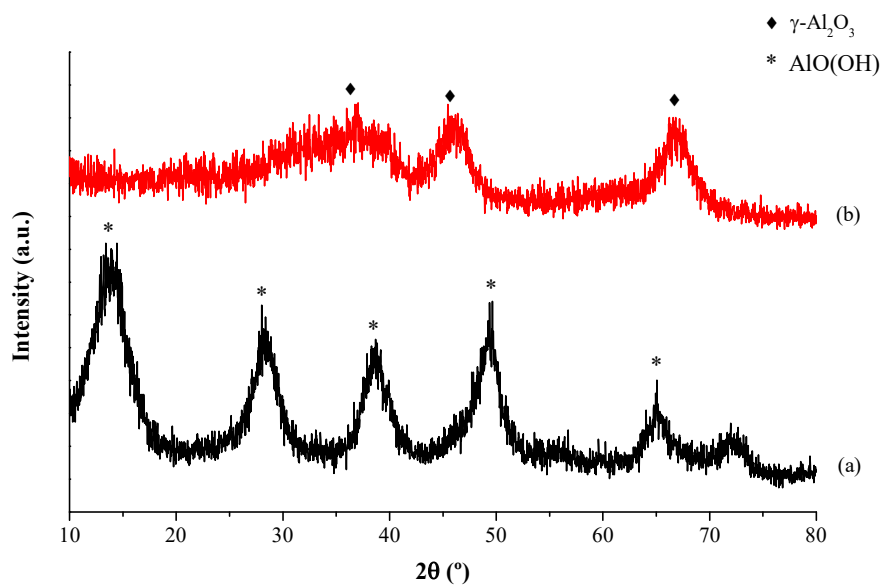


**Fig. 6.1.** XRD pattern of Al<sup>SG</sup> without thermal treatment (a), and after being calcined at 450 °C, Al<sup>SG</sup>, (b).

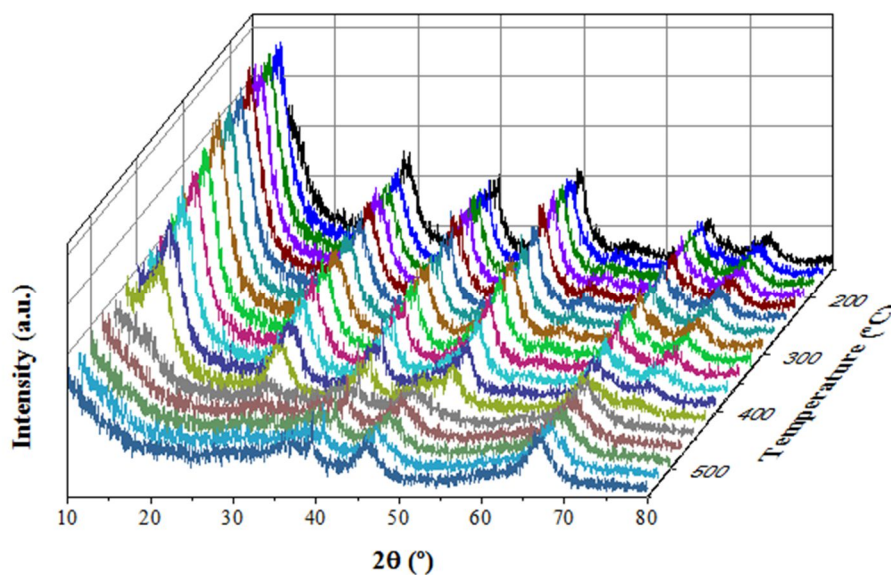


**Fig. 6.2.** Thermal evolution under air atmosphere of pseudo  $\gamma$ -AlO(OH) prepared by SG (Al<sup>SG</sup>) into  $\gamma$ -Al<sub>2</sub>O<sub>3</sub> (Al<sup>SG</sup>), measured by *in-situ* XRD.

The structure of Pt/WO<sub>x</sub> with a nominal W content of 10 wt% (real contents between 9 and 11 wt%) over the three Al-based supports employed (Al<sup>com</sup>, Al<sup>SG</sup> and Al<sup>SG'</sup>) were also studied by XRD. These are named as 2Pt9W Al<sup>com</sup>, 2Pt9W Al<sup>SG</sup> and 2Pt11W Al<sup>SG'</sup>. The diffraction patterns of these reduced catalysts, before (fresh) and after been utilised in the glycerol hydrogenolysis (used), are shown in Fig. 6.3.

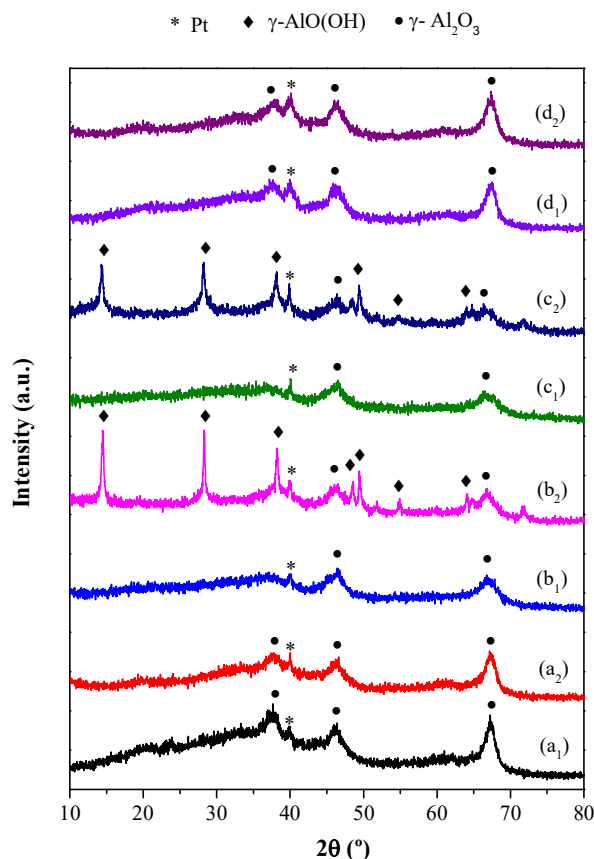


**Fig. 6.3.** XRD diffraction patterns of 2Pt9WAl<sup>com</sup> (a), 2Pt9WAl<sup>SG</sup> (b), 2Pt11WAl<sup>SG'</sup> (c), and 2Pt<sup>CVI</sup>9WAl<sup>com</sup> (d). The subscripts indicate the state of the catalyst: fresh reduced (1), and used (2).

It is worth noting that once the fresh catalysts were calcined at a temperature above 450 °C, the support phase was converted into  $\gamma$ -Al<sub>2</sub>O<sub>3</sub>, even when the WO<sub>x</sub> was incorporated into the Al<sup>SG'</sup>. This was verified by the presence of the diffraction peaks characteristic of the  $\gamma$ -Al<sub>2</sub>O<sub>3</sub> phase in all the fresh catalysts. However, the crystallinity of the used catalysts of Pt/WO<sub>x</sub> on Al<sup>SG</sup> and Al<sup>SG'</sup> increased, due to the fact that part of the  $\gamma$ -Al<sub>2</sub>O<sub>3</sub> support was transformed into its hydrate compound,  $\gamma$ -AlO(OH), during the reaction. This was detected by the appearance of very sharp peaks characteristic of well-crystallized  $\gamma$ -AlO(OH), the most intense located at  $2\theta = 14.4^\circ, 28.2^\circ, 38.1^\circ$  and  $49.4^\circ$  [6,8]. The aggressive hydrothermal conditions employed (200 °C, 45 bar of H<sub>2</sub> and 95

wt% liquid water) are very favourable for this transformation. The same phenomenon was found in the literature under similar conditions [11,12]. It leads to the conclusion that the supports prepared by SG are not stable under the reaction conditions employed, in contrast to the Al<sup>com</sup>. The SG preparation method must, therefore, be improved to avoid these phenomena.

By contrast, WO<sub>x</sub> species seem to be stable and well-anchored to the support, in all cases. The absence of WO<sub>3</sub> NPs indicated that there was neither migration nor repulsion of WO<sub>x</sub> from the surface of the catalysts, at least in a significant extent.

With regard to metal phases, some peaks characteristic of metallic Pt were detected in all catalysts, at reflection angles of 39.9°, 46.4° and 67.4° [14]. Moreover, it is interesting to note that there were no evidences of the presence of PtO<sub>x</sub>, which indicates that Pt was completely reduced under the pre-treatment conditions employed, and remained in the metallic state after the glycerol hydrogenolysis reaction.

Since the metallic Pt peaks were overlapped with those of  $\gamma$ -Al<sub>2</sub>O<sub>3</sub>, the Pt crystallite average size could not be accurately estimated using the Scherrer equation. Nevertheless, the XRD results allowed a qualitatively comparison between Pt dispersion of the fresh and used catalysts providing certain information about the catalyst stability. According to this, the most intense reflection of Pt, at 39.9° (indicated in the Fig. 6.3), seemed to be significantly sharper in the 2Pt9W Al<sup>com</sup> used catalyst, which suggests the sintering of Pt crystallites during the reaction. By contrast, there were insignificant changes between Pt characteristic peaks of those supported on Al<sup>SG</sup> and Al<sup>SG'</sup>.

### **6.2.1.2 Chemical composition and textural properties**

The textural properties of the bare supports, Al<sup>com</sup>, Al<sup>SG</sup> and Al<sup>SG'</sup>, were obtained by N<sub>2</sub> physisorption, and the adsorption/desorption isotherms are shown in Fig. 6.4.

According to the IUPAC classification [15], all supports showed type IV isotherms, characteristic of mesoporous solids, and presented an hysteresis loop due to capillary condensation into mesopores [16]. The type of the hysteresis loop is correlated with the texture of the adsorbent, giving an indication of the shape and size distribution of the catalyst pores [17]. The Al<sup>com</sup> support presented a type H3, characterized by ink-bottle type pores and asymmetrical triangular form. In contrast, the Al<sup>SG</sup> and Al<sup>SG'</sup> supports showed H2 hysteresis which is correlated with more complex pore networks formed by pores with ill-defined shape and wide pore size distribution

[18]. The textural properties of  $\text{WO}_x/\text{Al}_2\text{O}_3$  catalysts obtained by  $\text{N}_2$  physisorption are also provided in Table 6.1.

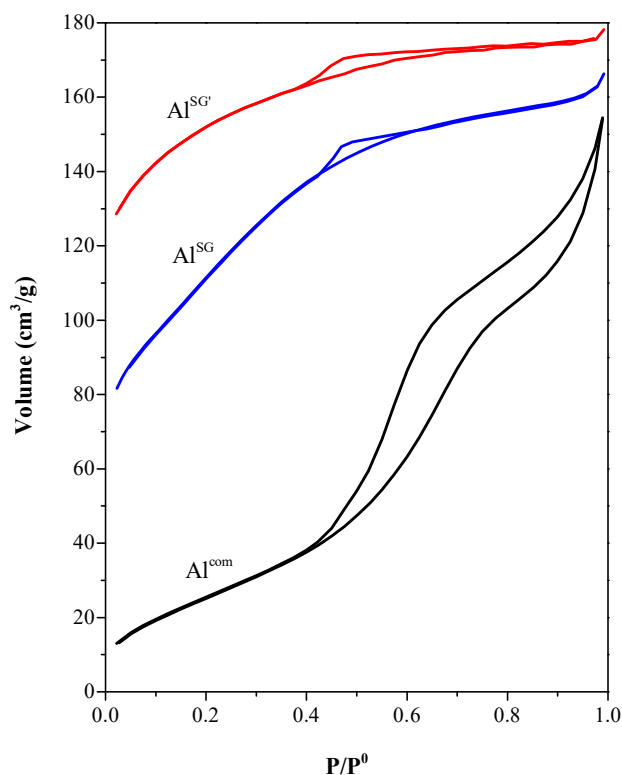


Fig. 6.4.  $\text{N}_2$  adsorption/desorption isotherms at  $-196\text{ }^\circ\text{C}$  of the bare Al-based supports:  $\text{Al}^{\text{com}}$ ,  $\text{Al}^{\text{SG}}$  and  $\text{Al}^{\text{SG}'}$ .

**Table 6.1.** Textural properties of the  $\text{WO}_x$  supported over Al-based supports and the bare supports obtained by  $\text{N}_2$ -physisorption.

Catalyst <sup>a</sup>	W composition (wt %)	$S_{\text{BET}}$ ( $\text{m}^2 \text{g}^{-1}$ )	$V_p$ ( $\text{cm}^3 \text{g}^{-1}$ )	$r_p$ ( $\text{Å}$ )
$\text{Al}^{\text{com}}$	-	140	0.26	38.4
$\text{Al}^{\text{SG}}$	-	286	0.32	23.1
$\text{Al}^{\text{SG}'}$	-	275	0.14	12.6
9W $\text{Al}^{\text{com}}$ (2.3)	8.5	110	0.20	76.7
9W $\text{Al}^{\text{SG}}$ (1.1)	8.4	307	0.27	18.2
9W $\text{Al}^{\text{SG} 800}$ (1.4)	8.7	181	0.25	28.5
15W $\text{Al}^{\text{SG}}$ (2.0)	14.6	-	-	-
11W $\text{Al}^{\text{SG}'}$ (1.5)	10.8	288	0.28	20.3
11W $\text{Al}^{\text{SG}' 800}$ (2.4)	10.9	126	0.25	30.5
23W $\text{Al}^{\text{SG}'}$ (3.8)	22.9	-	-	-

<sup>a</sup>  $\rho_w$  in brackets (expressed in W at.  $\text{nm}^{-2}$  of support).

According to the surface area, calculated by Brunauer-Emmett-Teller method ( $S_{\text{BET}}$ ), the WO<sub>x</sub> incorporation on Al<sup>com</sup> (9W Al<sup>com</sup>) reduced the  $S_{\text{BET}}$  and the pore volume ( $V_p$ ) of the bare support, which suggests a blockage or filling of some of the pores, especially the smallest ones as the increase in the average pore radio ( $r_p$ ) suggests. The opposite effect on  $S_{\text{BET}}$  was found when WO<sub>x</sub> was incorporated on the Al<sup>SG</sup> and the Al<sup>SG'</sup>. In view of the results, these supports did not suffer the pore blockage by the WO<sub>x</sub> species; on the contrary, higher surface areas were generated. Comparing the calcined 9W Al<sup>SG</sup> and 11W Al<sup>SG'</sup> samples, they showed similar textural properties,  $V_p$  and  $r_p$ , with the exception of a slightly lower  $S_{\text{BET}}$  for the later (307 vs. 288 m<sup>2</sup> g<sup>-1</sup>).

The increase in the calcination temperature, from 450 to 800 °C, has a greater effect on the  $S_{\text{BET}}$  of those samples: it decreased from 307 to 181 m<sup>2</sup> g<sup>-1</sup> for the 9W Al<sup>SG</sup> and from 288 to 126 m<sup>2</sup> g<sup>-1</sup> for the 11W Al<sup>SG'</sup> catalyst.

The chemical composition of the WO<sub>x</sub> supported on different Al-based materials, determined by the ICP-OES, is shown in Table 6.2. According to the ICP results, the real W loadings are quite near the nominal composition (2 wt% Pt and 10 wt% W), pointing out the effectiveness of the WI method for the incorporation of those metal oxides.

Since leaching is one of the main factors by which the catalyst may be deactivated during the glycerol hydrogenolysis [19], the chemical analysis of some fresh and used catalysts was also carried out by ICP-OES to study this phenomenon. The results are also summarized in Table 6.2.

**Table 6.2.** Bulk atomic ratios obtained from ICP-OES.

Catalyst <sup>a</sup>	Fresh composition (wt %)		Pt/Al		W/Al	
	Pt	W <sup>b</sup>	Fresh	Used	Fresh	Used
2Pt9W Al <sup>com</sup> (2.4)	1.8	8.5	0.0051	0.0058	0.0264	0.0233
2Pt9W Al <sup>SG</sup> (1.1)	1.8	8.5	0.0053	0.0051	0.0269	0.0265
2Pt11W Al <sup>SG'</sup> (1.5)	2.1	11.0	0.0065	0.0056	0.0355	0.0312
2Pt <sup>CVI</sup> 9W Al <sup>com</sup> (2.4)	1.9	9.1	0.0057	0.0058	0.0285	0.0263

<sup>a</sup>  $\rho_w$  in brackets (expressed in W at. nm<sup>-2</sup> of support).

<sup>b</sup> W content related to the Al-based support.

The ICP-OES results suggest that metal leaching did not take place up to a significant level for any of the investigated catalysts.

### 6.2.1.3 Raman spectroscopy

It is widely reported that the appearance of crystalline  $\text{WO}_3$  NPs may be an evidence that a close packed monolayer of surface  $\text{WO}_x$  has been achieved and that no additional exposed support sites remain for the anchoring of  $\text{WO}_x$  species [20]. However, Raman spectroscopy shows that a small fraction of  $\text{WO}_3$  begins to form three-dimensional clusters at  $\rho_w$  values below the theoretical monolayer content of 4-7 W at.  $\text{nm}^{-2}$  predicted in the literature [21,22]. In addition, these models assume that the structures of  $\text{WO}_x$  are similar to the one corresponding to crystalline  $\text{WO}_3$ . Therefore, the theoretical monolayer determinations based on such structural calculations are just rough approximations, as it occurs with similar oxophilic metal systems [23]. All in all, it is possible that the emergence of  $\text{WO}_3$  NPs takes place before a full monolayer formation, but what was clearly observed is that it has a worsening effect on the 1,3-PDO yield [24]. Therefore, their formation should be avoided.

The Raman spectroscopy technique was selected in order to establish the highest  $\rho_w$  values before the appearance of  $\text{WO}_3$  NPs ( $\rho_w^{\text{lim}}$ ) for each type of support. The spectra of the calcined  $\text{WO}_x$  over  $\text{Al}^{\text{SG}}$  and  $\text{Al}^{\text{SG}'}$  catalysts are shown in Fig. 6.5.

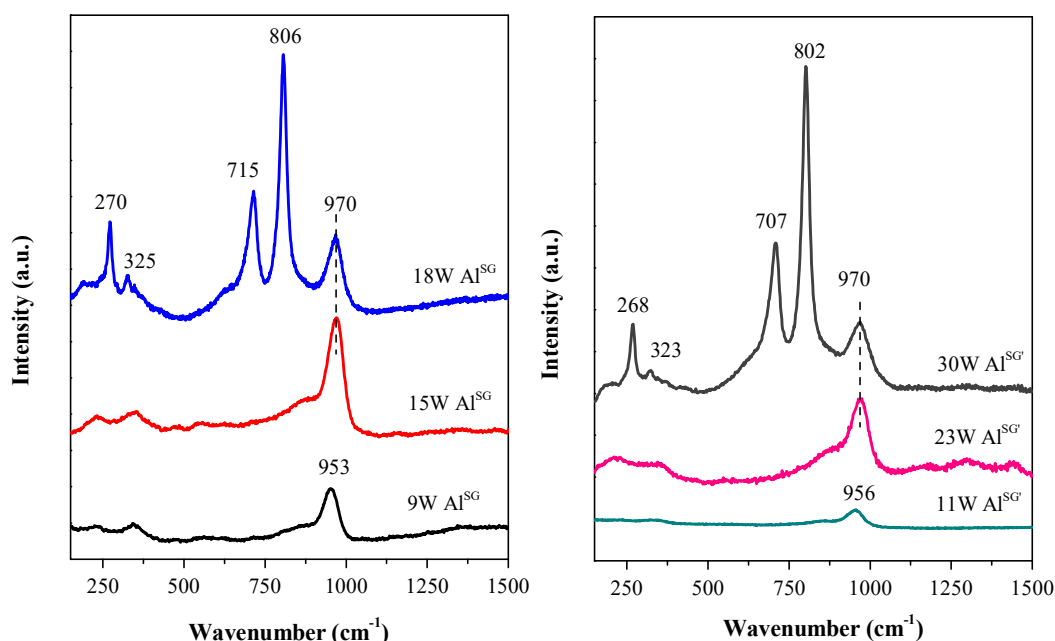
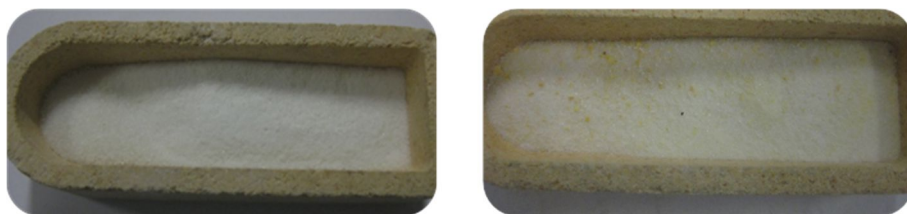


Fig. 6.5. Raman spectra of the calcined  $\text{WO}_x/\text{Al}$ -based catalyst.  $\text{Al}^{\text{SG}}$  (left) and  $\text{Al}^{\text{SG}'}$  (right) were used as supports.

It can be observed that the band corresponding to the symmetric stretching of  $\text{W}=\text{O}$  bonds of polytungstate [22] appears at 953 and 956  $\text{cm}^{-1}$  for the 9W  $\text{Al}^{\text{SG}}$  (1.1 W at.  $\text{nm}^{-2}$ ) and 11W  $\text{Al}^{\text{SG}'}$  (1.5 W at.  $\text{nm}^{-2}$ ) catalysts, respectively. This band shifted

towards higher wavenumbers with  $\rho_w$ , as the polytungstate concentration increased [20,25–27], reaching the 970  $\text{cm}^{-1}$  position for different  $\rho_w$ : 2.0 W at.  $\text{nm}^{-2}$  over Al<sup>SG</sup> support (15W Al<sup>SG</sup>) and 3.8 W at.  $\text{nm}^{-2}$  over Al<sup>SG'</sup> (23W Al<sup>SG'</sup>). At higher  $\rho_w$  very strong typical bands of WO<sub>3</sub> NPs were observed at around 800, 700 and 270  $\text{cm}^{-1}$ , which are assigned to the W–O stretching, W–O bending and W–O–W deformation modes of octahedrally coordinated WO<sub>3</sub> NPs [6]. Those NPs appeared at  $\rho_w \geq 2.7$  for Al<sup>SG</sup> support (18W Al<sup>SG</sup>) and at  $\rho_w \geq 5.7$  W at.  $\text{nm}^{-2}$  for Al<sup>SG'</sup> (30W Al<sup>SG'</sup>). Bulk WO<sub>3</sub> crystallites could also be visually identified by their light yellow colour, whereas the rest of WO<sub>x</sub> surface species are of white colour (see Fig. 6.6).



**Fig. 6.6.** Visual identification of bulk WO<sub>3</sub> crystallites (of yellow colour) in the 18W Al<sup>SG</sup>, 2.7 W at.  $\text{nm}^{-2}$  sample (right). The 15W Al<sup>SG</sup>, 2.0 W at.  $\text{nm}^{-2}$ , (left) is showed for comparison.

Regarding the WO<sub>x</sub> supported on Al<sup>com</sup>, the  $\rho_w^{\text{lim}}$  was previously found to be at around 2.4 W at.  $\text{nm}^{-2}$  (see Chapter 5). In this study, a similar catalyst was prepared achieving a  $\rho_w$  value of 2.3 W at.  $\text{nm}^{-2}$  (9W Al<sup>com</sup>), and therefore very close to the established  $\rho_w^{\text{lim}}$  value.

At first glance, it can be concluded that the maximum amount of WO<sub>x</sub>, which the support can accommodate before the appearance of the WO<sub>3</sub> NPs, depends on the Al-based starting material and preparation method. In spite that Al<sup>SG</sup> could incorporate a higher WO<sub>x</sub> loading before the appearance of WO<sub>3</sub> NPs, it did not achieve a higher  $\rho_w^{\text{lim}}$  than the 9W Al<sup>com</sup> catalyst (see Table 6.3). However, it is interesting to highlight that the Al<sup>SG'</sup> support, which according to XRD analysis (section 6.2.1.1) was composed by pseudo  $\gamma$ -AlO(OH), can accommodate a remarkably higher W loading before the appearance of WO<sub>3</sub> NPs, leading to the highest  $\rho_w^{\text{lim}}$  value (3.8 W at.  $\text{nm}^{-2}$ ). It was suggested that the surface WO<sub>x</sub> species primarily anchor to the Al<sub>2</sub>O<sub>3</sub> support by titrating the surface hydroxy groups [28–30]. The higher hydroxy concentration on  $\gamma$ -AlO(OH) with respect to  $\gamma$ -Al<sub>2</sub>O<sub>3</sub> type support may explain this behaviour.

Besides incorporating a higher WO<sub>x</sub> loading, another way to increase the  $\rho_w$  is to decrease the S<sub>BET</sub> of the catalyst by increasing the calcination temperature. Thus, two other catalysts with 10 wt% W nominal content over Al<sup>SG</sup> (1.4 W at.  $\text{nm}^{-2}$ ) and Al<sup>SG'</sup>

( $2.4 \text{ W at. nm}^{-2}$ ) were prepared and calcined at  $800 \text{ }^\circ\text{C}$ , instead of  $450 \text{ }^\circ\text{C}$ . In these cases, the  $\rho_{\text{W}}$  values were calculated using the real  $S_{\text{BET}}$  of the sample according to the formula showed in the Eq. 6.2, appeared also in the literature [31], since the  $S_{\text{BET}}$  of the supports calcined at  $800 \text{ }^\circ\text{C}$  were not available.

$$\rho_{\text{W}} [\text{W atoms nm}^{-2} \text{ of support}] = \frac{\left(\frac{x_{\text{W}}}{M_{\text{W}}}\right) NA}{S_{\text{sample}}/(1-x_{\text{WO}_3})} \quad \text{Eq. 6.2}$$

where  $x_{\text{W}}$  and  $x_{\text{WO}_3}$  are the mass fraction of the W and  $\text{WO}_3$  species in the final catalyst, NA is the Avogadro number,  $M_{\text{W}}$  is the W atomic weight, and  $S_{\text{sample}}$  is the  $S_{\text{BET}}$  of the calcined sample.

The Raman spectra of similar catalysts, with a 10 wt% W nominal content, at both calcination temperatures ( $450$  and  $800 \text{ }^\circ\text{C}$ ) are compared in Fig. 6.7. The symmetric stretching  $\text{W}=\text{O}$  band of polytungstates shifted towards higher wavenumbers (from approximately  $950$  to  $970 \text{ cm}^{-1}$ ) and the peak suffered a significant intensity increase, when the calcination temperature varied from  $450$  to  $800 \text{ }^\circ\text{C}$ . From this qualitatively comparison, it may be deduced that the polytungstates to monotungstates ratio increased with the calcination temperature since the  $\rho_{\text{W}}$  of the catalysts increased. However, this value remained below the  $\rho_{\text{W}}^{\text{lim}}$ , since no peaks related to  $\text{WO}_3$  NPs were detected.

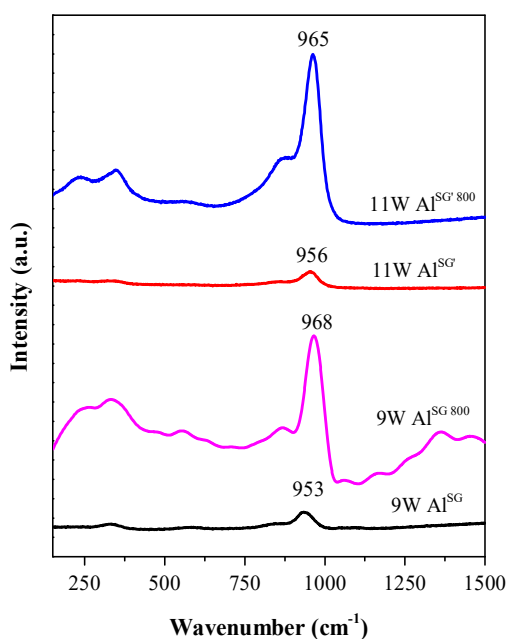


**Fig. 6.7.** Comparison of Raman spectra of  $9\text{W Al}^{\text{SG}}$  and  $11\text{W Al}^{\text{SG}}$  calcined at  $450 \text{ }^\circ\text{C}$  and  $800 \text{ }^\circ\text{C}$  (in the latter case the calcination temperature was indicated in the catalyst name).



Table 6.3 shows all the WO<sub>x</sub>/Al-based samples investigated by Raman spectroscopy and summarizes the main findings achieved.

**Table 6.3.** Summary of the WO<sub>x</sub>/Al-based samples investigated by Raman spectroscopy and the main findings achieved.

Catalyst	Calcination T	$\rho_w$ (W at. nm <sup>-2</sup> )	Stretching W=O position (cm <sup>-1</sup> )	Presence of NPs
9W Al <sup>com</sup>	450	2.3 <sup>a</sup>	973	No
9W Al <sup>SG</sup>	450	1.1 <sup>a</sup>	953	No
15W Al <sup>SG</sup>	450	2.0 <sup>a</sup>	970	No
18W Al <sup>SG</sup>	450	2.7 <sup>a</sup>	970	Yes
11W Al <sup>SG'</sup>	450	1.5 <sup>a</sup>	956	No
23W Al <sup>SG'</sup>	450	3.8 <sup>a</sup>	970	No
30W Al <sup>SG'</sup>	450	5.7 <sup>a</sup>	970	Yes
9W Al <sup>SG 800</sup>	800	1.4 <sup>b</sup>	968	No
11W Al <sup>SG' 800</sup>	800	2.4 <sup>b</sup>	965	No

<sup>a</sup>  $\rho_w$  calculated according to the Eq. 4.1 (Chapter 4).

<sup>b</sup>  $\rho_w$  calculated according to the Eq. 6.2.

#### 6.2.1.4 SEM

Morphological investigations of some reduced samples were carried out by SEM in order to determine the influence of the Al-based supports. For this research the Pt/WO<sub>x</sub> catalysts with the maximum loading of WO<sub>x</sub>, whose corresponding supports were able to incorporate WO<sub>x</sub> without the formation of tridimensional WO<sub>3</sub> NPs, were analysed: 2Pt9W Al<sup>com</sup>, 2Pt15W Al<sup>SG</sup> and 2Pt23W Al<sup>SG'</sup>.

SEM images of Pt/WO<sub>x</sub> supported Al<sup>com</sup> sample (Fig. 6.8) showed a different morphology as compared to those samples with Al<sup>SG</sup> and Al<sup>SG'</sup> as supports (Fig. 6.9 (a) and (b), respectively). The 2Pt9W Al<sup>com</sup> sample was composed by multiple layers of close-packed spheres. Different regions of the catalyst at higher magnifications are shown in Fig 6.8 (b) and (c). The Energy-dispersive X-ray spectroscopic (EDS) analysis allowed the differentiation between Pt and WO<sub>x</sub> particles (not shown). This was impossible neither by colour nor shape. These analyses were carried out in different characteristic zones of the catalyst and were marked in the images.

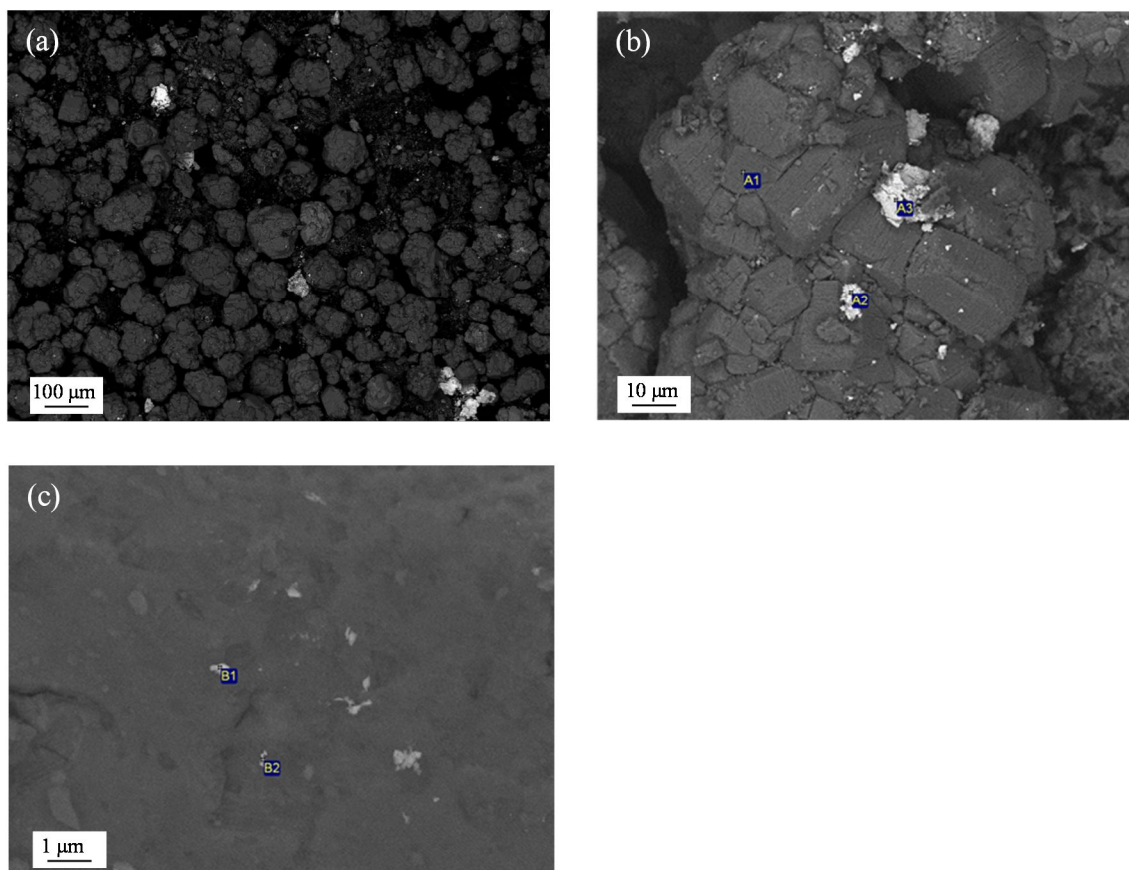


**Fig. 6.8.** SEM images taken from different zones of 2Pt9W Al<sup>com</sup> reduced fresh sample.

WO<sub>x</sub> particles were found well-dispersed over the Al<sup>com</sup> support (zone A1), in spite that they may also form some bigger agglomerates (A2, A3 and B1) to a lesser extent. By contrast, the Raman spectroscopy and the XRD analysis showed the absence of WO<sub>3</sub> NPs. This contradiction could be attributed to the difference in the analysis depth. While the Raman spectroscopy only investigates the surface of the sample, the SEM reaches a deeper layer under the catalyst surface [32].

The differentiation and identification of Pt particles was harder, and this led to the conclusion that Pt was well-dispersed over the Al<sup>com</sup> support. Few big agglomerates were scarcely found in B1 zone, which is in agreement with the quite small Pt size (about 5 nm) obtained by CO chemisorption (see Table 6.5).

Pt/WO<sub>x</sub> supported on Al<sup>SG</sup> (2Pt15W Al<sup>SG</sup>) and Al<sup>SG'</sup> (2Pt23W Al<sup>SG'</sup>) showed a quite similar morphology (Fig. 6.9).

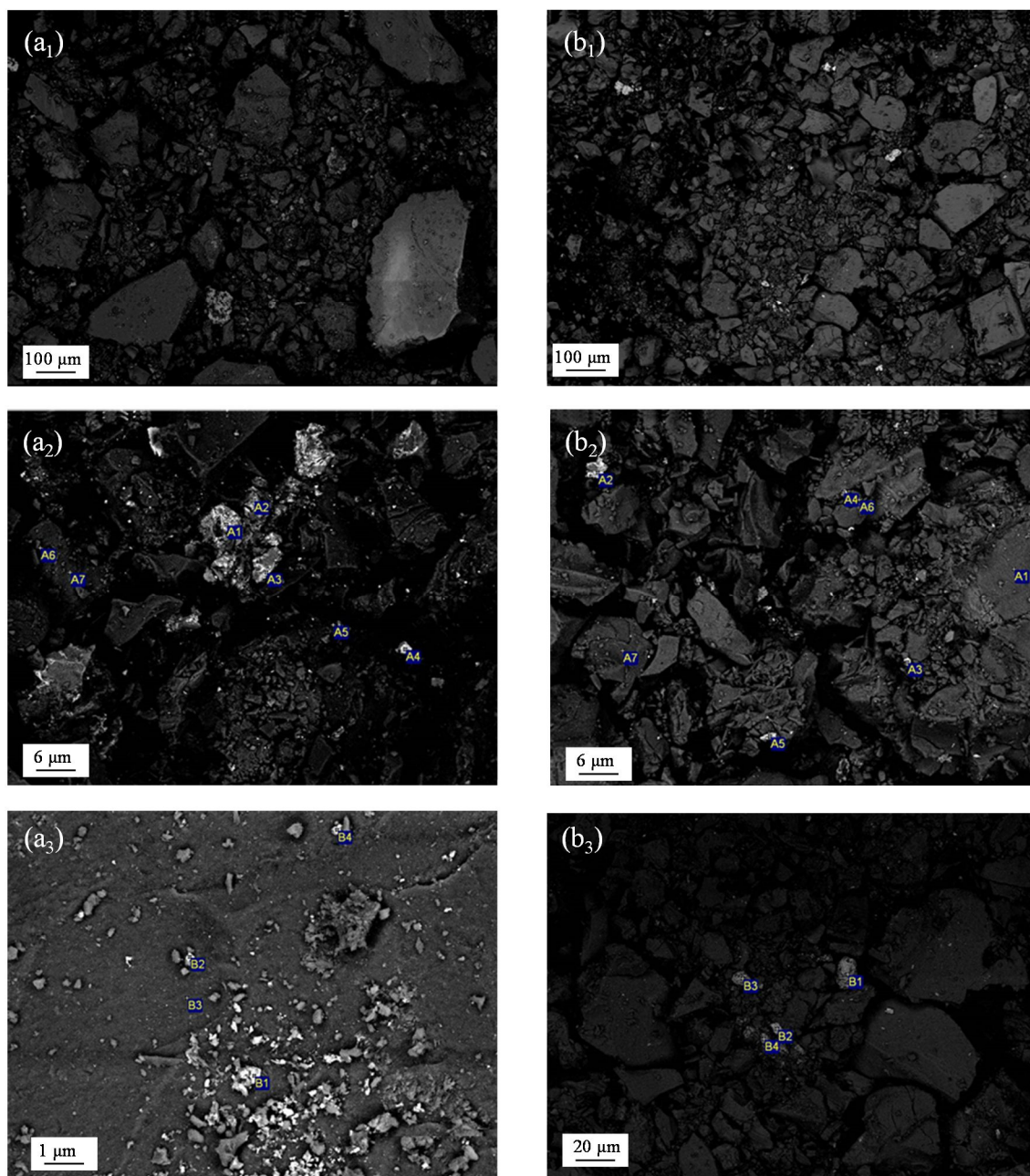


**Fig. 6.9.** SEM images 2Pt15W Al<sup>SG</sup> (a), and 2Pt23W Al<sup>SG</sup> (b). Subscripts 1 to 3 indicate different zones of the same catalyst.

None of them showed a plate-like structure characteristic of layered  $\gamma$ -AlO(OH) [10,33], which verifies the phase transformation, observed by XRD, from a pseudo  $\gamma$ -AlO(OH) to a  $\gamma$ -Al<sub>2</sub>O<sub>3</sub> phase that occurs during the calcination in air at temperatures higher than 450 °C.

Although the 2Pt23W Al<sup>SG</sup> sample showed a more homogeneous distribution, both samples formed aggregates with a wide range of morphologies. Quite big WO<sub>x</sub> agglomerates were found in 2Pt15W Al<sup>SG</sup> sample (zone A1-A4, A6, A7, B1, B2 and B4), whereas Pt particles were hardly observed (B3 zone). It can be concluded that WO<sub>x</sub>

was poorly distributed unlike the Pt. Regarding the 2Pt23W Al<sup>SG'</sup> sample, it showed smaller and better dispersed WO<sub>x</sub> particles (A1 and A7 zones) but poorly dispersed Pt (A2-A6 and B1-B4 zones).

#### 6.2.1.5 H<sub>2</sub>-TPR

The study of the reducibility of the surface species was carried out by H<sub>2</sub>-TPR, within the temperature range of 40-1000 °C. The TPR technique can also provide information about the dispersion of the metallic components, as well as of the metal-support and metal-metal interactions. The TPR profiles of the most relevant Al-supported Pt/WO<sub>x</sub> and WO<sub>x</sub> catalysts are shown in Fig. 6.10.

Within the investigated temperature range, the WO<sub>x</sub>/Al-based samples showed a broad reduction peak with a maximum around 900 °C for 11W Al<sup>SG'</sup> and 11W Al<sup>SG' 800</sup>, and higher than 1000 °C for 9W Al<sup>com</sup>. In spite that their reduction started at around 740 °C, they required very high temperatures (T >1000 °C) to achieve it entirely. According to the literature, those peaks at elevated temperatures are attributed to the reduction of the WO<sub>3</sub> (W<sup>6+</sup>→W<sup>0</sup>) strongly bonded to the γ-Al<sub>2</sub>O<sub>3</sub> support [34,35]. The difference between the maxima of around 100 °C could indicate the higher interaction between WO<sub>3</sub> with the Al<sup>com</sup> support. The absence of TPR peaks at lower temperatures indicates that surface WO<sub>3</sub> species were well-dispersed over the respective support (9W Al<sup>com</sup>, 11W Al<sup>SG'</sup> and 11W Al<sup>SG' 800</sup>), and, therefore, WO<sub>3</sub> NPs were not be formed [24,36], as it was previously confirmed by Raman spectroscopy.

All Pt-containing catalysts showed multiple reduction peaks between 40 °C and 270 °C, related to the reduction of different PtO<sub>x</sub> species [37,38]. It can be observed that the incorporation of Pt has a significant effect on the WO<sub>x</sub> reducibility. It facilitates their reduction probably through a H<sub>2</sub> spillover effect, which was also found in similar catalytic systems [39,40]. In addition, according to Jia et al. [41], the peaks whose maximum appeared between 420 and 480 °C could be assigned to the reduction of PtO<sub>2</sub> in high interaction with the support. However, the TPR profile of 2Pt Al<sup>com</sup> showed just a quite small shoulder in this region (at 455 °C). Therefore, there are not clear evidences to rule out whether the reduction peaks in the 400-500 °C temperature range could be attributed to PtO<sub>x</sub>-WO<sub>x</sub> or to PtO<sub>2</sub> species. Moreover, the 2Pt Al<sup>com</sup> sample also showed three main peaks with maxima at 83, 211 and 366 °C. With the presence of WO<sub>x</sub> (2Pt9W Al<sup>com</sup>), the temperature required for the reduction of PtO<sub>x</sub> species generally increased (peak maxima at 73, 260 and 427 °C).

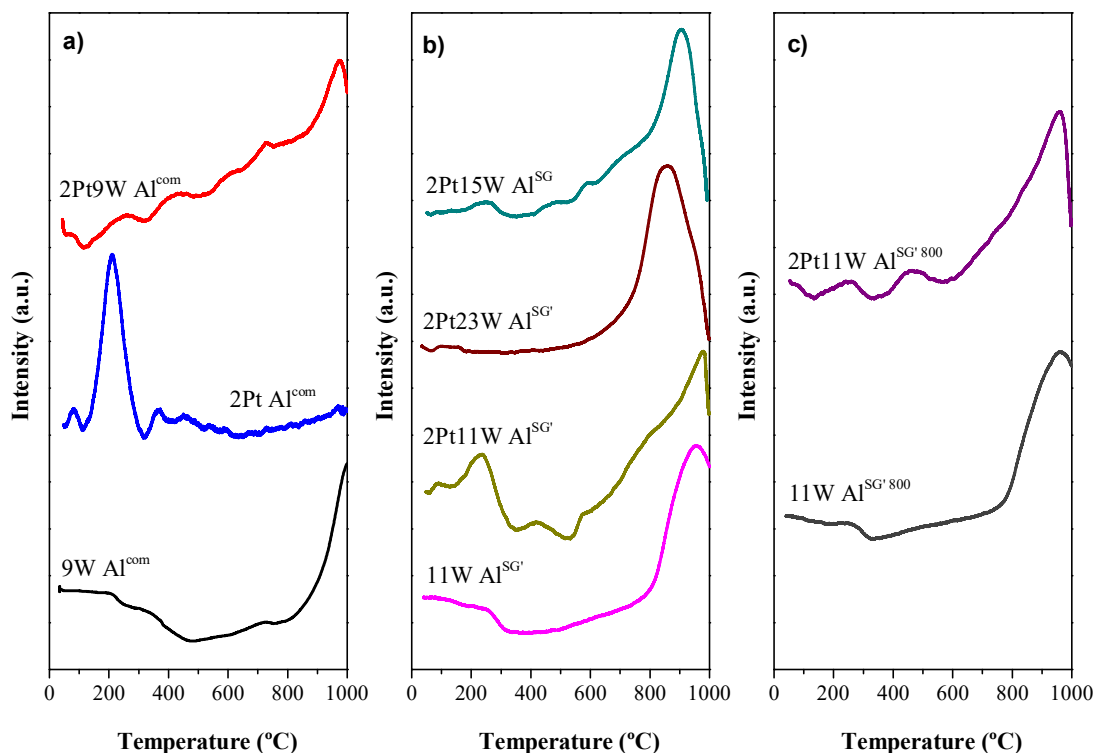


**Fig. 6.10** H<sub>2</sub>-TPR of the fresh calcined catalysts: WO<sub>x</sub> and Pt/WO<sub>x</sub> supported on Al<sup>com</sup> (a) and Al<sup>SG</sup>, WO<sub>x</sub>/ Al<sup>SG</sup> calcination at 450 and 800 °C (b and c, respectively). A catalyst supported on Al<sup>SG</sup> was also showed for comparison in Fig. b.

Comparing the TPR profiles of 2Pt9W Al<sup>com</sup>, 2Pt11W Al<sup>SG</sup> and 2Pt11W Al<sup>SG</sup>,<sup>800</sup>, it seems that the reduction of PtO<sub>x</sub>, in the 40-300 °C temperature range, required temperatures slightly higher when Al<sup>com</sup> was used as support instead of the Al<sup>SG</sup>. This indicates a possible higher interaction of PtO<sub>x</sub> species with the commercial support.

The 2Pt11W Al<sup>SG</sup> and 2Pt15W Al<sup>SG</sup> samples showed similar reduction peaks related to the reduction of PtO<sub>x</sub> species. However, only three very small peaks for PtO<sub>x</sub> reduction were observed for the 2Pt23W Al<sup>SG</sup> catalyst, at lower temperatures (40-150 °C). The unexpected low temperature peaks are indicative of the quite weak PtO<sub>x</sub> interaction with the support. The low intensity, due to small H<sub>2</sub> consumption, is consistent with the poor Pt dispersion observed in the SEM analysis of this sample. It is important to note that the peak at about 400 °C observed in previous cases, and corresponding to PtO<sub>2</sub> in high interaction with the support or to PtO<sub>x</sub>-WO<sub>x</sub> species, was not observed. In addition, the reduction of WO<sub>x</sub> did not start until 600 °C. All these evidences suggest a very low Pt-WO<sub>x</sub> interaction or proximity between those sites for this 2Pt23W Al<sup>SG</sup> catalyst, probably the lowest ones of all the investigated samples.

### 6.2.1.6 Activity tests

The effect of  $\rho_w$  was investigated in the aqueous glycerol hydrogenolysis, at 200 °C and 45 bar of H<sub>2</sub> for 16 h of reaction time.

As it occurred in our previous findings, the  $\rho_w$  played a key role in the selective formation of the 1,3-PDO compound. At low  $\rho_w$  values, 1.2 or 1.5 W at. nm<sup>-2</sup> for 2Pt9W Al<sup>SG</sup> and 2Pt11W Al<sup>SG</sup>, respectively, negligible amounts of 1,3-PDO were formed in the reaction (see Table 6.4 entries 2 and 3). These catalysts acted as common monometallic Pt/Al<sub>2</sub>O<sub>3</sub> catalytic systems, producing 1,2-PDO as the main product (selectivity > 88 %).

At higher  $\rho_w$ , 2.1 W at. nm<sup>-2</sup> for 2Pt15W Al<sup>SG</sup> and 3.9 W at. nm<sup>-2</sup> for 2Pt23W Al<sup>SG</sup>, the glycerol conversion increased, a fact which was not found with the Al<sup>com</sup> support (see Chapter 5), and the product distribution changed completely (Table 6.4, entries 4 and 5). Both PDOs became the major products showing together selectivities > 80 %. Interestingly, the selectivity towards 1,2-PDO decreased at the same time that the 1,3-PDO formation increased. In addition, the cracking reactions, which mainly led to EG and methanol, were almost suppressed. Nevertheless, the over-hydrogenolysis of PDOs formed quite high amounts of 1-PO (selectivity values > 14 %).

The higher concentration of polytungstate species as the  $\rho_w$  increases, according to the Raman spectroscopy results showed, may be the responsible of this behaviour. As it was pointed out in our previous studies (Chapter 5), dispersed monotungstates cannot accommodate the negative charge required to form and stabilise the Brønsted acid sites, unlike the extended network of WO<sub>x</sub> formed by polytungstate species [6,22,42].

However, in view of the previous results, it could be considered that the W loading is the controlling parameter in the reaction. In order to verify that  $\rho_w$  is actually the controlling parameter instead of the W loading, two Pt/WO<sub>x</sub>/Al-based catalysts with similar W content (9-11 wt%), but higher  $\rho_w$  than their homologous, were tested in the reaction. This was obtained by calcining the W/supports at higher temperatures (800 °C), leading to a lowering of the S<sub>BET</sub> of the samples (see Table 6.2) and, therefore, to an increase of the  $\rho_w$  values (but below the  $\rho_w^{\text{lim}}$  value). The activity test results are convincing: 2Pt9W Al<sup>SG 800</sup> and 2Pt11W Al<sup>SG 800</sup> catalysts (Table 6.4 entries 6 and 7) showed higher glycerol conversion than their homologous (Table 6.4 entries 4 and 5) and formed 1,3-PDO as one of their main products (selectivity > 40 %).

**Table 6.4.** Activity test results obtained after 16 h of reaction time, 200 °C and 45 bar of H<sub>2</sub>.

Entry	Catalyst <sup>a</sup>	Glycerol conversion (%)	Product selectivity (%)			
			1,3-PDO	1,2-PDO	1-PO	Cracking products <sup>b</sup>
1	2Pt9W Al <sup>com</sup> (2.4)	15.7	52.7	16.9	20.8	0.0
2	2Pt9W Al <sup>SG</sup> (1.2)	3.8	0.0	88.1	0.0	11.2
3	2Pt11W Al <sup>SG'</sup> (1.5)	3.4	0.0	89.0	0.0	11.0
4	2Pt15W Al <sup>SG</sup> (2.1)	9.2	45.4	36.4	14.4	3.8
5	2Pt23W Al <sup>SG'</sup> (3.9)	4.7	36.2	43.9	19.9	0.0
6	2Pt9W Al <sup>SG 800</sup> (1.4)	7.6	40.6	41.8	12.2	0.0
7	2Pt11W Al <sup>SG' 800</sup> (2.4)	10.1	42.9	33.4	14.4	0.0

<sup>a</sup>  $\rho_w$  in brackets (expressed in W at. nm<sup>-2</sup> of support).

<sup>b</sup> Cracking products: ethylene glycol (EG) and methanol, above all.

The relationship between the  $\rho_w$  and the selectivity towards 1,3-PDO is graphically shown Fig. 6.11. It was found that in order to obtain high selectivities towards 1,3-PDO there is an optimum  $\rho_w$  value between 2.0 and 2.4 W at. nm<sup>-2</sup>.

It is interesting to note that despite the 2Pt23W Al<sup>SG'</sup> was the sample presenting the highest  $\rho_w^{\text{lim}}$ , it showed an unexpected lower glycerol conversion and 1,3-PDO selectivity (Table 6.4 entry 5) than other catalysts with lower  $\rho_w$  values. In addition to this, the 2Pt9W Al<sup>com</sup> (2.4 W at. nm<sup>-2</sup>) sample provided the best results: 15.7 % glycerol conversion and 52.7 % selectivity towards 1,3-PDO (Table 6.4 entry 1). These results show that, besides the  $\rho_w$ , there are other catalytic properties that are also important in the selective production of 1,3-PDO.

In this regard, the H<sub>2</sub>-TPR results suggested that (section 6.2.1.5) the catalysts 2Pt9W Al<sup>com</sup>, 2Pt11W Al<sup>SG'</sup>, 2Pt11W Al<sup>SG' 800</sup> and 2Pt15W Al<sup>SG</sup> showed a direct Pt-WO<sub>x</sub> interaction or, at least, a very close proximity between Pt and WO<sub>x</sub> sites. This interaction was almost negligible for the 2Pt23W Al<sup>SG'</sup> sample, explaining quite well the low 1,3-PDO yield obtained despite its high  $\rho_w$  value. By contrast, Pt-WO<sub>x</sub> interactions became visible for those catalysts with more balanced loadings. These results suggest that a balance of Pt and WO<sub>x</sub> sites may be necessary in order to enhance those interactions or the closer proximity. This is the case of 2Pt11W Al<sup>SG'</sup>. However, this catalyst was not able to produce 1,3-PDO because the polytungstate concentration was not enough to generate the necessary Brønsted acidity.



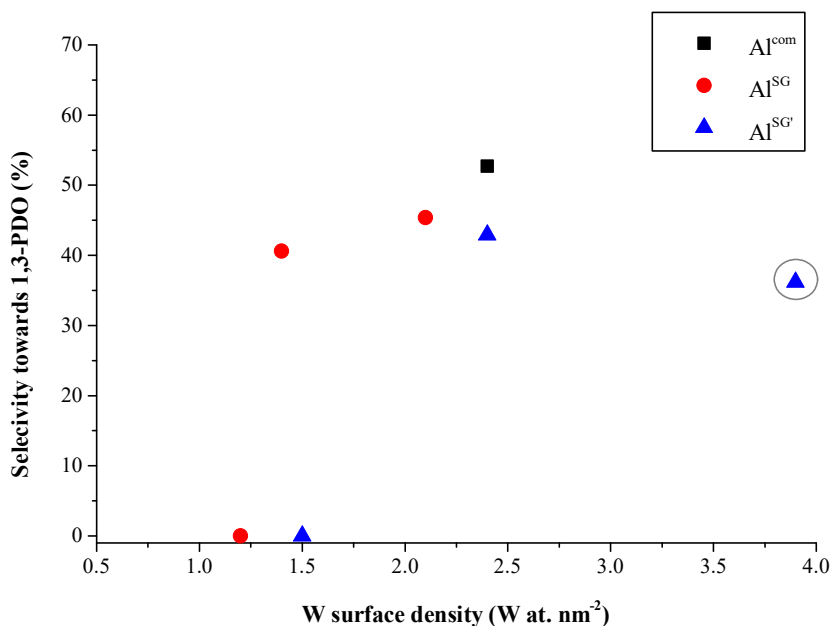


**Fig. 6.11.** Relationship between  $\rho_W$  and the selectivity towards 1,3-PDO for the different Pt/WO<sub>x</sub>/Al-based catalysts. The results are divided by the corresponding support. The circle showed an abnormal result.

## 6.2.2 Effect of the Pt dispersion and the Pt-WO<sub>x</sub> interactions

As a summary, in order to obtain 1,3-PDO selectively from glycerol it seems necessary a catalyst with a high concentration of polytungstate species, without the formation of WO<sub>3</sub> NPs, and with a high interaction or proximity between the metallic sites of Pt and the acid sites of WO<sub>x</sub>. In the current section, two strategies were carried out with the aim to improve the Pt-WO<sub>x</sub> interactions.

1. Improving the Pt dispersion of the catalyst which showed the best results up to now, 2Pt9W Al<sup>com</sup>, with the use of a non-conventional method for Pt deposition: the CVI method (section 6.2.2.1).
2. Increasing the Pt loading (section 6.2.2.2).

### 6.2.2.1 Effect of Pt dispersion

The 2Pt9W Al<sup>com</sup> catalyst was the one which gave the highest glycerol conversion and selectivity towards 1,3-PDO (see Table 6.4 entry 1). Since the metal dispersion is especially important in the heterogeneous catalysis with noble and precious metals [43], it was tried to improve the Pt dispersion of this catalyst. For this purpose, the CVI method was employed for the Pt deposition. According to the literature, the CVI method (sometimes found as CVD, chemical vapour deposition) has some advantages over conventional preparation techniques: (i) it facilitates a high metal



dispersion through the enhancement of the interaction (adsorption) between the organometallic precursor and the support [44,45], and (ii) the lack of a solvent decreases the likelihood of the surface contamination from residual solvent or the by-products of solvent decomposition during the heat treatment [43].

In order to verify the efficiency of the CVI method on the improvement of the Pt dispersion, the Pt particle size and metal dispersion of 2Pt<sup>CVI</sup>9W Al<sup>com</sup> and 2Pt9W Al<sup>com</sup> catalysts were measured by CO chemisorption. For the calculations, it was employed the most widely CO/Pt adsorption stoichiometry of 1 reported in the literature [46,47]. The results are displayed in the Table 6.5. It is worth noting that the conventional WI method led to the formation of smaller Pt particles than the CVI: a Pt size of 5.1 nm for the 2Pt9W Al<sup>com</sup> sample and 7.0 nm for the 2Pt<sup>CVI</sup>9W Al<sup>com</sup> sample. Thus, the CVI method was not effective to enhance the Pt dispersion (22.4 for WI and 17.3 % for CVI) on this catalytic system. The reason of this unexpected behaviour could reside in the higher reduction temperatures used for the sample prepared by CVI, 400 °C instead of 300 °C. However, this high temperature was required in order to fully pyrolyse the Pt-precursor employed in the synthesis (see section 4.1.3 of Chapter 4).

Both catalysts were tested in the glycerol hydrogenolysis reaction. The results mainly show a considerably lower glycerol conversion for the 2Pt<sup>CVI</sup>9W Al<sup>com</sup> catalyst than that obtained with 2Pt9W Al<sup>com</sup> (15.7 and 8.1 %, respectively), which seems to indicate that the Pt dispersion is also an important parameter in the glycerol hydrogenolysis. A higher Pt dispersion may lead to a higher hydrogen activation, required for the glycerol conversion, and to a higher Pt-WO<sub>x</sub> interaction.

Slightly lower selectivities towards 1,3-PDO were also found for 2Pt<sup>CVI</sup>9W Al<sup>com</sup> catalyst, of 46.8 % in contrast to the 52.7 % value obtained for 2Pt9W Al<sup>com</sup>. This could be due to the lower Pt-WO<sub>x</sub> interactions for the former catalyst.

**Table 6.5.** Pt particle size and dispersion obtained for the fresh reduced samples by CO chemisorption at 35 °C.

Catalyst	Pt size (nm)	Pt dispersion (%)
2Pt9WAl <sup>com</sup>	5.1	22.4
2Pt <sup>CVI</sup> 9WAl <sup>com</sup>	7.0	17.3
9Pt8WAl <sup>com</sup>	7.2	15.8
9Pt8WAl <sup>com</sup> *	26.4	4.1

\*Pre-treatment temperature: 450 °C (instead of 300 °C)

### 6.2.2.2 Effect of Pt loading

Once it was established that the 2Pt9W Al<sup>com</sup> was the catalyst which showed the best yield to the target product 1,3-PDO, the Pt loading was again risen up to 9 wt % in order to increase the Pt-WO<sub>x</sub> interactions (or improve their proximity) and promote the selective glycerol hydrogenolysis towards 1,3-PDO.

Fig. 6.12 shows the time-evolution of glycerol hydrogenolysis for 9Pt8W Al<sup>com</sup> at 200 °C and 45 bar of H<sub>2</sub>, which was examined along a period of 24 h.

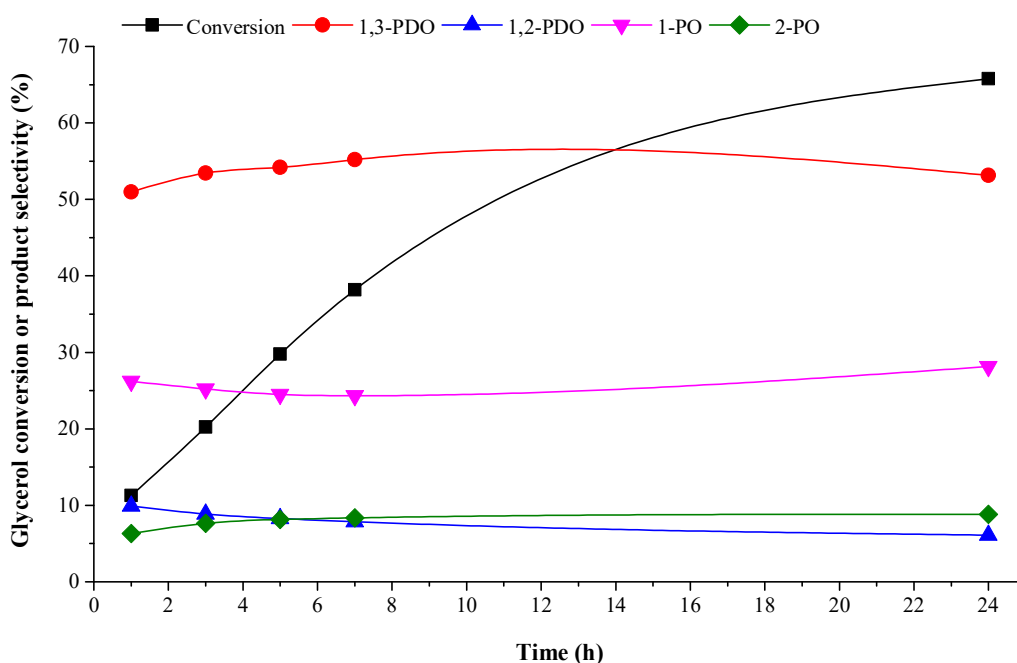


**Fig. 6.12.** Time-evolution of glycerol conversion and main product selectivities obtained for 9Pt8W Al<sup>com</sup> at 200°C and 45 bar of H<sub>2</sub>.

The glycerol conversion continuously increased during the 24 h reaction time, reaching a maximum of 65.8 % at 24 h. The selectivity towards 1,3-PDO remained quite stable, showing a little initial increase until 12 h, time from which it slightly decreased. In spite of this, the selectivity was > 50 % all the time. The opposite trend was found for 1-PO, suggesting a possible over-hydrogenolysis of 1,3-PDO giving rise to the monoalcohol. Regarding the selectivity towards 1,2-PDO, a constant drop was found as the selectivity towards 2-PO increased, indicating that 2-PO was formed through the over-hydrogenolysis of 1,2-PDO.

Extrapolating the results obtained with 9Pt8W Al<sup>com</sup> catalyst at 16 h and comparing with those obtained with the catalyst with 2 wt% Pt, as expected, glycerol

conversion increased with Pt content: from 15.7 % for 2 wt% to 59.4 % for 9 wt% Pt content. The effect on product selectivity is again more observable on 1,2-PDO, decreasing from 16.9 % to 6.4 % for 2 and 9 wt% Pt loading, respectively. At the same time, the selectivities towards 1,3-PDO and 1-PO slightly increased with the higher Pt content: from 52.7 to 55.9 % and from 20.8 to 25.8 %, respectively. By increasing the Pt content it seems possible to enhance the interactions between Pt and WO<sub>x</sub> species and promote the production of 1,3-PDO.

Although it is true that the Pt dispersion decreased with the Pt metal loading (see Table 6.5), the CO chemisorption results of 9Pt8W Al<sup>com</sup> revealed relatively small Pt particles of 7.2 nm (15.8 % Pt dispersion).

Moreover, the results of this work allow us comparing the effect of the temperature used in the pre-treatment (calcination and pre-reduction), since this is the unique difference between the 9Pt8W Al<sup>com</sup> catalyst tested in the Chapters 5 and 6 (calcined at 450 °C and 300 °C, respectively). As it was expected, the main difference was found in the glycerol conversion. This difference can be observed in Fig. 6.13.

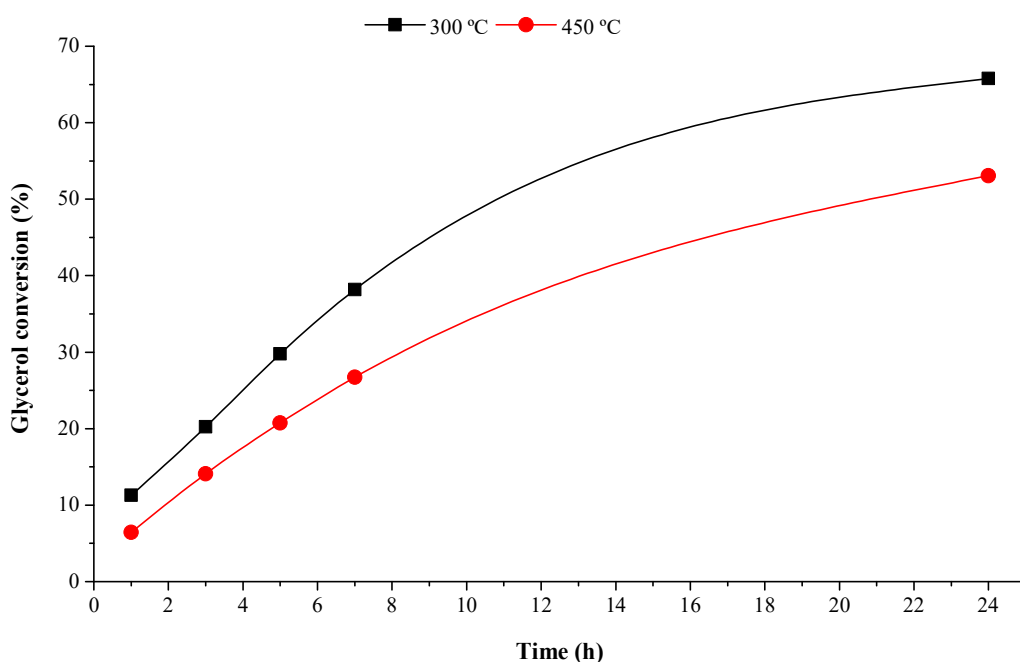


**Fig. 6.13.** Time-evolution of glycerol conversion obtained for 9Pt8W Al<sup>com</sup>, pre-treated at 450 °C and 300 °C. Reaction conditions: 200°C and 45 bar of H<sub>2</sub>.

According to the CO chemisorption results, the temperature used during the calcination and reduction pre-treatments has a large influence on the Pt metal size and,

therefore, on its dispersion on the catalysts surface. At 450 °C big Pt particles of 26.4 nm were found leading to a poor Pt dispersion of just a 4 % (see Table 5.2 of Chapter 5). Considerably smaller particles were obtained for the catalyst pre-treated at 300 °C: 7.2 nm and 17 % Pt dispersion. Thus, the Pt dispersion could explain quite well the greater glycerol conversion obtained for the 9Pt8W Al<sup>com</sup> catalyst pre-treated at 300 °C.

### 6.3 Conclusions

The results of this work allow a better understanding of the importance of some parameters involved in the glycerol hydrogenolysis to 1,3-PDO and of the Pt/WO<sub>x</sub> catalytic system.

The  $\rho_w$  was pointed out to be a crucial factor because it controls the kind of WO<sub>x</sub> species formed on the catalyst surface. It was found that the polytungstate species are the responsible of the Brønsted acid sites generation, which are related to the 1,3-PDO formation.

As the pseudo-AlO(OH) support presented a high concentration of hydroxy groups on its surface as compared to  $\gamma$ -Al<sub>2</sub>O<sub>3</sub>, it allowed the incorporation of larger W loadings and higher  $\rho_w$  without the emergence of the undesired WO<sub>3</sub> NPs ( $\rho_w^{\text{lim}}$ ). These results indicated that the hydroxy groups are the preferential anchoring sites for the WO<sub>x</sub> species. However, a balance between the WO<sub>x</sub> and Pt loadings seems to be necessary in order to enhance the Pt-WO<sub>x</sub> interactions or a closer proximity between these active sites.

Pt dispersion was also found as a key parameter in the reaction. The improvement of Pt dispersion leads to higher glycerol conversion values, since a higher number of Pt active sites are able to activate the hydrogen molecules. The selectivity towards 1,3-PDO was also increased by the improvement of Pt dispersion, which could be related to the enhancement of the Pt-WO<sub>x</sub> interactions or their proximity.

The best results were achieved with the 9Pt8W Al<sup>com</sup> catalyst showing a quite high 1,3-PDO yield of 35.0 % after 24 h reaction time.

## References

- [1] G.A. Lomi, E.E. Ki, G.C. Bo, R.P. Marinkovi, N. Sad, B.C. Lazara, Application of scanning electron microscopy in catalysis, *System*. 280 (2004) 67–77.
- [2] C.T. Campbell, Catalyst-support interactions: Electronic perturbations, *Nat. Chem.* 4 (2012) 597–598.
- [3] G. Toledo-Chávez, J.-C. Paniagua-Rodríguez, J. Zárate-Medina, R. Maya-Yescas, Reactions analysis during the synthesis of pseudo-boehmite as precursor of gamma-alumina, *Catal. Today*. (2015) In press.
- [4] D. Mishra, S. Anand, R.K. Panda, R.P. Das, Effect of anions during hydrothermal preparation of boehmites, *Mater. Lett.* 53 (2002) 133–137.
- [5] X. Wu, L. Zhang, D. Weng, S. Liu, Z. Si, J. Fan, Total oxidation of propane on Pt/WO<sub>x</sub>/Al<sub>2</sub>O<sub>3</sub> catalysts by formation of metastable Pt delta+ species interacted with WO<sub>x</sub> clusters, *J. Hazard. Mater.* 225-226 (2012) 146–154.
- [6] D.G. Barton, M. Shtein, R.D. Wilson, S.L. Soled, E. Iglesia, Structure and Electronic Properties of Solid Acids Based on Tungsten Oxide Nanostructures, *J. Phys. Chem. B.* 103 (1999) 630–640.
- [7] P.D.S. Santos, A.C.V. Coelho, H.D.S. Santos, P.K. Kiyohara, Hydrothermal synthesis of well-crystallised boehmite crystals of various shapes, *Mater. Res.* 12 (2009) 437–445.
- [8] D. Mishra, S. Anand, R.K. Panda, R.P. Das, Hydrothermal preparation and characterization of boehmites, *Mater. Lett.* 42 (2000) 38–45.
- [9] F. Hu, X. Wu, Y. Wang, X. Lai, Ultrathin  $\gamma$ -Al<sub>2</sub>O<sub>3</sub> nanofibers with large specific surface area and their enhanced thermal stability by Si-doping, *RSC Adv.* 5 (2015) 54053–54058.
- [10] A. Takagaki, C. Jung, S. Hayashi, Solid Lewis acidity of boehmite gamma-AlO(OH) and its catalytic activity for transformation of sugars in, *RSC Adv.* 4 (2014) 43785–43791.
- [11] H. Wang, Z. Yao, X. Zhan, Y. Wu, M. Li, Preparation of highly dispersed W/ZrO<sub>2</sub>-Al<sub>2</sub>O<sub>3</sub> hydrodesulfurization catalysts at high WO<sub>3</sub> loading via a microwave hydrothermal method, *Fuel*. 158 (2015) 918–926.
- [12] V.J. Ingram-Jones, R.C.T. Slade, T.W. Davies, J.C. Southern, S. Salvador, Dehydroxylation sequences of gibbsite and boehmite: study of differences between soak and flash calcination and of particle-size effects, *J. Mater. Chem.* 6 (1996) 73.
- [13] R.M. Ravenelle, J.R. Copeland, W. Kim, J.C. Crittenden, C. Sievers, W. Peachtree, et al., Structural Changes of  $\gamma$ -Al<sub>2</sub>O<sub>3</sub>-Supported Catalysts in Hot Liquid Water, *ACS Catal.* (2011) 552–561.
- [14] T. Hyde, Final Analysis: Crystallite Size Analysis of Supported Platinum Catalysts by XRD, *Platin. Met. Rev.* 52 (2008) 129–130.
- [15] K.S.W. Sing, D.H. Everett, R.A.W. Haul, L. Moscou, R.A. Pierotti, J. Rouquerol, et al., Reporting Physisorption Data for Gas/Solid Systems, in: G. Ertl, H. Knozinger, F. Schuth, J. Weitkamp (Eds.), *Handb. Heterog. Catal.*, 2nd ed., Wiley-VCH Verlag GmbH & Co. KGaA, 2008: pp. 1217–1230.
- [16] P.B. Balbuenat, K.E. Gubbins, Theoretical Interpretation of Adsorption Behavior of Simple Fluids in Slit Pores, *Langmuir*. 9 (1993) 1801–1814.

- [17] B. Lippens, J.H. de Boer, Studies on pore systems in catalysts V. The t method, *J. Catal.* 4 (1965) 319–323.
- [18] M. El Doukkali, A. Iriondo, P.L. Arias, J. Requies, I. Gandarías, L. Jalowiecki-Duhamel, et al., A comparison of sol-gel and impregnated Pt or/and Ni based  $\gamma$ -alumina catalysts for bioglycerol aqueous phase reforming, *Appl. Catal. B Environ.* 125 (2012) 516–529.
- [19] Y.S. Yun, D.S. Park, J. Yi, Effect of nickel on catalytic behaviour of bimetallic Cu–Ni catalyst supported on mesoporous alumina for the hydrogenolysis of glycerol to 1,2-propanediol, *Catal. Sci. Technol.* (2014) 3191–3202.
- [20] I.E. Wachs, T. Kim, E.I. Ross, Catalysis science of the solid acidity of model supported tungsten oxide catalysts, *Catal. Today.* 116 (2006) 162–168.
- [21] M.A. Vuurman, D.J. Stufkens, A. Oskam, G. Deo, I.E. Wachs, Combined Raman and IR study of  $\text{MO}_x\text{-V}_2\text{O}_5/\text{Al}_2\text{O}_3$  ( $\text{MO}_x = \text{MoO}_3, \text{WO}_3, \text{NiO}, \text{CoO}$ ) catalysts under dehydrated conditions, *J. Chem. Soc. Faraday Trans.* 92 (1996) 3259.
- [22] D.G. Barton, S.L. Soled, G.D. Meitzner, F. G.A., E. Iglesia, Structural and Catalytic Characterization of Solid Acids Based on Zirconia Modified by Tungsten Oxide, *J. Catal.* 181 (1999) 57–72.
- [23] I.E. Wachs, B.M. Weckhuysen, Structure and reactivity of surface vanadium oxide species on oxide supports, *Appl. Catal. A Gen.* 157. 157 (1997) 67–90.
- [24] S. García-Fernández, I. Gandarias, J. Requies, M.B. Güemez, S. Bennici, A. Auroux, et al., New approaches to the Pt/WO<sub>x</sub>/Al<sub>2</sub>O<sub>3</sub> catalytic system behavior for the selective glycerol hydrogenolysis to 1,3-propanediol, *J. Catal.* 323 (2015) 65–75.
- [25] T. Kim, A. Burrows, C. Kiely, I. Wachs, Molecular/electronic structure–surface acidity relationships of model-supported tungsten oxide catalysts, *J. Catal.* 246 (2007) 370–381.
- [26] M. Valigi, D. Gazzoli, I. Pettiti, G. Mattei, S. Colonna, S. De Rossi, et al., WO<sub>x</sub>/ZrO<sub>2</sub> catalysts Part 1 Characterization, *Appl. Catal. A Gen.* 231 (2002) 159–172.
- [27] M.N. Taylor, W. Zhou, T. Garcia, B. Solsona, A.F. Carley, C.J. Kiely, et al., Synergy between tungsten and palladium supported on titania for the catalytic total oxidation of propane, *J. Catal.* 285 (2012) 103–114.
- [28] M.M. Ostromecki, L.J. Burcham, I.E. Wachs, The influence of metal oxide additives on the molecular structures of surface tungsten oxide species on alumina. II. In situ conditions, *J. Mol. Catal. A Chem.* 132 (1998) 59–71.
- [29] A.M. Turek, I.E. Wachs, E. DeCanio, Acidic properties of alumina-supported metal oxide catalysts: an infrared spectroscopy study, *J. Phys. Chem.* 96 (1992) 5000–5007.
- [30] A. Karakonstantis, L., Bourikas, K., Lycourghiotis, Tungsten–Oxo-Species Deposited on Alumina, *J. Catal.* 162 (1996) 295–305.
- [31] C. Thomas, Should W Surface Density of WO<sub>x</sub>–ZrO<sub>2</sub> Catalysts be calculated with respect to the Specific Surface Area of the sample or That of ZrO<sub>2</sub> Only?, *J. Phys. Chem. C.* 115 (2011) 2253–2256.
- [32] L. Vilcocq, R. Koerin, A. Cabiac, C. Especel, S. Lacombe, D. Duprez, New bifunctional catalytic systems for sorbitol transformation into biofuels, *Appl. Catal. B Environ.* 148–149 (2014) 499–

- 508.
- [33] D. Papias, A. Krestou, Effect of synthesis parameters on precipitation of nanocrystalline boehmite from aluminate solutions, *Powder Technol.* 175 (2007) 163–173.
- [34] J. Cruz, M. Avalos-borja, R.L. Cordero, M.A. Bañares, J.L.G. Fierro, J.M. Palacios, et al., Influence of pH of the impregnation solution on the phosphorus promotion in W/Al<sub>2</sub>O<sub>3</sub> hydrotreating catalysts, *Appl. Catal. A Gen.* 224 (2002) 97–110.
- [35] Y. Fan, X. Bao, H. Wang, C. Chen, G. Shi, A surfactant-assisted hydrothermal deposition method for preparing highly dispersed W/ $\gamma$ -Al<sub>2</sub>O<sub>3</sub> hydrodenitrogenation catalyst, *J. Catal.* 245 (2007) 477–481.
- [36] H. Wang, Y. Wu, Z. Liu, Z. Yao, W. Zhao, Deposition of WO<sub>3</sub> on Al<sub>2</sub>O<sub>3</sub> via a microwave hydrothermal method to prepare highly dispersed W/Al<sub>2</sub>O<sub>3</sub> hydrosulfuration catalyst, *Fuel.* 136 (2014) 185–193.
- [37] A.S. Ivanova, E.M. Slavinskaya, R. V. Gulyaev, V.I. Zaikovskii, O. a. Stonkus, I.G. Danilova, et al., Metal-support interactions in Pt/Al<sub>2</sub>O<sub>3</sub> and Pd/Al<sub>2</sub>O<sub>3</sub> catalysts for CO oxidation, *Appl. Catal. B Environ.* 97 (2010) 57–71.
- [38] M. Paulis, H. Peyrards, M. Montes, Influence of Chlorine on the Activity and Stability of Pt/Al<sub>2</sub>O<sub>3</sub> Catalysts in the Complete Oxidation of Toluene, *J. Catal.* 199 (2001) 30–40.
- [39] S. Kuba, P. Lukinskas, R.K. Grasselli, B.C. Gates, H. Knözinger, Structure and properties of tungstated zirconia catalysts for alkane conversion, *J. Catal.* 216 (2003) 353–361.
- [40] M. Guemini, Y. Rezgui, Effect of pretreatment conditions on the catalytic performance of Ni-Pt-W supported on amorphous silica-alumina catalysts. Part 2. Catalysts prepared by a hybrid method, *Appl. Catal. A Gen.* 345 (2008) 164–175.
- [41] J. Jia, A study on reduction behaviors of the supported platinum – iron catalysts, (1999) 177–184.
- [42] J. Macht, E. Iglesia, Structure and function of oxide nanostructures: catalytic consequences of size and composition., *Phys. Chem. Chem. Phys.* 10 (2008) 5331–5343.
- [43] M.M. Forde, L. Kesavan, M.I. Bin Saiman, Q. He, N. Dimitratos, J.A. Lopez-Sanchez, et al., High activity redox catalysts synthesized by chemical vapor impregnation, *ACS Nano.* 8 (2014) 957–969.
- [44] B. Caussat, C. Vahlas, CVD and Powders: A Great Potential to Create New Materials, *Chem. Vap. Depos.* 13 (2007) 443–445.
- [45] P. Serp, R. Feurer, R. Morancho, P. Kalck, One-Step Preparation of Highly Dispersed Supported Rhodium Catalysts by Low-Temperature Organometallic Chemical Vapor Deposition, *J. O.* 157 (1995) 294–300.
- [46] Y. Izutsu, Y. Oku, Y. Hidaka, N. Kanaya, Y. Nakajima, J. Fukuroi, et al., Physicochemical Characterization of Highly Dispersed Platinum and Chromium on Zeolite Beta, *J. Phys. Chem. C.* (2014) 10746–10753.
- [47] K.E. Jeong, H.D. Kim, T.W. Kim, J.W. Kim, H.J. Chae, S.Y. Jeong, et al., Hydrogen production by aqueous phase reforming of polyols over nano- and micro-sized mesoporous carbon supported platinum catalysts, *Catal. Today.* 232 (2014) 151–157.

## **CHAPTER 7.**

### **Mechanistic study of the glycerol hydrogenolysis over Pt/WO<sub>x</sub>/Al<sub>2</sub>O<sub>3</sub> catalysts**





---

**Table of contents**

ABSTRACT.....	161
7.1 INTRODUCTION.....	162
7.2 EXPERIMENTAL .....	164
7.2.1 Catalyst preparation .....	164
7.2.2 Catalyst characterisation .....	164
7.2.3 Kinetic measurements.....	164
7.2.4 Activity test to determine the effect of the reacting atmosphere .....	164
7.3 RESULTS AND DISCUSSION .....	164
7.3.1 Catalyst characterisation .....	164
7.3.1.1 In-situ ATR spectroscopy .....	164
7.3.1.2 Ex-situ ATR-IR spectroscopy .....	172
7.3.2 Glycerol and products competition for the same active sites .....	175
7.3.3 Effect of the reacting atmosphere and hydrogen availability.....	177
7.4 OVERALL REACTION MECHANISM.....	180
7.5 CONCLUSIONS .....	182
REFERENCES.....	183



## Abstract

In spite of the intense work carried out, the overall reaction mechanism of the aqueous glycerol hydrogenolysis into propanediols (PDOs), in particular to the most valuable 1,3-PDO, still remains unclear. This fact together with the great deal of controversy about fundamental reaction parameters, such as the role of the oxophilic metal in the binding of glycerol or the intermediate species generated, has motivated to a deeper study of the reaction mechanism.

The glycerol hydrogenolysis was studied using Pt/WO<sub>x</sub>/Al<sub>2</sub>O<sub>3</sub> catalytic systems by *in-situ* attenuated total reflection infrared (ATR-IR) spectroscopy. This powerful technique is well-suited for studying adsorbed species on the catalyst surface such as reactants, intermediates and products, even in aqueous phase. Moreover, other *ex-situ* ATR-IR spectroscopic studies were also utilized to study the interactions of the reactants and products with the catalyst surface. The results suggest a different adsorption trend of glycerol when WO<sub>x</sub> is incorporated on the  $\gamma$ -Al<sub>2</sub>O<sub>3</sub> support.

The competitive adsorption between reactants and products for the same active sites and the effect of the hydrogen availability were also studied in the present work. They provided some new insights into the reaction pathways of glycerol hydrogenolysis which lead to a better understanding of the overall reaction mechanism.

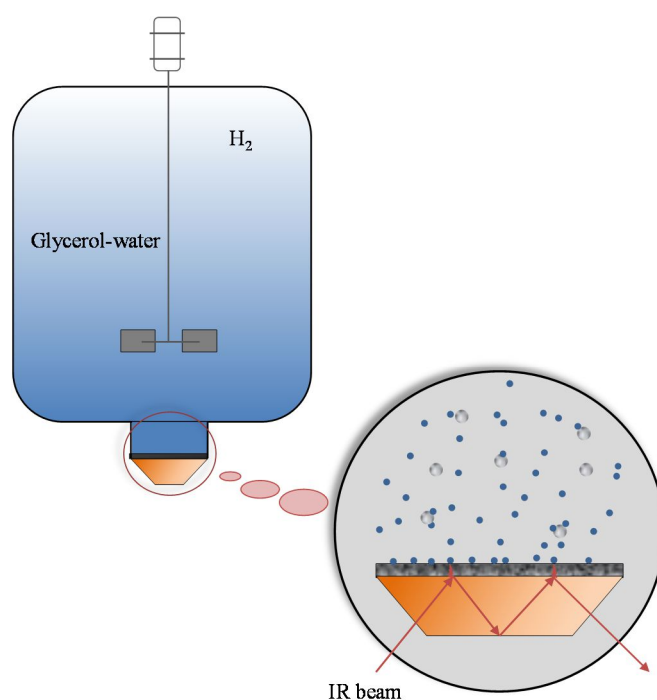


Fig. 7.1. Graphical abstract.

## 7.1 Introduction

A detailed understanding of the surface chemistry is fundamental in order to improve the performance of a catalyst as well as to design new efficient heterogeneous catalysts [1]. In this respect, infrared (IR) spectroscopy is one of the most powerful tools. Besides contributing to the surface chemistry knowledge, IR spectroscopy is a valuable tool for mechanistic studies as it can be applied *in-situ* providing fundamental information of adsorbed species during the reaction under working conditions [2].

The majority of *in-situ* IR spectroscopic studies are usually carried out in gas phase using the conventional transmission Fourier Transform infrared (FTIR) spectroscopy [3,4], in which the IR beam passes through the sample where it is partially absorbed [5]. However, liquid phase reactions present a greater challenge for *in-situ* spectroscopic studies and their study has been limited due to the large spectral interference caused by the strong IR absorption of the solvent [6]. Water, in particular, absorbs IR light in several important regions in the mid-IR range (4000-400 cm<sup>-1</sup>). This problem comes together with the very strong absorbance of most of the metal oxides, including the widely used Al<sub>2</sub>O<sub>3</sub> support [7,8]. Thus, conventional transmission FTIR techniques are not suitable to study the molecular vibrations at the solid-liquid interface.

Interestingly, the problems related to the use of aqueous environments can be minimized by using the *in-situ* attenuated total reflection infrared (ATR-IR) spectroscopy [9]. In general, the ATR-IR technique consists on directing the IR beam onto an internal reflection element (IRE), a crystal of relatively high refractive index. The IR beam undergoes a total reflection (single or multiple internal reflections) when the incident angle exceeds the critical angle. Upon total reflection, an evanescent wave is generated which projects orthogonally into the sample in intimate contact with the crystal [10]. The evanescent wave decays rapidly with the distance from the surface and, therefore, it is essential that the sample is in close contact with the IRE. Part of the energy of the evanescent wave is absorbed by the sample generating an absorption spectrum and the reflected radiation is returned to the detector [5]. The schematic representation of this phenomenon is shown in Fig. 7.2.

The resulting ATR-IR spectrum is similar to a conventional IR one, just only the higher intensities are obtained for longer wavelengths (shorter wavenumbers) because of the higher penetration depth at those wavenumbers [11]. This technique avoids the direct transmission of the beam through the sample, since the evanescent wave is

restricted to a region near the solid-liquid interface (of only few microns). In this way, the liquid interference is minimised while maximising the signals of the surface species [12,13]. The ATR technique is also attractive since little or no sample preparation is necessary in contrast to the conventional IR techniques [14].

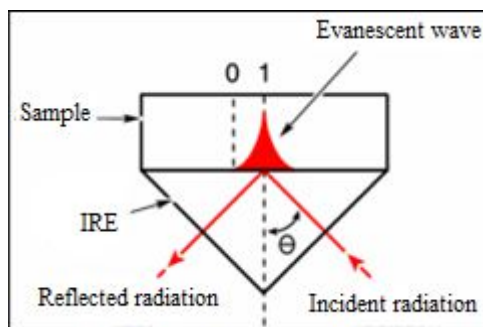


Fig. 7.2. Schematic representation of the ATR-IR work (single-reflection crystal).

Up to date, only few studies of the application of *in-situ* ATR-IR to aqueous phase reactions have been reported. Dumesic's group combined this technique with a kinetic study in order to understand the differences between methanol reforming over Pt/Al<sub>2</sub>O<sub>3</sub> in vapour or aqueous-phase reaction conditions [15]. More recently, Lefferts et al. applied this technique in the CO adsorption and aqueous phase oxidation [16], as well as in the nitrite hydrogenation [17], over noble metal supported catalysts, to determine the type of adsorbates and possible reaction intermediates. Another innovative work was carried out by the Weckhuysen's group applying *the in-situ* ATR-IR technique to investigate the Pt-based catalysts deactivation on aqueous phase reforming (APR) of crude glycerol [18]. These studies are some illustrative examples of the potential of this technique.

In this Chapter 7, the *in-situ* ATR-IR spectroscopy was used in the glycerol hydrogenolysis to PDOs in aqueous phase over Pt/WO<sub>x</sub>/Al<sub>2</sub>O<sub>3</sub> catalysts, aiming to study the nature of adsorbed species on the catalyst surface such as reactants, intermediates and products. As shown in the Chapter 5, these catalysts proved to be very effective in the reaction, affording very high yields of 1,3,-PDO [19]. Other *ex-situ* ATR-IR spectroscopic studies based on the same principle were also carried out to study the reactant adsorption modes on different catalyst surfaces. These spectroscopic studies in combination with the reaction kinetics shed some light on the overall reaction mechanism of the glycerol hydrogenolysis to PDOs.

## **7.2 Experimental**

### **7.2.1 Catalyst preparation**

The Pt/WO<sub>x</sub>/Al<sub>2</sub>O<sub>3</sub> catalysts used were prepared by sequential wetness impregnation method following the preparation procedure described in the section 4.1.1 of Chapter 4. The nomenclature used, *x*Pt<sub>y</sub>W(*z*), is also explained in the same section.

### **7.2.2 Catalyst characterisation**

The catalyst characterisation was made using *in-situ* as well as *ex-situ* ATR-IR spectroscopy. The equipment and operating conditions employed for both spectroscopic studies are detailed in the sections 4.4.12 and 4.4.13 of Chapter 4, respectively. Typically, in these studies the solid catalyst is immobilized on the IRE as it was explained in the section 4.2.

### **7.2.3 Kinetic measurements**

The kinetic study was carried out using the 9Pt8W catalyst and different reactants according to the procedure described in the section 4.3.2 of Chapter 4.

### **7.2.4 Activity test to determine the effect of the reacting atmosphere**

Some activity tests were carried out in a batch-autoclave in order to determine the effect of the reacting atmosphere (N<sub>2</sub> and H<sub>2</sub>) on the hydrogenolysis of glycerol over the 9Pt8W catalyst. The catalyst powder was reduced in a H<sub>2</sub> flow at 300 °C prior to the activity tests. The reaction conditions used for these experiments were: 220 °C, 45 bar of H<sub>2</sub> or N<sub>2</sub> and 16 h of reaction time. Other conditions and the experimental procedure for the activity tests were detailed in the section 4.3.1.

## **7.3 Results and discussion**

### **7.3.1 Catalyst characterisation**

#### **7.3.1.1 *In-situ* ATR spectroscopy**

Time-resolved ATR-IR spectra of the surface species adsorbed on the 9Pt8W catalyst during the hydrogenolysis of 5 wt% glycerol on water, at 200 °C and 45 bar of H<sub>2</sub>, are shown in Fig. 7.3. In order to minimise the contribution of any possible modification of the catalyst layer, as well as the expansion of the IRE with the

temperature, the catalyst layer coated on the IRE at the reaction temperature (200 °C) was used as background.

Two strong peaks characteristic of liquid water can clearly be observed: a very broad peak around 3460  $\text{cm}^{-1}$  which corresponds to the O-H stretching ( $\nu_{\text{OH}}$ ) mode and a peak at 1638  $\text{cm}^{-1}$  corresponding to the HOH scissor bending mode of water [9,20].

There are no evidences of the hydration of the  $\gamma\text{-Al}_2\text{O}_3$  support into  $\text{AlO}(\text{OH})$  (boehmite) during the reaction, usually evidenced by a sharp peak at 1064  $\text{cm}^{-1}$  assigned to OH deformations and shoulder bands at 3304 and 3124  $\text{cm}^{-1}$  to the stretching vibrational modes [21]. It was reported that the presence of both Pt and glycerol retards this transformation [18,21].

Interestingly, a peak centred around 2020  $\text{cm}^{-1}$  with a shoulder at 1988  $\text{cm}^{-1}$  was detected. It was also observed in the blank-experiment with water under the same reaction conditions (not shown) and, therefore, it cannot be ascribed to the formation of CO during the reaction, which is expected to appear in this region [16,22]. In the work carried out by Ortiz-Hernández et al. they observed two peaks in the same region (a peak centred at 2060  $\text{cm}^{-1}$  and a shoulder at 1990  $\text{cm}^{-1}$ ) exposing a Pt/ $\text{Al}_2\text{O}_3$  catalyst to a  $\text{H}_2$  flow in water [23]. In their work, they demonstrated that those peaks were likely trace amounts of CO or other carbonyl species formed from impurities in the catalyst layer.

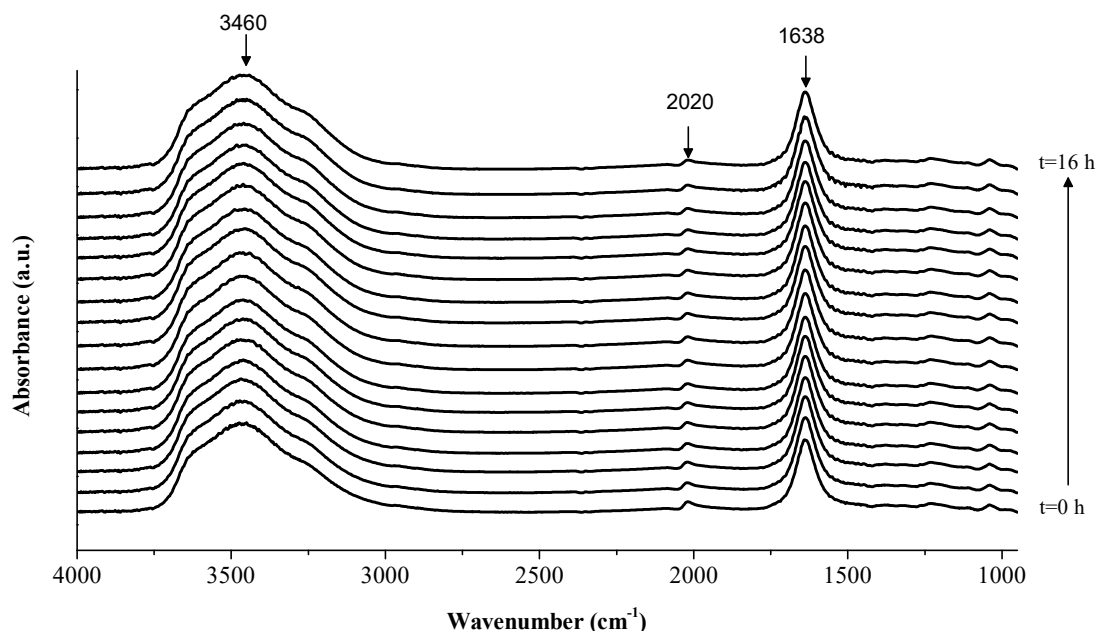


**Fig. 7.3.** Time-resolved *in-situ* ATR-IR spectra during the hydrogenolysis of 5 wt% glycerol on water over 9Pt8W at 200 °C and 45 bar of  $\text{H}_2$ .



Unfortunately, the strong absorption of water in mid-IR may hinder the observation of other bands related to the intermediates or products species. In order to eliminate the contribution of water adsorption, the water spectrum (blank-experiment) was subtracted from the time-resolved spectra. The resulted spectra in the 4000-950 cm<sup>-1</sup> region are shown in Fig. 7.4.

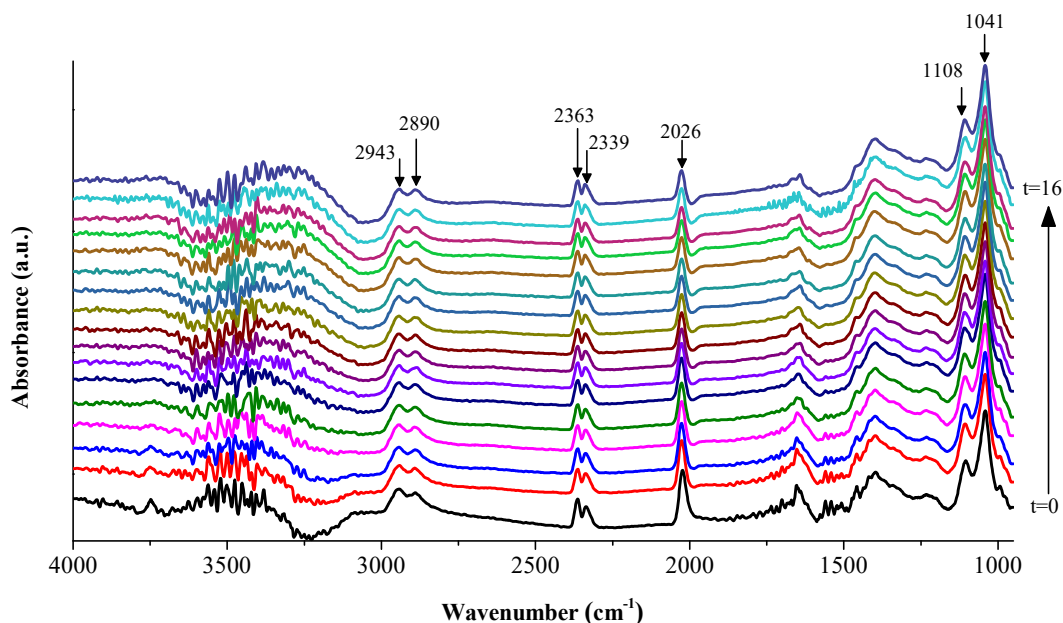


**Fig. 7.4.** Time-resolved *in-situ* ATR-IR spectra during the hydrogenolysis of 5 wt% glycerol in water over 9Pt8W (at 200 °C and 45 bar of H<sub>2</sub>) after water spectrum subtraction, in the complete region 4000-950 cm<sup>-1</sup>

First of all, it is necessary to highlight the difficulty to identify the adsorbed species since the majority of the compounds were alcohols and showed absorption bands at similar frequencies.

Moreover, because of the strong absorbance of water in the 3600-3000 cm<sup>-1</sup> region, and the noise that the spectra contained after water subtraction, the νOH mode of the reactant or the product species containing hydroxy groups cannot be resolved. The large noise that also appeared in the region around 1870-1450 cm<sup>-1</sup> could also hinder other bands [24]. This could be the case of the νC=O characteristic modes of some potential intermediates, such as aldehydes (1740-1720 cm<sup>-1</sup>), ketones (1725-1705 cm<sup>-1</sup>) and acids (1725-1700 cm<sup>-1</sup>) [25]. The peaks in the 2400-2000 cm<sup>-1</sup> region may correspond to some carbonyl species coming from impurities in the catalyst layer, as mentioned before: the peaks at 2363 and 2339 cm<sup>-1</sup> may be assigned to the adsorbed CO<sub>2</sub> [26] and the peak around 2026 cm<sup>-1</sup> to the linearly adsorbed CO [16].

Since the strongest and more defined bands were observed in the  $\nu\text{CH}$  ( $3000\text{--}2850\text{ cm}^{-1}$ ) and  $\nu\text{CO}$  ( $1150\text{--}950\text{ cm}^{-1}$ ) regions, those regions are represented in Fig. 7.5.

The good match between the position of the peaks found in these measurements and those detected in the work carried out by Sievers et al. on the adsorption of an aqueous glycerol solution on a  $\text{Pt}/\text{Al}_2\text{O}_3$  catalyst [27], demonstrated unequivocally that they correspond to glycerol. The peaks around  $2943$  and  $2890\text{ cm}^{-1}$  can be ascribed to the asymmetric and symmetric stretching modes of the  $\text{CH}_2$  group of glycerol, respectively ( $\nu_{\text{asym}}\text{CH}_2$  and  $\nu_{\text{sym}}\text{CH}_2$ ). Two other peaks at  $1108$  and  $1041\text{ cm}^{-1}$  were also detected, which correspond to the  $\nu\text{CO}$  of the secondary ( $\nu\text{CO } 2^\circ$ ) and of the primary carbons ( $\nu\text{CO } 1^\circ$ ) of glycerol. Weaker deforming modes ( $\delta$ ) likely associated with glycerol can be seen in the  $1400\text{--}1200\text{ cm}^{-1}$  region (see Fig. 7.4).

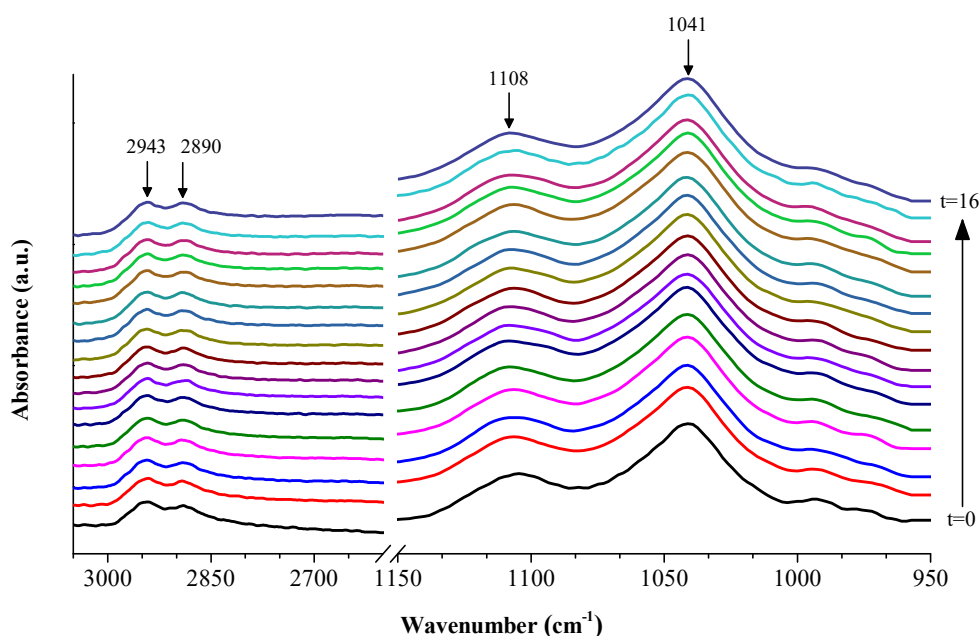


**Fig. 7.5.** Time-resolved *in-situ* ATR-IR spectra during the hydrogenolysis of 5 wt% glycerol in water over 9Pt8W (at  $200\text{ }^\circ\text{C}$  and 45 bar of  $\text{H}_2$ ) after water spectrum subtraction.

The quite low glycerol conversion achieved (18.6 %) after the 16 h reaction time may be one of the reasons for which qualitative changes cannot be observed: neither the presence of species different from glycerol nor significant changes in the peak height. Thus, in order to increase the conversion of glycerol and to reduce the strong adsorption of water on the catalyst surface, two experiments were carried out with higher initial glycerol concentrations (15 and 30 wt%). Fig. 7.6 shows the effect of glycerol concentration on the glycerol hydrogenolysis over the 9Pt8W catalyst under the same reaction conditions ( $200\text{ }^\circ\text{C}$ , 45 bar of  $\text{H}_2$  and 16 h of reaction time).

According to the results, the glycerol conversion notably increased from 18.6 to 38.8 % as its initial concentration in water was incremented from 5 to 30 wt% .

Regarding the product selectivities, the most remarkable fact was the decrease in the selectivity towards 1,2-PDO. It decreased from 58.7 % for 5 wt% of glycerol to 30.6 % for 15 wt% and remained almost constant for higher glycerol concentrations. The selectivity towards 1,3-PDO slightly decreased as the glycerol concentration increased (from 27.8 to 22.0 %, for 5 and 30 wt% glycerol). The downward trend of PDOs selectivities could be explained by their over-hydrogenolysis mainly in favour of 1-PO but also of 2-PO and other degradation products such as ethylene glycol (EG), ethanol and methanol.

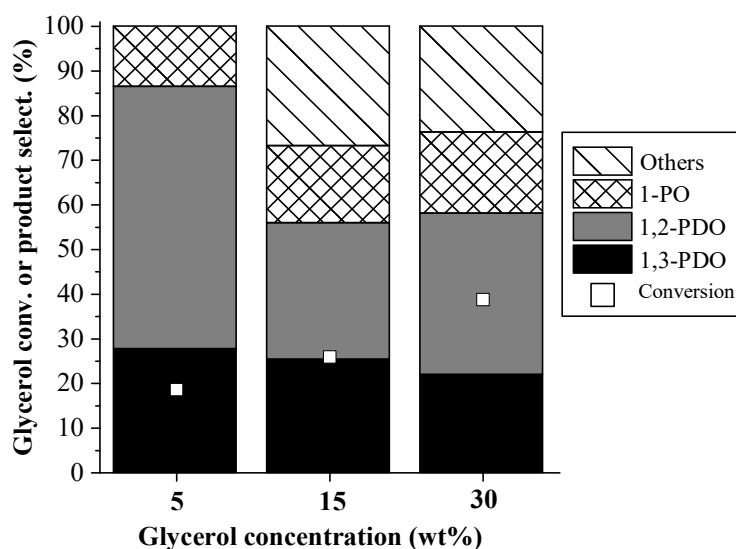


**Fig. 7.6.** Effect of glycerol concentration on the glycerol hydrogenolysis over 9Pt8W at 200 °C, 45 bar of H<sub>2</sub> and 16 h reaction time. Others: 2-PO, EG, ethanol and methanol.

For a deeper analysis, the water spectrum was subtracted from the time-resolved spectra of the hydrogenolysis of 15 wt% of glycerol. Fig 7.7 shows the  $\nu$ CH and the  $\nu$ CO regions of those spectra.

The same glycerol-related modes as those found in the hydrogenolysis of 5 wt% glycerol (Fig. 7.5) were detected. All glycerol-related peaks became weaker as the reaction time increased. This can be clearly seen in the  $\nu$ CO 2° mode at 1108 cm<sup>-1</sup>, which almost disappeared after 3 h of reaction time. This fact may correspond to that the higher initial concentration of glycerol led to a higher glycerol conversion and, therefore, a larger formation of the reaction products. According to this, there was a

higher competitive adsorption between the glycerol and the reaction products on the catalyst surface.

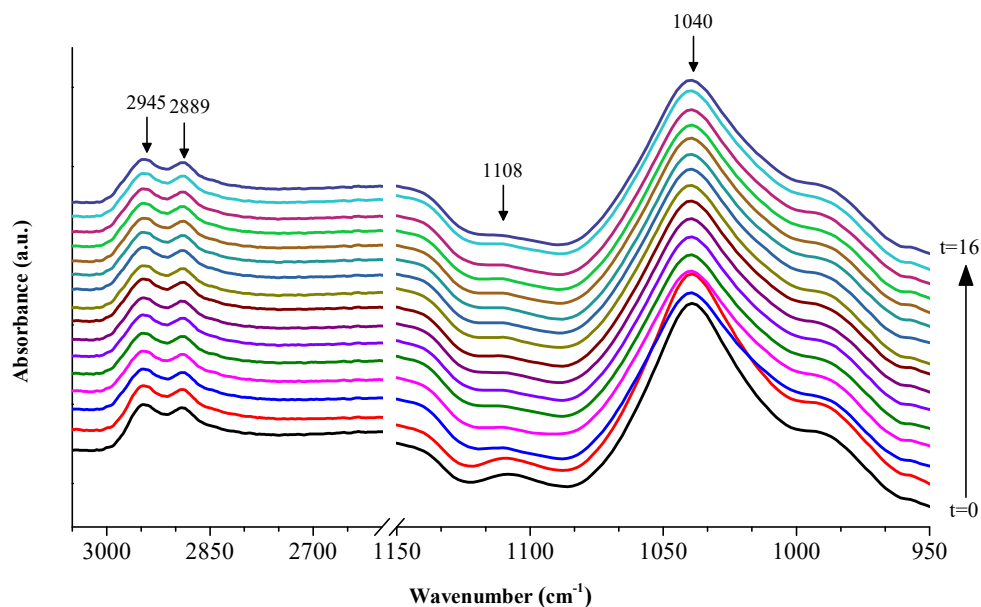


**Fig. 7.7.** Time-resolved *in-situ* ATR-IR spectra during the hydrogenolysis of 15 wt% glycerol in water over 9Pt8W (at 200 °C and 45 bar of H<sub>2</sub>) after water spectrum subtraction.

In a thorough work carried out by Sievers et al., the interactions between C2 and C3 polyols and  $\gamma$ -Al<sub>2</sub>O<sub>3</sub> catalyst, and the influence of co-adsorbed water on those interactions were investigated [28]. They found that the polyols with more hydroxy groups have stronger surface interactions on  $\gamma$ -Al<sub>2</sub>O<sub>3</sub> and a higher uptake from the aqueous solutions than those with fewer hydroxy groups. Besides glycerol was present in greater concentrations, this could also be one of the reasons to explain why glycerol was detected more clearly than any other reaction product under the operating conditions used.

Considering the hypothesis previously mentioned, the spectrum at initial time ( $t=0$ ) was subtracted from the time-evolution spectra of the hydrogenolysis of 15 wt% glycerol (Fig. 7.8). At  $t=0$  time glycerol is considered to be the unique compound adsorbed, to a large extent, on the catalyst surface. At  $t>0$  two strong negative peaks appeared at 1108 and 1038 cm<sup>-1</sup> associated with the  $\nu$ CO modes of glycerol. They revealed the lower adsorption of glycerol because of the competitive adsorption with the products formed along the reaction.

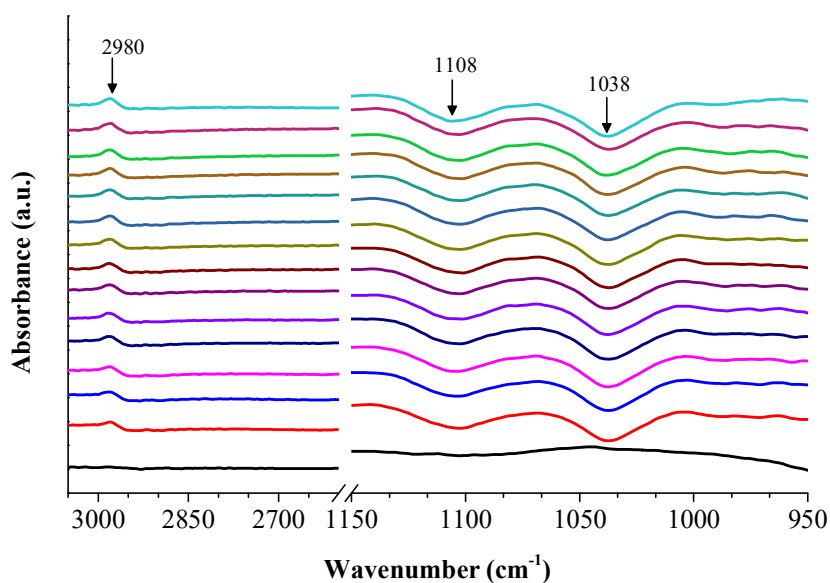


**Fig. 7.8.** Time-resolved *in-situ* ATR-IR spectra during the hydrogenolysis of 15 wt% glycerol in water over 9Pt8W (at 200 °C and 45 bar of H<sub>2</sub>) after spectrum at t=0 was subtracted.

Interestingly, a positive clearly defined peak appeared at 2980 cm<sup>-1</sup> (see Fig. 7.8 left), whose area increased as the reaction moved forward as it can be observed in Fig. 7.9. The appearance of positive peaks suggests the formation of products along the reaction. It is reasonable to qualitatively correlate the peak integrated-area to the extent of product formation.

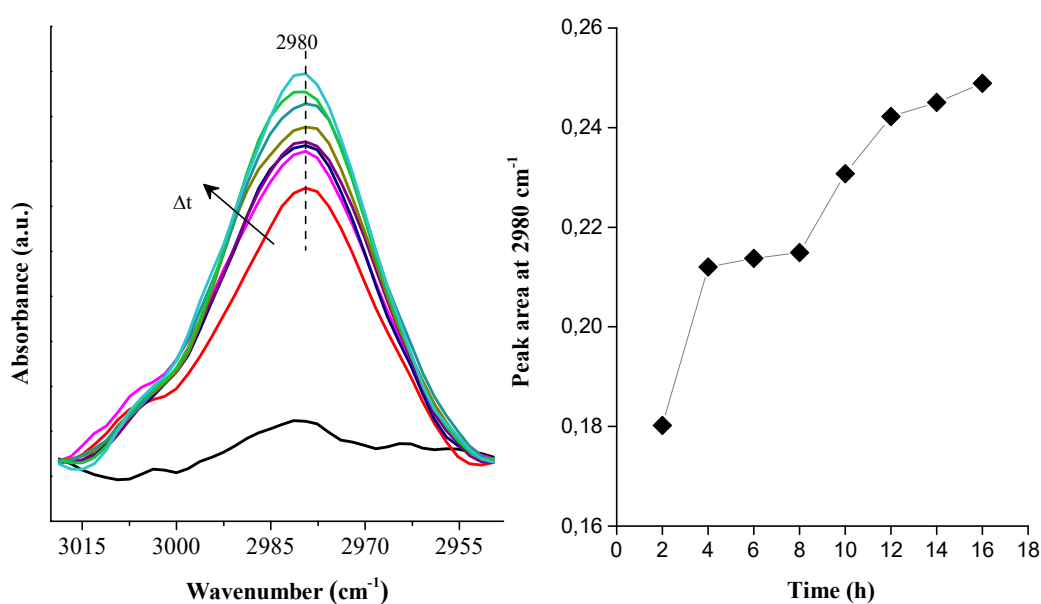


**Fig. 7.9.** The positive peak at 2980 cm<sup>-1</sup> developed in time (left) and the peak area evolution (right) during the hydrogenolysis of 15 wt% glycerol in water over 9Pt8W (at 200 °C and 45 bar of H<sub>2</sub>). Spectrum at t=0 subtracted.

The analysis of the hydrogenolysis of 30 wt% glycerol spectra, after the spectrum at  $t=0$  was subtracted, provided more information about the origin of the band around  $2980\text{ cm}^{-1}$ . Fig. 7.10 shows the  $\nu\text{CH}$  region of those spectra. A band at a similar position,  $2981\text{ cm}^{-1}$ , and other two at  $2933$  and  $2880\text{ cm}^{-1}$  were found, which may be ascribed to the  $\nu_{\text{asym}}\text{CH}_3$ ,  $\nu_{\text{asym}}\text{CH}_2$  and  $\nu_{\text{sym}}\text{CH}_2$  of 1,2-PDO, respectively [28].

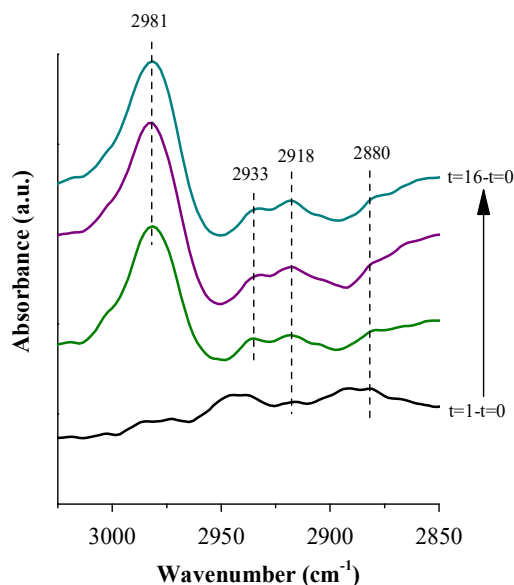


**Fig. 7.10.** Time-resolved *in-situ* ATR-IR spectra during the hydrogenolysis of 30 wt% glycerol on water over 9Pt8W (at  $200\text{ }^{\circ}\text{C}$  and  $45\text{ bar}$  of  $\text{H}_2$ ) after spectrum at  $t=0$  was subtracted, in the  $\nu\text{CH}$  region.

Despite that the surface species formed by other product species, such as 1-PO, 2-PO or ethanol, also exhibit  $\nu\text{CH}_3$  and  $\nu\text{CH}_2$  bands with nearly identical frequencies [29–31], it is reasonable to think that they could correspond to 1,2-PDO, since it is the major product in the reaction (30.6 and 36.1 % selectivity for the experiments with 15 and 30 wt% initial glycerol concentrations). In addition, the higher number of hydroxy groups of 1,2-PDO makes easier its adsorption on the catalyst surface [28], as it was explained above. The preliminary kinetic studies carried out in the current work (see section 7.3.2) shed more light on the matter and support this hypothesis. Obviously, the assignment of those peaks to 1,3-PDO is ruled out since this compound does not show the  $\nu\text{CH}_3$  mode.

Another peak centred at  $2918\text{ cm}^{-1}$  was observed and likely corresponds to the  $\nu_{\text{asym}}\text{CH}_2$  characteristic group [11]. According to the literature, it is quite far from the bands the bulk species (when they are not adsorbed) showed, the products analysed by GC-TCD-FID (PDOs, 1-PO, EG or ethanol) as well as the main intermediates involved in the reaction, acetol and propanal (detected in other experiments, see section 7.3.3),

and other suggested intermediates, such as acrolein [20,25]. Nevertheless, the formation of an adsorbed alkoxide coming from some of these compounds could shift the band position or originate a new band.

### 7.3.1.2 *Ex-situ* ATR-IR spectroscopy

The ATR-IR working is not limited to the *in-situ* measurements. It is also very useful for obtaining IR spectra of samples that cannot be readily examined by common transmission methods, such as thick or highly absorbing solids and liquid samples [11].

In this work, the  $\gamma$ -Al<sub>2</sub>O<sub>3</sub> support was impregnated with different glycerol aqueous solutions: 0.5, 1.0, 2.0 and 5.0 wt% of glycerol in water. Their different spectra are shown in Fig. 7.11. The weak signals obtained in the 0.5 wt% loading test did not allow a clear peak discrimination and, therefore, those results were not included. In these experiments, after glycerol was loaded on the sample, the bulk water was removed by applying high vacuum (HV). Thereby, the interactions between glycerol and the catalyst surface but also bulk glycerol signals can be observed (see Fig. 7.11). The existence of those reactant/surface interactions is demonstrated by the changes in the glycerol  $\nu$ CH and especially in the  $\nu$ CO modes related to those of bulk pure glycerol (directly loaded on the IRE).

As the glycerol concentration increased, the spectra became more similar to the bulk glycerol. The reason for this is that not only the signals from adsorbed glycerol molecules, but also the signals from the bulk molecules, just deposited on the surface, are increasingly more perceptible [28].

The  $\nu$ CO 2° was 1112 cm<sup>-1</sup> for the  $\gamma$ -Al<sub>2</sub>O<sub>3</sub> support impregnated with 1 wt% glycerol, and shifted to lower wavenumbers as the concentration of the aqueous solutions increased. It should be noted that the more remarkable change was observed for the  $\nu$ CO 1° mode, which changed from 1040 cm<sup>-1</sup> for 1 wt% to 1028 cm<sup>-1</sup> for the bulk pure glycerol spectra, meaning a shift of 12 cm<sup>-1</sup>. It indicates that the surface interaction between the 1° OH group of glycerol is stronger than that of the 2° OH group. The  $\nu$ CH<sub>2</sub> modes suffered small changes: the  $\nu_{\text{asym}}$  CH<sub>2</sub> and  $\nu_{\text{sym}}$  CH<sub>2</sub> modes changed from 2939 and 2885 cm<sup>-1</sup> for 1 wt% of glycerol to 2934 and 2880 cm<sup>-1</sup> for the bulk pure glycerol, respectively.

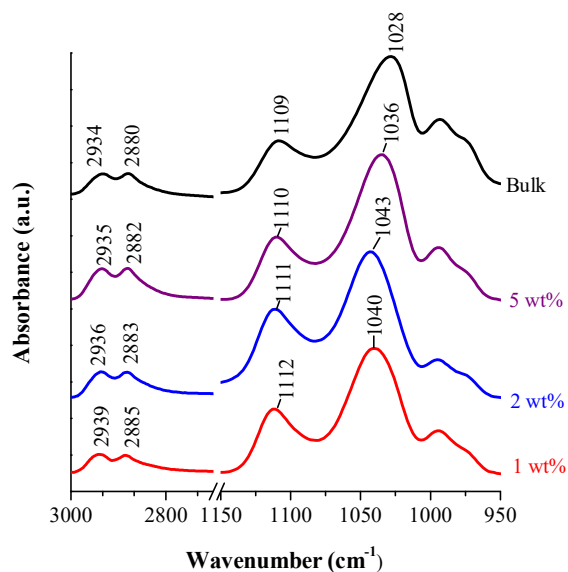


**Fig. 7.11.** ATR-IR spectra of the different glycerol loadings on  $\gamma$ -Al<sub>2</sub>O<sub>3</sub> support (1-5 wt%) after the removal of water by HV and the spectra of the bulk pure glycerol directly deposited on the ZnSe IRE.

In other similar studies carried out using transmission FTIR, when glycerol was adsorbed on the  $\gamma$ -Al<sub>2</sub>O<sub>3</sub> surface, the  $\nu$ CO modes of bulk glycerol (at 1108 and 1030 cm<sup>-1</sup>) disappeared and three new defined modes (at 1151, 1122, and 1075 cm<sup>-1</sup>) appeared in its place [28]. It means that glycerol was chemisorbed on the catalyst surface, which implies electron sharing between the adsorbate (glycerol) and the surface active sites. Thus, the electronic structure of the adsorbate changed [32].

Through the assignment of those new bands with the vibrational frequencies calculated using density functional theory (DFT) simulations, the authors proposed that glycerol readily forms a multidentate alkoxy species through its primary OH group with coordinatively unsaturated Al atoms of  $\gamma$ -Al<sub>2</sub>O<sub>3</sub>. They also suggested that the glycerol species exhibits a bridging alkoxy bond from one of its primary OH and a strong interaction with the remaining one.

In contrast, the interactions found in our study are not as strong as in the previously mentioned work. The smaller shifts indicate that the electronic structure of glycerol changed to a lesser extent and, therefore, it may only be physisorbed on the catalyst surface. The weak interactions between glycerol and  $\gamma$ -Al<sub>2</sub>O<sub>3</sub> may be mostly due to relatively weak van der Waals forces or hydrogen bonding [27]. However, it cannot be ruled out the formation of a stronger alkoxide under real reaction conditions.

The loading that produced the best balance between the signal from the adsorbed glycerol and those from the bulk glycerol was 1 wt%. Thus, this was the selected



loading to study the role of the WO<sub>x</sub> in the adsorption step of glycerol. The effect of the incorporation of Pt was not studied in the present work, since its role in the hydrogenolysis reaction is quite well-established: to activate the hydrogen molecules [33].

It is necessary to point out that the HV, which is used to remove the water from the impregnated samples, could induce or hide some interactions between glycerol and the catalyst surface. To make those interactions more visible, the spectrum of the samples with water was subtracted from the spectrum of glycerol loaded samples (denoted as WS). Then, they were compared with the spectra of the samples placed under HV. The νCO regions (1150-950 cm<sup>-1</sup>) of 1 wt% glycerol loaded on the γ-Al<sub>2</sub>O<sub>3</sub> support, as well as on the tungstated alumina (9W) are represented in Fig. 7.12.

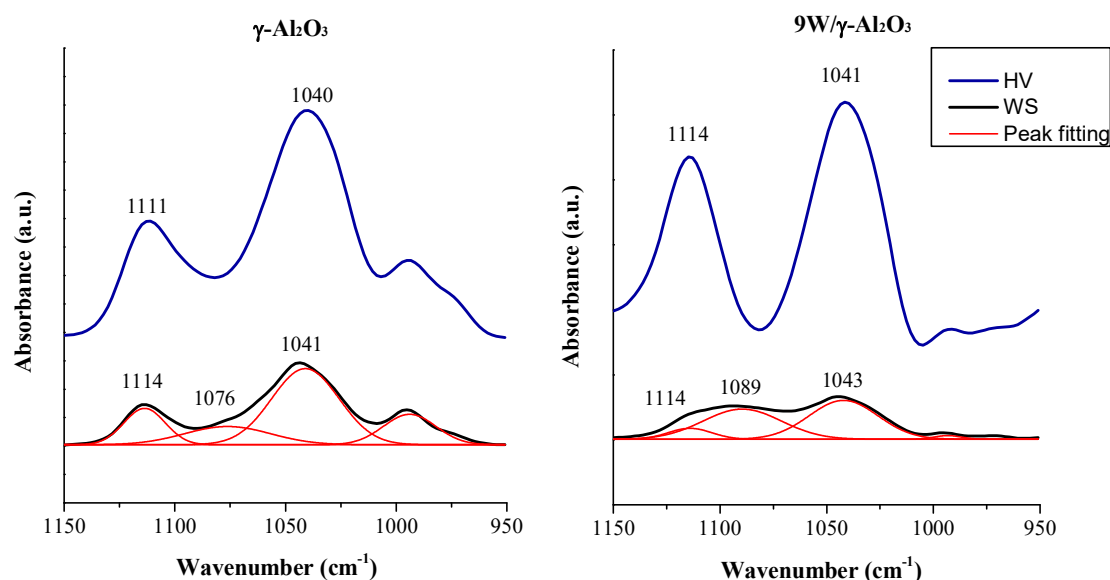


**Fig. 7.12.** Comparison of the ATR-IR spectra of 1 wt% glycerol in water loaded on γ-Al<sub>2</sub>O<sub>3</sub> and 9W/γ-Al<sub>2</sub>O<sub>3</sub> (9W), after the removal of water by high-vacuum (HV) and after the water spectrum was subtracted from the glycerol loaded sample (WS).

In general, the glycerol peaks appeared at higher wavenumbers for the WS spectra, since the HV favoured the glycerol desorption from the catalyst surface. Some peaks were also hidden after HV treatment as it is possible to see in the Fig. 7.12. Interestingly, very remarkable differences in the spectrum shapes and the band positions between the glycerol adsorption on γ-Al<sub>2</sub>O<sub>3</sub> and 9W can be observed, mainly in the WS spectra. The shift in the IR frequency is a complex matter; it could include the change in the dipole moment of the adsorbed molecule or small steric and electronic effects [24,34].

In spite that the nature of those shifts remains unclear, the very different spectra suggest, at least, a different interaction between glycerol and the catalyst surface when  $\text{WO}_x$  is incorporated on the  $\gamma\text{-Al}_2\text{O}_3$  support. However, they have something in common: the glycerol seems to be adsorbed by the terminal hydroxy group/s, since this mode suffered the highest shift related to the vibrational modes of bulk glycerol ( $\Delta\nu = 13\text{-}15\text{ cm}^{-1}$ ). The different strength of interaction is highlighted in the  $\nu\text{CO}$  mode region: the  $\nu\text{CO } 1^\circ$  band became weaker and a new broad band at  $1089\text{ cm}^{-1}$  appeared when glycerol is adsorbed on the 9W sample, whereas the  $\nu\text{CO } 2^\circ$  remained at the same position,  $1114\text{ cm}^{-1}$ . This fact suggests a stronger interaction between the primary OH groups of glycerol when  $\text{WO}_x$  is present over the  $\gamma\text{-Al}_2\text{O}_3$ .

In spite of these evidences, a more extended study should be necessary and the interactions shown by the experimental ATR-IR spectra should be validated using computational studies.

### 7.3.2 Glycerol and products competition for the same active sites

Kinetic measurements are often used to provide important information about the reaction mechanism [35]. In the present work, a preliminary kinetic study was performed in order to determine whether the main products of the glycerol hydrogenolysis compete for the same active sites of glycerol.

Based on the glycerol conversion results, shown in Fig. 7.13, it is clear that glycerol transformation was affected by the presence of all the products used as reactants. The inhibition of the glycerol conversion is due to the competition of products and glycerol for the same active sites. The PDOs, in particular, had a higher effect on the decrease in the glycerol conversion: 1,2-PDO reduced it from 11.6 % to 3.7 %, and, 1,3-PDO even to a lower value of 2.8 %, whereas 1-PO decreased the conversion to a lesser extent (to 6.7 %).

It is well known that the number of hydroxy groups has a great importance on the adsorption, since the possibilities for a molecule to be adsorbed increase with the number of those groups in the chain. It adds one more reason to confirm that 1,2-PDO was the adsorbed molecule most likely detected in the *in-situ* experiments with 15 and 30 wt% glycerol, after spectra at  $t=0$  was subtracted (see Fig. 7.9 and 7.10), instead of any other monoalcohol like 1-PO.

However, according to the work of Bronswijk et al. [36] the adsorption affinities of polyols increased with the increasing number of vicinal hydroxy groups present in

the chain. This is not the case of the current study since the adsorption seems to be stronger for 1,3-PDO than for 1,2-PDO. According to the *ex-situ* ATR-IR findings (section 7.3.2), glycerol was adsorbed by the terminal hydroxy group/s. It could be thought, therefore, that the PDOs adsorption occurred preferentially by the same groups. The stronger adsorption of 1,3-PDO, which exhibit two terminal hydroxy groups, than 1,2-PDO, of only one, is in good agreement with this adsorption trend.

In view of this result, it is not clear why the more strongly adsorbed 1,3-PDO was not detected in the *in-situ* ATR-IR measurements, unlike the adsorbed 1,2-PDO. The reason could lie in the fact that 1,3-PDO and glycerol exhibit bands at similar frequencies in the  $\nu$ CH region [20] which cancel out each other, since those attributed to the product formation were positive and those of reactant consumption negative, after spectra at  $t=0$  was subtracted (section 7.3.1.1). Moreover, the broad negative bands of glycerol in the  $\nu$ CO region made the differentiation of any peak in this region impossible.

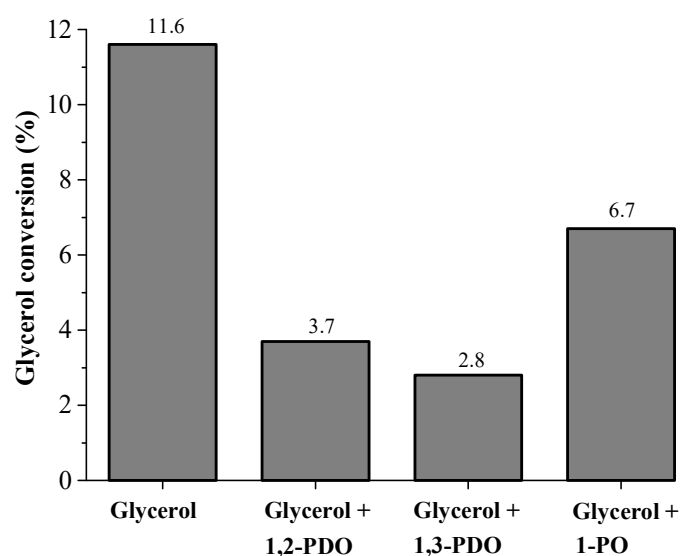


**Fig. 7.13.** Glycerol conversion values achieved in the hydrogenolysis reaction using different reactants (at 200 °C, 45 bar H<sub>2</sub> and 2 h reaction time). Concentration of glycerol in water = 5 wt. Glycerol:product molar ratio 1:1.

Once it was established that the main hydrogenolysis products compete for the same adsorption sites of glycerol, a more detailed kinetic study, using the Langmuir-Hinselwood kinetics to obtain the adsorption equilibrium constants in the rate equation, should be necessary in order to gain more knowledge about the reaction mechanisms.

### 7.3.3 Effect of the reacting atmosphere and hydrogen availability

The hydrogenolysis of glycerol, 1,2-PDO and 1,3-PDO were carried out over 9Pt8W catalyst under both H<sub>2</sub> and N<sub>2</sub> atmospheres. The activity test results are shown in Table 7.1 and 7.2, respectively. The principal objective of this study is to provide more information for the overall glycerol hydrogenolysis reaction.

In the literature, the most frequently proposed mechanism is the dehydration-hydrogenation route, in which glycerol is first dehydrated to acetol or 3-hydroxypropanal (3-HPA) and further hydrogenated to 1,2-PDO and 1,3-PDO, respectively [37]. Trace amounts of acetol were found in the glycerol hydrogenolysis under H<sub>2</sub> atmosphere, whereas the presence of 3-HPA was not detected. The acetol formation is thermodynamically more favoured than that of 3-HPA [38,39] and, therefore, 1,2-PDO is usually the major product among PDOs. However, in this case, the selectivity towards 1,3-PDO (38.5 %) was much higher than that towards 1,2-PDO (9.0 %). This fact could arise from two factors: (i) a different reaction mechanism was involved or, (ii) 1,2-PDO was more reactive than 1,3-PDO.

**Table 7.1.** Activity test results of the hydrogenolysis of glycerol and PDOs under H<sub>2</sub> atmosphere at 220 °C, 45 bar and 16 h of reaction time.

Reactant	Conv. (%)	Selectivity towards liquid products (%)									
		1,3-PDO	1,2-PDO	1-PO	2-PO	Acetol	Acetone	Propanal	Prop. acid	Ethanol	EG
Glycerol	80.3	38.5	9.0	36.9	7.2	*	3.1	0.0	*	3.9	0.0
1,3-PDO	23.9	-	0.0	80.8	0.0	0.0	0.0	0.0	2.3	7.9	0.0
1,2-PDO	26.6	0.0	-	70.8	15.5	0.0	5.1	0.0	0.0	0.0	0.0

\* Trace amounts

**Table 7.2.** Activity test results of the hydrogenolysis of glycerol and PDOs under N<sub>2</sub> atmosphere at 220 °C, 45 bar and 16 h of reaction time.

Reactant	Conv. (%)	Selectivity towards liquid products (%)									
		1,3-PDO	1,2-PDO	1-PO	2-PO	Acetol	Acetone	Propanal	Prop. acid	Ethanol	EG
Glycerol	22.2	0.0	57.3	7.3	0.0	21.4	0.0	0.0	0.0	5.9	5.0
1,3-PDO	46.4	-	0.0	42.2	0.0	0.0	0.0	2.1	4.2	6.8	0.0
1,2-PDO	13.8	0.0	-	29.7	0.0	22.7	6.2	0.0	0.0	17.8	0.0

However, under H<sub>2</sub> pressure both PDOs showed similar reactivity (see Table 7.1) indicating a higher formation of 1,3-PDO during the reaction. It is worth noting that the over-hydrogenolysis to 1-PO was the main reaction involved in the PDOs

conversion. This explains quite well why 1-PO was formed in high quantities when glycerol is used as reactant (36.9 % selectivity).

2-PO and acetone products were found when glycerol and 1,2-PDO were used as reactants. It was suggested that acetone is formed through the dehydration of 1,2-PDO, and the further hydrogenation lead to 2-PO formation. The reversibility of the hydrogenation of acetone to 2-PO [40] could explain why acetone was always present in the reaction medium (Eq. 7.1).



During the hydrogenolysis of glycerol and 1,3-PDO, small amounts of propionic acid were detected as well. This compound may be formed through Tishchenko or Cannizzaro type disproportionation, in which two molecules of aldehyde react to produce a primary alcohol and a carboxylic acid. It could be the case of the conversion of propanal, the dehydration product of both PDOs, to 1-PO and propionic acid, which was also proposed in previous works [41]. However, propanal was mainly hydrogenated to 1-PO.

The same experiments were performed under N<sub>2</sub> pressure in order to investigate the effect of the reacting atmosphere and the hydrogen availability. For an easier interpretation of the results, the products detected were divided in three groups:

- Hydrogenated products: PDOs, 1-PO, 2-PO, propane
- Dehydrated products: acetol, propanal, acetone, propionic acid
- Cracking products (C<3): EG, ethanol, ethane, CH<sub>4</sub>, CO<sub>2</sub>

The conversion value of glycerol under N<sub>2</sub> atmosphere (22.2 %) was extremely lower than under H<sub>2</sub> (80.3 %). This result seems to indicate that hydrogen plays an important role in the first step of the glycerol conversion mechanism. The lower availability of hydrogen affected the product distribution: the dehydrated products hugely increased under N<sub>2</sub> atmosphere as it can be seen in the Fig. 7.14. Among the dehydrated products, acetol was obtained with the highest selectivity (21 %). Nevertheless, the reversible hydrogenation of acetol to 1,2-PDO occurred to a large extent, being this the major product of the reaction (57.3 % selectivity). Moreover, other hydrogenated products, such as 1-PO, EG and ethanol, were also obtained but to a lesser extent. Since those reactions consumed hydrogen and it was not externally provided, it

should be *in-situ* generated by APR reactions of glycerol [42,43]. The APR of glycerol is a well-known process; the reaction stoichiometry is shown in the Eq. 7.2.



However, neither 1,3-PDO nor 2-PO (or acetone) products were detected in the hydrogenolysis of glycerol under inert  $\text{N}_2$ . This is an interesting fact that reveals that high availability of hydrogen is necessary for the glycerol conversion into those products.

The APR reactions have a great importance in the hydrogenolysis of 1,3-PDO and, surprisingly, its conversion was higher than under  $\text{H}_2$  (46.4 % under  $\text{N}_2$  vs 23.9 % under  $\text{H}_2$ ). The gas formation represented the 44.8 % of the total products formed, which was mainly composed by propane (3.1 %), ethane (23.1 %),  $\text{CO}_2$  (1.2 %) and  $\text{CH}_4$  (17.4 %). The excess of hydrogen generated in the reactions promoted the C-C hydrogenolysis of 1-PO to ethanol and  $\text{CH}_4$ , and further to ethane. The  $\text{CO}_2$  also reacted with hydrogen to yield  $\text{CH}_4$  [44]. This explains the high selectivity values towards cracking products,  $\text{CH}_4$  and ethane. In the liquid fraction, 1-PO was the major product (42.2 %). In addition, propanal and propionic acid were detected in the reaction products, which verifies the previously discussed formation of 1-PO and propionic acid.

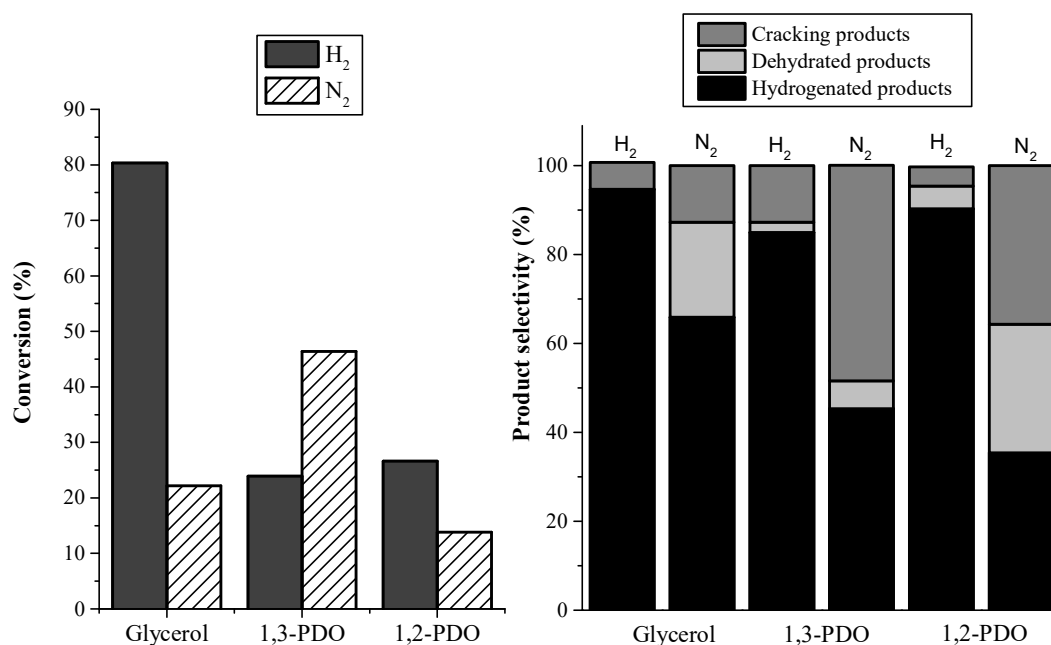


**Fig. 7.14.** Glycerol conversion (left) and product distribution (right), under  $\text{H}_2$  and  $\text{N}_2$  atmospheres (220 °C, 45 bar of  $\text{H}_2$  or  $\text{N}_2$  and 16 h of reaction time).

In contrast to 1,3-PDO, the conversion of 1,2-PDO under N<sub>2</sub> was lower than that obtained under H<sub>2</sub>. The main liquid products were 1-PO (29.7 %), acetol (22.7 %) and ethanol (17.8 %). Surprisingly, 2-PO was not among the reaction products, acetone was detected instead. It suggests, on the one hand, that higher amounts of hydrogen molecules must be provided in order to hydrogenated acetone into 2-PO, or that the chemical equilibrium was displaced to the acetone formation, under N<sub>2</sub> atmosphere. Again, the gases represented a high percentage of the total products, 23.6 %.

## 7.4 Overall reaction mechanism

The necessity of Brønsted acidity for the production of 1,3-PDO was widely proved in the literature [45–47] as well as in our previous works. We obtained the highest selectivity towards 1,3-PDO at the tungstate surface density showing the highest B/L ratio (at 2.4 W at. nm<sup>-2</sup>) [19]. However, there are some important evidences suggesting that the amount of Pt and the interactions between Pt and WO<sub>x</sub> active sites also affect the formation of 1,3-PDO. The characterization and activity test results from that study allowed us proposing a reaction mechanism. The new evidences found in the present research led to a better understanding of the reaction pathways and some of their fundamental aspects.

The new proposed mechanism (see Fig. 7.15) differs from the widely suggested dehydration-hydrogenation mechanism since it cannot explain the high selectivities towards 1,3-PDO (see Table 7.1). We propose that the WO<sub>x</sub> acid sites are involved in the hydrogenolysis of glycerol to 1,3-PDO by anchoring the primary hydroxy groups of glycerol according to our finding through *ex-situ* ATR-IR (section 7.3.1.2). A proton coming from a Brønsted acid site (provided by polytungstate species) protonates the internal hydroxy group of glycerol which possesses the highest proton affinity [48]. After dehydration, a secondary carbocation is formed.

The carbocation is then attacked by a hydride specie coming from the heterolytic activation of molecular H<sub>2</sub> on the Pt active sites [45,49]. At this point, the stabilisation and the fast hydrogenation of the secondary carbocation are of vital importance.

The polytungstate species present on the catalyst take part in the carbocation stabilisation by delocalizing the negative charge required. The stronger adsorption over those species (rather than on the  $\gamma$ -Al<sub>2</sub>O<sub>3</sub> support) may also be involved in the secondary carbocation stabilisation avoiding the releasing of the alkoxide before the hydride

attack. Furthermore, according to the results under  $H_2$  and  $N_2$  reacting atmospheres (section 7.3.3), the high availability of  $H_2$  and, therefore, hydride ions is indispensable in order to obtain 1,3-PDO. After the hydride attack, the hydrolysis of the alkoxide yields the 1,3-PDO compound.

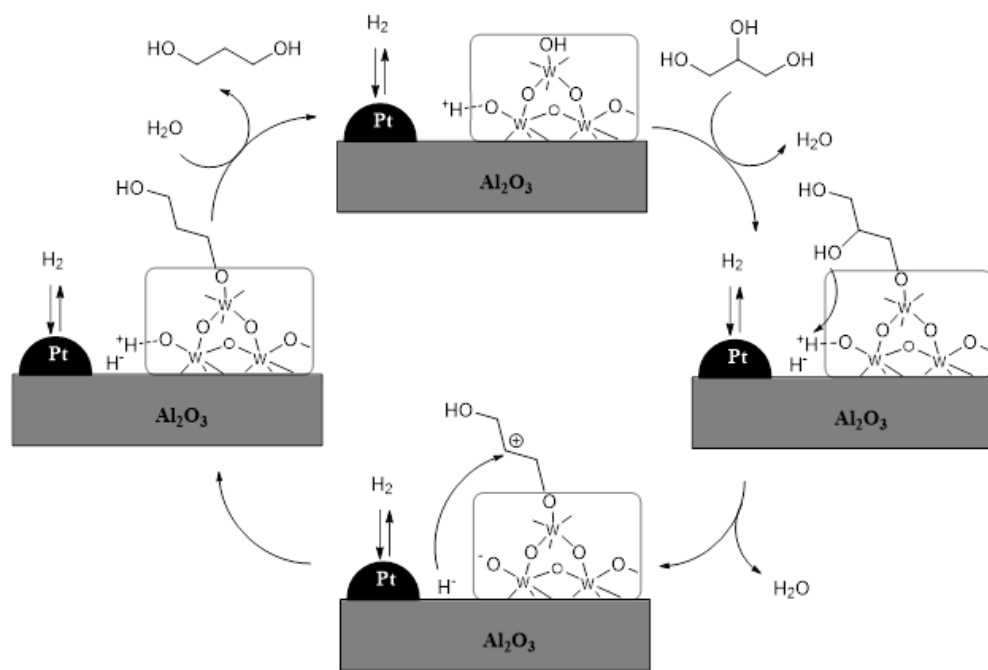


Fig. 7.15. Reaction mechanism proposed for the glycerol hydrogenolysis to 1,3-PDO.

According to our activity test results, a different reaction mechanism for the formation of 1,2-PDO should be involved, in which the Lewis acid sites, mainly of the  $\gamma$ -Al<sub>2</sub>O<sub>3</sub>, are implicated (see Fig. 7.16). The interaction of glycerol with Lewis acid sites is affected by steric constraints [50], in contrast to the glycerol protonation discussed above. According to this, the terminal hydroxy group of glycerol is more likely to interact with the Lewis acid sites. The migration of the proton of the secondary carbon to the oxygen of the Lewis site could release 2,3-dihydroxypropene which further suffer a keto-enol tautomerisation to yield acetol. The hydrogenation of acetol released the 1,2-PDO. This mechanism also explains the preferential formation of 1-PO rather than 2-PO from 1,2-PDO.



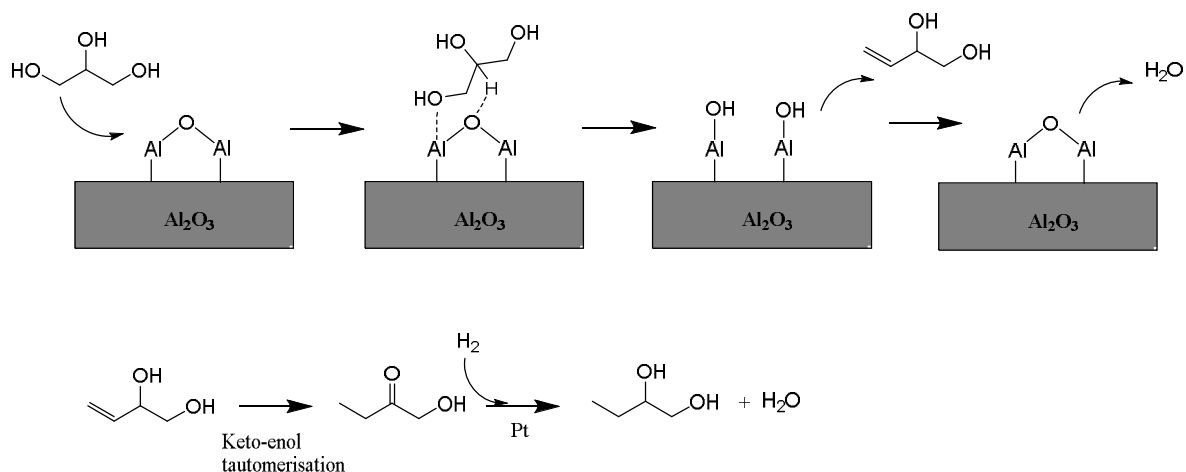


Fig. 7. 16. Reaction mechanism proposed for the glycerol hydrogenolysis to 1,2-PDO.

## 7.5 Conclusions

The *in-situ* ATR-IR spectroscopy has shown to be a powerful tool of catalyst characterisation since it could register the changes that a catalytic surface suffers during the reaction. It also allows characterising adsorbed molecules on heterogeneous catalysts in liquids with very strong absorbance, such as water, for which other conventional IR spectroscopies are not suitable. Although the measurements in water are still very hard, as this work highlighted, it was possible to measure in real-time the changes in adsorbed molecules/catalyst surface interactions as the reactant was consumed and the products were formed. Unfortunately, the similar nature of the majority of the products obtained in the glycerol hydrogenolysis, added an extra difficulty to this work: the product identification was very hard since all of them showed absorption bands at similar frequencies.

The application of the ATR-IR technique to the adsorption of glycerol aqueous solutions over  $\gamma$ -Al<sub>2</sub>O<sub>3</sub> and 9W provided mechanistic information about the initial adsorption step. Despite the adsorption seems to happen through the terminal hydroxy groups of glycerol over both catalysts, the adsorption strength seems to be stronger over the catalyst with WO<sub>x</sub>. This could contribute to stabilise the secondary carbocation formed during the hydrogenolysis of glycerol, before it is hydrogenated to 1,3-PDO.

The necessity of a high hydrogen availability in the medium was evident in the experiments under N<sub>2</sub> atmosphere, in which hydrogen was not provided externally. The high availability of Brønsted acid sites and the fast hydrogenation of the secondary carbocation seems to be the key parameters in order to boost the formation of 1,3-PDO.

## References

- [1] J.-M. Andanson, A. Baiker, Exploring catalytic solid/liquid interfaces by in situ attenuated total reflection infrared spectroscopy, *Chem. Soc. Rev.* 39 (2010) 4571.
- [2] T. Bürgi, A. Baiker, In Situ Infrared Spectroscopy of Catalytic Solid–Liquid Interfaces Using Phase-Sensitive Detection: Enantioselective Hydrogenation of a Pyrone over Pd/TiO<sub>2</sub>, *J. Phys. Chem. B.* 106 (2002) 10649–10658.
- [3] U. Hartfelder, C. Kartusch, J. Sá, J.A. van Bokhoven, In situ infrared spectroscopy on the gas phase hydrogenation of nitrobenzene, *Catal. Commun.* 27 (2012) 83–87.
- [4] J. Ryczkowski, IR spectroscopy in catalysis, *Catal. Today.* 68 (2001) 263–381.
- [5] B. Stuart, Infrared Spectroscopy, in: Kirk-Othmer (Ed.), *Kirk-Othmer Encycl. Chem. Technol.*, 5th ed., Wiley, 2000: pp. 1–20.
- [6] I. Ortiz-Hernández, C.T. Williams, In Situ Investigation of Solid - Liquid Catalytic Interfaces by Attenuated Total Reflection Infrared Spectroscopy, *Langmuir.* 19 (2003) 2956–2962.
- [7] C. Morterra, C. Emanuel, G. Cerrato, G. Magnacca, Infrared Study of some Surface Properties of Boehmite ( $\gamma$ -Al<sub>2</sub>O<sub>3</sub>), *J. Chem. Soc. Faraday Trans.* 88 (1992) 339–348.
- [8] M.A. Vuurman, D.J. Stufkens, A. Oskam, G. Deo, I.E. Wachs, Combined Raman and IR study of MO<sub>x</sub>-V<sub>2</sub>O<sub>5</sub>/Al<sub>2</sub>O<sub>3</sub> (MO<sub>x</sub> = MoO<sub>3</sub>, WO<sub>3</sub>, NiO, CoO) catalysts under dehydrated conditions, *J. Chem. Soc. Faraday Trans.* 92 (1996) 3259.
- [9] B.L. Mojet, S.D. Ebbesen, L. Lefferts, Light at the interface: the potential of attenuated total reflection infrared spectroscopy for understanding heterogeneous catalysis in water, *Chem. Soc. Rev.* 39 (2010) 4643.
- [10] G. Steiner, Section 5: Measurement Techniques, in: G. Gauglitz, D.S. Moore (Eds.), *Handb. Spectrosc.*, 2nd ed., Wiley-VCH, 2014: pp. 71–94.
- [11] V. Sablinskas, G. Steiner, M. Hof, R. Machán, Section 6: Applications, in: G. Gauglitz, D.S. Moore (Eds.), *Handb. Spectrosc.*, 2nd ed., Wiley-VCH, 2014: pp. 95–174.
- [12] D. Ferri, T. Bürgi, A. Baiker, Pt and Pt/Al<sub>2</sub>O<sub>3</sub> Thin Films for Investigation of Catalytic Solid–Liquid Interfaces by ATR-IR Spectroscopy: CO Adsorption, H<sub>2</sub>-Induced Reconstruction and Surface-Enhanced Absorption, *J. Phys. Chem. B.* 105 (2001) 3187–3195.
- [13] P.R. Griffiths, J.A. de Haseth, The handbook of infrared and Raman characteristic frequencies of organic molecules, in: D. Lin-Vien, N.B. Colthup, W.G. Fateley, J.G. Grasselli (Eds.), 2nd ed., John Wiley & Sons, 1991.
- [14] C. Keresszegi, T. Bürgi, T. Mallat, A. Baiker, On the role of oxygen in the liquid-phase aerobic oxidation of alcohols on palladium, *J. Catal.* 211 (2002) 244–251.
- [15] R. He, R.R. Davda, J. a Dumesic, In Situ ATR-IR Spectroscopic and Reaction Kinetics Studies of Water–Gas Shift and Methanol Reforming on Pt / Al<sub>2</sub>O<sub>3</sub> Catalysts in Vapor and Liquid Phases, *J. Phys. Chem. B.* (2005) 2810–2820.
- [16] S.D. Ebbesen, B.L. Mojet, L. Lefferts, In situ ATR-IR study of CO adsorption and oxidation over Pt/Al<sub>2</sub>O<sub>3</sub> in gas and aqueous phase: Promotion effects by water and pH, *J. Catal.* 246 (2007) 66–73.

- [17] S.D. Ebbesen, B.L. Mojet, L. Lefferts, In situ ATR-IR study of nitrite hydrogenation over Pd/Al<sub>2</sub>O<sub>3</sub>, *J. Catal.* 256 (2008) 15–23.
- [18] D.A. Boga, F. Liu, P.C. a. Bruijninx, B.M. Weckhuysen, Aqueous-phase reforming of crude glycerol: effect of impurities on hydrogen production, *Catal. Sci. Technol.* (2015).
- [19] S. García-Fernández, I. Gandarias, J. Requies, M.B. Güemez, S. Bennici, A. Auroux, et al., New approaches to the Pt/WO<sub>x</sub>/Al<sub>2</sub>O<sub>3</sub> catalytic system behavior for the selective glycerol hydrogenolysis to 1,3-propanediol, *J. Catal.* 323 (2015) 65–75.
- [20] NIST, Standard Reference Database, (n.d.). <http://webbook.nist.gov/chemistry/name-ser.html>.
- [21] K. Koichumanova, K.B. Sai Sankar Gupta, L. Lefferts, B.L. Mojet, K. Seshan, An in situ ATR-IR spectroscopy study of aluminas under aqueous phase reforming conditions, *Phys. Chem. Chem. Phys.* 17 (2015) 23795–23804.
- [22] D. Ferri, T. Bürgi, A. Baiker, Probing boundary sites on a Pt/Al<sub>2</sub>O<sub>3</sub> model catalyst by CO<sub>2</sub> hydrogenation and in situ ATR-IR spectroscopy of catalytic solid–liquid interfaces, *Phys. Chem. Chem. Phys.* 4 (2002) 2667–2672.
- [23] I. Ortiz-Hernandez, D. Jason Owens, M.R. Strunk, C.T. Williams, Multivariate analysis of ATR-IR spectroscopic data: Applications to the solid-liquid catalytic interface, *Langmuir.* 22 (2006) 2629–2639.
- [24] B. Stuart, Infrared Spectroscopy, in: *Kirk-Othmer Encycl. Chem. Technol.*, John Wiley & Sons, Inc., 2000.
- [25] M.R. Silverstein, F.X. Webster, D.J. Kiemle, *Spectrometric Identification of Organic Compounds*, 7th ed., Wiley, New York, 2005.
- [26] A. Cho, H. Kim, A. Iino, A. Takagaki, S. Ted Oyama, Kinetic and FTIR studies of 2-methyltetrahydrofuran hydrodeoxygenation on Ni<sub>2</sub>P/SiO<sub>2</sub>, *J. Catal.* 318 (2014) 151–161.
- [27] J.R. Copeland, G.S. Foo, L. a. Harrison, C. Sievers, In situ ATR-IR study on aqueous phase reforming reactions of glycerol over a Pt/gamma-Al<sub>2</sub>O<sub>3</sub> catalyst, *Catal. Today.* 205 (2013) 49–59.
- [28] J.R. Copeland, X. Shi, D.S. Sholl, C. Sievers, Surface Interactions of C<sub>2</sub> and C<sub>3</sub> Polyols with  $\gamma$ -Al<sub>2</sub>O<sub>3</sub> and the Role of Coadsorbed Water, *Langmuir.* 29 (2013) 581–593.
- [29] M. Dömök, M. Tóth, J. Raskó, A. Erdohelyi, Adsorption and reactions of ethanol and ethanol-water mixture on alumina-supported Pt catalysts, *Appl. Catal. B Environ.* 69 (2007) 262–272.
- [30] M.I. Zaki, M. a. Hasan, L. Pasupulety, In Situ FTIR Spectroscopic Study of 2-Propanol Adsorptive and Catalytic Interactions on Metal-Modified Aluminas, *Langmuir.* 17 (2001) 4025–4034.
- [31] A. V Deo, I.G. Dalla Lana, Infrared study of the adsorption and mechanism of surface reactions of 1-propanol on  $\gamma$ -alumina and  $\gamma$ -alumina doped with sodium hydroxide and chromium oxide, *J. Phys. Chem.* 73 (1969) 716–723.
- [32] R.I. Masel, Principles of adsorption and reaction on solid surfaces, in: John Wiley & Sons, Illinois, 1996: pp. 108–234.
- [33] M. Y. Nakagawa, T. and K. Tomishige, Catalytic materials for the hydrogenolysis of glycerol to 1,3-propanediol, *J. Mater. Chem. A.* 2 (2014) 6688–6702.

- [34] S.D. Ebbesen, B.L. Mojet, L. Lefferts, CO adsorption and oxidation at the catalyst-water interface: an investigation by attenuated total reflection infrared spectroscopy., *Langmuir*. 22 (2006) 1079–85.
- [35] E.S. Vasiliadou, A.A. Lemonidou, Kinetic study of liquid-phase glycerol hydrogenolysis over Cu/SiO<sub>2</sub> catalyst, *Chem. Eng. J.* 231 (2013) 103–112.
- [36] W. Van Bronswijk, H.R. Watling, Z. Yu, A study of the adsorption of acyclic polyols on hydrated alumina, *Colloids Surfaces A Physicochem. Eng. Asp.* 157 (1999) 85–94.
- [37] M.A. Dasari, P.P. Kiatsimkul, W.R. Sutterlin, G.J. Suppes, Low-pressure hydrogenolysis of glycerol to propylene glycol, *Appl. Catal. A Gen.* 281 (2005) 225–231.
- [38] J. TenDam, K. Djanashvili, F. Kapteijn, U. Hanefeld, Pt/Al<sub>2</sub>O<sub>3</sub> Catalyzed 1,3-Propanediol Formation from Glycerol using Tungsten Additives, *ChemCatChem*. 5 (2013) 497–505.
- [39] L. Huang, Y. Zhu, H. Zheng, G. Ding, Y. Li, Direct conversion of glycerol into 1,3-propanediol over Cu-H<sub>4</sub>SiW<sub>12</sub>O<sub>40</sub>/SiO<sub>2</sub> in vapor phase, *Catal. Letters*. 131 (2009) 312–320.
- [40] I. Gandarias, P.L. Arias, J. Requies, M.B. Güemez, J.L.G. Fierro, Hydrogenolysis of glycerol to propanediols over a Pt/ASA catalyst: The role of acid and metal sites on product selectivity and the reaction mechanism, *Appl. Catal. B Environ.* 97 (2010) 248–256.
- [41] A. Wawrzetz, B. Peng, A. Hrabar, A. Jentys, a. a. Lemonidou, J. a. Lercher, Towards understanding the bifunctional hydrodeoxygenation and aqueous phase reforming of glycerol, *J. Catal.* 269 (2010) 411–420.
- [42] A.O. Menezes, M.T. Rodrigues, A. Zimmaro, L.E.P. Borges, M.A. Fraga, Production of renewable hydrogen from aqueous-phase reforming of glycerol over Pt catalysts supported on different oxides, *Renew. Energy*. 36 (2011) 595–599.
- [43] D.L. King, L. Zhang, G. Xia, A.M. Karim, D.J. Heldebrant, X. Wang, et al., Aqueous phase reforming of glycerol for hydrogen production over Pt-Re supported on carbon, *Appl. Catal. B Environ.* 99 (2010) 206–213.
- [44] D. Roy, B. Subramaniam, R. V. Chaudhari, Aqueous phase hydrogenolysis of glycerol to 1,2-propanediol without external hydrogen addition, *Catal. Today*. 156 (2010) 31–37.
- [45] L.-Z. Qin, M.-J. Song, C.-L. Chen, Aqueous-phase deoxygenation of glycerol to 1,3-propanediol over Pt/WO<sub>3</sub>/ZrO<sub>2</sub> catalysts in a fixed-bed reactor, *Green Chem.* 12 (2010) 1466.
- [46] J. Oh, S. Dash, H. Lee, Selective conversion of glycerol to 1,3-propanediol using Pt-sulfated zirconia, *Green Chem.* 13 (2011) 2004.
- [47] S. Zhu, Y. Zhu, S. Hao, L. Chen, B. Zhang, Y. Li, Aqueous-phase hydrogenolysis of glycerol to 1,3-propanediol over Pt-H<sub>4</sub>SiW<sub>12</sub>O<sub>40</sub>/SiO<sub>2</sub>, *Catal. Letters*. 142 (2012) 267–274.
- [48] M.R. Nimlos, S.J. Blanksby, X. Qian, M.E. Himmel, D.K. Johnson, Mechanisms of Glycerol Dehydration, *J. Phys. Chem. A*. 110 (2006) 6145–6156.
- [49] S. Triwahyono, T. Yamada, H. Hattori, Kinetic study of hydrogen adsorption on Pt/WO<sub>3</sub>-ZrO<sub>2</sub> and WO<sub>3</sub>-ZrO<sub>2</sub>, *Appl. Catal. A Gen.* 250 (2003) 65–73.
- [50] A. Alhanash, E.F. Kozhevnikova, I. V. Kozhevnikov, Gas-phase dehydration of glycerol to acrolein catalysed by caesium heteropoly salt, *Appl. Catal. A Gen.* 378 (2010) 11–18.





## **CHAPTER 8.**

### **Conclusions and future work**









The current PhD thesis has focussed on a deep study of the glycerol hydrogenolysis over a novel catalytic system: the combination of the highly reducible Pt metal with the oxophilic W metal (in form of  $\text{WO}_x$ ), supported on alumina. The accomplishment of each of the parts of this thesis has allowed approaching to the main objective: the development of advanced catalytic systems for the selective aqueous phase C–O bond hydrogenolysis reactions. Although glycerol hydrogenolysis was chosen as the model reaction, all the knowledge developed along the research could be of great interest for its use in the valorisation of the more complicated biomass-derived polyols.

In this Chapter 8 the most relevant conclusions achieved in each of the Chapters are summarized, and some interesting ideas for future research are suggested.

**The role of Pt and  $\text{WO}_x$  active phases of the bimetallic Pt/ $\text{WO}_x$ / $\text{Al}_2\text{O}_3$  catalysts:**

This work proved that the bimetallic Pt/ $\text{WO}_x$ / $\text{Al}_2\text{O}_3$  catalytic system was highly efficient for the selective C–O hydrogenolysis of glycerol to 1,3-propanediol (1,3-PDO), and helped in the understanding of fundamental parameters of both, the catalytic system and the reaction. These are the main conclusions:

1. The incorporation of  $\text{WO}_x$  enhanced the total acidity of the  $\gamma\text{-Al}_2\text{O}_3$  based catalysts, whereas Pt metal active sites were not acidic.
2. The tungsten surface density ( $\rho_w$ ) was found to be a crucial parameter on the catalytic behaviour, as it controlled the type of  $\text{WO}_x$  species deposited on the catalyst surface, mainly: monotungstates, polytungstates and  $\text{WO}_3$  crystalline nanoparticles ( $\text{WO}_3$  NPs). The ratio of Brönsted to Lewis acid sites (B/L) increased with the  $\rho_w$  due to the polytungstate formation. These species are the unique able to delocalize the negative charge required for the formation of Brönsted acid sites. The B/L ratio increased with increasing  $\rho_w$ , until the emergence of  $\text{WO}_3$  NPs.
3. The selectivity towards 1,3-PDO depended on the  $\rho_w$ : the maximum yield to 1,3-PDO was achieved with the highest content of polytungstate species (2.4 W at.  $\text{nm}^{-2}$ ) but before the appearance of  $\text{WO}_3$  NPs. The selective formation of 1,3-PDO is, therefore, related to the presence of highly dispersed, and accessible to reactants, polytungstate species.

4. The synergy between the acid sites of  $\text{WO}_x$  and the metallic ones of Pt played a key role in the reaction. A larger interaction between Pt and  $\text{WO}_x$  sites, or a closer proximity between them, was suggested to be responsible of the greatly enhancement of glycerol conversion and 1,3-PDO selectivity, at high Pt contents.

**Influence of the support of bimetallic Pt- $\text{WO}_x$  catalyst on glycerol hydrogenolysis:**

The results of this work allow a better understanding of the importance of some of the parameters involved in the glycerol hydrogenolysis to 1,3-PDO. Remarkable yields to 1,3-PDO were also achieved:

5. The pseudo-boehmite support (pseudo  $\gamma\text{-AlO(OH)}$ ) presented a high concentration of hydroxy groups on its surface as compared to  $\gamma\text{-Al}_2\text{O}_3$ , which allowed a higher  $\rho_w$  without the emergence of the undesired  $\text{WO}_3$  NPs. These results indicated that the hydroxy groups are the preferential anchoring sites for the  $\text{WO}_x$  species.
6. It was unequivocally demonstrated that the  $\rho_w$ , and not the W loading, was the parameter which controlled the formation of polytungstates, which are directly related with the Brønsted acid sites generation required for the selective 1,3-PDO formation.
7. A balance between the acid and metal sites was found necessary in order to enhance the Pt- $\text{WO}_x$  interactions or the close proximity between these active sites. In this regard, Pt dispersion plays a key role.
8. The best results were achieved with the 9Pt/8W/ $\gamma\text{-Al}_2\text{O}_3$  (commercial support) catalyst. It showed a considerably high yield to 1,3-PDO of 35.0 % (in 24 h at 200 °C and 45 bar of  $\text{H}_2$ ).

**Mechanistic study of the glycerol hydrogenolysis over Pt/ $\text{WO}_x$ / $\text{Al}_2\text{O}_3$  catalysts:**

Through the use of powerful characterisation tools, like attenuated total reflection infrared (ATR-IR) spectroscopy, together with the knowledge acquired from preliminary kinetic studies and from the experiments under  $\text{N}_2$  atmosphere, a novel reaction mechanism for the glycerol hydrogenolysis to 1,3-PDO was proposed. These are the findings which guided to the proposal of the mechanism:

9. The adsorption of glycerol on the active sites of the catalyst seemed to take place by the terminal hydroxy group/s of glycerol regardless the presence of  $\text{WO}_x$ . However, the stronger adsorption strength over the catalyst with  $\text{WO}_x$  was proposed to contribute in the stabilization of the secondary carbocation formed during the glycerol hydrogenolysis.
10. In the experiments carried out under  $\text{N}_2$  atmosphere, the availability of hydrogen was quite limited and only 1,2-PDO, among both PDOs, was obtained. The high availability of hydrogen in the medium was, therefore, found necessary in order to lead to the 1,3-PDO formation. Therefore, the fast hydrogenation of the secondary carbocation formed after the adsorption of glycerol seems to be a key step in the selective production of 1,3-PDO.

In a near future, the results of this work could be improved by increasing the hydrogen availability. One of the strategies carried out would consist in the use of hydrogen donors, such as 2-propanol which have already proved to be highly effective as a hydrogen source for the glycerol hydrogenolysis process to 1,2-PDO with different catalytic systems (based on Ni-Cu/ $\text{Al}_2\text{O}_3$ ).

Moreover, all the knowledge acquired in the glycerol hydrogenolysis over Pt/ $\text{WO}_x$ / $\text{Al}_2\text{O}_3$  could be applied in the hydrogenolysis of biomass-derived polyols structurally analogous to glycerol, such as sorbitol and xylitol, greatly increasing the diversity of the biorefinery. Moreover, obtaining 1,3-PDO from these building blocks, which have not been obtained yet, could make the process greatly interesting.





## APPENDIX: List of acronyms

$(I_W/I_{Al})_{XPS}$	Ratio of the W4f and Al2p photoelectrons
$(W/Al)_{bulk}$	Bulk W/Al atomic ratio
1,2-PDO	1,2-propanediol
1,2-PeD	1,2-pentanediol
1,3-PDO	1,3-propanediol
1,5-PeD	1,5-pentanediol
1-PO	1-propanol
2-MF	2-methylfuran
2-MTHF	2-methyltetrahydrofuran
2-PO	2-propanol
3-HPA	3-hydroxypropanal
A15	Amberlyst 15
AIP	Aluminum isopropoxide, $Al[OCH(CH_3)_2]_3$
$Al_2O_3$	Alumina
$Al^{com}$	Commercial $\gamma-Al_2O_3$
$AlO(OH)$	Boehmite
$Al^{SG}$	$\gamma-Al_2O_3$ prepared by SG
$Al^{SG'}$	$\gamma-AlO(OH)$ prepared by SG
APR	Aqueous phase reforming
ASA	Amorphous silico-alumina
ASA	Amorphous silico-alumina
ATR-IR	Attenuated total reflection infrared
B/L	Brönsted/Lewis ratio
BET	Brunauer-Emmett-Teller
BJH	Barrett–Joyner–Halenda
CsTPA	Cesium salt of 12-tungstophosphoric acid
CTH	Catalytic transfer hydrogenation
$Cu_2Cr_2O_5$	Copper chromite
CVI	Chemical vapour impregnation
DFT	Density functional theory



DMI	1,3-dimethyl-2-imidazolidinone
DMO	Dimethyl oxalate
DOE	Department of Energy
EDS	Energy-dispersive X-ray spectroscopy
EG	Ethylene glycol
EIA	United States Energy Information Agency
EXAFS	Extended X-Ray Absorption Fine Structure
FID	Flame ionization detector
FTIR	Fourier transform infrared
GC	Gas chromatograph
GHG	Greenhouse-gases
H <sub>2</sub> -TPR	Temperature programmed reduction of H <sub>2</sub>
HDO	Hydrodeoxygenation
HLT	Hydrotalcite
HSiW	12-tungstosilicic acid, H <sub>4</sub> SiW <sub>12</sub> O <sub>40</sub>
HV	High vacuum
ICP-OES	Inductively coupled plasma optical emission spectrometry
IEA	International Energy Agency
IR	Infrared
IRE	Internal reflection element
K-M	Kerkhof-Moulijn
MCT	Mercury cadmium telluride
M <sub>w</sub>	Atomic weight of W in the final catalyst
m-WO <sub>3</sub>	monoclinic-WO <sub>3</sub> phase
NA	Avogadro number
Nb <sub>2</sub> O <sub>5</sub>	Niobia
NO <sub>x</sub>	Nitrogen oxides
NPs	Nanoparticles
OECD	Organization for Economic Cooperation and Development
PDF	Power diffraction files
PDOs	Propanediols
PTT	Polytrimethylene terephthalate
PyH <sup>+</sup>	Pyridinium ion
Qinit	Initial differential heat of NH <sub>3</sub> adsorption

---

$r_p$	Average pore ratio
RTP	Room temperature and pressure
$S_{BET}$	Surface area calculated by Brunauer-Emmett-Teller method
SEM	Scanning electron microscopy
SG	Sol-gel
$S_{sample}$	$S_{BET}$ of the sample
TCD	Thermal conductivity detector
TEM	Transmission electron microscopy
TGs	Triglycerides
TPA	12-tungstophosphoric acid
TPD-NH <sub>3</sub>	Temperature-programmed desorption of NH <sub>3</sub>
V <sub>irr</sub>	Irreversible volume of NH <sub>3</sub>
$V_p$	Pore volume
V <sub>tot</sub>	Total number of acid sites
WI	Wetness impregnation
WS	Water spectrum subtracted from the glycerol loaded sample
XPS	X-ray photoelectronic spectroscopy
XRD	X-ray diffraction
$x_w$	Mass fraction of W in the final catalyst
$x_{WO_3}$	Mass fraction of WO <sub>3</sub>
ZnSe	Zinc selenide
ZrO <sub>2</sub>	Zirconia
$\rho_w$	Tungsten surface density
$\rho_w^{lim}$	Maximum tungsten surface density before the WO <sub>3</sub> NPs formation



